DURABILITY AND REINFORCING STEEL CORROSION OF HIGH PERFORMANCE SELF-CONSOLIDATING CONCRETE

by

© Ahmed Abdallah Abouhussien, B.Sc.

A thesis submitted to the

School of Graduate Studies

in partial fulfillment of the requirements for the degree of

Master of Engineering

Faculty of Engineering and Applied Science

Memorial University of Newfoundland

May 2013

St. John's, Newfoundland, Canada

ABSTRACT

This study investigated the strength and durability of high performance self-consolidating concrete (HPSCC) incorporating metakaolin. The statistical design of experiments was utilized to study the effects of mixture proportions and curing conditions on the performance of HPSCC. A total of 9 mortar, 26 concrete mixtures, and 80 prism samples were tested. The first stage compared the strength and durability of mortars containing metakaolin to other supplementary cementitious materials (SCM's). The second stage tested 20 HPSCC mixtures to optimize the fresh, hardened, and durability properties, and the service life time of the HPSCC mixtures. The optimum HPSCC mixture with metakaolin was then compared to an additional three HPSCC mixtures containing different SCM's and to two normal concrete (NC) mixtures. Finally, the third stage involved testing 80 prism samples using an accelerated corrosion test method under ten alternative curing techniques. The results of this investigation yielded an optimum HPSCC mixture with a total binder of 490 kg/m^3, a water-to-binder ratio of 0.39, and a 19.9% replacement of cement by MK. The results of this investigation also showed that MK replacement proved to be the most significant variable affecting the chloride permeability, decline of permeability over time, and the service life time of the structure.

ACKNOWLEDGEMENTS

I want to express my great appreciation to my supervisor Dr. Assem Hassan for offering this great chance and for his continuous guidance during my Master's program and for his help during my first accommodation in St. John's.

Many thanks to Mr. Justin Mayo for his assistance with preparing all mixtures and his support during testing. Without his help this work would not have been completed.

Words cannot express my thankfulness to the support and encouragement provided by my parents and sisters during my studies.

The funding provided from Dr. Assem Hassan, School of Graduate Studies, Mitacs-Accelerate Internship Program, and the RDC OISRA grant should also be acknowledged.

I would also like to extend my thanks to the technicians of the concrete, soil, and structures laboratories. Special thanks to Mr. Shawn Organ for his assistance in preparing and assisting in the running of the various set-ups and test programs.

Finally, I would embrace this opportunity to thank all my friends for encouraging me to finish this work, especially Engineers Amen Elgharbawy, Waleed Jerjawi, Ziad Hassoun, and all other colleagues in the Engineering department.

Table of Contents

List of Tables

List of Figures

List of Symbols, Nomenclature or Abbreviations

ANOVA = Analysis of Variance

ASTM = American Society for Testing and Materials

BBD = Box-Behnken Design

C. A. = Coarse Aggregate

C/F = Coarse to Fine Aggregate Ratio

CCD = Central Composite Design

CSA = Canadian Standard Association

D_a = Apparent Chloride Diffusion Coefficient

d_f = Degrees of Freedom

F. A. = Fine Aggregate

FA = Fly Ash

f_c' = Characteristic Compressive Strength (MPa)

HPSCC = High Performance Self-Consolidating Concrete

HRWRA = High Range Water Reducer Admixture

m = Diffusion Decay Index

MK = Metakaolin

NC = Normal Concrete

RCPT = Rapid Chloride Permeability Test

PFA = Pulverized Fuel Ash

RHA = Rice Husk Ash

RSM = Response Surface Methodology

SB = Silica Breccia

SCC = Self-Consolidating Concrete

SCM = Supplementary Cementitious Material

S_f = Segregation Factor

SF = Silica Fume

SG = Slag Cement

VMA = Viscosity Modifying Admixtures

W/B = Water-to-Binder Ratio

1. Introduction

1.1 Background

Self-consolidating concrete (SCC) is a type of concrete that can achieve consolidation under its own weight without any type of compaction or mechanical vibration. It can flow easily through congested reinforcement, filling the formwork without segregation or bleeding problems (Khayat 1999; Lachemi et al. 2003). These advantages of SCC at the construction stage have widened its use for different structural applications in North America and worldwide. However, when SCC is used for structures in severe environments, such as offshore structures, the durability of SCC is considered to a critical design aspect. These structures deteriorate at an increasing rate owing to the corrosion of embedded steel rebar. As a result, the need for a special concrete that can achieve excellent filling ability, passing ability, desirable segregation resistance, high strength, and sufficient durability is urgently increasing (Russell 1999). This superior SCC mixture can be defined as high performance self-consolidating concrete (HPSCC). The production of HPSCC is normally achieved by: a) increasing the quantity of fines in the mixture, which could be achieved by incorporating one or more supplementary cementitious materials (SCM's); b) adding viscosity modifying admixtures (VMA) or high range water reducer admixtures (HRWRA) (Khayat et al. 2001; Hassan et al. 2012); and/or c) decreasing the coarse aggregate content in the mixture (Khayat et al. 1997; Lachemi et al. 2005). Different SCM's have been successfully used for the production of HPSCC, such as fly ash, ground granulated blast furnace slag, volcanic ash, cement kiln dust, rice husk ash, and silica fume (Lachemi et al. 2003).

Metakaolin is a relatively new SCM; it has been widely used for the production of high strength and high performance concrete over the past two decades (Zeljkovic 2009). In the recent years, metakaolin was introduced for the production of HPSCC. The behaviour of metakaolin in HPSCC mixtures was found to be similar to that in normal concrete mixtures, which enhances the overall mechanical and durability performance (Hassan et al. 2012). Silica breccia, also known as Aplite, is a newly discovered supplementary cementing material (SCM) that has shown to have some pozzolanic effect when mixed with cement. Like any other SCM, pulverized silica breccia reacts with the calcium hydroxide formed during Portland cement hydration, creating additional cementitious products that modify the mixture structure and enhance its overall strength and durability performance.

Unfortunately, the production of HPSCC usually warrants a high cost, which is attributed to the high cement contents, high percentage of SCM's, and high doses of HRWRA. For this reason, optimizing HPSCC mixtures is vitally required to minimize these additives in order to reduce the cost of the cubic metre of such mixtures. Statistical design of experiments is a useful tool to optimize the mixture components of SCC. Additionally, prediction models can be developed to evaluate the response at different levels of the governing factors. By using such models, the numerical optimization can then be performed to minimize or maximize the response (Ghezal et al. 2002; Patel et al. 2004; Sonebi 2004; Dogan et al. 2009).

Reinforced concrete structures in marine environments, especially those subjected to high percentages of chlorides, should be given a special design consideration to extend their service life. The reason behind this limitation is the increasing number of deteriorating

structures due to concrete durability problems (Boddy et al. 1999; Hooton et al. 2002). The most critical factor for this deterioration is the corrosion of embedded reinforcing steel (Hassan et al. 2009). The corrosion occurs when the chlorides from deicing salts, groundwater, or seawater penetrate the concrete cover and reach the reinforcing steel. Once the percentage of the chloride around the steel bar exceeds the threshold needed for corrosion initiation, the corrosion starts and is followed by propagation through steel bars, which eventually leads to a mass loss and a delimitation of the concrete cover (Hooton et al. 2002).

Chloride permeability is a significant property of the concrete representing its resistance to chloride ingress. Such a property directly affects the time for chlorides to reach the reinforcing bars and consequently the corrosion initiation time. Moreover, most of the models used for predicting the corrosion initiation time account for the resistance of concrete to chlorides (Boddy et al. 1999; Ehlen et al. 2009). HPSCC with low permeability and dense microstructure is proved to extend the time needed for corrosion to occur (Hassan et al. 2009). In fact, the total service life time for the structures in marine environments can be increased using high performance, or less permeable, concretes (Hooton et al. 2002; Sujjavanich et al. 2005). Assessment of concrete permeability can be performed using one of the following standard tests: Rapid Chloride Penetration Test (ASTM C1202) and/or Chloride Bulk Diffusion Test (ASTM C1556).

Recently, different methods were developed for predicting the service life of concrete structures exposed to harsh environments. These methods usually monitor the service life of concrete structures in two periods, including initiation and propagation periods. Most of these methods calculate the service life as a function of the chloride diffusion through

the concrete (Boddy et al. 1999). In these models, a simplified Fickian diffusion approach is applied assuming that the chloride diffusion is the dominant mechanism of rebar corrosion and that the corrosion starts after a sufficient percentage of chlorides reach the bar surface (chloride threshold). In general, the chloride permeability of concrete, in most of the service life prediction methods, is the key factor in measuring the service life time. It is not certain, however, whether the chloride threshold value well represents the sufficient value of chlorides causing corrosion of steel bars; and furthermore, if the chloride permeability is exactly demonstrated by the chloride diffusion coefficient measured as per ASTM C1556.

1.2 Research Objectives and Significance

The purpose of this research was to design and optimize HPSCC mixtures containing metakaolin with respect to fresh, mechanical, and durability characteristics and the service life time. Statistical models were produced to investigate the effects of total binder content, water-to-binder ratio, and percentage of metakaolin replacement on the properties of HPSCC. Two curing techniques were also adopted, including air and water curing, for a period of 28 days to study the effect of curing on the compressive strength, chloride permeability, and service life time of HPSCC. The significance of this study is to design an HPSCC mixture that can achieve the balance between the optimum fresh properties of self-consolidating concrete (filling ability, passing ability, segregation resistance) and the high strength and durability of the mixture. This research also utilized results obtained from an electrically accelerated corrosion test to evaluate the current available methods for service life prediction. Moreover, the research discusses and

evaluates some relationships between different methods for evaluating the chloride permeability of concrete. The results obtained from this investigation are of special interest for engineers considering the use of metakaolin in the production of HPSCC.

1.3 Scope of Research

This study was accomplished by achieving the research milestones throughout three successive experimental stages. The first stage of the study was performed to compare the commercially available SCM's (silica breccia, fly ash, slag, and silica fume) to metakaolin by testing the strength and the durability of different mortar samples. The strength and durability performance of mortar samples of eight tested mortar mixtures were evaluated based on the results of the pozzolanic activity index, sodium sulfate attack, and the alkali-silica reactivity tests. Based on the results of this stage, metakaolin was selected (owing to its superior performance) to be further tested in the production of HPSCC in the second stage.

The second stage was implemented to investigate the effects of mixture proportions and curing techniques on the fresh, mechanical, and durability characteristics and the service life time of 26 different HPSCC mixtures. The fresh, hardened, and durability performance and the service life time of the 26 HPSCC mixtures were compared based on two sets of tests. The first set of tests was implemented to evaluate the fresh properties of the mixture, including slump flow, V-funnel, L-box, J-ring, and air content tests. The second set of tests involved compressive strength, rapid chloride permeability test (RCPT), and chloride diffusion tests. The service life times were predicted for the 26 HPSCC mixtures by means of Fick's second law of diffusion. In addition, the second

stage involved exploiting a statistical analysis of experiments method (central composite design, or CCD method) to obtain an optimum HPSCC mixture among 20 HPSCC mixtures containing metakaolin. The optimum mixture was then evaluated by comparing its mechanical and durability properties to those of other HPSCC mixtures containing fly ash, slag, and silica fume along with two additional normal concrete mixtures.

Finally, the third stage of the study was conducted to investigate the effect of different curing techniques on the mechanical and durability characteristics of HPSCC and to evaluate the prediction of the service life times obtained from Fick's second law of diffusion. This study was based on an accelerated corrosion test performed on 80 prism samples cast with different concrete covers (20, 30, 40, and 60 mm). These tested concrete prisms were subjected to ten alternative curing scenarios in hot, cold, and normal temperatures prior to testing.

1.4 Thesis Outline

The structure of this thesis is composed of five chapters as follows:

Chapter 1 describes the research background, objectives, significance, milestones, and an overview of the overall program of the study.

Chapter 2 includes a review of the literature in the areas of HPSCC, corrosion of reinforcing steel, and service life prediction methods.

Chapter 3 contains the detailed experimental program including the materials, mixture proportions, and methodology of the experimental testing.

Chapter 4 shows the raw results and the discussion of each test, as well as the developed statistical models and relationships between different tests.

Chapter 5 presents the conclusions and recommendations that were drawn from the overall investigations.

2. Literature Review

2.1 High Performance Self-Consolidating Concrete (HPSCC)

High performance self-consolidating concrete (HPSCC) can be characterized by its excellent flow and passing ability, workability, segregation resistance, high strength, and superior durability performance. These characteristics require both incorporating HRWRA and relatively high replacement levels of SCM's. Lachemi et al. (2003) produced SCC containing FA and SG as SCM's, which showed overall enhancement in the fresh properties as well as a reduction in the overall cost of their mixtures. However, their mixtures had relatively low 28-days compressive strengths, which were 31-46 MPa in SG mixtures and 26-48 MPa in FA mixtures. Patel et al. (2004) investigated the effect of using high volumes of FA on the fresh, hardened, and durability properties of SCC. Although their results showed low HRWRA demands, good fresh properties, and low chloride permeability, the compressive strength of their mixtures was also relatively low (<52 MPa).

Sonebi (2004) developed a medium-strength (35 MPa) SCC mixture containing pulverized fuel ash (PFA) as a SCM with relatively low costs. His results saw an enhancement in the fresh properties of HPSCC by using high volumes of PFA. Safiuddin et al. (2012) produced HPSCC mixtures with rice husk ash (RHA) with a satisfactory fresh, hardened, and durability performance. Their results suggested that approximately 15% replacement of RHA was the optimum replacement level. Hassan et al. (2012) tested HPSCC incorporating both SF and MK, and the results showed that both SF and MK had significant effects on the fresh and hardened properties of the mixture. Moreover, their

results showed that MK had better fresh properties, strength, and durability than SF counterpart mixtures.

2.2 Fresh Properties of HPSCC

As previously mentioned, HPSCC mixtures should maintain high flowing ability, workability, passing ability, viscosity, stability, and segregation resistance. These properties are determined based on applying several tests on the freshly mixed HPSCC mixtures. Khayat (1999) measured the flow ability and workability of SCC mixtures by performing the slump flow, V-funnel tests, filling capacity, and settlement of concrete tests. Based on his results, the main requirements of satisfactory workability of the SCC mixtures are defined in Figure 2.1. Moreover, Khayat et al. (2004) examined the stability of SCC mixtures by performing T_{500} flow time, J-ring, L-box, U-box, and pressure bleed tests. Their results recommended using the L-box along with the slump flow test to evaluate the passing ability and deformability of the SCC mixture, and meanwhile using the pressure bleed test to evaluate the stability of the SCC mixtures.

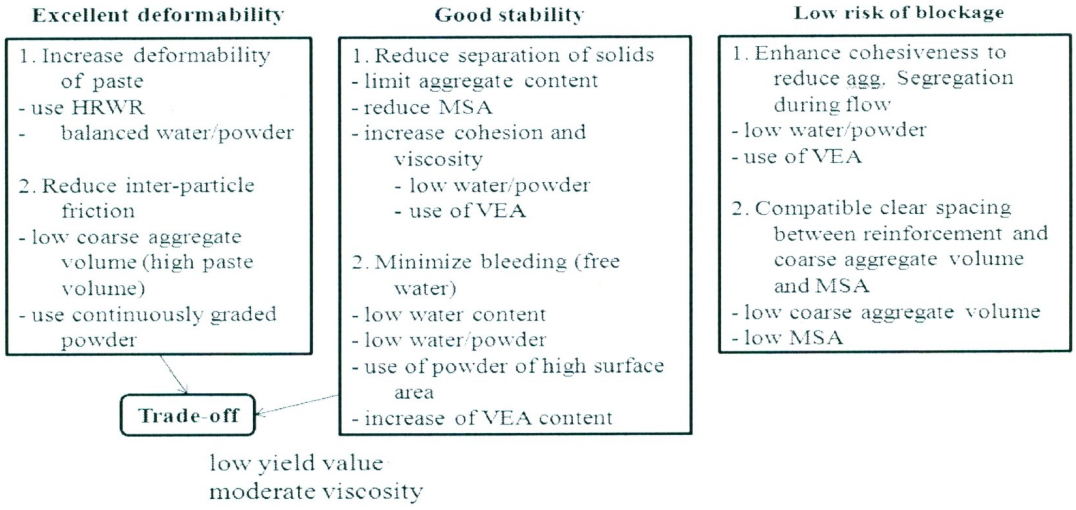

Figure 2.1: Requirement of Workability of SCC Mixtures (Khayat 1999)

The use of SCM's in proportioning HPSCC mixtures shows, in general, an improvement in the overall fresh properties of the mixture. However, the optimum percentages of SCM's replacement and HRWRA dosages are varied with each SCM based on its chemical compositions. Lachemi et al. (2003) compared the fresh properties of SCC mixtures containing FA and SG, and their results showed that both FA and SG required lower HRWRA amounts than those required for the control mixture. In addition, their results showed that SG had lower HRWRA demand than that found in FA mixtures, and about the same viscosity was obtained from both SCM's. Patel et al. (2004) also found that increasing the percentage of FA in their SCC mixtures decreased the HRWRA demand and increased the flow ability of the mixture. On the contrary, Hassan et al. (2012) found that increasing the MK content in their HPSCC mixtures showed a significant increase in the HRWRA demand as well as in the plastic viscosity of the mixture. Furthermore, their results showed an increase in the passing ability of the mixture containing MK when compared to the same mixtures with SF replacement.

2.3 Compressive Strength of HPSCC

2.3.1 Effect of SCM's

The use of supplementary cementing materials (SCM's) such as ground granulated blast furnace slag, fly ash, metakaolin, and/or silica fume has become common in the production of concrete owing to their superior effect in enhancing the mixture strength and durability. SCM's are incorporated to produce impermeable and dense concrete (Boddy et al. 2000). SCM's are classified as low reactive (limestone powder), cementitious (natural cement and hydraulic lime), pozzolanic (silica fume and Class F fly

ash), and both cementitious and pozzolanic (ground granulated blast furnace slag and Class C fly ash). The incorporation of one or more types of SCM's, together with a low water-to-cement ratio, has been proven to greatly improve the microstructure over that of concrete with ordinary water-to-cement ratio (Larbi 1993; Mehta et al. 1993).

SCM particles have a very high surface area, which consumes part of the mixing water to get their surface wet, and results in there being very little free water left in the mixture for bleeding. In addition, the SCM improves the concrete microstructure by means of either filler effect and/or chemical effect in the form of pozzolanic reaction (Mehta 1981). At early ages, the filler effect of SCM is responsible for the improvement in densification of the microstructure. The SCM improves packing of the hydration products, especially around the aggregate particles. At later ages, the chemical effect (pozzolanic reaction) adds to the improvement of the microstructure. The pozzolanic reaction of SCM is caused mainly by its reaction with the calcium hydroxide crystals that previously nucleated around the SCM particles (Larbi 1993). The pozzolanic reaction produces more calcium silicate hydrate (C-S-H) gel, which is the main cementitious product from the hydration of normal cement. C-S-H effectively ties together the hydration products and the unhydrated cement particles leading to a more homogeneous and denser matrix. These improvements in the microstructure lead to a significant increase in the compressive strength and durability of concrete. SCM that has higher pozzolanic activity is believed to be more effective in reducing concrete porosity (Sadok et al. 2011).

2.3.2 Effect of Metakaolin on the Strength of HPSCC

As with any other SCM, incorporating MK in the HPSCC was found to increase the compressive strength of the mixture. For example, Madandoust et al. (2012) tested HPSCC containing 0-20% of MK and their results showed a noticeable increase in the compressive strength (20 to 60 MPa), at all testing ages, by adding MK from 0-20%. The same trends were obtained from the study performed by Hassan et al. (2012) on HPSCC mixtures. Moreover, their results showed higher compressive strengths at 28 days obtained from MK than those of SF mixtures. These results yielded an optimum replacement level of MK of approximately 20% and any further increase in the MK percentages had no effect on the compressive strength of HPSCC. The performance of MK in the normal concrete mixtures also showed an increase in the compressive strength regardless of the water-to-binder ratios (Khatib 2008; Zeljkovic 2009).

2.4 Durability of Concrete

Durability of concrete is the property of concrete to last a longer amount of time without feasible deteriorations. Such a property includes the resistance of concrete to weathering action, chemical attack, and abrasion. Concrete with improved durability characteristics is expected to extend the overall service life of the structure (Hooton et al. 2002). The enhanced durability characteristics can evidently delay the onset of corrosion and, as a result, the time to first repair.

The durability of concrete can be examined by evaluating its resistance to chloride penetration, freezing and thawing, salt scaling, alkali-silica reactivity, sulfate resistance, and drying shrinkage. Two key factors affecting the durability of concrete include: a)

ultimate compressive strength and b) concrete permeability. The permeability of concrete can be described either by water permeability or chloride permeability. However, the permeability of concrete can be better represented by its ability to allow chlorides to pass through concrete pores (chloride permeability). The chloride permeability of concrete is influenced by several factors, including water-to-binder ratio, incorporating SCM's, curing conditions, and the total binder content.

The durability performance of normal vibrated concrete is considered well known nowadays. However, there is a lack of information regarding the durability performance of HPSCC. The production of HPSCC is usually done by decreasing the amount of coarse aggregates in the mixture, and having a slightly higher water-to-binder ratio and HRWRA (Hassan et al. 2009). As a result, the compressive strength and overall durability behaviour of HPSCC is expected to be different than that of normal vibrated concrete. On the other hand, the incorporation of SCM's in HPSCC mixtures can enhance its long-term durability performance (Hassan et al. 2012).

2.4.1 Effect of SCM's on Durability of HPSCC

The durability of HPSCC was evaluated by Hassan et al. (2009) in terms of drying shrinkage, freezing and thawing, salt scaling, and rapid chloride permeability tests (RCPT). The HPSCC mixtures included in their study contained metakaolin (MK) and silica fume (SF) with different levels of cement replacement. Their results showed a superior behaviour of HPSCC mixtures containing MK and SF when compared to their normal concrete counterparts. Based on the overall strength and durability performance, the optimum replacement level in terms of the durability performance for MK mixtures

was 20% while for SF it was 8%. Moreover, their results showed that MK had overall better durability performance than that of SF counterpart mixtures.

Guneyisi et al. (2011) compared the durability performance of different SCC mixtures containing metakaolin, fly ash, and ground granulated blast furnace slag. Their evaluation was based on the results of chloride ion permeability, water permeability, and sorptivity tests. Their results showed that the permeability of SCC mixtures was significantly affected by the type and amount of the used SCM. Moreover, their results indicated that MK was the most effective SCM in decreasing the chloride ion permeability compared to other SCM's (FA and SG).

2.4.2 Chloride Permeability Test Methods

Chloride permeability is a significant property of the concrete representing its resistance to chloride ingress. Such a property directly affects the time for chlorides to reach the reinforcing bars and consequently the corrosion initiation time. Most of the models used for corrosion prediction account for the resistance of concrete to chlorides (Boddy et al. 1999; Ehlen et al. 2009). Concrete with low permeability and dense microstructure is expected to extend the time needed for corrosion to occur. In fact, the total service life time for the structures in marine environments can be increased using high performance, or less permeable, concretes (Hooton et al. 2002; Sujjavanich et al. 2005). Assessment of concrete permeability can be performed using one of the following standard tests: Rapid Chloride Penetration Test (ASTM C1202) and/or Chloride Bulk Diffusion Test (ASTM C1556).

2.5 Curing of Concrete

Curing of concrete is the process of maintaining adequate temperature and moisture content during the concrete's early age to ensure it develops the designed properties. Curing has a significant effect on the concrete's hardened properties including durability, strength, chloride permeability, abrasion resistance, and resistance to freezing, thawing, and deicers. This significant effect is due to the longer hydration time, which leads to an increase of the strength and durability of concrete (Mehta 1981; Larbi 1993). Several curing techniques can be adopted to improve the properties of concrete. One of these methods is moist curing, which can be used to obtain higher strength than air curing (Gonnerman et al. 1928). Figure 2.2 shows the effect of the moist curing period on the strength development when compared to air curing. Alternatively, concrete can be cured by applying curing compounds or by covering the freshly placed and finished concrete with impermeable sheets or wet burlap.

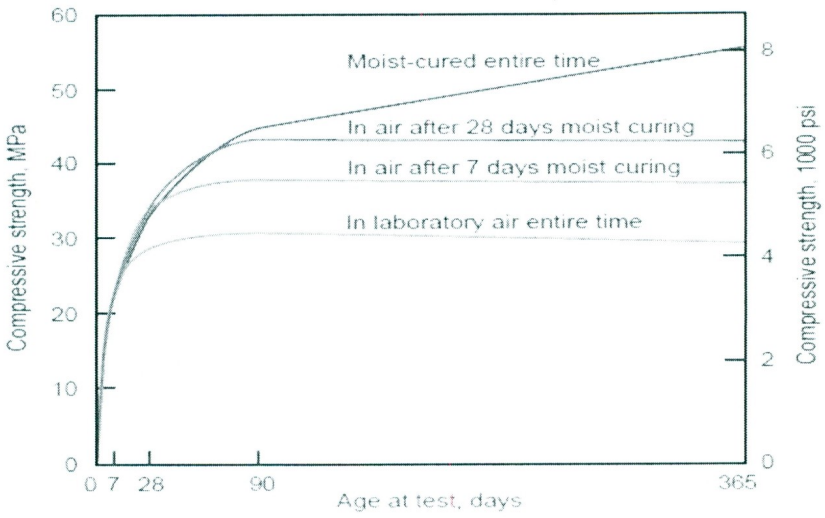

Figure 2.2: Effect of Moist Curing on Strength Development (Gonnerman et al. 1928)

Another important factor influencing the hydration process is the curing temperature. Temperatures below 10° C (50° F) are not preferred regarding the development of the strength (Copeland et al. 1955). Figure 2.3 shows the effects of different curing temperatures (from 10° C to 50° C) on the compressive strength of concrete. The increase in the temperature from 10° C to 50° C showed to increase the early age compressive strength of concrete (1 day). However, this increase in the curing temperature (10° C to 50° C) was found to decrease the 28-days compressive strength (Kosmatka et al. 2002).

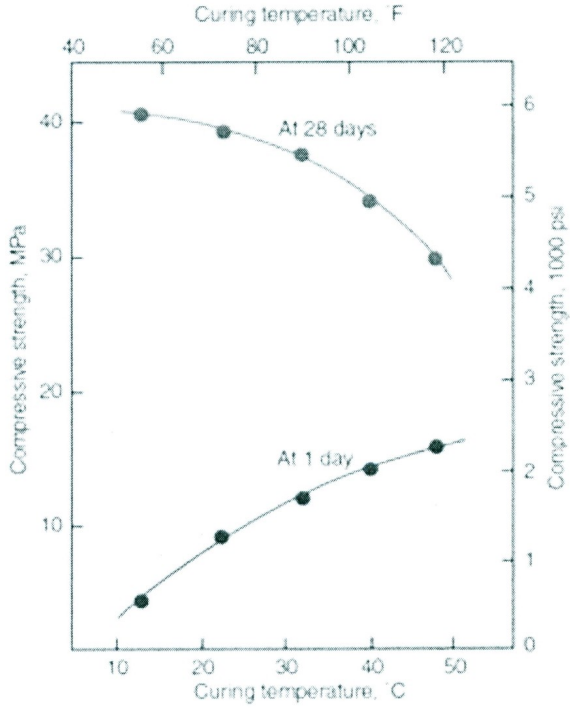

Figure 2.3: Effect of Curing Temperature on Compressive Strength (Verbeck et al. 1968)

2.6 Corrosion of Reinforcing Steel in Concrete

2.6.1 Mechanism of Corrosion

Corrosion is an electrochemical process that includes the flow of charges (electrons and ions). Although steel's natural tendency is to undergo corrosion reactions, the alkaline

environment of concrete (pH of 12 to 13) provides steel with corrosion protection. At the high pH, a thin oxide layer forms on the steel and prevents metal atoms from dissolving. This passive film does not actually stop corrosion; it reduces the corrosion rate to an insignificant level (Martin-Peréz et al. 1998). However, corrosion can occur when the passive layer is destroyed. The destruction of the passive layer occurs when the alkalinity of the concrete is reduced or when the chloride concentration in concrete is increased to a certain level (chloride threshold).

2.6.2 Accelerated Test Methods for Corrosion

Since corrosion of steel is a slow process, researchers use the accelerated corrosion tests. These tests are used to evaluate the loss of bond of corroding reinforcement, the effect of mineral admixtures in reducing reinforcement corrosion, and to compare different protection techniques (Shamsad 2009). The majority of techniques used for accelerating corrosion are based on the method of impressed current (galvanostatic method). This method is based on applying a constant current from a DC source to the steel embedded in concrete in order to induce significant corrosion in a short period of time (Sujjavanich et al. 2005). After a specified period of time, the degree of corrosion can be measured by using Faraday's law in terms of the percentages of mass loss. Typical set up for accelerated corrosion test as performed by Hassan et al. (2009) is presented in Figure 2.4.

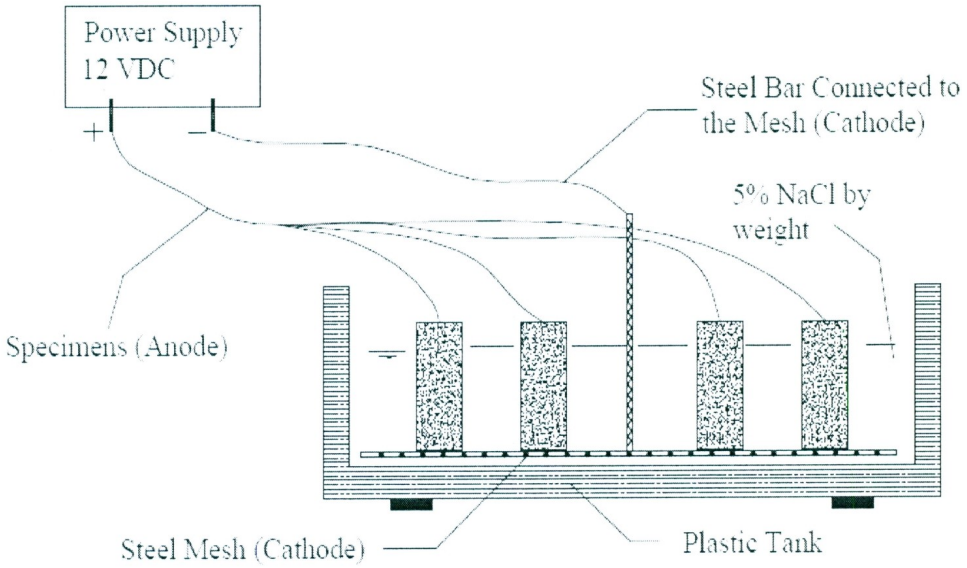

Figure 2.4: Schematic Representation of the Accelerated Corrosion Test (Hassan et al. 2009)

2.7 Service Life Time Prediction of Concrete Structures in Marine Environments

Recently, different methods were developed for predicting the service life of concrete structures exposed to severe environments. These methods identify the total service life of concrete structures as two periods, including initiation and propagation periods (Tuutti 1982). The initiation stage is the period of time at which the corrosion starts to initiate, while the propagation stage represents the period at which sufficient damage is detected in the reinforcing steel. Most of these methods calculate the initiation period as a function of the chloride diffusion through the concrete towards the steel bar (Boddy et al. 1999). In these models, a simplified Fickian diffusion approach is applied assuming that the chloride diffusion is the dominant mechanism. In general, the chloride permeability of concrete, in most of the service life prediction methods, is the key factor in measuring the service life time.

An example of these models was used in developing commercially available software for predicting the service life time (Ehlen et al. 2009). This model is similar to the more complex model proposed by Boddy et al. (1999); however, it accounts for both time and temperature in calculating the coefficient of diffusion of concrete. The initiation period in this model is defined as the period of time needed for sufficient chlorides to penetrate the concrete cover and accumulate at the surface of the embedded steel bars. This sufficient quantity represents the chloride threshold at which corrosion initiates. The model then uses Fick's second law of diffusion to estimate the initiation time under a number of limitations regarding the homogeneity of concrete properties and chloride concentrations. Researchers have focused on measuring the chloride threshold value and the chloride transport rate based on experimental tests and/or field results. For instance, Trejo et al. (2003) proposed a method for experimentally measuring the chloride threshold values for two types of steel reinforcement. In this method, the diffusion of chlorides towards the steel bars was accelerated by applying a potential gradient across two electrodes. An anode was embedded at the bar surface, while a cathode was placed in a chloride ion solution of 3.5% concentration. Corrosion initiation was detected by evaluating the polarization resistance of the steel reinforcement by a statistical analysis procedure.

2.8 Statistical Design of Experiments

Owing to its variety of advantages, the statistical design of experiments has been widely used in proportioning concrete mixtures. Statistical models can be developed to predict the properties of concrete at different levels of the mixture variables and to optimize the responses. Different methods have been successfully used in the concrete mixture design;

for instance, factorial designs, fractional factorial designs, and response surface methodology (RSM). These methods include the procedures of analysis of variance (ANOVA) for testing statistical significance of factors and regression analysis for developing prediction models. A limited number of researchers are using the factorial design in the design of concrete mixtures. However, the RSM methods are widely applied in the optimization of the concrete mixtures and more recently in optimizing SCC (Lachemi et al. 2003; Patel et al. 2004; Sonebi 2004; Dogan et al. 2009). The RSM methods are typically used in the applications of optimization of the responses that an HPSCC mixture has, and/or when these responses exhibit significant curvature (nonlinear effects). The RSM uses two alternative experimental designs: central composite design (CCD) and Box-Behnken Design (BBD). The CCD method enables studying the effects of the variable at five different levels (versus three in BBD) with almost the same number of runs (Schmidt et al. 1994). As a result, the CCD method can be used to study a wider range of the variables than can be studied using the BBD method.

2.8.1 Optimizing SCC Using CCD Method and Prediction Methods

The CCD method has already been used to optimize the SCC mixture to maximize or minimize the responses of the mixture, both at the fresh and hardened stages. For example, Ghezal et al. (2002) utilized the CCD method to optimize SCC containing limestone filler. The resulting prediction models were successfully employed in the selection of SCC mixture proportions that can maintain high strength at a relatively low cost. Another study conducted by Sonebi (2004) examined the use of statistical analysis for SCC mixture design. In his research, the statistical models were applied to optimize

the mixture proportions of SCC containing pulverized fuel ash. Different variables were studied, including the content of cement and pulverized fuel ash, water-powder ratio, and the dosage of the HRWRA. The models tested the filling ability, passing ability, segregation, compressive strength, and cost of SCC mixtures. The results of optimization yielded the desired levels of each ingredient of a medium strength SCC with minimum costs.

Patel et al. (2004) developed statistical models to predict the behaviour of SCC containing high volumes of fly ash. These models included the fresh, hardened, and durability performance of SCC mixtures. Their target was to exploit the statistical models to minimize the amount of the HRWRA and maximize the strength and durability of SCC. The factors examined were total binder content, percentage of fly ash, percentage of HRWRA, and water-to-binder ratio. Their results showed a valuable exploitation of the statistical methods to optimize SCC mixtures.

Dogan et al. (2009) also compared different pozzolanic materials by applying the CCD method for normal concrete. Their comparison was based on the chloride permeability of normal vibrated concretes containing fly ash, granulated blast furnace slag, and silica fume. A rapid chloride permeability test (RCPT) was performed to examine the chloride permeability of such concretes, both for air curing and water curing conditions. The results showed that the use of the CCD method was an appropriate technique for the design and optimization of concrete regarding the RCPT.

3. Experimental Program

3.1 Materials

In this program, type GU Canadian Portland cement similar to ASTM Type I, with a specific gravity of 3.15, was used for both mortar and HPSCC mixtures. The metakaolin (MK) used in this research was delivered from the Eastern United States by Advanced Cement Technologies, conforming to ASTM C-618 Class N, with a specific gravity of 2.56. The slag (SG) used in this investigation was similar to ASTM Type I, with a specific gravity of 2.89. Fly ash (FA) Class F was employed in this project similar to ASTM Type I, with a specific gravity of 2.26. The silica fume (SF) present in this study was similar to ASTM Type I, with a specific gravity of 2.27. The silica breccia (SB) tested herein was ground to four different grain sizes (<75 μm, <45 μm, <30 μm, and <20 μm) with a specific gravity of 2.7. The original material was obtained from one of the largest deposits of silica breccia, which was discovered in Finnvolldalen, Norway. The chemical properties of cement and all other SCM's are shown in Table 3.1.

A high range water reducer admixture (HRWRA), similar to ASTM Type F (ASTM C494), was applied to achieve the required workability of mortar mixtures and the required slump flow of HPSCC mixtures. The specific gravity, volatile weight, and pH of the HRWRA were 1.2, 62%, and 9.5, respectively. Natural sand was used for the production of mortar mixtures for alkali-silica reactivity and sulfate resistance tests, and for casting the HPSCC mixtures. In addition, silica sand was included as fine aggregate for the pozzolanic activity mortar mixtures. The natural and silica sand each had a specific gravity of 2.70 and water absorption of 1%. Both 10 mm and 20 mm maximum

size natural crushed stones were included as coarse aggregates in the HPSCC mixtures, with a specific gravity of 2.70 and water absorption of 1%.

Table 3.1: Chemical Properties of Cement and Other SCM's

Chemical Properties %	Cement	Metakaolin	Slag	Silica Fume	Fly Ash	Silica-Breccia
SiO_2	19.6	51-53	40.3	>85	52	82.1
Al_2O_3	5.5	42-44	8.4	-	23	8.8
Fe_2O_3	2.4	<2.2	0.5	-	11	0.8
FeO	-	-	-	<5	-	-
TiO_2	-	<3.0	-	-	-	0.03
C	-	-	-	<10	-	-
P_2O_5	-	<0.2	-	-	-	<0.01
SO_4	-	<0.5	-	-	-	-
CaO	62.4	<0.2	38.7	<5	5	0.8
MgO	2.5	<0.1	11.1	<5	-	0.04
Cr_2O_3	-	-	-	-	-	<0.01
MnO	-	-	-	-	-	0.02
SrO	-	-	-	-	-	0.01
BaO	-	-	-	-	-	0.03
Na_2O	-	<0.05	-	-	-	2.3
C_3S	52.3	-	-	-	-	-
C_2S	16.8	-	-	-	-	-
C_3A	10.5	-	-	-	-	-
C_4AF	7.2	-	-	-	-	-
K_2O	-	<0.4	0.4	-	-	3.1
L.O.I.	2.1	<0.5	0.7	-	-	0.7

3.2 Stage 1: Strength and Durability of Mortars Containing Different SCM's

In this stage, the strength and durability of an MK mortar mixture were tested and compared to seven other mortar mixtures with other SCM's (SG, FA, SF, and four SB samples). The tests involved flow table, pozzolanic activity index, alkali-silica reactivity, and sulfate resistance tests. As a result, three different mortar mixtures were warranted for the three different tests. The tests description and the mixture proportions of each mortar mixture containing MK and different SCM's are described in detail as follows:

3.2.1 Flow Table Test (ASTM C230)

The flow table test was completed in both the pozzolanic activity index and sulfate resistance tests to control the amount of mixing water, measured in mL, to be enough to produce a flow of 100±5%, according to the ASTM C230 standard. Sufficient amounts of HRWRA were added to the mortar mixture until reaching the required workability, which is determined in this test by achieving a flow of 100±5%.

3.2.2 Pozzolanic Activity Index Test (CSA A3004-E1)

The pozzolanic activity test involved mixing a small batch of mortar consisting of hydrated lime, silica sand, and the mineral admixture. The amount of each material and the amount of water was specified as per the CSA A3004-E1 standard. The mixture proportions for the eight different mortar mixtures, including MK and seven other SCM's samples, were calculated based on the CSA A3004-E1 standard and are shown in Table 3.2. After mixing, a minimum of three 50 x 50 x 50 mm cube specimens were cast and then stored in a moist room at 23±2° C for 24±2 hours. After this time the samples were removed from the moist room then sealed and stored at 55±2° C for seven days until the time of the test. The three cube specimens were then tested to measure the compressive strength according to the ASTM C109 standard.

Table 3.2: Mixture Proportions for the Pozzolanic Activity Test Mixtures in Stage 1

Sample	W/B	Hydrated Lime (gm)	HRWRA (mL)	Flow (mm)	Silica Sand (gm)	SCM (gm)	Water (mL)
FA	0.6	53.9	1.5	209	485.7	117.1	111.2
MK	0.8	48.9	3.8	205	440.9	120.4	135.5
SG	0.6	52.4	-	210	471.8	145.5	118.7
SF	0.8	50.5	4.4	205	454.1	109.9	128.3
SB <20 μm	0.6	53.2	-	205	479.1	138.0	114.8
SB <30 μm	0.6	53.8	-	207	484.1	139.4	112.1
SB <45 μm	0.6	53.5	-	210	481.6	138.7	113.4
SB <75 μm	0.6	53.5	-	212	481.6	138.7	113.4

3.2.3 Alkali-Silica Reactivity Test (CSA A23.2-25A)

The alkali-silica reactivity test involved mixing a mortar batch for moulding at least three bar specimens (25 x 25 x 127 mm). After 24 hours of mixing, the specimens were removed from the mould and the initial length was measured by means of a standard length comparator. The change in the length of the specimens was then measured after 24 hours submergence in water at 80±2° C. The samples were then submerged in preheated sodium hydroxide (1N NaOH) for a period of 14 days at 80±2° C. The rate of expansion at 2, 7, and 14 days was calculated as specified in the CSA standards, CSA A23.2-25A. The mixture proportions for the nine different mortar mixtures, including control, 20% MK, 30% FA, 30% SG, 8% SF, and four selected SB samples (10%) were made as per CSA A23.2-25A and are shown in Table 3.3. It should be mentioned that the water-to-binder ratios (W/B) were kept constant as specified in the CSA A23.2-25A standard. In addition, the replacement of cement by each SCM was selected based on the optimum level for the SCM found in similar studies (Boddy et al. 2000; Hassan et al. 2009; Sadok et al. 2011).

Table 3.3: Mixture Proportions for the Alkali-Silica Reactivity Test Mixtures in Stage 1

Sample	W/B	Replacement Level %	Cement (gm)	Graded Sand (gm)	SCM (gm)	Water (mL)
Control	0.4	-	97.8	266.6	-	135.6
FA	0.4	30	66.9	260.6	39.9	132.5
MK	0.4	20	77.5	264.2	23.9	134.4
SG	0.4	30	68.1	265.2	31.8	134.9
SF	0.4	8	89.4	265.0	10.8	134.8
SB <20 μm	0.4	10	87.7	265.8	11.4	135.1
SB <30 μm	0.4	10	87.7	265.8	11.4	135.1
SB <45 μm	0.4	10	87.7	265.8	11.4	135.1
SB <75 μm	0.4	10	87.7	265.8	11.4	135.1

3.2.4 Sulfate Resistance Test (CSA 3004-C8)

In this test, the change of length of six mortar bars (25 x 25 x 127 mm) representing each tested specimen was monitored as specified in the CSA standard, CSA 3004-C8. The mortar bars were cured in a 35° C water bath until their companion cubes reached a minimum strength of 20.0±1.0 MPa. The companion cubes were made from the same specimen batch and were tested at different times until their strength reached 20.0±1.0 MPa. The mortar bars were then stored in a sodium sulfate solution (Na_2SO_4) for up to one year with measurements taken at the specified intervals. The reading increments included 1, 2, 3, 4, 8, 13, and 15 weeks after the placement of the bars in the sulfate solution. Subsequent readings were taken at 4, 6, 9, and 12 months. The water-to-binder ratio was kept almost constant (around 0.45) as specified in the CSA standards, CSA 3004-C8. The flow table test was performed after mixing to maintain the same flow diameters for all mortars, according to the ASTM C230 standard. Table 3.4 shows the mixture proportions for the nine different mortar mixtures.

Table 3.4: Mixture Proportions for the Sulfate Resistance Test Mixtures in Stage 1

Sample	W/B	Replacement Level %	Cement (gm)	HRWRA (mL)	Flow Table (mm)	Graded Sand (gm)	SCM (gm)	Water (mL)
Control	0.5	-	1100	-	215	3020	-	530
FA	0.5	30	750	-	205	2960	320	500
MK	0.5	20	870	5	208	3000	220	530
SG	0.5	30	880	-	208	3010	220	500
SF	0.5	8	1000	4	205	3000	90	530
SB <20 μm	0.5	10	1000	-	211	3010	100	520
SB <30 μm	0.5	10	1000	2.5	209	3010	100	530
SB <45 μm	0.5	10	1000	-	205	3010	100	530
SB <75 μm	0.5	10	1000	-	207	3010	100	500

3.3 Stage 2: Optimizing HPSCC Mixture Using Statistical Analysis (CCD Method)

After completing the first stage, the results recommended that MK was the most preferred SCM for both strength and durability performance; as a result, MK was selected to be further tested to produce the optimum HPSCC in this stage. A total of 20 HPSCC mixtures containing MK were designed by applying the Box-Wilson central composite design (CCD) method (Schmidt et al. 1994). Three factors varied throughout the 20 mixtures, including total binder content (A = 400-500 kg/m^3), water-to-binder ratio (B=0.35-0.45), and percentage of metakaolin replacement of cement (C = 0-25%). The coarse-to-fine aggregate ratio was kept constant (0.9) for all the mixtures. The amount of HRWRA was determined based on maintaining a slump flow of approximately 650±50 mm (as per ASTM C1611). Upon achieving this slump value, the first set of fresh properties tests was implemented. The fresh properties tests included slump flow, time to reach 500 mm diameter (T_{500}) with the slump flow, J-ring flow diameter, T_{500} with J-ring ($T_{500}J$), air content tests (based on ASTM C1611; C1621; C231, respectively), V-funnel, and L-box tests (according to The European Guidelines for Self-Compacting Concrete,

2005). These tests examine the HRWRA demand (slump flow), viscosity (T_{500} and V-funnel), passing ability (J-ring and L-box), flowing ability ($T_{500}J$), segregation (repeated V-funnel), and air content of each HPSCC mixture.

After completing the tests for the fresh properties, (100 mm diameter x 200 mm length), cylinders were cast and cured for a period of 28 days for testing compressive strength and chloride permeability/diffusion. Two curing regimes were used: the first regime was to submerge the samples in water for 28 days, while the second regime was to store them in air for the whole 28-day period. Both regimes were performed at a controlled temperature of about 23° C. After the completion of the curing period, the compressive strength, rapid chloride permeability (RCPT), and chloride diffusion tests were performed on both air- and water-cured samples. The RCPT test was replicated at 90 and 180 days to measure the decrease in the chloride permeability versus the concrete's age. Using the chloride diffusion coefficients obtained from the chloride diffusion test, the service life time of the 20 mixtures was predicted by means of Fick's second law of diffusion. Next, a statistical analysis was performed on the results from each test and prediction models for each test (response) were developed. The statistical analysis was completed by commercially available software for the design and analysis of experiments.

Finally, using these models, the optimum level of each factor was determined. In addition, the optimum HPSCC mixture was tested for validating the prediction models by comparing the results obtained from the models and the actual tests.

3.3.1 Mixture Design and HPSCC Proportions Using CCD Method

The design of mixtures was obtained after determining the different levels of each factor by using the CCD method. This method divides the design space into three parts: the full-factorial part, the axial part, and the central part (Schmidt et al. 1994). The three parts together yielded the 20 runs that were represented by 20 HPSCC mixtures included in the study. The three parts consist of examining the studied factors at five different levels by the criteria shown in Table 3.5. The first part, the full-factorial, involved studying the three factors or variables (k = 3) at two levels only (-1 and +1 in coded factors) with a total number of runs of $n_f = 2k = 8$ runs. Secondly, the axial part defined as $n_a = 2k = 6$ runs and the coded factors were identified as the coded values of -1.68 and +1.68. The selection of the coded values of the axial part was designed to obtain a rotatable experimental design region, which can be achieved by using the value of $\alpha = \pm (2k)^{1/4} = \pm 1.68$ (Schmidt et al. 1994). By maintaining a rotatable design, the uncertainty of determined response surface symmetry can then be fixed. The remaining runs were set at the centre, or $n_c = 6$, with a coded value of 0, as shown in Table 3.5. The aim of using these centre points was to estimate the experimental error and to maintain orthogonality. Furthermore, testing at the centre points is more effective for variables that show nonlinear effects on the responses, if any. A minimum number of centre points was calculated by the equation proposed by Schmidt et al. (1994), $n_c = [4 \times (n_f+1)^{0.5}] - 2k = 6$ runs.

Table 3.5: The Range of Factors and their Coded Values

Factor	Range	Coded Values				
		-1.68	-1	0	1	1.68
A	400 – 500 (kg/m^3)	400	420	450	480	500
B	0.35 – 0.45	0.35	0.37	0.4	0.43	0.45
C	0 – 25%	0	5.1	12.5	19.9	25

The coded values of each factor were calculated based on Equation 3.1 for five different levels of each variable, as described in Table 3.5. For example, the coded value of water-to-binder ratio of 0.37 can be estimated by using Equation 3.1 as follows: Coded Factor = (0.37 – 0.4) / (0.5 * 0.06) = -1. The overall range of variables was selected based on reviewing the literature of proportioning HPSCC containing metakaolin (Hassan et al. 2009; Vejmelková et al. 2011; Hassan et al. 2012).

$$Coded\ Factor = \frac{(Actual\ Value - Central\ Value)}{0.5\ x\ (Range\ between\ Maximum\ and\ Minimum\ Values)} \qquad (3.1)$$

The total number of runs (mixtures) was 20, as described above. By using the previously described levels of each factor for each mixture, the mixture proportions were calculated by applying the absolute volume method. Table 3.6 outlines the mixture proportions for each run (mixture) in a random order based on the mixing time.

Table 3.6: Mixture Proportions for HPSCC Mixtures

Mix. No.	A: Binder Content (kg/m^3)	B: W/B	C: MK Replacement (%)	Cement (kg/m^3)	MK (kg/m^3)	C. A. (kg/m^3)	F. A. (kg/m^3)	Water (L/m^3)
1	420	0.37	19.9	336.4	83.6	868.4	964.9	155.4
2	480	0.37	5.1	455.5	24.5	822.9	914.4	177.6
3	450	0.4	12.5	393.8	56.3	828.9	920.9	180.0
4	450	0.4	12.5	393.8	56.3	828.9	920.9	180.0
5	480	0.43	19.9	384.5	95.5	781.1	867.9	206.4
6	450	0.45	12.5	393.8	56.3	801.2	890.2	202.5
7	450	0.35	12.5	393.8	56.3	856.6	951.8	157.5
8	400	0.4	12.5	350.0	50.0	873.6	970.7	160.0
9	420	0.37	5.1	398.6	21.4	874.1	971.2	155.4
10	450	0.4	25	337.5	112.5	823.8	915.4	180.0
11	420	0.43	19.9	336.4	83.6	837.4	930.5	180.6
12	450	0.4	12.5	393.8	56.3	828.9	920.9	180.0
13	480	0.43	5.1	455.5	24.5	787.5	875.0	206.4
14	420	0.43	5.1	398.6	21.4	843.0	936.7	180.6
15	450	0.4	12.5	393.8	56.3	828.9	920.9	180.0
16	450	0.4	12.5	393.8	56.3	828.9	920.9	180.0
17	480	0.37	19.9	384.5	95.5	816.6	907.3	177.6
18	500	0.4	12.5	437.5	62.5	784.1	871.3	200.0
19	450	0.4	12.5	393.8	56.3	828.9	920.9	180.0
20	450	0.4	0	450.0	0	833.9	926.6	180.0

C. A. and F. A. are Coarse and Fine Aggregates, respectively

3.3.2 Mixing and Fresh Properties Testing

The 20 HPSCC mixtures at this stage were mixed according to the procedures described in the ASTM C192 test standard. After mixing, the tests for fresh properties were completed by the following procedure:

3.3.2.1 Slump Flow Test (ASTM C1611)

The slump flow test was performed according to the ASTM C1611 by filling the standard slump cone with the freshly mixed HPSCC, as shown in Figure 3.1. The cone was then

lifted up in approximately 3-5 second periods until the mixture completely stopped flowing on the base plate. Three diameters of the mixture spread were measured and recorded as the slump flow diameter (mm). This test also included recording the required time for the mixture to flow after lifting the cone until reaching a 500 mm diameter (T_{500}).

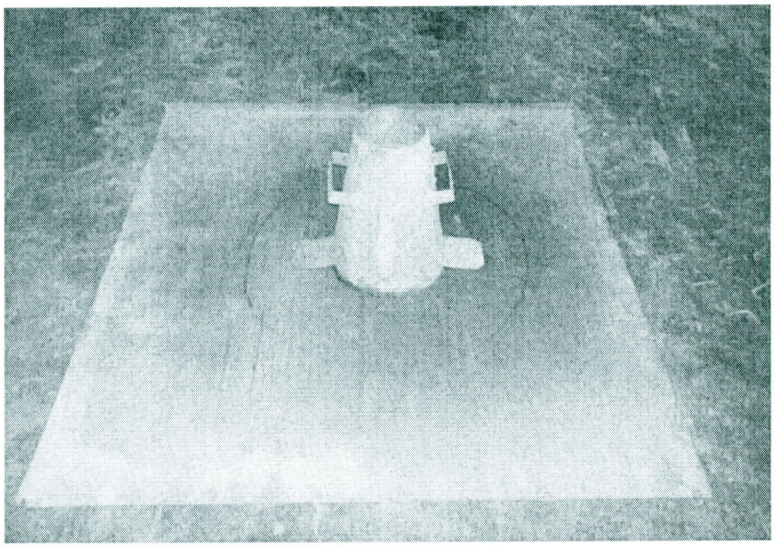

Figure 3.1: Slump Flow Testing Apparatus

3.3.2.2 J-Ring Test (ASTM C1621)

The J-ring test was intended to simulate the obstruction of the J-ring bars to the flowing and passing ability of the HPSCC, as per the ASTM C1621 standard. This test is similar to the slump flow test except for the obstructing J-ring seen in Figure 3.2. The results also include the flow diameter with J-ring and the 500 mm flow time with J-ring ($T_{500}J$).

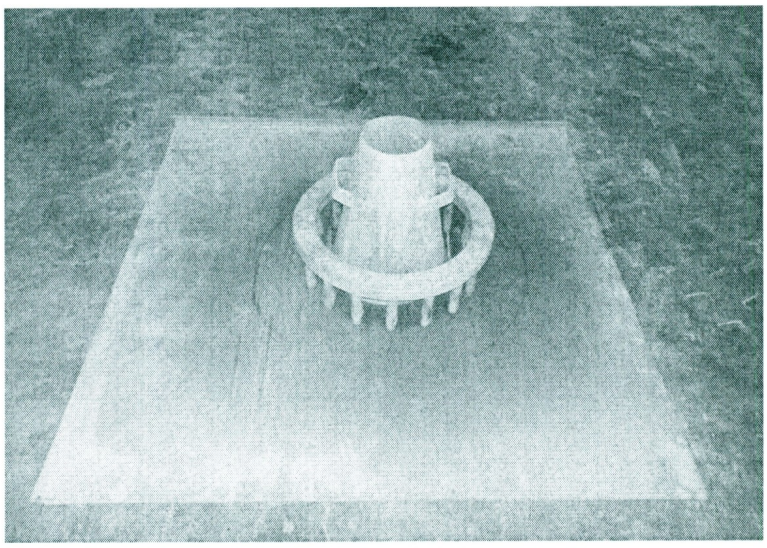

Figure 3.2: J-Ring Testing Apparatus

3.3.2.3 V-Funnel Test

The V-funnel test was used to measure the viscosity and the segregation factor of the HPSCC according to the European Project Group (2005). The test measures the time for the mixture to empty out from the V-shaped funnel seen in Figure 3.3. This time is called the initial V-funnel time (seconds), which is directly related to the mixture viscosity. In addition, the test was repeated after five minutes of filling the V-funnel and this time was denoted as final V-funnel time (seconds). The segregation factor can then be calculated using both initial and final V-funnel times, which represents the segregation resistance of the mixture, by substituting in Equation 3.2. The low values of segregation factor indicate high segregation resistance and vice versa.

$$S_f = \frac{(Final\ \ V-Funnel)-(Initial\ \ V-Funnel)}{Initial\ V-Funnel} \qquad (3.2)$$

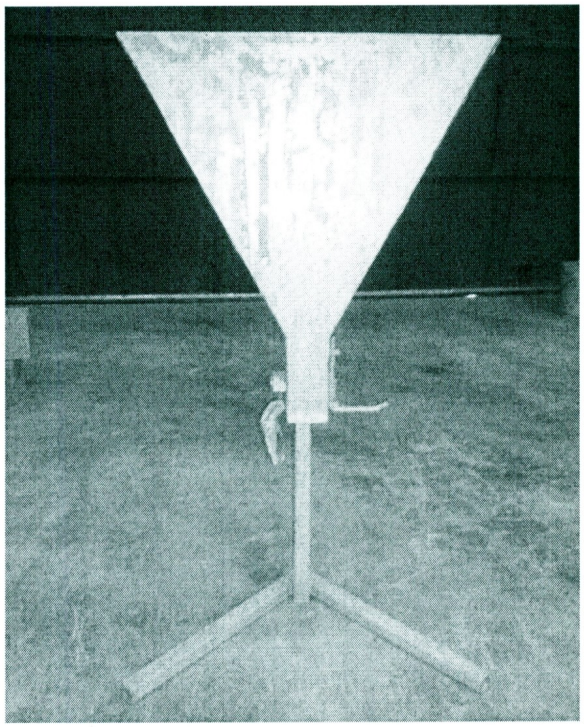

Figure 3.3: V-Funnel Test Apparatus

3.3.2.4 L-Box Test

The L-box test was also used to evaluate the passing ability of the HPSCC mixtures based on the European Project Group (2005). This test was implemented by filling the vertical part of the L-shaped apparatus shown in Figure 3.4 with the gates in the closing position. The gate was immediately opened and the mixture started to flow horizontally, passing through the vertical obstructing bars until the mixture stopped moving. The heights measurements before the obstructing bars (H1) and at the very end of the horizontal part (H2) were obtained. The ratio H2/H1, which represents the passing ability of the HPSCC mixture, was then calculated. The high H2/H1 ratio indicates the high passing ability of

the HPSCC mixture, which warrants the low difference in heights before and after the obstructing bars.

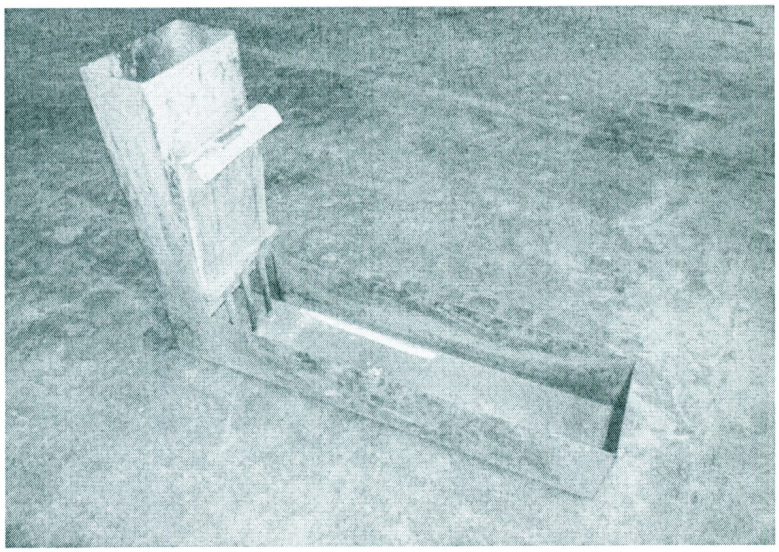

Figure 3.4: L-Box Test Apparatus

3.3.2.5 Air Content Test (ASTM C231)

The air content of the tested HPSCC mixtures was measured according to the ASTM C231 standard test method. In this method, the device shown in Figure 3.5 was utilized to measure the air voids contents of the freshly mixed HPSCC mixtures by the pressure method, as per ASTM C231.

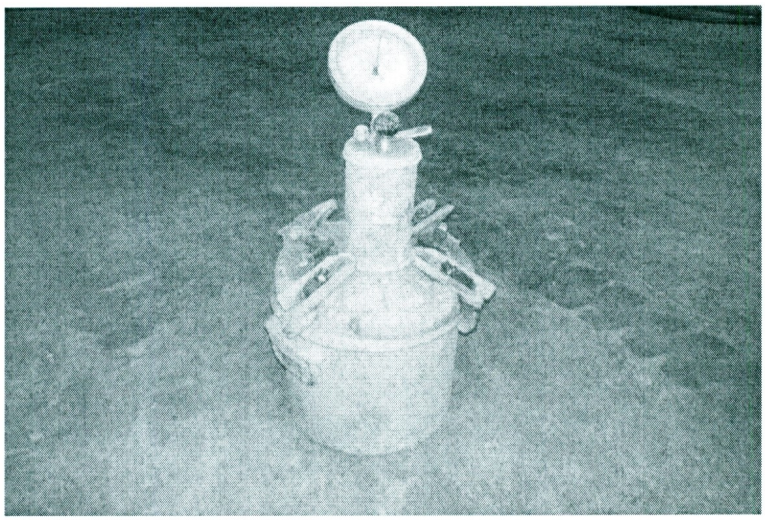

Figure 3.5: Air Content Test Device

3.3.3 Testing of Hardened HPSCC Specimens

At the age of 28 days, the 100 mm x 200 mm cylinder samples were tested to measure the compressive strength and chloride permeability/diffusion of HPSCC mixtures. Moreover, the chloride permeability (RCPT) was further tested at 90 and 180 days. These tests done to evaluate the hardened characteristics of the HPSCC mixtures are described below:

3.3.3.1 Compressive Strength of Cylinders (ASTM C39)

The compressive strength (f_c') of both air- and water-cured cylinder samples were measured by the compression test machine presented in Figure 3.6 conforming to the ASTM C39 standard test method. The test involved testing a minimum of three cylinders of each HPSCC mixture at a loading rate of 0.25 MPa/sec and reporting the average strengths.

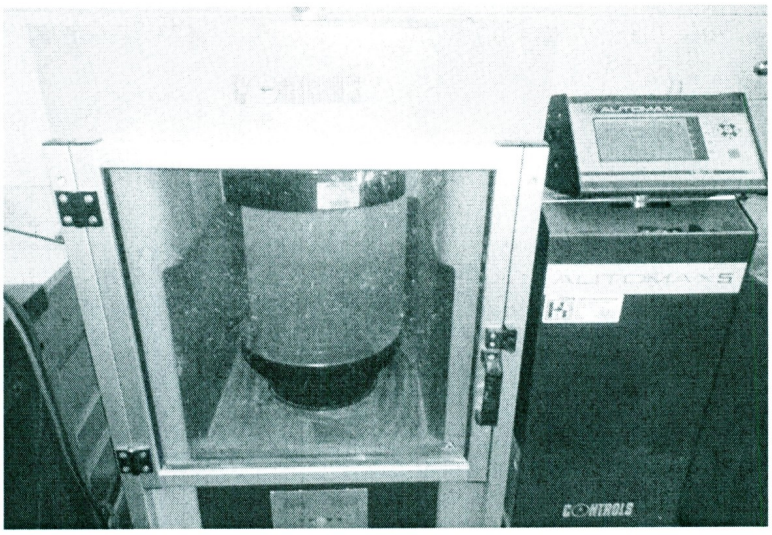

Figure 3.6: Compression Testing Machine

3.3.3.2 RCPT (ASTM C1202)

The chloride permeability of the 20 HPSCC mixtures was primarily evaluated by means of the rapid chloride permeability test (RCPT). The RCPT is a standard test method (ASTM C1202) that evaluates the level of chloride permeability as five different levels (High, Moderate, Low, Very Low, Negligible). These different levels are classified on the basis of the total electrical current passed through 2-inches (51-mm) thick slices of 4-inches (102-mm) nominal diameter cylinders during a 6-hour period. A potential difference of 60 V DC is maintained across the ends of the specimen, one of which is immersed in a sodium chloride solution (NaCl), the other in a sodium hydroxide solution (NaOH). The total charge passed (coulombs) was found to be related to the resistance of the specimen to chloride ion penetration. As a result, the standard test device seen in Figure 3.7 was utilized to measure the chloride permeability of the 20 HPSCC mixtures at 28, 90, and 180 days.

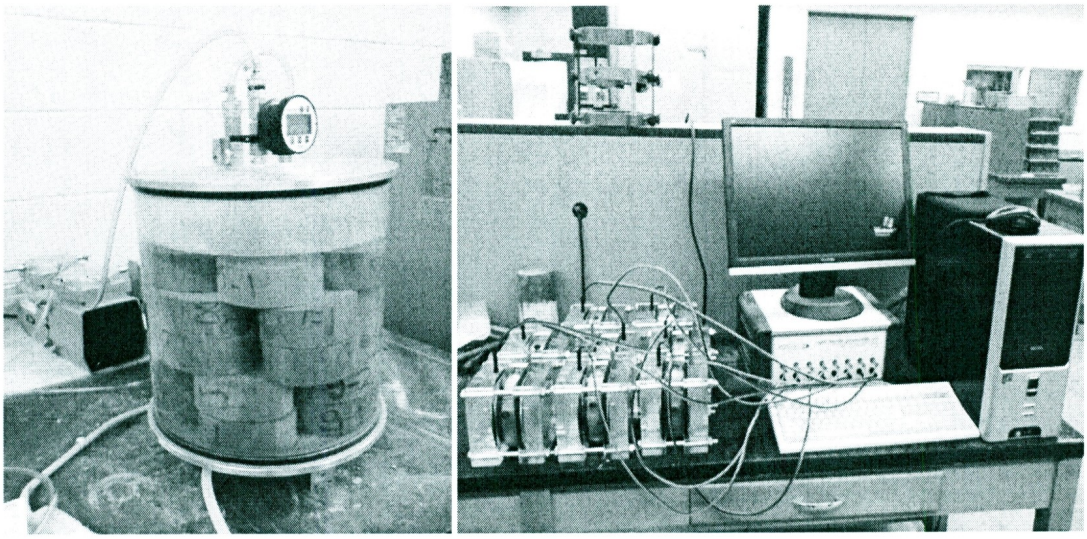

Figure 3.7: RCPT Equipment

3.3.3.3 Chloride Diffusion Test (ASTM C1556)

The chloride diffusion test was also used to evaluate the chloride permeability of the 20 HPSCC mixtures. This test method is similar to the Norway standard method (NT BUILD 443, 1995), which is defined as a standard ASTM C1556 test method for the assessment of chloride diffusion into hardened concrete. It is based on immersing cylinder samples in 16.5% NaCl solution for at least 35 days. A 35-day immersion period is adopted in this test program for both air- and water-cured cylinders of the 20 tested mixtures. The cylinder samples were coated with epoxy coating on all surfaces except for the top surface. After the immersion period, powder samples were extracted at different depths from the exposed surface for analysis of chloride contents. The chloride ion content of the collected powder samples was measured using the chloride meter device, seen in Figure 3.8, after a storage period of 24 hours in bottles of a specific extraction liquid. The chloride content profile (chloride content versus diffusion depth) for each mixture was

plotted and used to determine the apparent chloride diffusion coefficient (D_a) by analysis against Fick's second law of diffusion.

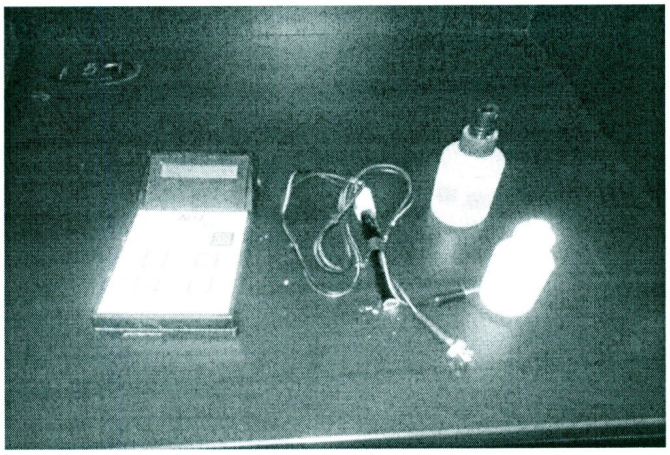

Figure 3.8: Chloride Meter Device

3.3.4 Testing Optimum HPSCC Mixture Containing Metakaolin

After analyzing the results of testing the 20 HPSCC mixtures, the numerical optimization was implemented and yielded the optimum HPSCC mixture containing MK. This mixture was then tested under the same previously described tests for validating the statistical models obtained from the ANOVA. Furthermore, this optimum mixture was compared to an additional three HPSCC (containing 30% FA, 30% SG, and 8% SF) and two NC mixtures. These five additional mixtures were similarly designed based on the mixture proportions of the optimum HPSCC containing MK. Table 3.7 shows the mixture proportions of the six additional samples tested in stage 2. It can be seen that the six mixtures had the same binder contents (490 kg/m^3) and the same water-to-binder ratios (0.39). The MK replacement level of 19.9% was found as the optimum level (see the results of the numerical optimization in section 4.2.4). In addition, the replacement levels of FA, SG, and SF were assumed as the optimum levels based on the results of testing

these SCM's in the production of HPSCC (Hassan et al. 2009; Sadok et al. 2011). Regarding the NC mixtures, two mixtures were included to examine different coarse aggregate sizes, denoted as NC1 (10 mm Coarse Aggregate) versus NC2 (20 mm Coarse Aggregate).

Table 3.7: Mixture Proportions of the Six Additional Mixtures Tested in Stage 2

Mix. No.	A: Binder Content (kg/m^3)	B: W/B	C: SCM Replacement (%)	C/F Ratio	C. A. Size (mm)	Cement (kg/m^3)	SCM (kg/m^3)	C. A. (kg/m^3)	F. A. (kg/m^3)	Water (L/m^3)
MK	490	0.39	19.9	0.9	10	392.3	97.7	795.9	884.3	191.1
SG	490	0.39	30	0.9	10	343.0	147.0	799.5	888.3	191.1
FA	490	0.39	30	0.9	10	343.0	147.0	782.0	868.9	191.1
SF	490	0.39	8	0.9	10	450.8	39.2	798.7	887.5	191.1
NC1	490	0.39	0	0.9	10	490.0	0	804.7	894.1	191.1
NC2	490	0.39	0	0.9	20	490.0	0	804.7	894.1	191.1

C.A. and F.A. are the Coarse and Fine Aggregates, respectively
C/F is the Coarse-to-Fine Aggregates Ratio

3.4 Stage 3: Accelerated Corrosion Test

In this stage, the **mixture number 20** (Table 3.6) was selected from stage 2 to be further investigated in stage 3. This mixture was selected as a control mixture that contained no SCM (MK) to study the effect of curing on the strength, durability, and reinforcement steel corrosion. The mixture was used for casting different samples, which were cured for a total period of 28 days under ten different curing techniques yielding ten different concrete qualities. The samples included (100 mm x 200 mm) concrete cylinders and a total of 80 prism samples containing one embedded steel bar at the middle of each prism. The chloride permeability of the ten concrete qualities samples were evaluated based on the ASTM standard test methods (see sections 3.3.3.2 and 3.3.3.3): Rapid Chloride

Penetration Test (ASTM C1202) and Chloride Bulk Diffusion Test (ASTM C1556). The apparent chloride diffusion coefficient (D_a) at 28 days was also measured for the ten samples based on the ASTM C1556 test method. These coefficients were exploited for predicting the service life time of each concrete sample by applying Fick's second law of diffusion. For comparison, an accelerated corrosion test was implemented on the 80 prism samples cast with the same mixture and cured under the same ten curing techniques.

3.4.1 Curing of Samples

After the mixing of the selected mixture (number 20) and obtaining the required slump flow, 80 prism samples with a 20M (200 mm diameter) steel bar at the centre were cast. The 80 samples were divided into four groups representing four variable concrete covers: 20 mm (20 prisms), 30 mm (20 prisms), 40 mm (20 prisms), and 60 mm (20 prisms). The samples maintained equal clear concrete covers from all sides (20, 30, 40, and 60 mm) by means of concrete spacers while each having the same length (250 mm). The dimensions of the samples were 60 mm x 60 mm x 250 mm for the 20 mm covers; 80 mm x 80 mm x 250 mm for the 30 mm covers; 100 mm x 100 mm x 250 mm for the 40 mm covers; and 140 mm x 140 mm x 250 mm for the 60 mm covers. In addition, 50 (100 mm x 200 mm) cylinders were also cast for compressive strength and chloride permeability/diffusion testing. The samples (prisms and cylinders) were then cured under ten different curing techniques, including air, water curing, heat, and cold temperatures, as described in Table 3.8. The curing techniques are divided into four general categories, including air curing at lab temperature (23° C), water curing at 23° C, heated-water curing at 50° C, and cold-air curing at 3-5° C. Different periods were associated with each curing technique in each

curing category, as seen in Table 3.8. At 28 days, all the samples were removed from the different curing spots and left to dry before testing. The cylinders from each curing regime were tested to measure the compressive strength and chloride permeability for each curing system. Meanwhile, the 80 prisms were used for the accelerated corrosion test.

Table 3.8: Different Curing Techniques

Curing Technique	Description	28-Days f_c' (MPa)
1	28 Days in Air at 23° C	53.2
2	28 Days in Water at 23° C	76.2
3	3 Days in Water then Air, both at 23° C	73.3
4	7 Days in Water then Air, both at 23° C	75.4
5	3 Days in Water at 23° C then Air at 3-5° C	65.9
6	7 Days in Water at 23° C then Air at 3-5° C	69.2
7	28 Days in Air at 3-5° C	47.5
8	1 Day in Water at 50° C then Water at 23° C	58.9
9	3 Days in Water at 50° C then Water at 23° C	59.4
10	7 Days in Water at 50° C then Water at 23° C	57.9

3.4.2 Test Set-Up and Prism Specimens

The accelerated corrosion experiment was set up similar to other studies performed by Hassan et al. (2009), as shown in Figure 3.9. The samples were connected to a DC power supply acting as anode (+), while the steel mesh was positioned under the samples as cathode (-). The samples were connected as parallel connections to the circuit board to maintain a constant volt (12 Volts) throughout the whole experiment. The 80 samples were totally submerged in a 5% NaCl solution in a container, as seen in Figure 3.9 (Hassan et al. 2009).

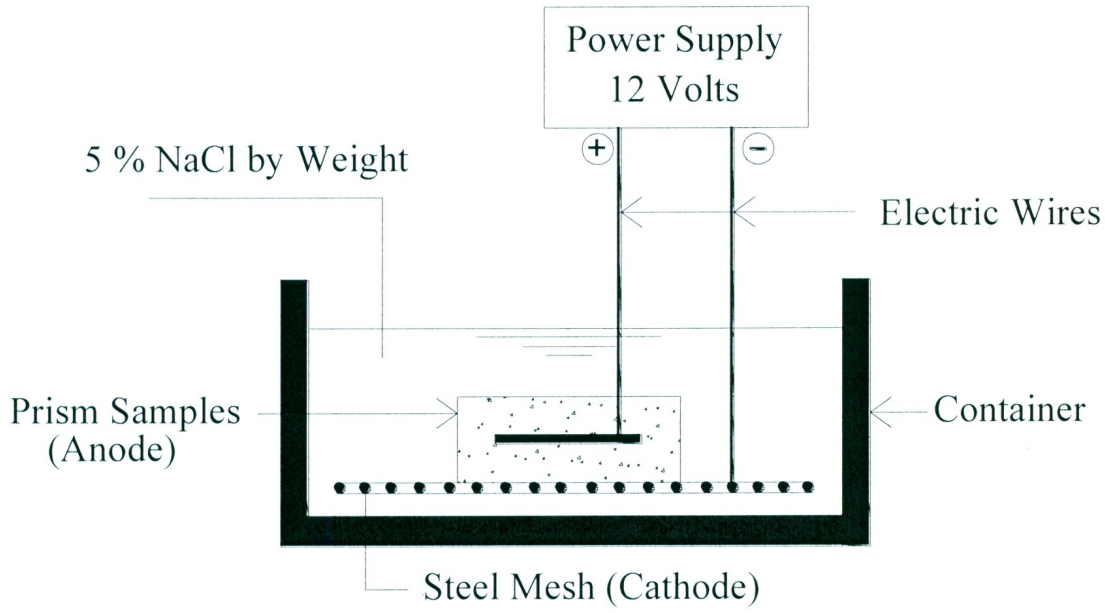

Figure 3.9: Accelerated Corrosion Test Set-Up

The 80 prism samples were subjected to an accelerated corrosion test in two stages, including non-severe corrosion stage (40 prism samples) and severe corrosion stage (40 prism samples). The samples tested in the non-severe stage were denoted as 1, while those samples in the severe corrosion stage were numbered as 2. The 40 samples in each stage were totally submerged in the NaCl solution in two different tanks, as described in Figure 3.10. In the non-severe stage, the samples were removed from the tank once the first crack was detected, at which point the experiment was completed for these samples. On the other hand, the severe corrosion stage was extended until sufficient damage, defined as exhibiting a crack of 4 mm or more, was reached in the sample. The 40 samples in each stage were divided into four groups of ten prisms based on four concrete covers (20, 30, 40, and 60 mm) and ten curing techniques (1 through 10). The samples were designated based on the degree of corrosion, cover thickness, and curing technique.

For example, the sample tested in stage 1 (non-severe stage) with 40 mm concrete cover and cured in water for 28 days (curing technique 2) was designated as 1-40-2.

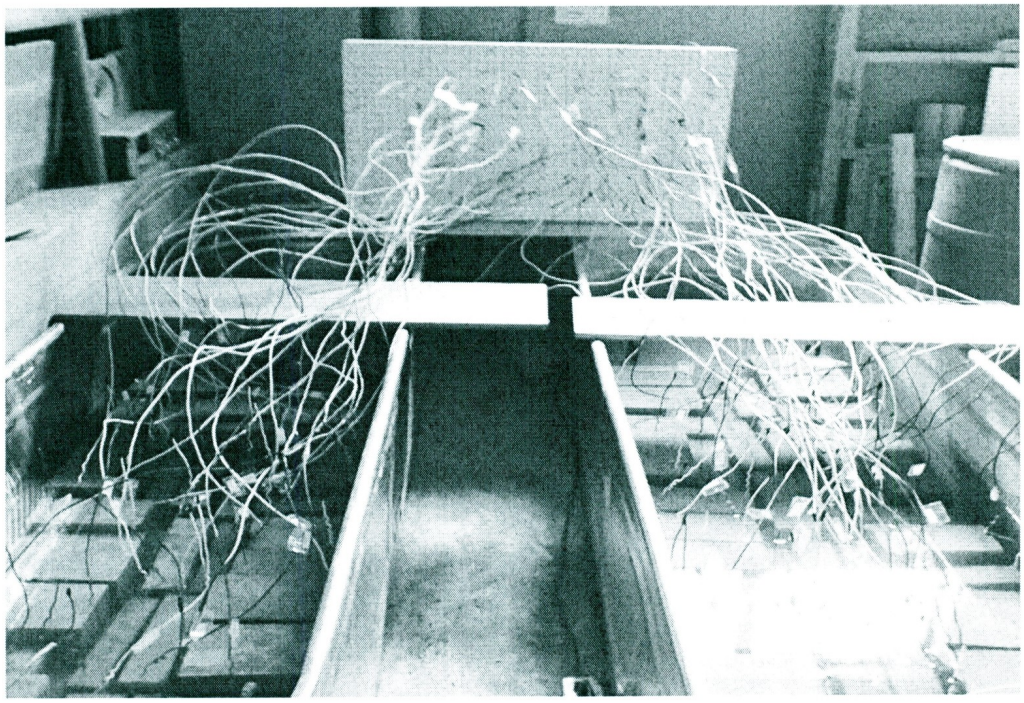

Figure 3.10: Tanks for Accelerated Corrosion Test (Right Tank = Non-Severe Corrosion Stage and Left Tank = Severe Corrosion Stage)

3.4.3 Corrosion Monitoring Using Current Measurements

The readings of the electrical current (mA) passing through the bar embedded into the sample were fairly representative of the degree of corrosion present on the bar surface (Hassan et al. 2009). The current readings were taken on a daily basis for both non-severe and severe corrosion stages. The readings were stopped upon reaching the first crack in the non-severe stage and exhibiting a crack of 4 mm thick in the severe corrosion stage.

3.4.4 Corrosion Monitoring Using Half-Cell Potentials (ASTM C876)

The corrosion activity was alternatively monitored using the ASTM C876 standard test method. The half-cell device described in Figure 3.11 was used to measure the potential difference between the reference electrode and the embedded bar. The results obtained from the device were exploited to examine the probability of corrosion occurring on the bar surface. The probability of corrosion is classified into three different levels based on the half-cell reading. A reading of (-0.2 V) or more positive value indicates that there is a greater than 90% probability that no corrosion is present. While a reading between (-0.2 to -0.35 V) represents that corrosion activity of the reinforcing steel in that area is uncertain. If the potentials read more negative than (−0.35 V), there is a greater than 90% probability of corrosion, as per ASTM C876.

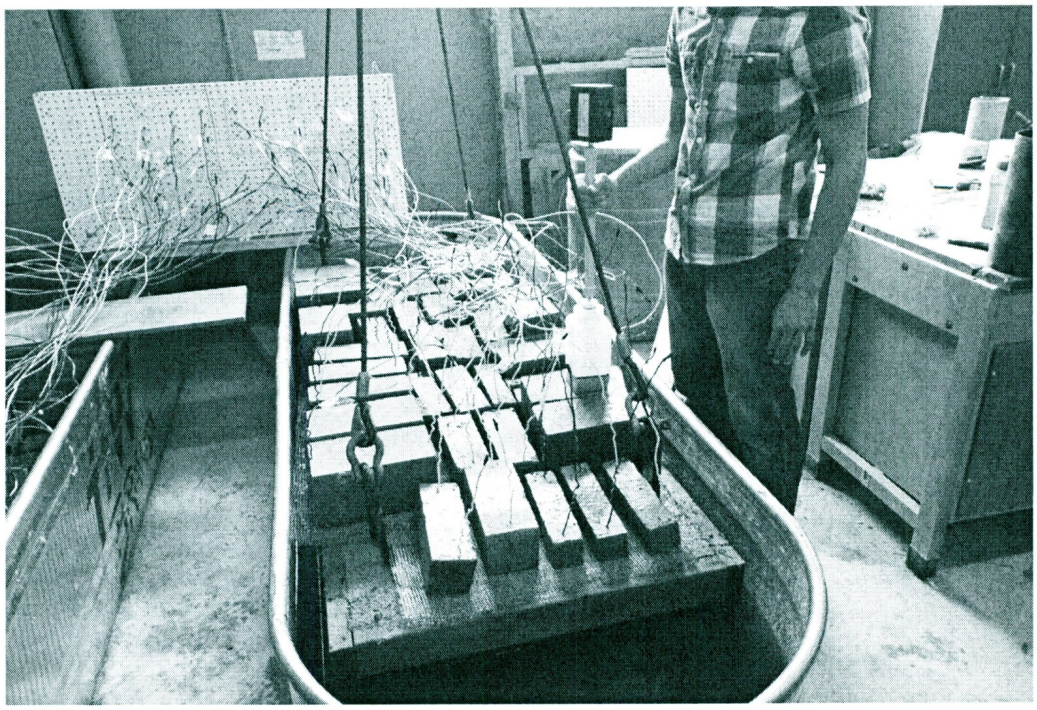

Figure 3.11: Half-Cell Potentials Test

3.4.5 Chloride Ion Content Measurements

The chloride ion content near the bar surface was measured after removing each sample from the accelerated corrosion test by means of a chloride-meter, as seen in Figure 3.8. The aim for this reading was to determine the chloride threshold value at which corrosion initiates and correlate it with the results obtained from half-cell and accelerated corrosion test. The chloride ion content of the concrete powder extracted near the bar surface was measured by submerging the reference electrode into the bottle of extraction liquid containing the powder sample. The percentage of powder to liquid was 3 grams of powder to 20 mL of liquid, and the chloride ion content is expressed as a ratio to the mass of concrete (% wt of concrete).

3.4.6 Mass Loss in Corroded Bars

The percentage of the mass loss in the embedded bar for the 80 tested prisms was experimentally evaluated with respect to the initial mass (W_i) of the bars after removing the prism from the experiment. The final weight (W_f) of each bar was measured and the percentage of mass loss was calculated using Equation 3.3.

$$\%\ Mass\ Loss = \frac{W_i - W_f}{W_i}\ x\ 100 \qquad (3.3)$$

3.5 Sources of Error

The experimental work in this investigation was associated with some sources of error at the stage of mixing, curing, and testing concrete samples. In mixing stage, errors may be attributed to the precision of the weighing scales, mixing temperature, and moisture condition of the mixer. The curing stage may include errors resulting from any

unexpected change of curing temperature. During testing the samples under different tests, the homogeneity of the samples from the same batch may also lead to some discrepancies in the test results. However, mixing, curing, and testing of concrete in this experimental program were conducted based on the ASTM standard methods.

4. Results and Discussion

4.1 Strength and Durability of Mortars Containing Different SCM's

The main objective of this stage was to select the best SCM type to be used for optimizing the durability of HPSCC Mixture in stage 2. The results from the standard test methods performed during this stage are shown and discussed below:

4.1.1 Pozzolanic Activity Index Test Results

Figure 4.1 shows the results obtained from the pozzolanic activity index tests on the eight tested mortar mixtures. It is clear from the figure that the 20% MK mixture exhibited the maximum compressive strength (14.5 MPa) after 7 days compared to other SCM's. Although SB samples had the minimum strength, the sample with particle size <20 μm achieved a relatively high strength (6.83 MPa). In addition, this sample was the only SB mixture that fulfilled the minimum strength of 5.5 MPa as per CSA A3004-E1 standard.

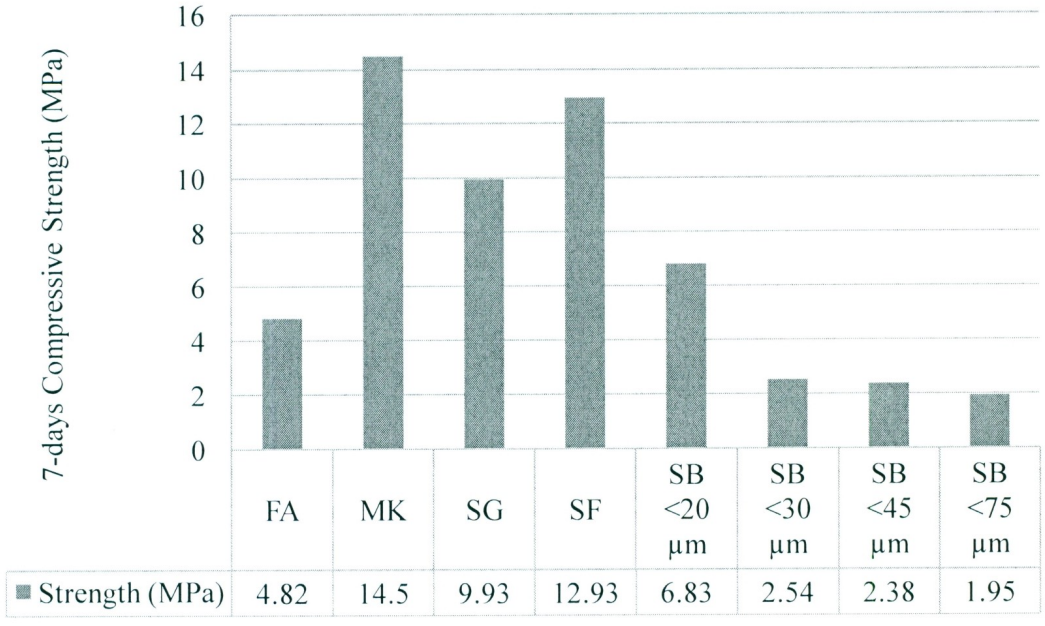

Figure 4.1: Pozzolanic Activity Index Test Results

4.1.2 Alkali-Silica Reactivity Test Results

Table 4.1 presents the rate of expansion resulting from the alkali-silica reactivity test for the nine tested mixtures at different intervals up to 14 days. A maximum expansion of 0.1% at 14 days is allowed for the sample to be qualified as an alternative supplementary cementing material, as per CSA A3004-E1. It is clear from the table that all SB samples exhibited expansions higher than 0.1%. However, SB <30 μm sample had an expansion smaller than the control sample. In addition, SF and SG samples had higher expansions than FA and MK, which may be attributed to the relatively low replacement levels used in the mixtures of slag and silica fume. The minimum expansion (0.093%) was found in MK mortar bars, while the SB <20 μm had the maximum expansions (0.206%) after 14 days. It should be mentioned that the expansion results for the SB samples were previously expected because of its natural silica content (see Appendix A).

Table 4.1: Expansions Rates for Alkali-Silica Reactivity Test

Sample	Expansions Rate %		
	2-Days	7-Days	14-Days
Control	0.083	0.113	0.156
FA	0.065	0.094	0.099
MK	0.078	0.078	0.093
SG	0.078	0.105	0.149
SF	0.08	0.109	0.134
SB <20 μm	0.076	0.098	0.206
SB <30 μm	0.059	0.088	0.155
SB <45 μm	0.08	0.123	0.192
SB <75 μm	0.087	0.119	0.167

4.1.3 Sulfate Resistance Test Results

The change of length of the mortar bars was periodically reported and the rate of expansion was calculated compared to the initial length. The rate of expansion was

calculated as the average expansion of the six mortar bars every week until a period of eight months had elapsed, as seen in Figure 4.2. It is clear from the graph that the 20% MK mortar mixture exhibited the minimum expansions after eight months, compared to different SCM's. It can also be seen that the minimum expansion among SB mortars was shown for SB <20 μm, which had an expansion less than the control mortar. However, the difference between the expansions of SB samples was not significant. It can be concluded that all mortar samples are acceptable in terms of maximum expansions after eight months, as all expansions were below 0.1%, as per CSA A3004-E1 (see Appendix B).

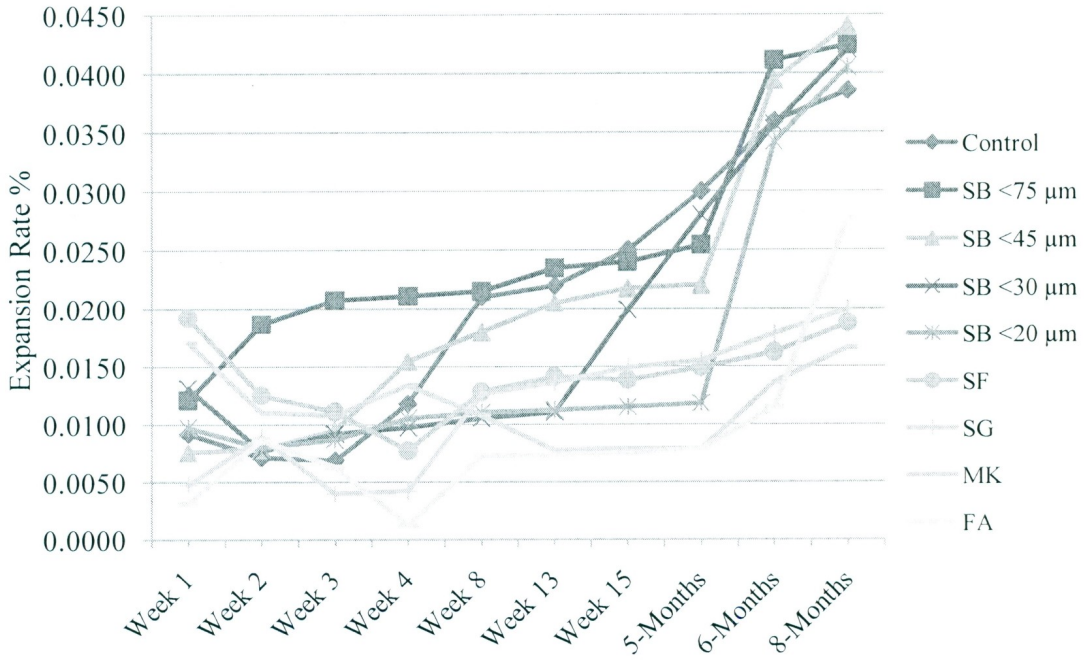

Figure 4.2: Rate of Expansions for Sulfate Resistance Test

It can be concluded from the results of mortar testing that the optimum behaviour in terms of strength and overall durability was obtained by using MK with 20% replacement of

cement. As a result, between all tested SCM's, MK was selected to be used in the HPSCC mixtures for further investigation.

4.2 Optimizing HPSCC Mixture Using Statistical Analysis (CCD Method)

The raw results from each test were subjected to a statistical analysis by means of the commercially available program for experimental design. This program performs nonlinear regression analysis for each response (test result) based on preselected variables. The variables presented in this program include A: Binder content (kg/m^3), B: W/B, and C: MK replacement (%). Eventually, the software yields an equation of the response and response surface diagrams for each test result. The developed equations are usually based only on the most significant variables (factors) and their interactions. The equation may be linear or nonlinear depending on the behaviour of the response throughout the range of variables. Linear equations contain main variables and their interactions, while nonlinear formulas include higher order variables (quadratic factors).

The significance of variables and their interactions is determined after completing the analysis of variance (ANOVA). The ANOVA tests the probability values (Probability > F), which indicate that the factor is significant if its value is < 0.05. In addition, the degree of significance among the significant factors can be determined based on the F-value for each factor. The factor with a higher F-value is considered more significant than other factors with lower F-values. On this basis, the significant variables and the degree of importance for each response were selected to form the prediction equations. These equations exhibit some coefficients, which depend on the contribution of each variable. The factor with lower value of Probability > F and higher F-value is preceded by higher

coefficients in the respective equation. The equations can be interpreted in forms of coded values or actual values of significant variables. For simplifying the equations, the form of actual values of each variable was applied for all models presented in this thesis.

4.2.1 Fresh Properties of HPSCC

Fresh properties tests were conducted to measure the HRWRA demand, viscosity, passing ability, flow ability, and segregation of different HPSCC mixtures. The results obtained from each test are presented in Table 4.2 and the derived prediction model for each response are described below in detail:

Table 4.2: Raw Results of the Fresh Properties for HPSCC Mixtures

Mix. No.	HRWRA Dose (L/m^3)	Slump Flow (mm)	T_{500} (Sec)	J-Ring Flow (mm)	$T_{500}J$ (Sec)	Slump-J-Ring (mm)	V-Funnel (Sec)		S_f*	L-Box Ratio H2/H1	Air %
							Initial	Final			
1	10.4	629	9.5	604	13.5	25	40	63	0.58	0.65	1.7
2	4.0	640	2.5	605	4.5	35	30	48	0.60	0.55	1.7
3	4.6	610	3.2	580	5.5	30	24	40	0.67	0.67	2.3
4	4.6	650	3.7	621	5.8	29	26	43	0.65	0.69	2.1
5	4.9	653	2.0	641	3.0	12	5	6	0.20	0.93	3.3
6	3.3	625	2.5	605	3.7	20	4	5	0.25	0.77	2.4
7	15.4	673	5.5	636	8.6	37	34	59	0.74	0.5	1.5
8	8.1	635	7.2	600	9.3	35	32	55	0.72	0.52	1.8
9	8.7	600	8.5	560	11.8	40	36	89	1.47	0.45	2.0
10	7.3	662	4.5	645	5.6	17	30	45	0.50	0.78	1.8
11	6.1	650	4.7	634	6.2	16	34	48	0.41	0.83	1.4
12	5.3	640	3.5	615	4.4	25	22	35	0.59	0.6	1.8
13	2.6	673	1.5	659	2.3	14	3.5	4.5	0.29	0.69	1.4
14	3.6	625	3.8	604	6.5	21	8	13	0.63	0.68	1.2
15	4.7	640	4.2	610	5.9	30	23	38	0.65	0.64	1.7
16	4.6	635	4	603	5.3	32	29	46	0.59	0.59	1.9
17	9.6	653	6.5	625	8.25	28	24	36	0.50	0.8	0.9
18	4.3	625	3.3	605	3.9	20	10	13	0.30	0.7	1.9
19	5.3	635	4.5	608	5.8	27	27	45	0.67	0.66	2.0
20	2.3	625	3	592	4.0	33	15	34	1.27	0.55	2.0

* S_f = Segregation Factor

4.2.1.1 HRWRA Demand of HPSCC

The slump flow test was performed for each HPSCC mixture after adding a minimum dosage of the HRWRA. The test was repeated by adding additional amounts of HRWRA to reach the diameter of approximately 650±50 mm. The values of the slump flow diameters ranged between 600-673 mm, with non-significant differences between the 20 mixtures (see Table 4.2). It can also be seen in Table 4.2 that different values of HRWRA demand were warranted depending on the mixture proportions. Thus, the analysis of variance (ANOVA) was performed for the demand of HRWRA and the most significant factors were determined, as seen in Table 4.3. These factors were B, C, A, B^2, A^2, and AC, respectively in order of significance. The water-to-binder ratio (factor B) was the most significant factor, as it had the lowest P-value and the highest F-value compared to other significant factors (see Table 4.3). It can also be seen from Table 4.3 that all these significant factors exhibited P-values (Prob. > F) lower than 0.05.

Figures 4.3, 4.4, 4.5, and 4.6 show the effects of the significant factors and interactions on the HRWRA demand (L/m^3). These figures demonstrate the single effect of each factor on the response (HRWRA demand L/m^3) while maintaining the values of the other two factors at the centre (A = 450 kg/m^3, B = 0.4, C = 12.5%). Furthermore, response surface diagrams for the HRWRA results are shown in Figures 4.7, 4.8, and 4.9. These figures show the effects of each couple of factors on the 3D surface of the respective response (HRWRA demand L/m^3). Moreover, these figures can be used to determine the optimum level of each factor based on the desired response values (maximize or minimize). It should be noted that these 3D surface figures are more useful in determining the optimum level of each factor when nonlinear relationships exist.

Table 4.3: ANOVA Table for HRWRA Response

Response	1	HRWRA Dose				
Transform:	Natural Log	Constant:		0		
ANOVA for Response Surface Reduced Quadratic Model						
Analysis of variance table [Partial sum of squares - Type III]						
Source	Sum of Squares	d_f	Mean Square	F-Value	P-Value (Prob. > F)	Significance
Model	4.09	6	0.68	42.33	< 0.0001	Significant
A-Binder Content	0.46	1	0.46	28.59	0.0001	Significant
B-W/B	1.94	1	1.94	120.26	< 0.0001	Significant
C-Replacement	1.26	1	1.26	78.55	< 0.0001	Significant
AC	0.08	1	0.08	4.80	0.0472	Significant
A^2	0.08	1	0.08	5.18	0.0405	Significant
B^2	0.29	1	0.29	18.14	0.0009	Significant
Residual	0.21	13	0.02			
Lack of Fit	0.18	8	0.02	4.43	0.0591	Not Significant
Pure Error	0.03	5	0.01			
Correlation Total	4.30	19				

d_f = Degrees of Freedom

4.2.1.1.1 Effect of Binder Content on the HRWRA Demand of HPSCC

Figure 4.3 presents the effects of the total binder content (kg/m^3) on the HRWRA demand (L/m^3). The figure shows the values of the HRWRA dose for different binder contents (420-480 kg/m^3) while having the other factors at the centre point (W/B = 0.4 and MK Replacement = 12.5%). The variations in the HRWRA dose are indicated as the solid line in Figure 4.3. This line may be either a straight one for linear responses or a curved one in the case of nonlinear responses. It is clear from the figure that the relation between the binder content and the HRWRA demand is almost nonlinear. As a result, a curved line was warranted for this case, which was also proved by having the factor A^2 significantly affecting the HRWRA demands (see Table 4.3). The figure also includes the results of the HRWRA dose for the six preselected centre points (circles at the centre denoted as design

points). Moreover, the dotted lines represent the 95% confidence band on the mean prediction at any given binder content. It is obvious from the graph that the increase of the binder content (from 420 to 480 kg/m^3) resulted in a reduction of the HRWRA demand by approximately 25%. However, this result is only valid at 12.5% MK replacement value owing to the significant interaction between the two factors A and C (AC). As a result, the effect of the binder content on the HRWRA demand is shown at different values of MK replacement in Figure 4.4.

It can be seen from the figure that the change in the HRWRA dose by increasing the total binder was different at each MK replacement. The bottom part of Figure 4.4 represents the effect of increasing the binder content (from 420 to 480 kg/m^3) at 5.1% MK replacement. From this part, the increase in the total binder content resulted in a reduction of the HRWRA by approximately 40%. The top part of Figure 4.4 includes the effect of increasing the binder content (from 420 to 480 kg/m^3) at 19.9% MK replacement. It can be noticed from this part that the reduction of the HRWRA demand is nearly 14%.

In general, it can be concluded that increasing the binder content in MK mixtures resulted in lower HRWRA demands (see Figures 4.3 and 4.4). This trend was reported by Khayat (2000) and his results were attributed to the reduction of the interparticle friction resulting from adding more fine materials into the SCC mixture. Another study conducted by Assaad et al. (2005) demonstrated that increasing the binder content can produce SCC having comparable slump flow diameters with lower HRWRA dosages.

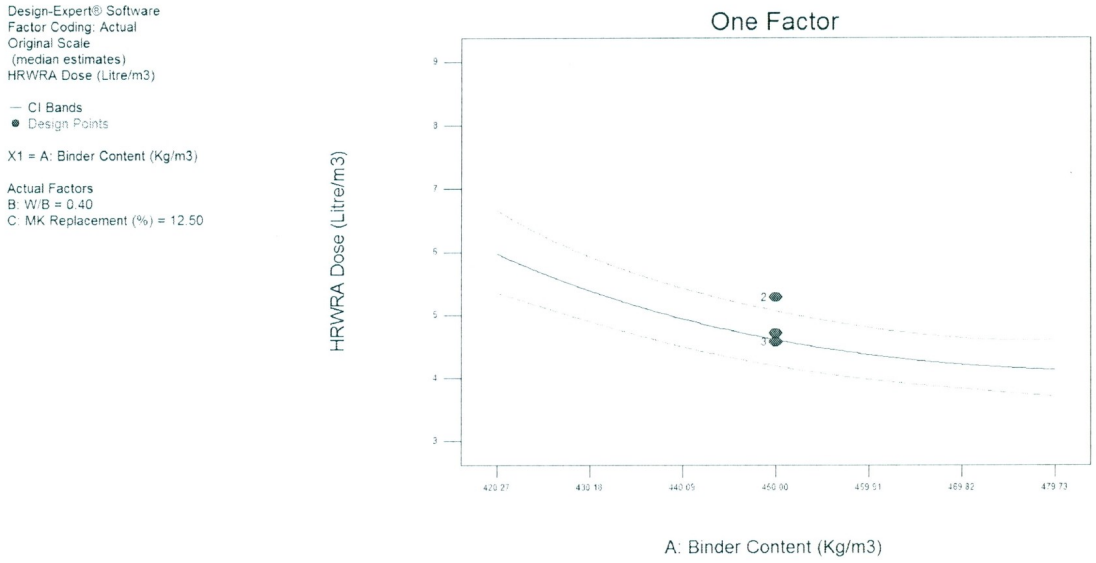

Figure 4.3: Effect of Binder Content (kg/m^3) on HRWRA Dose (L/m^3)

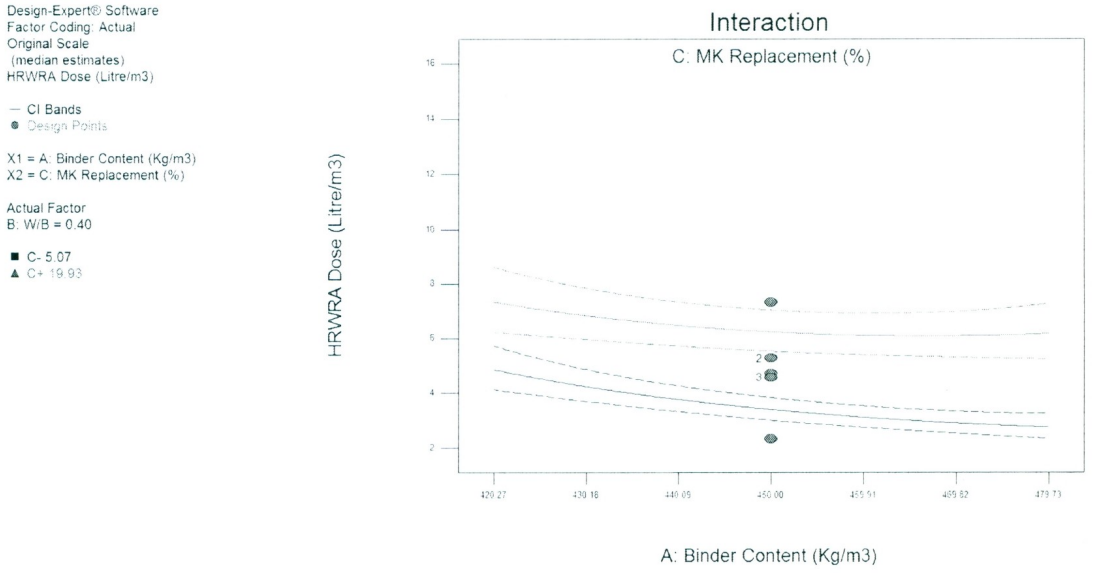

Figure 4.4: Effect of Interaction between Binder Content (kg/m^3) and MK Replacement (%) on HRWRA Dose (L/m^3)

4.2.1.1.2 Effect of Water-to-Binder Ratio on the HRWRA Demand of HPSCC

The effect of water-to-binder ratio on the HRWRA dose can be seen in Figure 4.5, which demonstrates a nonlinear relationship between the W/B and HRWRA dose. The figure

shows that increasing the W/B from 0.37 to 0.47 minimized the HRWRA dose by approximately 50%. This reduction was attributed to the enhanced workability of the mixtures with high W/B ratios > 0.4 compared to other mixtures. However, the HRWRA was needed to achieve the desired slump flow diameter in all tested mixtures. This result reflects that the water-to-binder ratio is the most significant factor affecting the HRWRA demand, as previously concluded from Table 4.3 (maximum F-value). This finding matches the results from the study performed by Felekoglu et al. (2006), which included testing a wide range of water-to-binder ratios (0.37 to 0.6) in proportioning SCC mixtures.

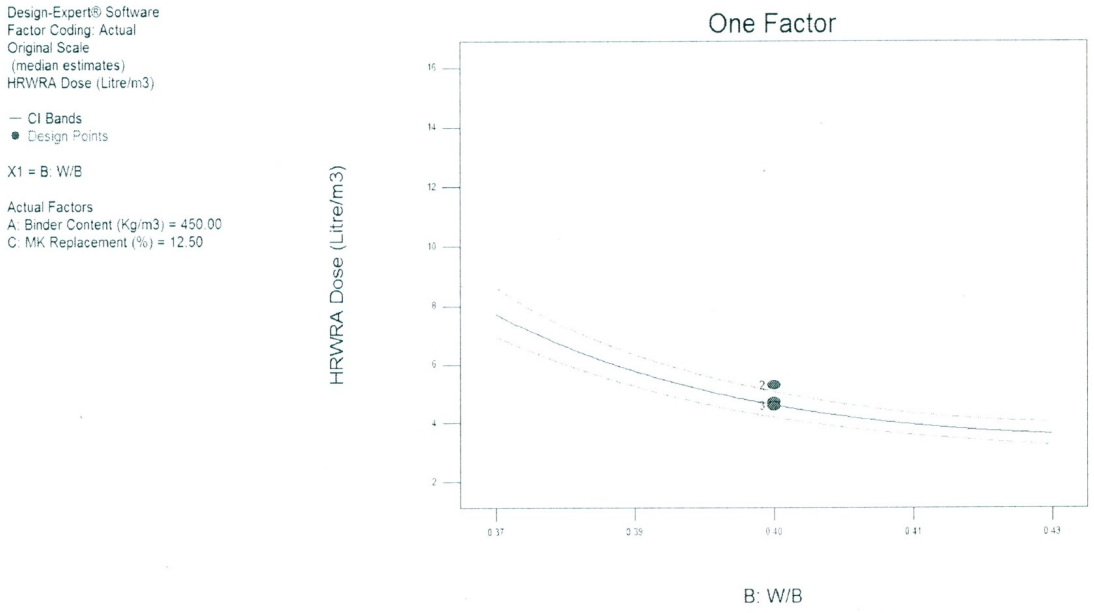

Figure 4.5: Effect of W/B Ratio on HRWRA Dose (L/m^3)

4.2.1.1.3 Effect of Metakaolin Replacement on the HRWRA Demand of HPSCC

The single effect of the MK replacement on the HRWRA demand is shown in Figure 4.6. From the figure, a linear relationship can be seen showing that the increase of the

replacement of MK yielded higher HRWRA demand. A percentage of increase in the HRWRA dose of about 40% can be noticed from the figure when increasing the MK percentage from 5.1 to 19.9%. This trend matched the results of other research accomplished by Hassan et al. (2012) and Madandoust et al. (2012), indicating that incorporating high replacements of MK required high amounts of HRWRA.

However, this linear relationship is valid only for a binder content of 450 kg/m^3 owing to the interaction effect of AC. The effect of MK replacement on the HRWRA is shown in Figure 4.7 involving two values of binder content. At a binder content of 420 kg/m^3 (top line of Figure 4.7), an increase of nearly 30% was warranted owing to the change in the MK replacement from 5 to 19.9%. At higher binder content (480 kg/m^3), higher increase in the HRWRA demand (50%) was obtained because of the increase of MK replacement from 5.1 to 19.9% (bottom line of Figure 4.7). It should be noted that this result was expected, since at high binder contents the amount of MK in the mixture was greater than that at low binder contents, which required higher doses of HRWRA.

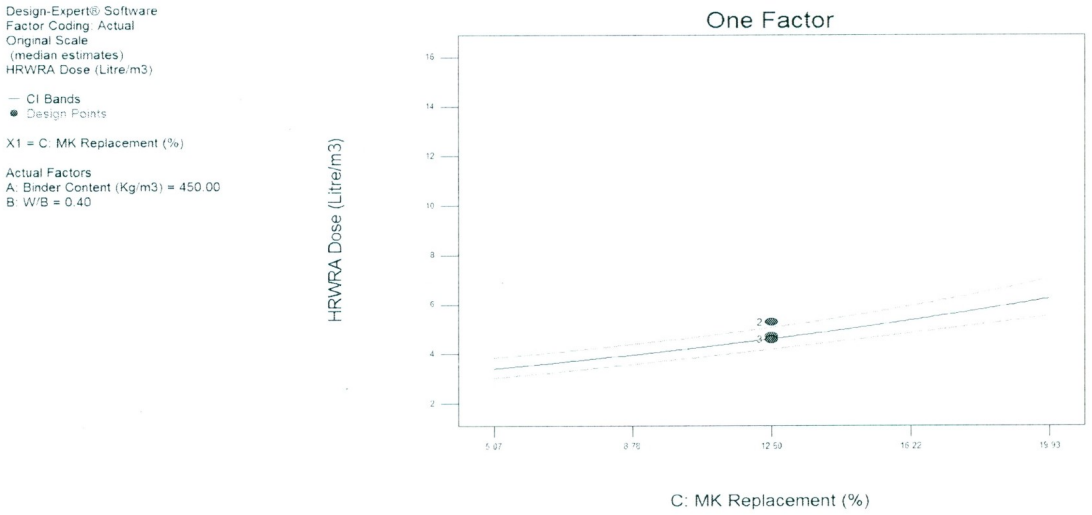

Figure 4.6: Effect of MK Replacement (%) on HRWRA Dose (L/m^3)

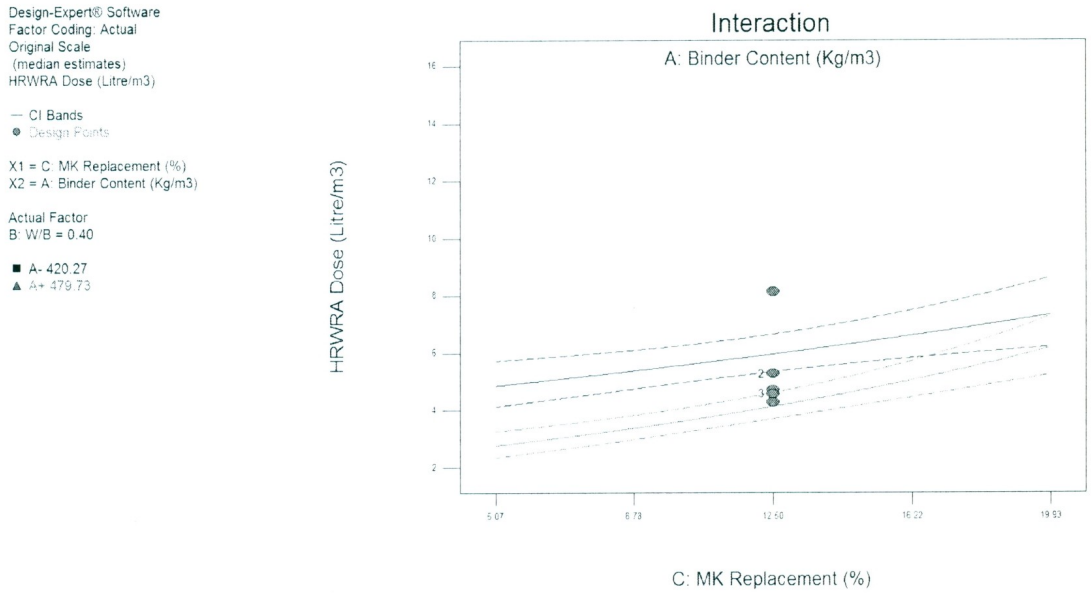

Figure 4.7: Effect of Interaction between Binder Content (kg/m^3) and MK Replacement (%) on HRWRA Dose (L/m^3)

The response surface of the HRWRA demand that relates the effects of total binder content and MK replacement is seen in Figure 4.8. This figure was produced by maintaining the third factor at the centre point (W/B = 0.4). From the figure, the minimum HRWRA can be obtained by setting the binder content at 480 (kg/m^3) and the MK replacement at 5.1%. The second response surface of the HRWRA demand includes the effects of total binder and water-to-binder ratio, shown in Figure 4.9. By assuming the MK replacement is 12.5%, the minimum HRWRA may be achieved by using a binder content of 480 (kg/m^3) and W/B of 0.43, as seen in Figure 4.9. Finally, the response surface of the HRWRA demand between the water-to-binder ratio and MK replacement is presented in Figure 4.10. A minimum HRWRA dose can be fulfilled by adding 5.1% MK replacement and water-to-binder ratio of 0.43, while keeping the total binder content at 450 (kg/m^3).

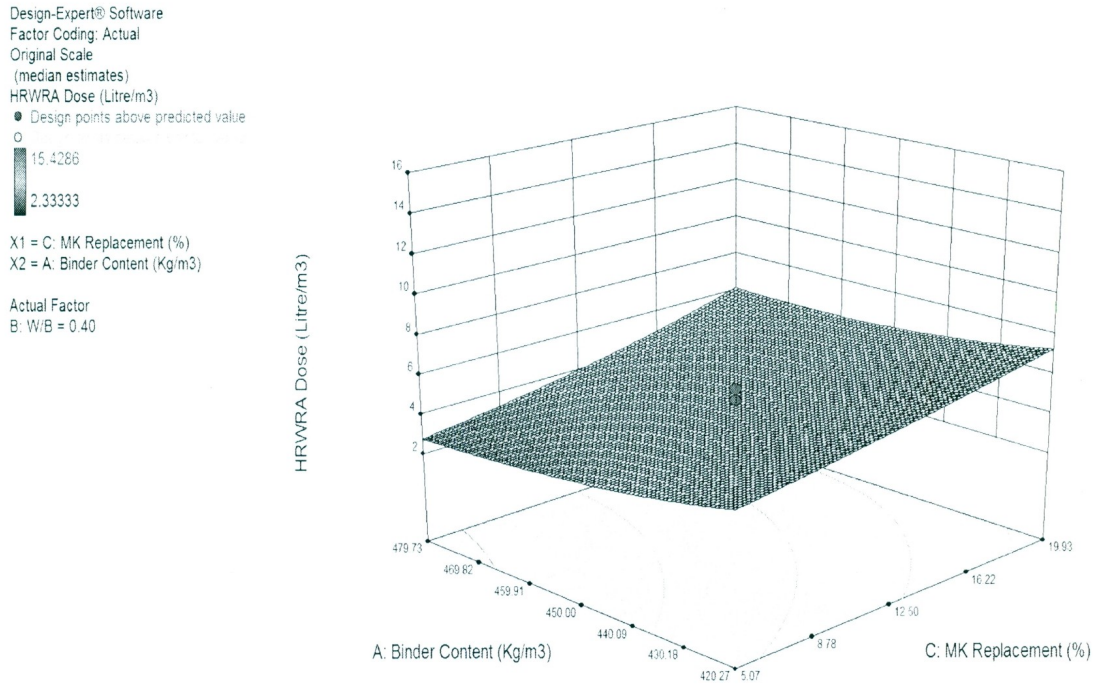

Figure 4.8: Response Surface of HRWRA Dose (L/m^3) versus Binder Content (kg/m^3) and MK Replacement (%)

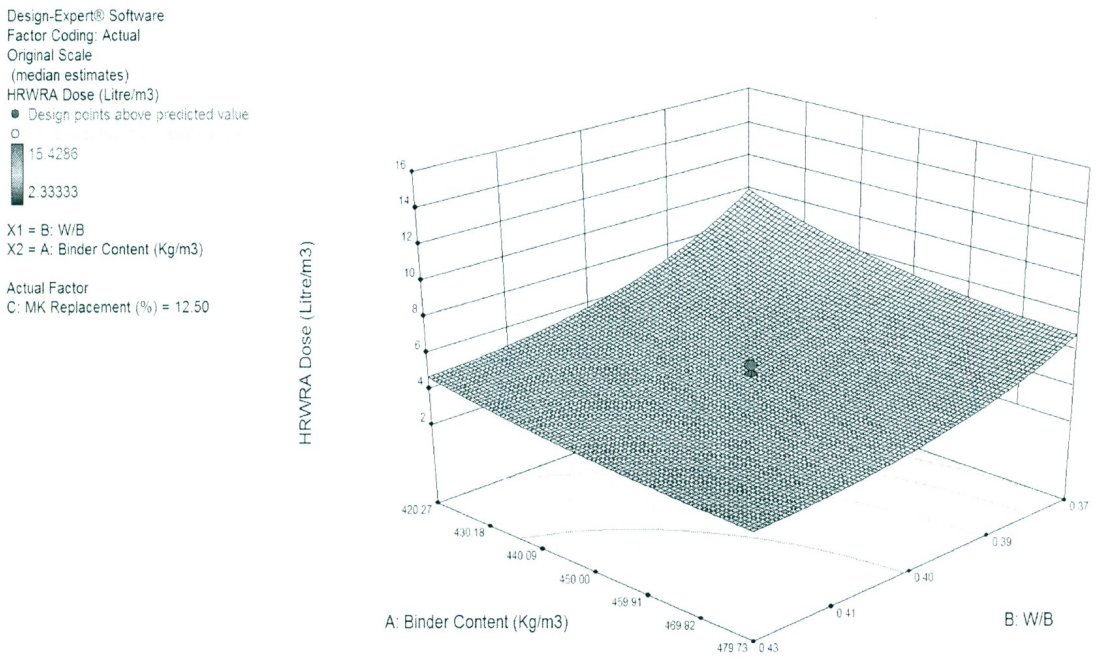

Figure 4.9: Response Surface of HRWRA Dose (L/m^3) versus Binder Content (kg/m^3) and W/B Ratio

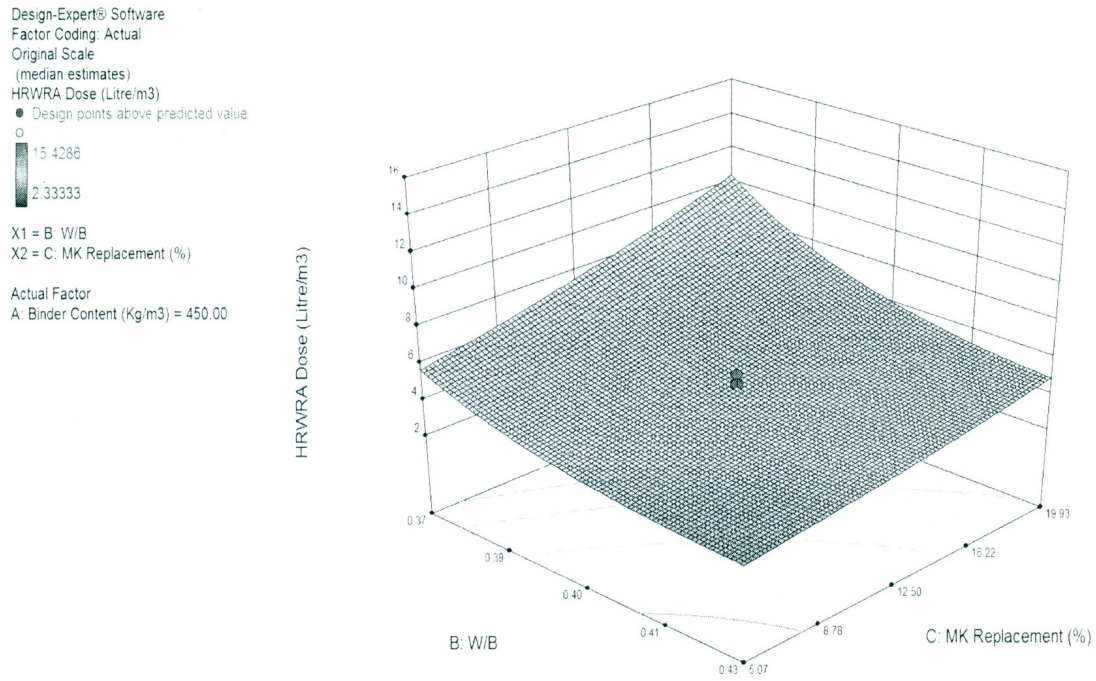

Figure 4.10: Response Surface of HRWRA Dose (L/m^3) versus W/B Ratio and MK Replacement (%)

It is clear from the figures that increasing the water-to-binder ratio, decreasing the percentage of MK, and the increase of the binder content resulted in a reduction of the HRWRA demand. These results matched the results from other studies performed for SCC containing SCM's (Lachemi et al. 2003; and Khayat et al. 2004). A statistical model was developed to predict the HRWRA dose under varying mixture proportions. The model relates the significant factors (B, C, A, B^2, A^2, and AC) together in Equation 4.1 in a logarithmic form to predict the dose of HRWRA (L/m^3) based on the mixture proportions, with an R^2 value of (0.95).

$$Ln\ HRWRA\ Dose\ (L/m^3) = 54.35 - 0.089\ x\ A - 140.898\ x\ B - 0.159\ x\ C + 0.00045\ x\ A\ x\ C + 0.000086\ x\ A^2 + 160.291\ x\ B^2 \quad \textbf{(4.1)}$$

4.2.1.2 Viscosity of HPSCC

The viscosity of the HPSCC mixtures is evaluated based on the results of the T_{500} and the V-funnel tests. The raw results and the derived models from each test are discussed below in detail:

4.2.1.2.1 T_{500} Results

As mentioned earlier, the slump flow diameter of the 20 mixtures was kept constant (650±50 mm) for all mixtures; however, the measured time to reach a diameter of 500 mm (T_{500}) was relatively different. This difference was expected owing to the different viscosity associated with each mixture related to its proportions. The maximum value of T_{500} was 9.5 seconds, and it was obtained in mixture number 1 (A = 420 kg/m^3, B = 0.37, and C = 19.9%). This high value of T_{500} reflected the highest viscosity, which was attributed to the low binder content, low water-to-binder ratio, and high replacement of MK. On the other hand, a minimum value of 1.5 seconds occurred in mixture number 13 (A = 480 kg/m^3, B = 0.43, and C = 5.1%), which demonstrated the minimum viscosity. These results revealed that the increase of the water-to-binder ratio, and/or binder content, and/or incorporating lower MK replacement decreased the viscosity of HPSCC (see Appendix C, Response 2-One Factor Effects). In addition, the results from the ANOVA (see Appendix C, Response 2-ANOVA Table) for the viscosity (T_{500}) indicated that the most significant factors affecting the mixture viscosity were A, B, and C, respectively (in order of significance). Using these factors, the model for calculating the viscosity was produced as shown in Equation 4.2 in the logarithmic form, with an R^2 value of (0.85).

$$Ln\,T_{500}\,(Sec) = 10.77 - 0.012\,x\,A - 11.14\,x\,B + 0.022\,x\,C \qquad \textbf{(4.2)}$$

4.2.1.2.2 V-Funnel Test Results

The V-funnel test was completed over the 20 mixtures primarily to measure the filling ability and viscosity of HPSCC. The test was performed initially and the amount of time for the concrete to flow out was recorded as initial V-funnel. After performing the ANOVA on the initial V-funnel test, the significant factors were found to be B, A, C, AC, and BC, respectively in order of significance (see Appendix C, Response 3-ANOVA Table). It should be noted that the effects of the three factors on the V-funnel test results were similar to those obtained from T_{500} tests. As a result, the increase of the water-to-binder ratio, total binder, and the decrease of the MK replacement also minimized the viscosity presented by the V-funnel test. Equation 4.3 shows the prediction model for the initial V-funnel time as a function of the significant factors ($R^2 = 0.94$).

$$Initial\ V-Funnel\ (Seconds) = 220.78 + 0.016\ x\ A - 528.66\ x\ B + 2.61\ x\ C - 0.0195\ x\ A\ x\ C + 16.69\ x\ B\ x\ C \quad (4.3)$$

4.2.1.2.3 Effect of Binder Content on the Viscosity of HPSCC

As mentioned earlier, the ANOVA results showed that the binder content has a significant effect on the HPSCC viscosity in both T_{500} and V-funnel tests. The increase in the binder content from 420 to 480 kg/m^3 yielded a drop in the viscosity (T_{500} time) by almost 45% (see Appendix C, Response 2-Effect of A). Moreover, this rise in the binder content showed to decrease the initial V-funnel time by approximately 43% (see Appendix C, Response 3-Effect of A). These results were attributed to the increase in the paste volume as a result of incorporating more binding materials. This reduction in the viscosity by increasing the binder content was also reported by Koeler et al. (2005). Gencel et al.

(2011) also found a reduction in the viscosity of SCC (V-funnel) by increasing the binder content from 470 to 570 kg/m^3.

4.2.1.2.4 Effect of Water-to-Binder Ratio on the Viscosity of HPSCC

The increase in the water-to-binder ratio also resulted in a decrease in the viscosity of HPSCC obtained by T_{500} and V-funnel tests. A drop in the V-funnel of nearly 55% was noticed after increasing the W/B ratio from 0.37 to 0.43 (see Appendix C, Response 3-Effect of B). In addition, this increase in the W/B ratio yielded a reduced viscosity (T_{500}) by almost 50% (see Appendix C, Response 2-Effect of B). Lachemi et al. (2003) also found that increasing the W/B ratio (0.35 to 0.45) led to lower flow times (viscosity) of SCC containing fly ash and slag. Moreover, Madandoust et al. (2012) observed a reduction of the viscosity (T_{500} and V-funnel times) of SCC containing MK when W/B ratio was increased from 0.32 to 0.45.

4.2.1.2.5 Effect of Metakaolin Replacement on the Viscosity of HPSCC

On the contrary, the replacement of MK showed to increase the viscosity of HPSCC based on results of T_{500} and V-funnel tests. By increasing the MK percentage from 5.1 to 19.9%, a 40% increase in the T_{500} time was observed (see Appendix C, Response 2-Effect of C). The initial V-funnel time also saw an increase of about 44% when the MK replacement changed from 5.1 to 19.9% (see Appendix C, Response 3-Effect of C). These results were expected from incorporating high replacement of MK, which resulted in an increase of the viscosity of HPSCC. The viscosity of SCC containing MK was studied by Hassan et al. (2012) and Madandoust et al. (2012) and a similar behaviour of MK was reported.

4.2.1.3 Passing Ability of HPSCC

The passing ability of the HPSCC mixtures can be expressed as a function of the difference between slump flow and J-ring diameter and/or L-box test. The test results and the prediction models from each test are presented below in detail:

4.2.1.3.1 Slump – J-Ring Results

The results from the J-ring test included the flow diameter and $T_{500}J$ time (see Table 4.2). The results demonstrated that the J-ring diameters were, in general, lower than the diameters of the slump flow. However, the mixture with the highest passing ability should have the minimum difference between the J-ring and slump flow diameters. The results showed that mixture number 5 (A = 480 kg/m^3, B = 0.43, and C = 19.9%) had the minimum difference (12 mm) between the two diameters. This result was expected, as the proportions of such mixture exhibited high water-to-binder ratio (0.43), high binder content (480 kg/m^3), and high percentage of MK (19.9%). The maximum difference (40 mm) was associated with mixture number 9, which had low water-to-binder ratio (0.37), low binder content (420 kg/m^3), and low replacement of MK (5.1%).

The prediction model for the J-ring diameter was developed by using the difference between the slump flow and J-ring diameters. The factors B, C and A (respectively in terms of significance) were found to be the most significant factors governing the passing ability of HPSCC (see Appendix C, Response 4-ANOVA Table). It was found that increasing the water-to-binder ratio, dosage of MK, and/or total binder content enhanced the passing ability of HPSCC. The model given in Equation 4.4 represents the difference between the slump flow and J-ring diameters ($R^2 = 0.8$).

$$Slump - JRing\ Diameter\ (mm) = 167.67 - 0.094\ x\ A - 230.51\ x\ B - 0.551\ x\ C \qquad (4.4)$$

4.2.1.3.2 L-Box Test Results

The passing ability was also tested by the L-box test in which the ratio between the heights before and after the obstructing bars was measured (H2/H1). The same trend from the J-ring test was detected when analyzing the results from the L-box test (Table 4.2). It is clear from Table 4.2 that the mixture with the minimum difference between J-ring and slump flow (number 5) exhibited the maximum ratio of 0.93 in the L-box test. Similarly, the mixture with the maximum difference between J-ring and slump flow (number 9) had the minimum ratio of L-box test (0.45). The prediction model for the L-box test is described in Equation 4.5 with the significant factors B, C, and A affecting the L-box ratio (R^2 = 0.86). In this model, the factor B (W/B ratio) was the most significant factor, followed by C (MK %), and finally (factor C) the binder content (see Appendix C, Response 5-ANOVA Table).

$$H2/H1 = -1.353 + 0.00164\ \ x\ A + 2.818\ x\ B + 0.0121\ x\ C \qquad (4.5)$$

4.2.1.3.3 Effect of Binder Content on the Passing Ability of HPSCC

The results from slump flow, J-ring, and L-box tests showed an enhancement in the passing ability of the HPSCC mixtures by increasing the binder content (A). For instance, the difference between the slump flow and J-ring diameters was decreased by around 17% (indicating better passing ability) by increasing the binder content from 420 to 480 kg/m^3 (see Appendix C, Response 4-Effect of A). In addition, the L-box ratio exhibited an increase of approximately 17% when the binder content was increased from 420 to 480 kg/m^3 (see Appendix C, Response 5-Effect of A). These results indicated a significant

improvement in the passing ability (high L-box ratio and low difference between slump and J-ring) by incorporating higher binder contents. This trend was also reported in similar studies on the fresh properties of SCC (Assaad et al. 2005; Koehler 2007; and Nanthagopalan et al. 2009).

4.2.1.3.4 Effect of Water-to-Binder Ratio on the Passing Ability of HPSCC

As mentioned previously, the water-to-binder ratio was considered the most significant factor affecting the passing ability of HPSCC mixture. The difference between the slump and J-ring diameters was minimized by approximately 40% when the water-to-binder ratio was changed from 0.37 to 0.43 (see Appendix C, Response 4-Effect of B). This increase in the water-to-binder ratio also resulted in a rise of the L-box ratio by nearly 30%, which reflected a notable improvement in the passing ability of HPSCC mixtures (see Appendix C, Response 5-Effect of B). Similar results were obtained in a study conducted by Madandoust et al. (2012) on SCC containing MK when the W/B ratio was increased from 0.32 to 0.45.

4.2.1.3.5 Effect of Metakaolin Replacement on the Passing Ability of HPSCC

The MK replacement (factor C) came in second place in order of significance for the effect it had on the passing ability of HPSCC mixture. When the MK percentage was increased from 5.1 to 19.9%, the passing ability of the mixture was improved. For example, a reduction of 25% was found in the difference between slump and J-ring diameters as a result of increasing the percentage of MK from 5.1 to 19.9% (see Appendix C, Response 4-Effect of C). Accordingly, the L-box ratio was increased by approximately 33% owing to this rise in the MK replacement (see Appendix C, Response

5-Effect of C). This result was expected because of the high viscosity provided by MK, which maximized the mixture's passing ability (Hassan et al. 2012).

4.2.1.4 Flowing Ability of HPSCC

The J-ring test also included measuring the time to reach a 500 mm diameter through the ring ($T_{500}J$). This test examined the flow time after passing the obstructing J-ring bars, which may be used to indicate the flowing ability of the HPSCC mixture. The most significant factors governing the value of this test were found to be A, B, and C, respectively in order of importance (see Appendix C, Response 6-ANOVA Table). The change in these factors (A, B, and C) showed a similar effect on the $T_{500}J$ to that on the values of the T_{500} test. The prediction model obtained from this test is shown in Equation 4.6 in a logarithmic form ($R^2 = 0.89$).

It should be mentioned that all values of $T_{500}J$ were higher than the values of T_{500} without the ring, as expected. This difference existed because of the obstructing bars of the J-ring, which affected the flowing ability of the mixture. In the mixtures with high flowing ability (for example, number 13), the difference between T_{500} and $T_{500}J$ was not significant (1.5 seconds for T_{500} versus 2.3 seconds for $T_{500}J$). Meanwhile, the mixtures with low flowing ability exhibited higher difference between T_{500} and $T_{500}J$. For example, in mixture number 1 (A = 420 kg/m^3, B = 0.37, and C = 19.9%) the value of $T_{500}J$ was 13.5 seconds, significantly higher than that of T_{500} (9.5 seconds).

$$Ln\,T_{500}J\ (Seconds) = 11.14 - 0.012\ x\ A - 11.023\ x\ B + 0.015\ x\ C \qquad \textbf{(4.6)}$$

4.2.1.4.1 Effect of Binder Content on the Flowing Ability of HPSCC

As previously discussed, the binder content was the most significant factor affecting the $T_{500}J$ time (flowing ability of HPSCC). It can be noticed that an increase in the flowing ability (lower $T_{500}J$ times) of nearly 50% occurred as a result of increasing the binder content from 420 to 480 kg/m^3 (see Appendix C, Response 6-Effect of A). This result may be attributed to the decrease in the viscosity and the increase in the passing ability owing to incorporating higher volumes of fine materials.

4.2.1.4.2 Effect of Water-to-Binder Ratio on the Flowing Ability of HPSCC

The water-to-binder ratio was ranked as the second significant factor affecting the flowing ability of the HPSCC mixtures. A reduction in the $T_{500}J$ time (approximately 45%) was reported when the water-to-binder ratio increased from 0.37 to 0.43 (see Appendix C, Response 6-Effect of B). This result reflected the expected improvement in the flowing ability of SCC mixtures by increasing the water-to-binder ratio (Khayat et al. 2002).

4.2.1.4.3 Effect of Metakaolin Replacement on the Flowing Ability of HPSCC

The MK replacement showed a counter effect on the $T_{500}J$ time (flowing ability of HPSCC). As a result, the increase of MK replacement (5.1 to 19.9%) showed to increase the $T_{500}J$ time (flowing ability of HPSCC) by nearly 25% (see Appendix C, Response 6-Effect of C). This result can be attributed to the high viscosity associated with SCC mixtures incorporating MK as partial replacements. This finding was also reported in the study performed by Hassan et al. (2012), showing that the addition of MK reduced the flowing ability of SCC mixtures. It should be noted that the addition of HRWRA may

also have an effect on the flowing ability of HPSCC mixtures. However, the effect of HRWRA dose on the flowing ability was not studied in this investigation.

4.2.1.5 Segregation of HPSCC

The V-funnel test was repeated by filling the funnel and leaving the concrete to settle for five minutes. After this period, the time required for the concrete to empty out was then measured (final V-funnel). The purpose of repeating the test was to check if the mixture exhibited any segregation and to study the thixotropy of the mixture. The segregation could have occurred because of settling of the coarse aggregate towards the bottom. Using the initial and final V-funnel times, the segregation factor was calculated by substituting in Equation 3.2 (see section 3.3.2.3). The results of the segregation factor are shown in Table 4.2.

It is clear from the values of both initial and final V-funnel times that the final times were higher than the initial times, as expected. The difference between the initial and final times ranged between 1 to 53 seconds, present in mixtures number 13 (A = 480 kg/m^3, B = 0.43, and C = 5.1%) and 9 (A = 420 kg/m^3, B = 0.37, and C = 5.1%), respectively. The values of the segregation factor ranged between 0.2 (in mixture number 5) and 1.47 (in mixture number 9). According to these results, the segregation factor can be minimized by maintaining higher water-to-binder ratio, binder content, and percentage of MK. It should be noted that this factor may also depend on the HRWRA dosage. Higher HRWRA dosage may affect the mixture thixotropy, which could influence the difference between the initial and final V-funnel times. However, the chemical composition of the HRWRA plays a significant role in this effect. For the final V-funnel test, the significant

factors were B, A, BC, and C, respectively in order of significance (see Appendix C, Response 7-ANOVA Table). Factors B, A, C, B^2, A^2, AC, and C^2 were found to significantly govern the segregation factor, respectively (see Appendix C, Response 8-ANOVA Table). Equations 4.7 and 4.8 show the prediction models for the final V-funnel time and segregation factor in a logarithmic form ($R^2 = 0.92$; $R^2 = 0.97$, respectively).

$$Final\ V-Funnel\ (Sec) = 707.58 - 0.47\ x\ A - 1154.67\ x\ B - 16.67\ x\ C + 42.09\ x\ B\ x\ C \quad (4.7)$$

$$Ln\ S_f = -44.61 + 0.111\ x\ A + 126.6\ x\ B - 0.25\ x\ C + 0.00041\ x\ A\ x\ C - 0.00014\ x\ A^2 - 172.31\ x\ B^2 + 0.0012\ x\ C^2 \quad (4.8)$$

4.2.1.5.1 Effect of Binder Content on the Segregation of HPSCC

The binder content was found as one of the significant factors affecting the segregation factor of the HPSCC mixtures. Increasing the total binder content (from 420 to 480 kg/m^3) showed a reduction in the segregation factor by approximately 33%, which indicated an enhancement in the segregation resistance (see Appendix C, Response 8-Effect of A). This enhancement of the segregation resistance was attributed to the increase in the total binding materials and was also reported in other similar studies (Su et al. 2001).

4.2.1.5.2 Effect of Water-to-Binder Ratio on the Segregation of HPSCC

The water-to-binder ratio was considered the most significant factor affecting the segregation factor of the HPSCC mixtures. The increase in the water-to-binder ratio from 0.37 to 0.43 was found to decrease the required amounts of HRWRA, as previously discussed. This low percentage of HRWRA eventually yielded a notable reduction in the

segregation factor (about 50%). However, the range of the study did not include high water-to-binder ratios (> 0.45) and/or different HRWRA types, which may show differences in the segregation factor results. Increasing the water-to-binder ratios above 0.5 may result in excessive bleeding and segregation of the mixture.

4.2.1.5.3 Effect of Metakaolin Replacement on the Segregation of HPSCC

The MK replacement percentage is also considered a significant factor affecting the segregation factor of the HPSCC mixtures. The increase of the MK replacement from 5.1 to 19.9% resulted in a reduction in the segregation factor of approximately 35% (see Appendix C, Response 8-Effect of C). This result could be attributed to the increased passing ability of the mixtures containing high replacement of MK. The increased passing ability reduced the opportunity for the coarse aggregate to separate from the paste matrix and allowed the paste to efficiently carry the coarse aggregate, which minimized the risk of segregation (Zhu et al. 2003).

4.2.1.6 Air Content of HPSCC

The air content test was implemented for the 20 mixtures and the results yielded a range of 0.9 to 3.3%, as shown in Table 4.2. It should be noted that no air entrainment agent was added in the mixtures and the measured air content represented the trapped air. The model to evaluate the air content of HPSCC mixtures is shown in Equation 4.9 ($R^2 = 0.7$). The ANOVA showed that the significant factors governing the amount of the trapped air were AB and BC, respectively in order of significance (see Appendix C, Response 9-ANOVA Table). It should be noted that the three studied factors (A, B, and C) were

considered not significant (had P-value > 0.05); however, these factors were included in the model owing to the significant effects of their interactions (AB and BC).

$$Air\ Content\ (\%) = 90.85 - 0.184\ x\ A - 226.24\ x\ B - 0.717\ x\ C + 0.47\ x\ A\ x\ B + 1.81\ x\ B\ x\ C \quad (4.9)$$

4.2.2 Mechanical and Durability Properties of HPSCC

The compressive strength at 28 days, chloride permeability (RCPT and chloride diffusion) at 28 days, and RCPT at 90 and 180 days were reported for the 20 mixtures, as shown in Table 4.4, both for air and water curing.

Table 4.4: Mechanical and Durability Properties of HPSCC Mixtures

Mix. No.	28-Days f_c' (MPa)		28-Days RCPT (Coulombs)		90-Days RCPT (Coulombs)		180-Days RCPT (Coulombs)		28-Days D_a (m^2/sec)	
	Air	Water	Air	Water	Air	Water	Air	Water	Air	Water
1	70.3	74.8	329	293	258	210	209	169	1.01E-12	8.90E-13
2	73.5	74.0	1156	1132	1091	1044	939	894	4.24E-12	4.01E-12
3	74.1	76.5	400	341	367	315	326	290	1.82E-12	1.04E-12
4	75.8	77.8	390	365	358	335	325	302	1.65E-12	1.11E-12
5	64.1	72.5	571	288	470	247	402	221	2.37E-12	7.77E-13
6	62.0	67.3	760	439	704	398	673	376	3.57E-12	2.22E-12
7	77.7	78.3	361	329	346	315	300	272	1.25E-12	9.97E-13
8	60.9	62.1	542	356	482	327	394	275	2.29E-12	1.15E-12
9	51.1	54.1	2066	1518	1627	1188	1480	1081	6.05E-12	5.26E-12
10	72.8	79.9	451	315	277	193	226	157	2.24E-12	9.54E-13
11	62.6	68.9	678	345	462	232	402	197	2.76E-12	1.06E-12
12	73.6	79.1	412	367	371	332	335	300	2.05E-12	1.07E-12
13	54.8	61.1	1948	1319	1832	1228	1628	1105	5.74E-12	4.57E-12
14	49.3	58.1	2649	1597	2395	1441	2124	1293	6.97E-12	5.38E-12
15	70.9	77.8	407	373	365	334	324	295	1.98E-12	1.13E-12
16	73.1	80.2	405	327	360	290	318	257	1.85E-12	9.97E-13
17	78.6	82.3	280	240	218	187	185	159	5.50E-13	4.22E-13
18	78.2	82.2	388	351	326	294	305	276	1.58E-12	8.69E-13
19	75.9	81.9	397	347	352	307	295	259	1.79E-12	1.08E-12
20	55.3	57.0	3987	3739	3173	2842	2446	2024	8.43E-12	7.29E-12

4.2.2.1 28-Days Compressive Strength of HPSCC

An ANOVA analysis was completed similarly for both results from air and water curing to select the most significant factors affecting the 28-days compressive strength. The significant factors were found to be C, B, A, C^2, A^2, B^2, and AB, respectively in order of significance (see Appendix C, Responses 10 and 11-ANOVA Tables). In addition, the associated models were developed in Equations 4.10 and 4.11 (R^2 = 0.92; R^2 = 0.94, respectively). It is clear from the equations that both models are based on the same variables representing the same trend. However, as seen in Table 4.4, the results of water-curing samples exhibited higher values than air-curing counterparts, as expected. The maximum strength was obtained from mixture number 17 (A = 480 kg/m^3, B = 0.37, and C = 19.9%) in both air- and water-cured samples; while the minimum was associated with mixture number 9 (A = 420 kg/m^3, B = 0.37, and C = 5.1%), as seen in Table 4.4. This result was attributed to the high binder content, high replacement of MK, and the low water-to-binder ratio included in the mixture (number 17).

$$28-Days\ f_c'(Air\ Curing) = -1556.48 + 4.03\ x\ A + 3493.7\ x\ B + 2.75\ x\ C - 3.36\ x\ A\ x\ B - 0.003\ x\ A^2 - 2687.76\ x\ B^2 - 0.08\ x\ C^2\ (MPa) \quad \textbf{(4.10)}$$

$$28-Days\ f_c'(Water\ Curing) = -1648.77 + 4.29\ x\ A + 3610.22\ x\ B + 2.78\ x\ C - 2.94\ x\ A\ x\ B - 0.003\ x\ A^2 - 2994.08\ x\ B^2 - 0.08\ x\ C^2\ (MPa) \quad \textbf{(4.11)}$$

4.2.2.1.1 Effect of Binder Content on the Compressive Strength of HPSCC

The binder content was increased from 420 to 480 kg/m^3 in both air- and water-cured samples. This increase resulted in approximately 10% higher compressive strength of air-cured samples (see Appendix C, Response 10-Effect of A). In addition, the compressive strength of water-cured samples was increased by nearly 12.5% by increasing the binder

content (see Appendix C, Response 11-Effect of A). These results were expected from increasing the total cementing material in the mixture and matched the results from other investigations (Lachemi et al. 2003; and Patel et al. 2004).

4.2.2.1.2 Effect of Water-to-Binder Ratio on the Compressive Strength of HPSCC

The water-to-binder ratio exhibited a slightly higher effect on the results of compressive strength, as previously mentioned. The results showed that increasing the water-to-binder ratio from 0.37 to 0.43 yielded a drop in the compressive strength. For instance, the compressive strength of air-cured samples reduced by roughly 15% as a result of this increase of water-to-binder ratio (see Appendix C, Response 11-Effect of B). Moreover, approximately the same strength reduction rate (15%) was observed from water-cured samples because of this increase in water-to-binder ratio (see Appendix C, Response 11-Effect of B). These trends are attributed to the reduction in the hydration process (chemical reactions of cement) and the formation of large capillary pores as the water content in the mixture increases (Mehta et al. 1993).

4.2.2.1.3 Effect of Metakaolin Replacement on the Compressive Strength of HPSCC

The MK replacement showed the most significant effect on the compressive strength of both air- and water-cured samples. When the MK replacement increased from 5.1 to 19.9%, the strength of both air- and water-cured samples increased by nearly 20% (see Appendix C, Responses 10 and 11-Effect of C). It should be noted that further increase in the MK replacement (> 20%) resulted in no improvement in the compressive strength. This result revealed that the optimum replacement of MK was 20%, which was reported in the study conducted by Hassan et al. (2012).

4.2.2.1.4 Effect of Curing on the Compressive Strength of HPSCC

The results of the compressive strength for both air- and water-cured samples are plotted in Figure 4.11 for all HPSCC mixtures. The compressive strength of water-cured samples was slightly higher than their air-cured counterparts. The difference of the compressive strengths between the water- and air-cured samples was not significant in almost all mixtures, except for mixtures number 5, 6, 11, 13, and 14. This relatively high difference was attributed to the high water-to-binder ratio (> 0.4) present in these mixtures. In general, the results showed that by using high MK replacement, low water-to-binder ratio, and high binder content the compressive strength can be maximized in both air- and water-curing samples.

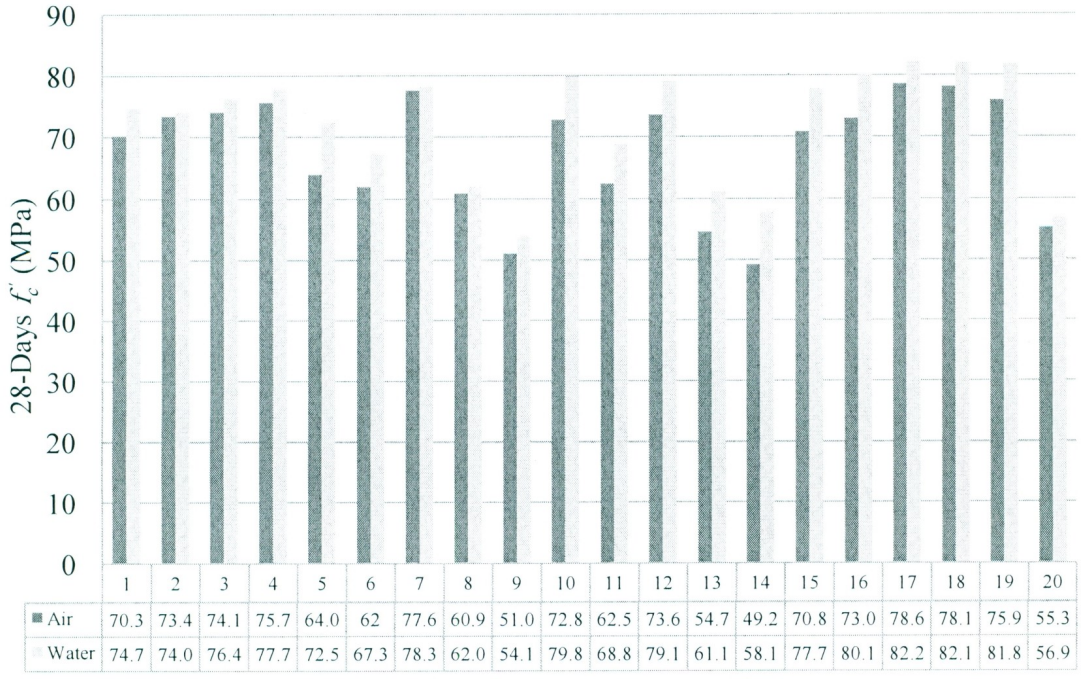

	1	2	3	4	5	6	7	8	9	10	11	12	13	14	15	16	17	18	19	20
Air	70.3	73.4	74.1	75.7	64.0	62	77.6	60.9	51.0	72.8	62.5	73.6	54.7	49.2	70.8	73.0	78.6	78.1	75.9	55.3
Water	74.7	74.0	76.4	77.7	72.5	67.3	78.3	62.0	54.1	79.8	68.8	79.1	61.1	58.1	77.7	80.1	82.2	82.1	81.8	56.9

Figure 4.11: 28-Days Compressive Strength of HPSCC Mixtures

4.2.2.2 28-Days RCPT of HPSCC

Following the same analysis procedure, the prediction models for chloride permeability at 28 days were obtained in the logarithmic form of the total charge passed in the RCPT. The model in Equation 4.12 predicts the chloride permeability of air-curing samples. In this model, the most important variables were C, C^2, B, B^2, A, and A^2 (respectively in order of significance), with $R^2 = 0.97$. Alternatively, the model for water-curing samples included only C, C^2, B, A as the most significant factors, respectively, with ($R^2 = 0.98$), as seen in Equation 4.13 (see Appendix C, Responses 12 and 13-ANOVA Tables). It is obvious from Table 4.4 that minimum chloride permeability was obtained from mixture number 17 (A = 480 kg/m^3, B = 0.37, and C = 19.9%), which had the maximum compressive strength. On the contrary, the maximum permeability was related to mixture number 20 (A = 450 kg/m^3, B = 0.4, and C = 0), which had no MK (0%). This result manifests the effect of MK in reducing the chloride permeability of HPSCC.

$$Ln\ 28-Days\ RCPT\ (Air\ Curing) = 55.75 - 0.104\ x\ A - 122.66\ x\ B - 0.31\ x\ C + 0.000111\ x\ A^2 + 163.98\ x\ B^2 + 0.0086\ x\ C^2 \quad (Coulombs) \qquad (4.12)$$

$$Ln\ 28-Days\ RCPT\ (Water\ Curing) = 8.37 - 0.0022\ x\ A + 2.55\ x\ B - 0.294\ x\ C + 0.0076\ x\ C^2 \quad (Coulombs) \qquad (4.13)$$

4.2.2.2.1 Effect of Binder Content on the 28-Days RCPT of HPSCC

The increase in the binder content from 420 to 480 kg/m^3 resulted in a 20% reduction of the 28-days RCPT reading (indicating a lower chloride permeability) of air-cured samples (see Appendix C, Response 12-Effect of A). This reduction was expected from increasing the total binder material in the mixture, which resulted in more hydration product to fill the gaps in the concrete microstructure and eventually decreased the concrete

permeability (Mehta 1981). However, the increase of the binder content did not show a significant effect on the 28-days RCPT of the water-cured samples (see Appendix C, Response 13-Effect of A). This result may be attributed to the enhanced microstructure of the water-cured samples compared to the air-cured samples.

4.2.2.2.2 Effect of Water-to-Binder Ratio on the 28-Days RCPT of HPSCC

Increasing the water-to-binder ratio from 0.37 to 0.43 showed a counter effect on the chloride permeability of HPSCC. This increase yielded a relatively high increase in the 28-days RCPT (approximately 50%) in the air-cured samples (see Appendix C, Response 12-Effect of B). On the other hand, the water-cured samples exhibited little increase in the 28-days RCPT as a result of higher water-to-binder ratios (see Appendix C, Response 13-Effect of B). It should be noted that using relatively high water-to-binder ratios resulted in increasing the capillary pores, which led to higher permeability of the concrete (Larbi 1993). These results also matched other studies on the chloride permeability of SCC (Patel et al. 2004).

4.2.2.2.3 Effect of Metakaolin Replacement on the 28-Days RCPT of HPSCC

As mentioned earlier, the MK replacement was seen as the most significant factor affecting the 28-days RCPT of HPSCC mixtures. As the MK percentage increased from 5.1 to 19.9%, the 28-days RCPT results were significantly decreased (approximately 75%) in both air- and water-cured samples (see Appendix C, Responses 12 and 13-Effect of C). These results indicated the superior effect of MK in minimizing the chloride permeability of HPSCC regardless of the curing type. It should be noted that the addition

of higher replacements of MK (> 20%) showed higher RCPT values; as a result, the 20% of MK replacement was deemed the optimum percentage (Hassan et al. 2012).

4.2.2.2.4 Effect of Curing on the 28-Days RCPT of HPSCC

The results of the RCPT test indicate that the chloride permeability is low when the total passed charge in coulombs is low. Figure 4.12 indicates that an identical trend was obtained from the chloride permeability of both air- and water-cured samples. In the chart, the water-cured samples showed lower permeability than air-cured ones throughout the 20 mixtures. In addition, the significant difference between water- and air-cured results was also obvious within the same mixtures that exhibited a noticeable difference in the 28-days compressive strength (5, 6, 11, 13 and 14). This difference indicated that water curing is a significant factor affecting the strength and permeability of HPSCC, especially when higher water-to-binder ratios are used (> 0.4).

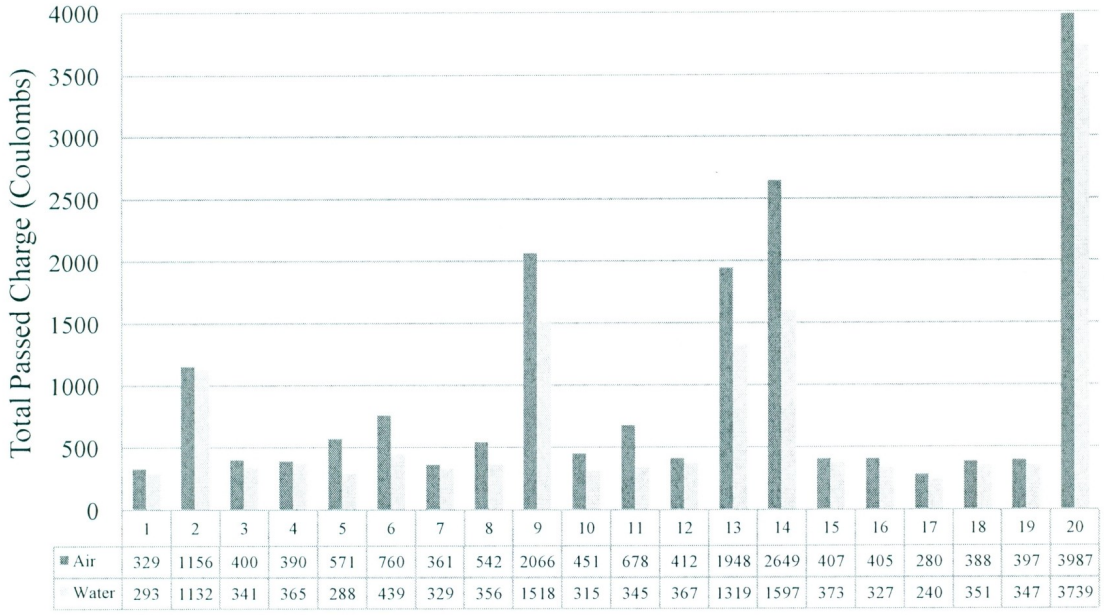

	1	2	3	4	5	6	7	8	9	10	11	12	13	14	15	16	17	18	19	20
Air	329	1156	400	390	571	760	361	542	2066	451	678	412	1948	2649	407	405	280	388	397	3987
Water	293	1132	341	365	288	439	329	356	1518	315	345	367	1319	1597	373	327	240	351	347	3739

Figure 4.12: 28-Days RCPT of HPSCC Mixtures

4.2.2.3 Effect of Curing Time on the RCPT of HPSCC

The RCPT test was replicated for the 20 mixtures at this stage on 90 and 180 days for both air- and water-cured samples. The results from the 90 and 180-days tests are shown and compared to the 28-days counterparts, as seen in Figure 4.13. It is clear from the figure that all mixtures exhibited a significant decrease in the RCPT values from 28 days to 180 days, as expected. These results were attributed to the effect of the hydration process during the curing period, which decreased the permeability of the concrete (Mehta 1981; Larbi 1993).

Although the 20 mixtures had an almost identical trend of decline of permeability versus time, different percentages of reduction based on the mixture proportions were warranted for each mixture. These percentages of change are represented by the factor called a diffusion decay index (m). This coefficient is an important property of the concrete as it is used in the service life prediction models; for example, the model presented in the Life365 software (Bentz et al. 2012). These models consider using this coefficient to represent the change in the chloride permeability over time (Boddy et al. 1999; Gjørv 2002; Ehlen et al. 2009). The coefficient m was found to be affected by the mixture proportions, including binder content, water-to-binder ratio, and incorporating SCM's (Boddy et al. 2001; Nokken et al. 2006).

Based on the assumption that the change in the RCPT values is almost linear with the curing time in the logarithmic scales (Figures 4.14 and 4.15), the factor m was calculated as shown in Table 4.5. The factor m was calculated for the 20 mixtures using Equation 4.14 (Boddy et al. 2001; Nokken et al. 2006; Zeljkovic 2009) for both air- and water-cured samples. The values of the m coefficient ranged between 0.065 and 0.374. The

absolute minimum and maximum values were obtained from mixtures number 6 (A = 450 kg/m^3, B = 0.45, and C = 12.5%) and 10 (A = 450 kg/m^3, B = 0.4, and C = 25%), respectively. Minimum values of 0.065 and 0.083 were obtained from the mixture number 6 when cured in air and water, respectively. These values may be attributed to the highest water-to-binder ratio used in this mixture (0.45). However, mixture number 7 (A = 450 kg/m^3, B = 0.35, and C = 12.5%) had the minimum water-to-binder ratio (0.35) and the values of m were also low (0.099 and 0.102). These results may be associated with to the nonlinear effect of the water-to-binder ratio on m values. The maximum m values were 0.371 and 0.374 and were associated to mixture number 10 in air- and water-cured samples, respectively. These maximum m values were warranted owing to the highest replacement level used in this mixture (25%). It should be noted that mixture number 20 (A = 450 kg/m^3, B = 0.4, and C = 25%) had the same binder content and water-to-binder ratio as number 10 but did not contain MK. As a result, this mixture (20) had lower m values than number 10 (0.263 versus 0.371). These trends were also found to be present in a study performed by Zeljkovic (2009) on normal concrete containing MK.

$$RCPT = RCPT_{ref} \; x \left(\frac{T_{ref}}{T}\right)^m \qquad \textbf{(4.14)}$$

Where:

$RCPT$ = The RCPT Reading at any time T,

T = Target Time of Prediction,

$RCPT_{ref}$ = RCPT at the Time T_{ref}, and

T_{ref} = Time at which RCPT Reading is Known (28-Days).

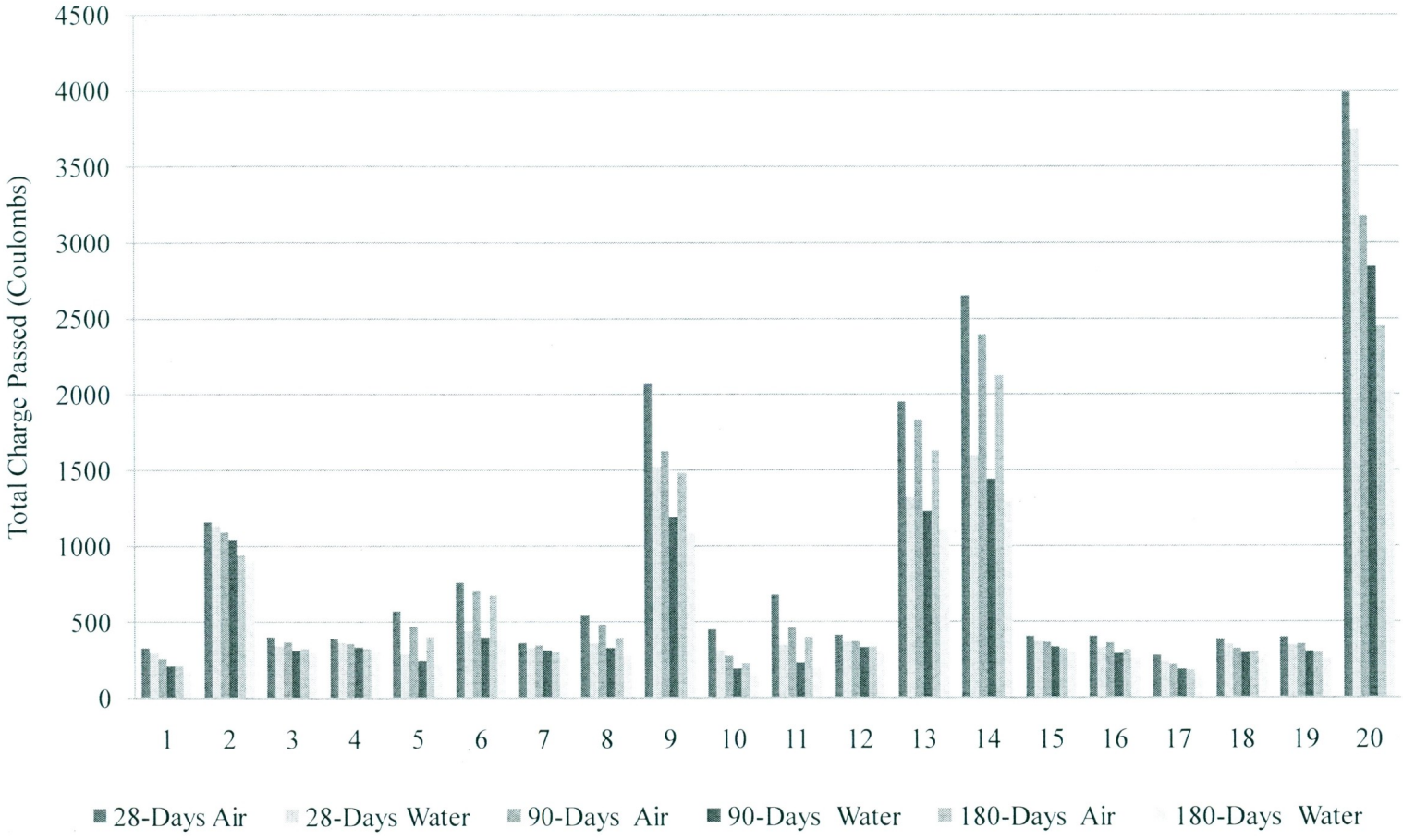

Figure 4.13: RCPT Permeability versus Time for the 20 HPSCC Mixtures

Table 4.5: *m* Coefficients for Air- and Water-Cured Samples

Mixture Number	m_{air}	m_{water}
1	0.244	0.296
2	0.112	0.127
3	0.110	0.087
4	0.098	0.102
5	0.189	0.142
6	0.065	0.083
7	0.099	0.102
8	0.171	0.139
9	0.179	0.182
10	0.371	0.374
11	0.281	0.301
12	0.111	0.108
13	0.096	0.095
14	0.119	0.113
15	0.123	0.126
16	0.130	0.129
17	0.223	0.221
18	0.129	0.129
19	0.160	0.157
20	0.263	0.330

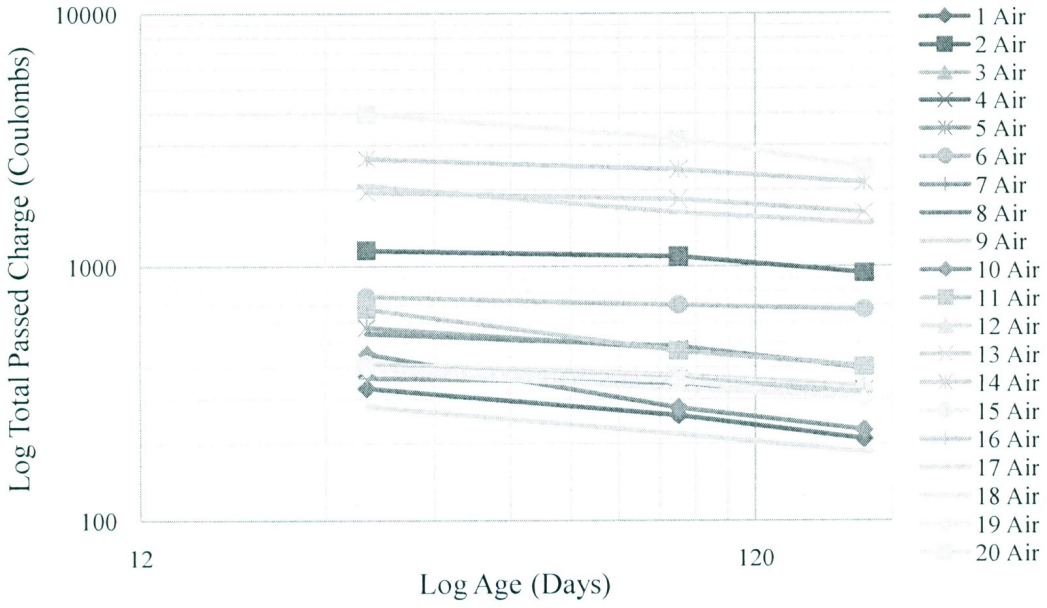

Figure 4.14: RCPT Values versus Age for Air-Cured Samples

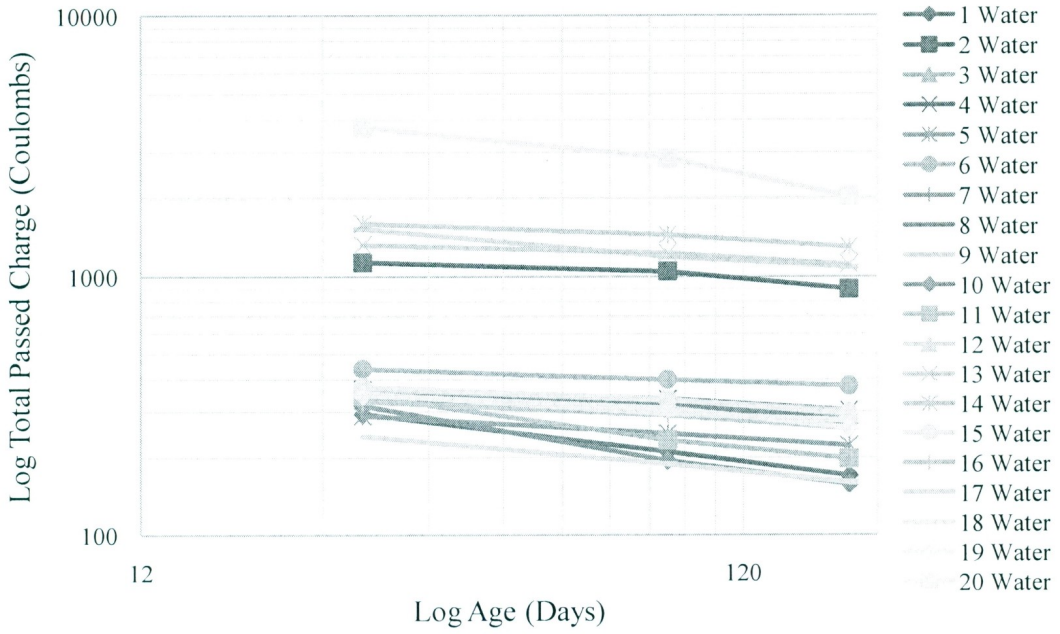

Figure 4.15: RCPT Values versus Age for Water-Cured Samples

In addition to the aforementioned relationships, the prediction models for the 90 and 180-days RCPT were developed for both air- and water-cured samples. These equations are based on the most significant factors governing the 90 and 180-days RCPT values (see Appendix C, Responses 14, 15, 16 and 17-ANOVA Tables). These significant factors are C, C^2, B, B^2, and A, respectively in order of significance, as shown in Equations 4.15, 4.16, 4.17, and 4.18 ($R^2 = 0.97$; $R^2 = 0.99$; $R^2 = 0.96$; and $R^2 = 0.98$, respectively).

$$Ln\,90-Days\ RCPT\ (Air\ Curing) = 34.199 - 0.00364\ x\ A - 129.68\ x\ B - 0.276\ x\ C + 172.723\ x\ B^2 + 0.0069\ x\ C^2 \quad (Coulombs) \qquad \textbf{(4.15)}$$

$$Ln\,90-Days\ RCPT\ (Water\ Curing) = 19.84 - 0.0013\ x\ A - 58.55\ x\ B - 0.261\ x\ C + 76.66\ x\ B^2 + 0.0059\ x\ C^2 \quad (Coulombs) \qquad \textbf{(4.16)}$$

$$Ln\,180-Days\ RCPT\ (Air\ Curing) = 35.818 - 0.003\ x\ A - 140.59\ x\ B - 0.26\ x\ C + 187.13\ x\ B^2 + 0.0062\ x\ C^2 \quad (Coulombs) \qquad \textbf{(4.17)}$$

$$Ln\,180-Days\ RCPT\ (Water\ Curing)=20.971-0.0007\ x\ A-67.49\ x\ B$$
$$-0.24\ x\ C+88.73\ x\ B^2+0.005\ x\ C^2\quad (Coulombs) \qquad \textbf{(4.18)}$$

Furthermore, two prediction models to calculate the factor (m) based on the most significant factors were obtained from the ANOVA over the results of the 20 HPSCC mixtures (Appendix C, Responses 18 and 19-ANOVA Tables). Equation 4.19 measures m for air-cured concretes relating the most significant factors C^2, C, A, B^2, and B, respectively ($R^2 = 0.93$). In addition, Equation 4.20 predicts m for water-cured concretes with the most important factors C^2, C, and A, respectively ($R^2 = 0.83$).

$$m_{air}=-2.263-0.00067\ x\ A+14.365\ x\ B-0.0241\ x\ C$$
$$-18.357\ x\ B^2+0.00121\ x\ C^2 \qquad \textbf{(4.19)}$$

$$m_{water}=0.6352-0.0008\ x\ A-0.0315\ x\ C+0.0015\ x\ C^2 \qquad \textbf{(4.20)}$$

4.2.2.4 Relationship between 28-Days RCPT and 28-Days Diffusion Coefficient

Apparent chloride diffusion coefficient (D_a) at the age of 28 days was measured experimentally as part of the bulk chloride diffusion test. The chloride diffusion coefficient represents the permeability of concrete, which may be alternatively obtained from the RCPT technique. The bulk chloride diffusion test requires a minimum submersion period of 35 days to allow sufficient chlorides to penetrate the concrete pores up to at least 10 mm depth. For this reason, a relationship that relates the RCPT with the D_a was deemed necessary. In addition, the prediction models that relate the coefficient D_a with the most important factors affecting the chloride permeability for both air and water curing (see Appendix C, Responses 20 and 21-ANOVA Tables) are presented in Equations 4.21 and 4.22 ($R^2 = 0.94$; and $R^2 = 0.95$, respectively). As seen in Equation 4.21, the factors that mostly affected the air-cured coefficient D_a were C, B, C^2, BC, and

A, respectively in order of significance. On the other hand, the factors C, C^2, B, B^2, and A were the most significant effects governing the water-cured coefficient D_a, respectively in order of significance (Equation 4.22).

$$Ln\,28-Days\,D_a\,(Air\ Curing)=10.368-0.0048\,x\,A-2.78\,x\,B-0.67\,x\,C+1.144\,x\,B\,x\,C+0.0055\,x\,C^2\quad(x\,10E-14\,m^2/\sec) \tag{4.21}$$

$$Ln\,28-Days\,D_a\,(Water\ Curing)=33.795-0.0048\,x\,A-128.71\,x\,B-0.266\,x\,C+167.92\,x\,B^2+0.0064\,x\,C^2\quad(x\,10E-14\,m^2/\sec) \tag{4.22}$$

Figure 4.16 shows the relationship between the RCPT and apparent chloride diffusion coefficient D_a for air- and water-cured samples at 28 days. It is obvious from the figure that an almost linear relationship exists in both air- and water-cured samples. As a result, a linear equation was developed to predict the coefficient D_a by substituting the RCPT value. This equation will be used for the quick estimation of the chloride diffusion after performing the RCPT procedure, which requires only 6 hours instead of 35 days. Equation 4.23 can be utilized to estimate the apparent chloride diffusion coefficient D_a for air- and water-cured samples as a function of the RCPT (coulombs) for the HPSCC mixtures containing MK (R^2 = 0.9). It should be noted that the use of this equation is limited to the range of factors studied in the current research.

$$28-Days\,D_a=7.522E-13+2.196E-15\,x\,RCPT\quad(m^2/\sec) \tag{4.23}$$

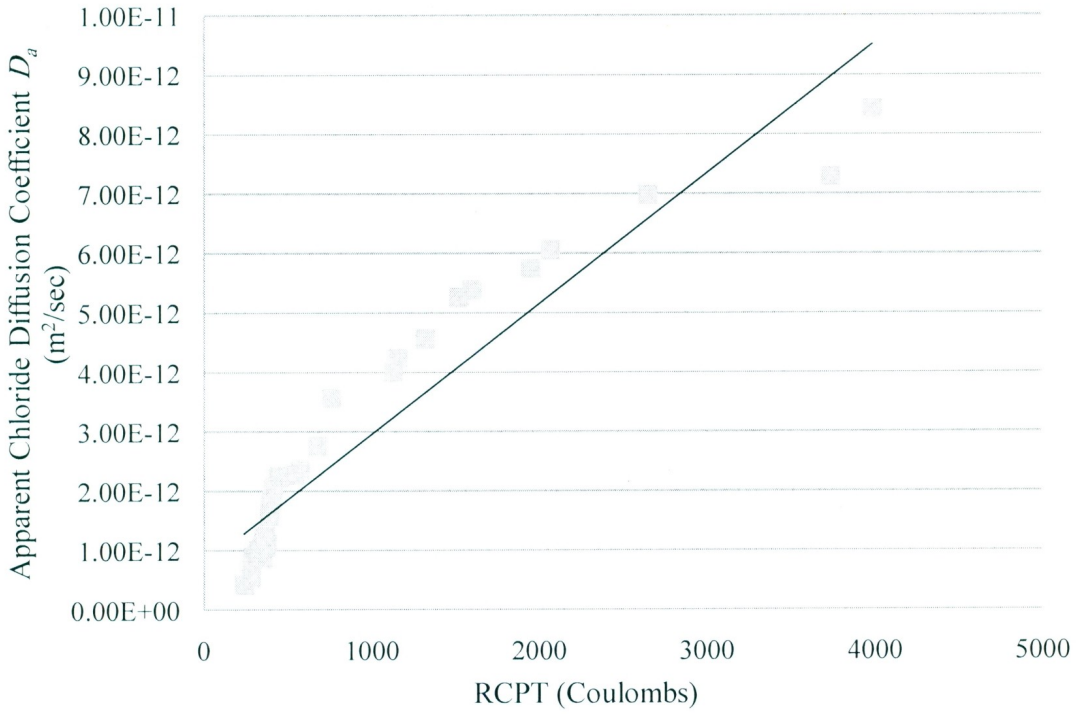

Figure 4.16: Relationship between D_a and RCPT for Air- and Water-Cured Samples

4.2.3 Service Life Time Prediction of HPSCC Using Fick's Law

After measuring the apparent chloride diffusion coefficients (D_a) and the diffusion decay index (m) for each curing technique, the following assumptions were made to predict the service life time for the 20 tested HPSCC mixtures:

- The structure has a clear concrete cover of 60 mm,
- The chloride threshold value is 0.05% (% weight of concrete) as given from the literature (Trejo et al. 2003; Ehlen et al. 2009),
- The chloride diffusion is the dominant mechanism and is governed by Fick's second law of diffusion in the differential Equation 4.24 (Gjørv 2002);

$$\frac{dC}{dt} = D_a \; x \; \frac{d^2C}{dx^2} \qquad \textbf{(4.24)}$$

Where: C = the chloride content, D_a = the apparent diffusion coefficient, x = the depth from the exposed surface, and t = time.

- The chloride diffusion coefficients shown in Table 4.4 (at 28 days) decreases periodically as a function of time because of the cement hydration process. As a result, the chloride diffusion should be calculated at different time periods using the following Equation 4.25 (Bentz et al. 2012):

$$D(t) = D_{ref} \; x \left(\frac{t_{ref}}{t}\right)^{m} \qquad \textbf{(4.25)}$$

Where: $D(t)$ = diffusion coefficient at time t,

D_{ref}= diffusion coefficient at time t_{ref} (28 days), and

m = diffusion decay index (Table 4.5).

- The surface chloride concentration (C_s) of the simulated structure had reached the maximum value of 0.8% weight of concrete (or more) at the start time of chloride diffusion.

The solution for estimating the time of corrosion initiation was implemented using a finite difference application of Equation 4.24. The values of chloride diffusion coefficient were varied at different time steps using Equation 4.25, until the value of chloride concentration near the rebar surface reached the chloride threshold value. At this stage, the time was reported, which indicated the corrosion initiation for each sample, as seen in Figure 4.17.

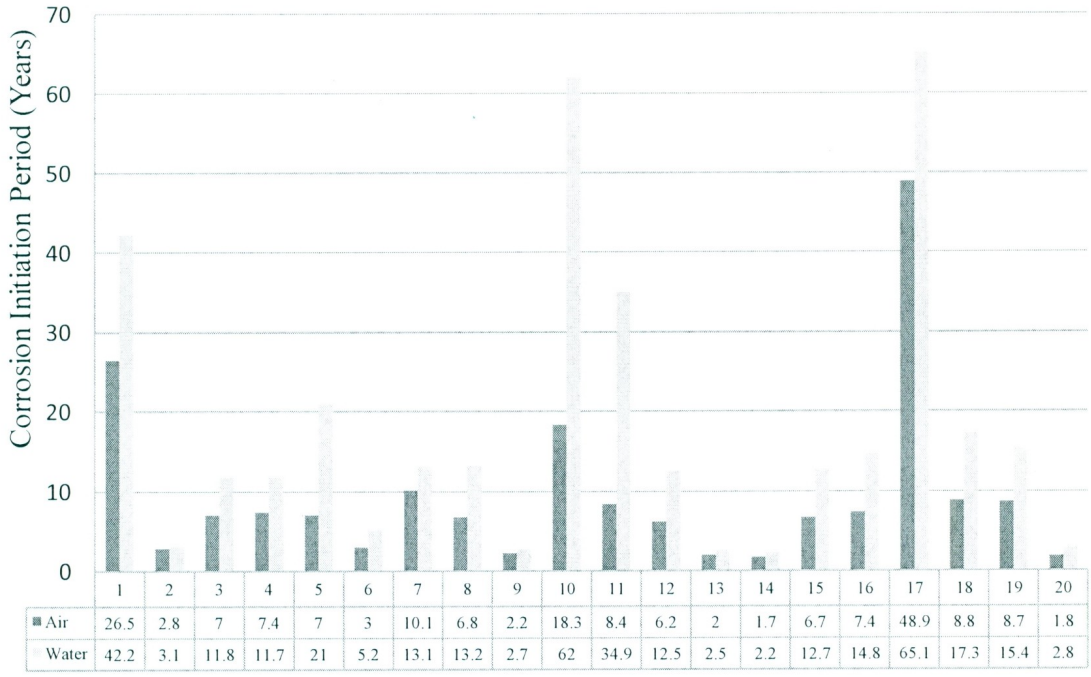

	1	2	3	4	5	6	7	8	9	10	11	12	13	14	15	16	17	18	19	20
Air	26.5	2.8	7	7.4	7	3	10.1	6.8	2.2	18.3	8.4	6.2	2	1.7	6.7	7.4	48.9	8.8	8.7	1.8
Water	42.2	3.1	11.8	11.7	21	5.2	13.1	13.2	2.7	62	34.9	12.5	2.5	2.2	12.7	14.8	65.1	17.3	15.4	2.8

Figure 4.17: Corrosion Initiation Periods for Air- and Water-Cured Samples

It is clear from the figure that different mixtures and curing procedures significantly affected the time for corrosion to start. Moreover, a wide range of the initiation periods was obtained from the 20 HPSCC mixtures (1.7-65.1 years). This wide range manifests the effect of the durability performance of the HPSCC on the corrosion initiation time and the overall service life time of structures in harsh environments.

It should be mentioned that the initiation period calculated herein was based on assuming that the maximum surface chloride concentration (0.8%) was accumulated previously. This assumption is not real for actual structures, as it may take years for chlorides to build up at the surface of the exposed structure. However, this assumption was made as the conducted chloride diffusion test had a maximum surface chloride concentration during

the whole test. Therefore, the results obtained above can be used as a comparative study only and cannot represent the actual corrosion time.

4.2.3.1 Effect of Curing on Corrosion Initiation Times

As seen in Figure 4.17, all water-cured samples showed higher initiation times than their air-cured counterparts. This trend was expected owing to the lower chloride permeability of water-cured samples than air-cured ones in both the RCPT and chloride diffusion tests. Nevertheless, the differences in the corrosion initiation times between air- and water-cured samples were not constant for all HPSCC mixtures. The maximum difference was 43.7 years and was obtained in the mixture number 10 (A = 450 kg/m^3, B = 0.4, and C = 25%), which had the maximum replacement level of MK. This difference was attributed to the higher effect of curing on the mixtures containing high percentages of MK. In this mixture, water curing decreased the chloride diffusion coefficient from 2.24E-12 to 9.54E-13, which significantly affected the initiation times. A significant difference (>10 years) was also obtained from mixtures number 1, 5, 11, and 17. These mixtures were cast with 19.9% MK replacement; as a result, increasing the MK percentage greatly increased the difference between air and water curing. On the other hand, the minimum difference was 0.3 years in mixture number 2 (A = 480 kg/m^3, B = 0.37, and C = 5.1%), which exhibited a lower percentage of MK (5.1%). For instance, mixture number 17 (A = 480 kg/m^3, B = 0.37, and C = 19.9%) had a difference of 16.2 years, which was attributed to the increase in the MK from 5.1 to 19.9%. It can be concluded that incorporating high percentages of MK resulted in noticeable differences between the initiation times from air- and water-cured samples from the same HPSCC mixture.

4.2.3.2 Effect of HPSCC Mixture Proportions on Corrosion Initiation Times

It can be noticed from Figure 4.17 that different corrosion initiation periods were associated with different HPSCC mixtures. These results were expected as the 20 mixtures exhibited various diffusion coefficients (D_a), which represents the most important factor in the corrosion process. As a result, the mixture with the minimum diffusion coefficients was number 17 (A = 480 kg/m^3, B = 0.37, and C = 19.9%), which yielded the maximum corrosion initiation periods (48.9 and 65.1). The mixture with the minimum corrosion initiation periods (1.7 and 2.2) was number 14 (A = 420 kg/m^3, B = 0.43, and C = 5.1%). It should be noted that the mixture number 20 (A = 450 kg/m^3, B = 0.4, and C = 0%) was expected to show the minimum corrosion initiation times owing to its high diffusion coefficients (maximum among all 20 mixtures). However, the diffusion decay index (m) was higher in mixture number 20 than in number 14 (0.33 versus 0.113), which on the long age of the concrete yielded lower diffusion coefficients in mixture number 20. The results from Fick's law were used to develop prediction models for the service life time to predict the time of corrosion initiation as a function of mixture proportions. These models were obtained after performing ANOVA on the initiation times for the 20 HPSCC mixtures. In the first model (air curing), the factors C, B, and BC were found to be the most significant factors governing the initiation time for air-cured samples, respectively in order of significance (see Appendix C, Response 22-ANOVA Table). The second model (water curing) contains only C and B, which were proved to be the most important factors affecting the initiation time of water-cured samples (see Appendix C, Response 23-ANOVA Table). These models are shown in the logarithmic form, as seen in Equations 4.26 and 4.27 (R^2 = 0.93; and R^2 = 0.92, respectively).

$$Ln\ Corrosion\ Initiation\ Time\ (Air\ Curing) = -1.0571 + 3.5577\ x\ B + 0.685\ x\ C - 1.413\ x\ B\ x\ C \quad (Years) \tag{4.26}$$

$$Ln\ Corrosion\ Initiation\ Time\ (Water\ Curing) = 3.718 - 8.116\ x\ B + 0.157\ x\ C \quad (Years) \tag{4.27}$$

4.2.4 Optimization of HPSCC Mixture and Models Validation

By reviewing the results from both the fresh and hardened properties of the 20 mixtures, the optimum mixtures were number 5 (A = 480 kg/m^3, B = 0.43, and C = 19.9%) and 17 (A = 480 kg/m^3, B = 0.37, and C = 19.9%), respectively. These two mixtures both had a binder content of 480 kg/m^3 and an MK percent of 19.9%. It is clear that the mixture with high water-to-binder ratio (0.43) had the optimum fresh properties (mixture number 5), as expected. Moreover, the mixture with low water-to-binder ratio (0.37) had the maximum strength and the minimum chloride permeability/diffusion (mixture number 17). In order to determine one mixture achieving the balance between fresh properties, strength, and durability, the numerical optimization tool was utilized. This tool is available with the method of central composite design (CCD) in the commercially used software. The target in this technique was established to maximize the flow ability, passing ability, and compressive strength, and to minimize the chloride permeability of the HPSCC mixture. In this optimization, the developed prediction models were used, along with the predefined targets, in a number of trials which maintained the desired criteria.

The results yielded an optimum HPSCC mixture having the following ingredients: A (Total Binder = 490 kg/m^3), B (W/B = 0.39), and C (MK Ratio = 19.9%). This optimum mixture was tested under the same procedure to validate the prediction models;

the results are compared in Tables 4.6 and 4.7. It can be seen that the results obtained from the prediction models are relatively close to the actual test results. However, the small differences can be attributed to the higher dosage of the HRWRA added in the actual test than the required amount predicted in the model. It should be mentioned that the differences are lower in the results of compressive strength and chloride permeability than those in the fresh properties. The results also showed that the equations underestimated the predicted corrosion times owing to the cumulative errors from predicting the values of the diffusion coefficients (D_a) and diffusion decay index (m).

Table 4.6: Comparison of the Fresh Properties of Tested and Predicted HPSCC Optimum Mixture

Mixture Number	HRWRA Dose L/m^3	T_{500} (Sec)	T_{500}J (Sec)	Slump – J-Ring (mm)	V-Funnel (Sec)		S_f*	L-Box Ratio H2/H1	Air %
					Initial	Final			
Predicted	7.71	3.25	4.29	21	13	24	0.35	0.79	2.1
Tested	10.77	3.5	4	18	8	11	0.38	0.8	1.0

S_f*= Segregation Factor

Table 4.7: Comparison of the Hardened Properties of Tested and Predicted HPSCC Optimum Mixture

Mixture Number	28-Days f_c' (MPa)		28-Days RCPT (Coulombs)		90-Days RCPT (Coulombs)		180-Days RCPT (Coulombs)		28-Days D_a (m^2/sec)		Initiation Times (Years)	
	Air	Water	Air	Water	Air	Water	Air	Water	Air	Water	Air	Water
Predicted	80.11	84.67	299	239	217	187	180	157	1.01 E-12	5.46 E-13	19.8	39.2
Tested	74.65	82.1	268	217	248	196	185	160	5.81 E-13	4.33 E-13	35.2	44.9

4.2.5 Comparison of Optimum HPSCC Mixture Containing Metakaolin, Other SCM's Mixtures, and Normal Concrete Mixtures

The optimum HPSCC mixture containing MK obtained previously from the numerical optimization process was tested and compared to counterpart mixtures containing other SCM's. The three alternative HPSCC mixtures contained 30% slag (SG), 30% fly ash (FA), and 8% silica fume (SF), while the total binder contents and water-to-binder ratios (0.39) were kept constant (see Table 3.7, Section 3.3.4). The optimum replacement levels of other SCM's were selected after reviewing the literature for each SCM for the production of SCC (Lachemi et al. 2003; and Hassan et al. 2012). In addition, two additional normal concrete mixtures (NC1, NC2) were included in the comparison without any SCM's. NC1 and NC2 contained total binder of 490 kg/m^3, W/B of 0.39, and coarse-to-fine aggregate ratio of 0.9 (see Table 3.7, Section 3.3.4). However, NC1 contained coarse aggregate the size of 10 mm and NC2 had a greater coarse aggregate size (20 mm). The tests included fresh, hardened, and durability tests. These tests were performed by exactly the same procedures as previously completed for the 20 HPSCC mixtures. The results are described in Tables 4.8 and 4.9.

4.2.5.1 Fresh Properties of the Selected Mixtures

Table 4.8 shows the fresh properties of the optimum HPSCC containing MK and three other HPSCC mixtures with SG, FA, and SF. The tests included slump flow, J-ring, V-funnel, L-box, and air content tests to compare the fresh properties of the optimum MK mixture to other SCM's. In addition, the standard slump and air content tests were only applied for NC mixtures.

Table 4.8: Fresh Properties Test Results for the Optimized Mixtures

Mix. No.	HRWRA Dose (L/m^3)	Slump Flow (mm)	T_{500} (Sec)	J-Ring Flow (mm)	$T_{500}J$ (Sec)	Slump-J-Ring (mm)	V-Funnel (Sec)		S_f**	L-Box Ratio H2/H1	Air %
							Initial	Final			
MK	10.77	650	3.5	632	4.0	18	8	11	0.38	0.80	1.0
SG	1.54	667	2.2	628	3.3	39	6	9	0.50	0.70	0.9
FA	2.00	650	3.0	622	3.5	28	7	10	0.43	0.77	1.4
SF	3.08	635	2.0	570	6.0	65	7.5	13	0.73	0.63	1.2
NC1	-	85*	-	-	-	-	-	-	-	-	2.0
NC2	-	170*	-	-	-	-	-	-	-	-	1.7

*Slump Height in NC Mixtures, S_f **= Segregation Factor

4.2.5.1.1 Slump Test for NC Mixtures

The standard slump test was implemented for the NC mixtures and the slump heights were measured as shown in Table 4.8. The NC mixtures were mixed without any HRWRA and the slump heights were 85 and 170 mm (for NC1 and NC2, respectively). The higher slump height (170 mm) was obtained in NC2, which had the 20 mm maximum stone size, versus 85 mm in NC1, which had a stone size of 10 mm.

4.2.5.1.2 HRWRA Demand of the HPSCC Mixtures

All other fresh properties tests were only performed for the HPSCC mixtures after adding sufficient HRWRA dosage to obtain the target slump flow diameter (650±50 mm). It can be seen from Table 4.8 that MK required the maximum HRWRA dose (10.77 L/m^3), while the three other SCM's required comparable doses (1.54 to 3.08 L/m^3). The 30% SG mixture exhibited the minimum HRWRA amount of 1.54 L/m^3. These amounts of HRWRA were added to obtain slump flow diameters of approximately 650±50 mm. The slump flow diameters ranged between 635 and 667 mm, which lie in the presumed range and with no significant differences between the tested HPSCC mixtures.

4.2.5.1.3 Viscosity and Segregation Resistance of the HPSCC Mixtures

The T_{500} times were measured for the four HPSCC mixtures in the slump flow test. These times represent the viscosity of the mixture and ranged between 2.0 and 3.5, as seen in Table 4.8. The maximum T_{500} (3.5 sec) was associated with MK and the minimum (2.0 sec) was obtained in the SF mixture. This result showed that MK exhibited the maximum viscosity when compared to other SCM's. In addition, the initial V-funnel directly reveals the viscosity of the HPSCC along with the T_{500} times. As expected, the MK mixture showed the maximum viscosity or the maximum initial V-funnel time (8 sec). The minimum viscosity in terms of the initial V-funnel test was obtained from the SG mixture (6 sec).

The V-funnel test was repeated after five minutes and the segregation factor was calculated (see Table 4.8). Although the MK mixture had the maximum initial V-funnel, it exhibited the minimum segregation factor (0.38). This result indicated that MK had the superior performance in minimizing the segregation of the HPSCC mixture. It should be noted that the maximum segregation factor of 0.73 was obtained from the SF mixture that had the lowest passing ability between the tested mixtures. This result may be attributed to the low percentage of silica fume (8%) present in the tested mixture.

4.2.5.1.4 Passing Ability of the HPSCC Mixtures

The tested mixtures showed different flow diameters in the J-ring test from those obtained in the slump flow test, which related to the passing ability of HPSCC. As a result, the differences between the slump flow and J-ring diameters showed a wide range of 18 to 65 mm. The minimum difference (18 mm) was obtained from MK mixture, whereas the SF

mixture exhibited the maximum difference (65 mm). The results from the L-box tests also indicate the passing ability of the HPSCC mixtures. The four mixtures showed different ratios in the L-box test, which ranged from 0.63 to 0.8. The maximum L-box ratio (0.8) was achieved in MK mixture, which reflected the high passing ability of the HPSCC mixture. SF mixture showed the minimum passing ability because of the low ratio of the L-box test (0.63). The results from the L-box test matched the results from the difference between slump and J-ring diameters presented in Table 4.8. The minimum difference (18 mm) was associated with the maximum L-box ratio (0.8) in the MK mixture. Following this approach, the maximum difference (65 mm) was related to the minimum L-box ratio (0.63) of the SF mixture. As a result, the MK mixture was considered the optimum mixture in terms of the passing ability.

4.2.5.1.5 Flowing Ability of the HPSCC Mixtures

The results of the $T_{500}J$ test showed a different trend from that of T_{500}, as it depends on the flowing ability of the mixture. It is clear from the table that all $T_{500}J$ times were higher than T_{500} times, in general. Ultimately, the mixture of the minimum flowing ability (SF) exhibited the maximum $T_{500}J$ (6.0 sec). Both MK and FA had a difference of 0.5 second between the two tests, which indicated the superior flowing ability of MK and FA in the HPSCC.

4.2.5.1.6 Air Tests for the Selected Mixtures

Finally, the air content test was performed over the six tested mixtures, including four HPSCC and two NC mixtures. The values of the trapped air content in the HPSCC mixtures ranged between 0.9 and 1.4. It can also be seen from Table 4.8 that NC mixtures

exhibited slightly higher air contents (1.4 to 2.0). However, the difference between HPSCC and NC mixtures was not significant.

4.2.5.2 Mechanical and Durability Properties of the Selected Mixtures

The compressive strength at 28 days; RCPT at 28, 90, and 180 days; and bulk chloride diffusion tests were performed on the six selected mixtures. The results are shown in Table 4.9.

Table 4.9: Mechanical and Durability Properties of the Selected Mixtures

Mix. No.	28-Days f_c' (MPa)		28-Days RCPT (Coulombs)		93-Days RCPT (Coulombs)		180-Days RCPT (Coulombs)		28-Days D_a (m^2/sec)	
	Air	Water	Air	Water	Air	Water	Air	Water	Air	Water
MK	74.65	82.1	268	217	248	196	185	160	5.81E-13	4.33E-13
SG	42.44	54.32	1715	1120	1572	584	1325	320	2.46E-12	1.16E-12
FA	50.035	66.03	2450	1325	1954	378	1632	208	3.80E-12	1.23E-12
SF	62.08	71.44	1180	509	705	431	425	288	7.77E-13	6.99E-13
NC1	54.04	62.74	2773	2309	2267	1957	1925	1760	4.72E-12	3.96E-12
NC2	51.125	57.52	3396	2614	2680	2087	2250	1825	6.17E-12	5.33E-12

4.2.5.2.1 28-Days Compressive Strength of the Selected Mixtures

Figure 4.18 shows the compressive strength for the selected mixtures after air and water curing periods of 28 days. It is clear from the figure that all water-cured samples exhibited higher strength than their air-cured counterparts for all tested HPSCC and NC mixtures. These results were expected and matched the results obtained from testing the 20 HPSCC mixtures in the previous stage. It can be seen from the figure that MK had the maximum compressive strength in both air- and water-cured samples (74.65 and 82.1, respectively). This mixture showed approximately 10 MPa higher than the closer mixture (SF), which obtained 62.08 and 71.44 MPa in air- and water-cured samples, respectively.

Following SF, the FA and SG were the third and the fourth HPSCC mixtures, respectively. On the other hand, MK and SF had higher strengths than NC mixtures cured in air and water. NC1 had a slightly higher compressive strength than NC2, which was attributed to the lower coarse aggregate size in NC1 (10 mm) than that in NC2 (20 mm).

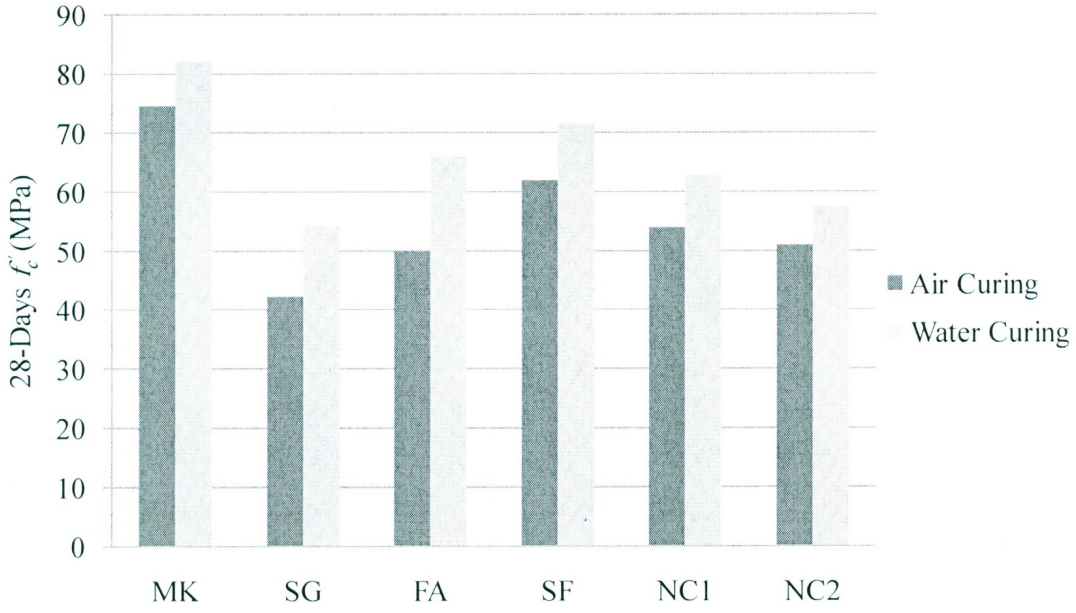

Figure 4.18: 28-Days Compressive Strength for Air- and Water-Cured Samples

4.2.5.2.2 RCPT Results of the Selected Mixtures

As seen in Figure 4.19, the RCPT results followed similar trends to those obtained from the 28-days compressive strength. The minimum charge passed (RCPT) was found in the MK mixture, which indicated the minimum chloride permeability in both air- and water-cured samples. As concluded before, SF had the second lowest RCPT after the MK mixture, followed by SG and FA, respectively. In addition, all HPSCC mixtures had lower RCPT values than NC mixtures, in general, as average RCPT values. This result manifested the effect of the use of SCM's in reducing the chloride permeability of

HPSCC and the superior behaviour of the optimized MK HPSCC mixture compared to NC in both the compressive strength and chloride permeability. On the other hand, NC mixtures demonstrated different RCPT values based on the coarse aggregate size. For example, NC2 had slightly higher RCPT than NC1 owing to the greater coarse aggregate size used in NC2 than NC1 (20 mm versus 10 mm). This result shows that the increase in the coarse aggregate size resulted in higher RCPT values.

The effect of curing on the RCPT of HPSCC and NC mixtures can be clearly observed from Figure 4.19. From the figure, all water-cured samples showed to have lower RCPT values compared to their counterparts cured in air. In addition, the longer curing period decreased the RCPT from 28 to 93 and ultimately 180 days for both air- and water-cured samples. However, in some cases the effect of water curing was shown to be more dominant than the curing period length. For example, in SG, FA, SF, and NC2 the 28-days RCPT of water-cured samples was lower than the 93 days RCPT of the same samples cured in air.

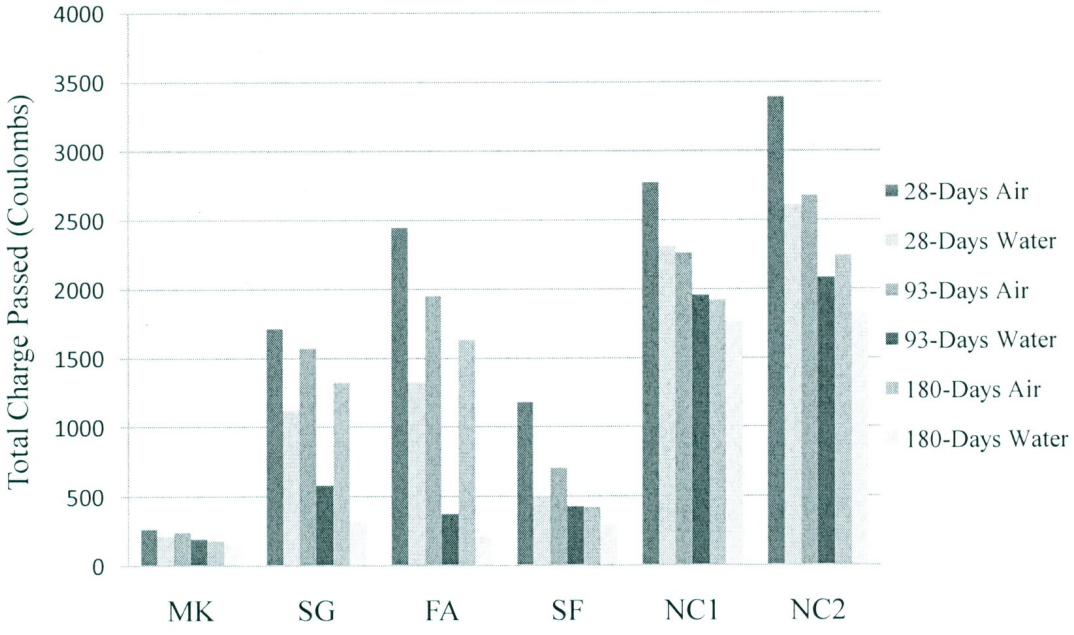

Figure 4.19: RCPT Results for the Selected Mixtures

4.2.5.2.3 Chloride Diffusion Coefficients of the Selected Mixtures

The apparent chloride diffusion coefficients for the six selected mixtures was measured as part of the bulk chloride diffusion test, as shown in Figure 4.20, for air- and water-cured samples. As expected, MK had the minimum chloride diffusion coefficients in both air- and water-cured samples. Meanwhile, the NC2 had the absolute maximum chloride diffusion factors (6.17E-12, 5.33E-12 m^2/sec) for both air- and water-cured samples. In addition, all water-cured samples attained lower chloride diffusion coefficients than air-cured counterparts. It is obvious from Figure 4.21 that a linear relationship was warranted between RCPT and chloride diffusion coefficients. Both air-cured and water-cured samples for all tested HPSCC and NC mixtures exhibited this trend.

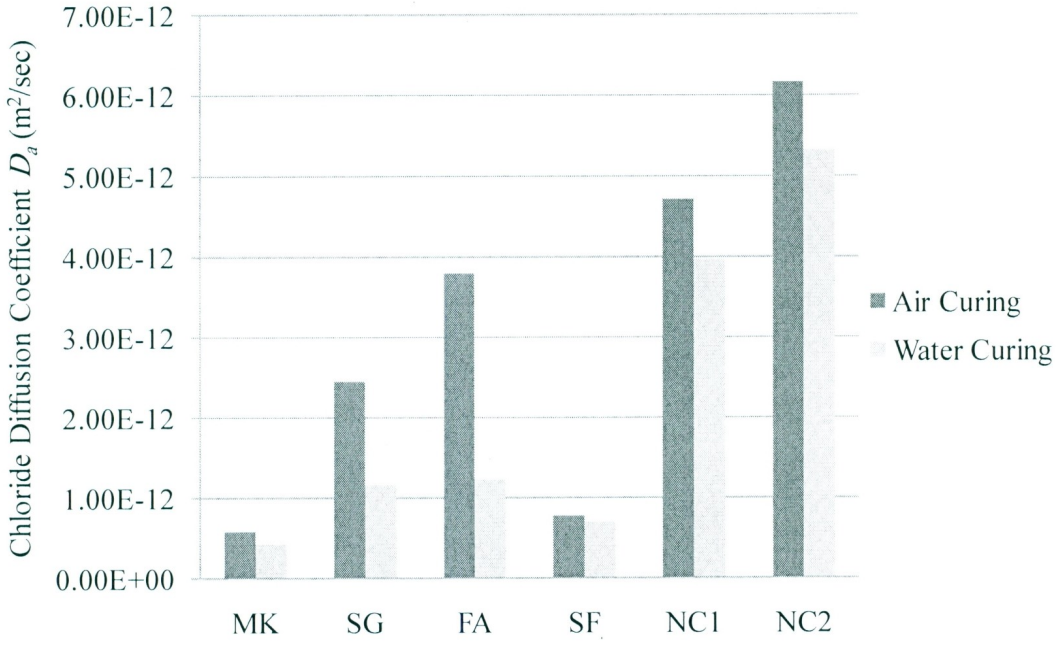

Figure 4.20: Chloride Diffusion Coefficients for Air- and Water-Cured Samples

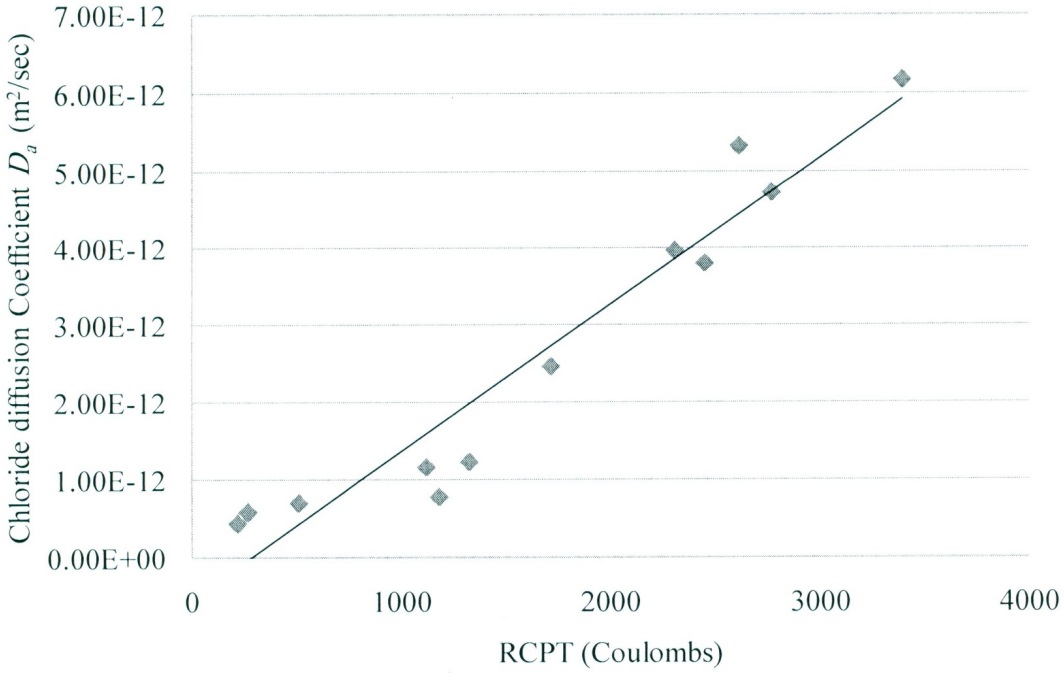

Figure 4.21: Relationship between RCPT and Diffusion Coefficients for Selected Mixtures

4.3 Accelerated Corrosion Test

In this stage, only one HPSCC mixture containing no SCM's was selected for further investigation, including the effect of ten different curing techniques on the compressive strength, RCPT, chloride diffusion, and accelerated corrosion tests. This investigation was performed to validate the derived service life prediction models described in stage 2. In addition, this stage contains an optimization of the accelerated corrosion tests for a more accurate prediction of the real service life time of concrete structures. The results from each test were evaluated based on different curing techniques and are discussed in detail as follows:

4.3.1 Effect of Different Curing Techniques on the Compressive Strength

The compressive strength of cylinders representing ten different curing conditions was measured and compared (see Figure 4.22). It can be seen that different curing techniques had a significant effect on the 28-days compressive strength. The maximum compressive strength (76.16 MPa) was associated with curing technique 2 (28-days water), while the minimum compressive strength (47.45 MPa) was obtained from technique 7 (28-days cold air), as expected. It is obvious that longer water curing periods increased the compressive strength at 28 days. In addition, all water-cured samples exhibited higher strengths than those in both cold- and heat-cured samples. For example, the average compressive strength of the water-cured samples (techniques 2, 3, and 4) was higher than cold (techniques 5, 6, and 7) and heat-cured samples (techniques 8, 9, and 10) by 20% and 23%, respectively.

It is also clear from the chart that the subsequent cold curing performed in techniques 5 and 6 decreased the compressive strength by approximately 10% when compared to that found with techniques 3 and 4. However, approximately the same strength reduction (10%) was obtained from both air curing (technique 1) and cold curing (technique 7) for the 28-days curing periods. When comparing technique 7 to other cold curing techniques 5 and 6, it can be seen that the increase of the cold-temperature curing period resulted in decreasing the compressive strength at 28 days by nearly 30%. Moreover, the heat curing at the early age (1-7 days) resulted in a general decrease in the strength with no significant differences found between heat-curing techniques. The maximum strength achieved with heat curing is 3 days in heat (technique 9), but with a slight difference from other techniques (8 and 10).

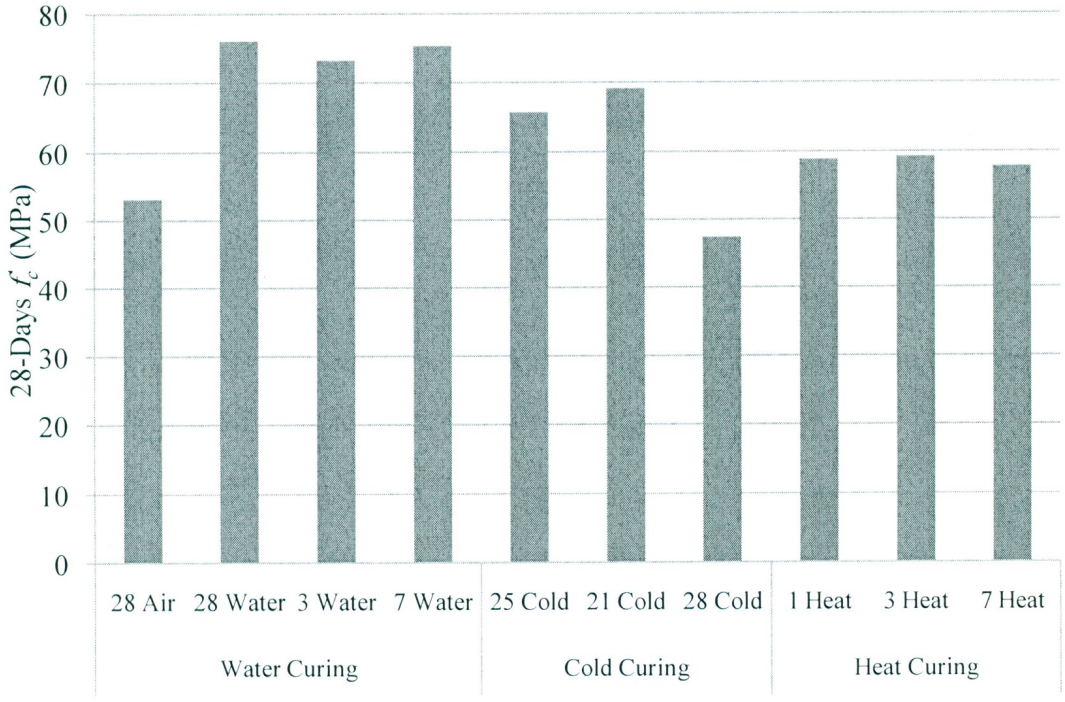

Figure 4.22: 28-Days Compressive Strength for Different Curing Techniques

4.3.2 Effect of Different Curing Techniques on RCPT

The results, presented in Figure 4.23, showed that different curing techniques had a significant effect on the RCPT results. These results ranged between 2072 and 3700, which are classified as moderate penetrability, as per ASTM C1202. The sample with the minimum permeability was number 2, which was cured in water for 28 days at 23° C. On the other hand, the maximum permeability was associated with sample number 10, which was cured in heated water at 50° C for a period of 7 days. Furthermore, cold curing samples (number 5, 6 and 7) had an average permeability of 2716, which was lower than the air-cured sample (number 1). Figure 4.23 also shows that the water-cured samples (2, 3 and 4) had almost similar RCPT permeability. In fact, the increase in the water curing period at 23° C slightly decreased the chloride permeability (2130 to 2072 coulombs). On the other hand, when samples 5 and 6 were subsequently cured in air after water curing periods, the permeability was increased by approximately 15%. Ultimately, when sample 7 was cured in cold air (3-5° C), the chloride permeability was higher than the normal air-cured sample (technique 1). It is obvious that heat-cured samples (8, 9 and 10) exhibited the maximum average chloride permeability.

It is also clear that as the heat-curing period increases, the total charge passing increases, which represented higher permeability. The minimum RCPT between heat-cured samples was obtained from technique 8, followed by technique 9, and finally technique 10. However, the difference between techniques 8, 9, and 10 was not significant.

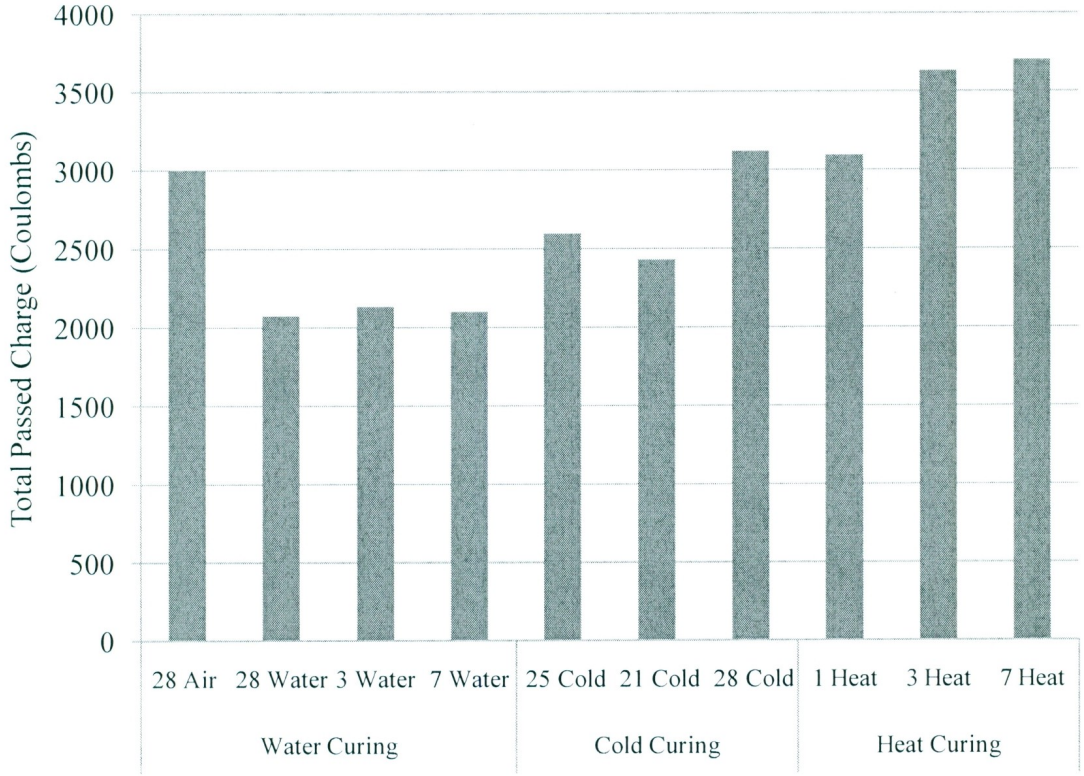

Figure 4.23: RCPT Results of Different Curing Techniques

4.3.3 Effect of Different Curing Techniques on Chloride Diffusion Coefficients

Alternatively, the results from the chloride diffusion test also indicated a significant effect of curing on the chloride diffusion coefficient. Again, it is clear from Figure 4.24 that a minimum chloride diffusion coefficient of 7.52E-12 m^2/sec was associated with the mixture with minimum RCPT coulombs (technique 2). Moreover, a maximum value of 1.8E-11 m^2/sec was obtained from sample number 10. In fact, the effect of using different curing techniques on the chloride diffusion coefficients yielded an identical effect of that on the RCPT permeability. This effect can be clearly described by the linear relationship between RCPT and diffusion coefficients (Figure 4.25).

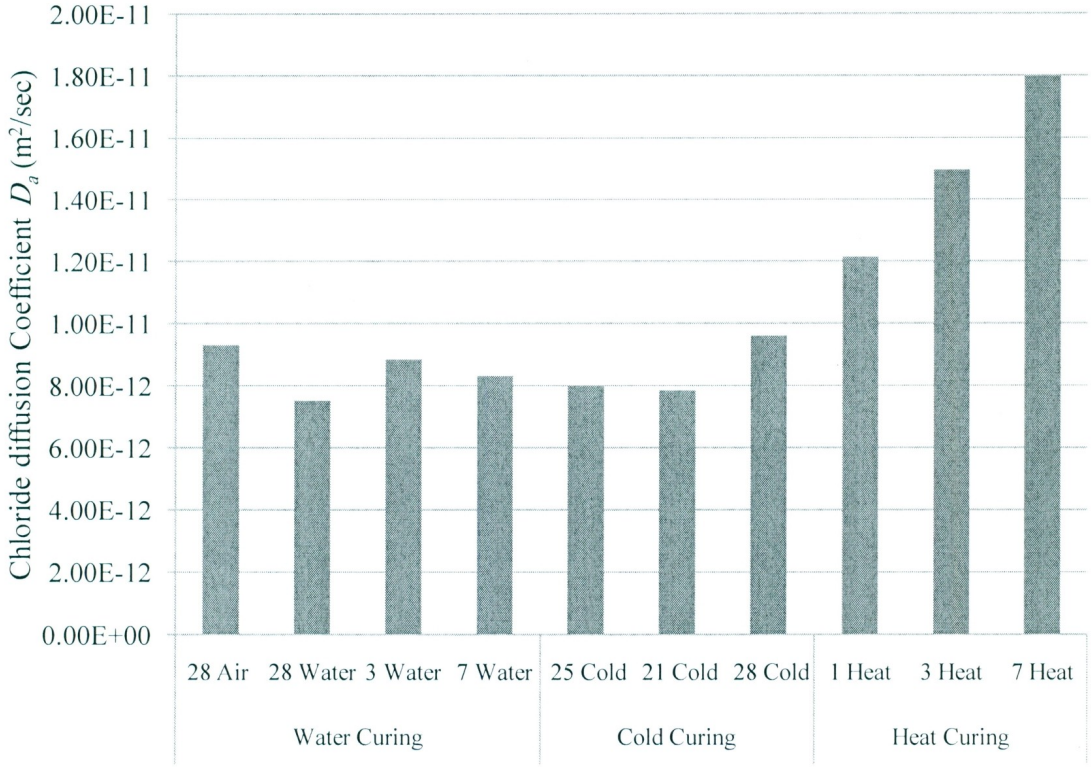

Figure 4.24: Chloride Diffusion Coefficients for Different Curing Techniques

Using this linear relationship, the diffusion coefficient can be estimated by substituting the RCPT value in Equation 4.28 (R^2 = 0.67). It should be noted that this equation is based on a limited number of mixtures. More samples with a wider range of values can present a more accurate equation. However, equation 4.28 can provide an estimation for the chloride permeability after only six hours, instead of 35 days.

$$Chloride\ Diffusion\ Coefficient\ D_a\ (m^2/\text{sec}) = -2.4718E-12 + 4.9208E-15\ x\ RCPT\ (Coulombs) \quad \textbf{(4.28)}$$

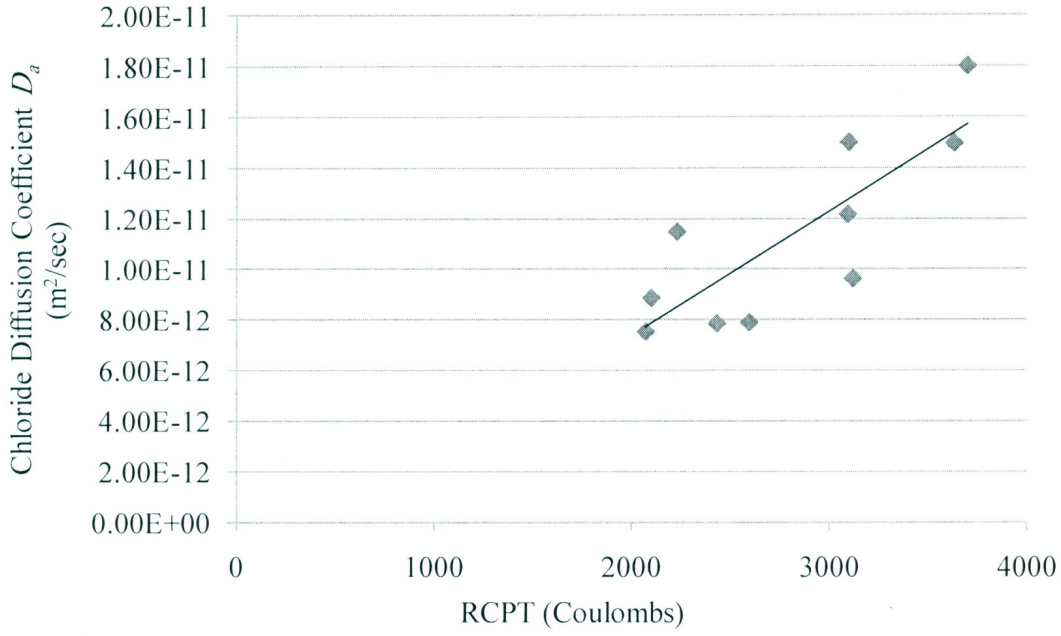

Figure 4.25: Relationship between RCPT and Chloride Diffusion Coefficients

4.3.4 Effect of Different Curing Techniques on Accelerated Corrosion Times

The results obtained from the initiation periods calculated in stage 2 showed that corrosion requires a relatively long period (years) to start. For this reason, an accelerated corrosion was performed on 80 different samples by the procedure described in chapter 3. The corrosion activity of the 80 samples tested for the accelerated corrosion was monitored by means of electrical current measurements and half-cell potentials (as per ASTM C876). A total of 80 prism samples were divided into 40 samples for non-severe corrosion stage and 40 for severe corrosion stage. Each of the 40 samples were based on the ten different curing techniques applied on four different prism sizes cast with different concrete covers (20, 30, 40, and 60 mm).

4.3.4.1 Non-Severe Corrosion Stage

In this stage, the 40 samples were monitored on a daily basis by recording their current and half-cell readings. Once the first crack was detected, the crack width, chloride content near the bar surface, and mass loss in the rebar were measured. The results of these measurements are described in Table 4.10.

It is clear from the table that the 40 samples took different times to crack based on the cover thickness and the curing regime. It is clear from the table that the increase of the concrete cover from 20 mm to 60 mm showed an increase in the time of crack initiation. The minimum average time of about 3 days was obtained from the 20 mm samples; followed by the 30 mm samples, which took 9 days to crack; and then the 40 mm samples, which took an average of 18 days to crack. The maximum average time was 43 days and was obtained from the 60 mm cover samples, as expected. These results demonstrated the effect of the concrete cover on the time to cracking of concrete. The increase of the concrete cover resulted in longer periods for chlorides to penetrate through the cover and reach the embedded bars and eventually initiate corrosion. These results matched the results obtained from similar studies (for example, Vu et al. 2000).

On the other hand, different curing techniques showed different cracking times between the ten samples having the same cover (20, 30, 40, and 60 mm). The first cracked samples were those cured in air and heat, followed by cold-cured samples, and finally water-cured samples. For example, the 60 mm cover heat-cured samples started to crack at an average of 24 days (1-60-8, 1-60-9, and 1-60-10), which were cured in heated water (at 50° C) for 1,3, and 7 days, respectively. Following the heat-cured samples, the air-cured samples at

23° C (1-60-1) cracked at 25 days. Next, the samples cured in cold air at 3-5° C (1-60-5, 1-60-6, and 1-60-7) cracked at an average period of 49 days. Finally, the water-cured samples at 23° C (1-60-2, 1-60-3, and 1-60-4) exhibited an average time to cracking of 62 days. In addition, similar trends were obtained from other samples having 20, 30, and 40 mm concrete cover. It can be concluded that the first samples to crack were those cured in heated water for 7 days (curing technique 10). The 28-days water-cured samples (curing technique 2) had the longest times to crack of all tested samples. These results were attributed to the low resistivity of the samples cured with technique 10 and the high resistivity of samples cured with technique 2. This resistivity was also observed from the results of the RCPT and chloride diffusion tests.

It can be also seen in Table 4.10 that different cracking times were obtained in each curing type (including water, cold, and heat) based on the period of applying such techniques. In water-cured samples (at 23° C), for the 60 mm cover samples as an example, increasing the water-curing period from 3 to 28 days resulted in an extension of the cracking times by approximately 10%. Extending the cold-air curing period (at 3-5° C) from 21 to 28 days was found to decrease the cracking times by nearly 6% (in 60 mm cover). Moreover, longer heat curing periods (at 50° C) from 1 to 7 days yielded a reduction in the time to cracking by about 15% (in 60 mm samples). It should be noted that the trends obtained from 60 mm cover samples were almost identical in other concrete covers (20, 30, and 40 mm).

As seen in Table 4.10, all samples at the cracking stage had half-cell potential readings less than -350 mV. These high half-cell potentials indicated that corrosion probability is greater than 90%, as per ASTM standard C876. The passing currents, percentages of mass

loss, and chloride contents at cracking stage are also shown in Table 4.10. It is obvious that neither the different curing techniques nor the concrete covers showed significant effects on these measurements.

Table 4.10: Results for the 40 Samples in Non-Severe Corrosion Stage

Prism Sample	Number of Cracks	Maximum Crack Size (mm)	Chloride Content % wt. of Concrete	Mass Loss %	Final Time at Cracking (Days)	Cracking Current (mA)	Cracking Half-Cell (mV)
1-20-1	1	0.3302	0.775	0.85	2	176.5	-600
1-20-2	*	0	0.411	0.00	4.5	82.6	-600
1-20-3	1	0.0635	0.459	0.00	3.5	96.5	-600
1-20-4	2	0.1397	0.358	0.00	3.5	74.1	-600
1-20-5	3	0.1905	0.679	0.00	3	99.8	-600
1-20-6	1	0.0635	0.541	0.00	3	93.1	-600
1-20-7	3	0.2667	0.655	0.42	3	173.7	-600
1-20-8	1	0.1397	0.628	0.00	2.5	138.2	-580
1-20-9	1	0.2413	0.662	0.00	2	169.1	-600
1-20-10	2	0.1651	0.695	0.00	2	123	-610
1-30-1	1,*	0.2032	0.609	0.00	8	47.7	-463
1-30-2	1	0.3556	0.7	0.00	12	90.3	-523
1-30-3	1	1.0795	1.5	0.69	11	187.2	-514
1-30-4	1	0.1778	0.6	0.46	11	67	-532
1-30-5	1	0.445	0.921	11.16	10	120.3	-566
1-30-6	2	0.47	0.846	0.47	9	87.5	-561
1-30-7	2	0.548	1.185	0.93	9	170.3	-570
1-30-8	*	N/A	0.3	0.69	6.5	58.2	-445
1-30-9	4	0.2032	0.523	0.00	6.5	91.1	-610
1-30-10	1	0.5969	0.554	0.46	6.5	127.6	-590
1-40-1	1	0.1524	0.339	0.00	15.5	32.5	-400
1-40-2	1	0.1143	0.21	0.52	24.5	52.8	-455
1-40-3	1	0.9525	0.396	1.04	22.5	78.8	-475
1-40-4	1	0.612	0.367	0.52	23	73.6	-490
1-40-5	1	0.5842	0.278	1.55	22	73	-551
1-40-6	1	0.7239	0.364	1.55	21	120.6	-534
1-40-7	3	0.28194	0.515	0.52	20	49.3	-490
1-40-8	*	N/A	0.094	0.00	13	34.6	-445
1-40-9	1	0.3302	0.688	0.52	11	86	-534

1-40-10	1	0.6731	0.943	1.04	10	118.6	-507
1-60-1	3	0.53	0.182	0.68	25	54.2	-520
1-60-2	4	1.143	0.364	2.72	65	90.2	-538
1-60-3	2	0.889	0.175	1.36	58	77.5	-560
1-60-4	4	1.0287	0.14	2.03	63	77	-502
1-60-5	3	0.432	0.148	1.37	51	52.1	-510
1-60-6	3	1.0795	0.27	3.33	49	100.9	-585
1-60-7	1	0.3429	0.291	0.68	48	54.4	-582
1-60-8	*	N/A	0.161	0.34	27	30.3	-363
1-60-9	1	1.016	0.178	0.00	24	44.8	-421
1-60-10	1	0.8382	0.275	1.01	23	44.9	-397

* = Local Corrosion

4.3.4.2 Severe Corrosion Stage

In this stage, the 40 counterpart samples were monitored on a daily basis until obtaining a minimum crack width of 4 mm, which was considered sufficient damage in the sample. At this time, the current, half-cell, chloride content near the bar surface, and mass loss in the rebar were measured. The results of these measurements are described in Table 4.11.

It is obvious from the table that these 40 samples exhibited longer times at this stage to reach a crack of 4 mm or higher when compared to stage 1. Moreover, the effects of the curing techniques and concrete cover on the total time to damage were identical to the measured times of cracking. However, the differences between the time of cracking and the time of damage showed to be approximately constant for the samples with covers 20, 30, and 40 mm. The average differences of the 20, 30, and 40 mm cover samples were 8, 9, and 11 days, which may be considered not significant. As a result, the length of the times of damage for these samples showed exactly the same trend as that of the cracking times. Finally, the 60 mm samples had relatively higher differences, as the average difference of these ten samples was 26 days. These results were attributed to the fact that

at the stage of damage the effect of concrete resistivity was not a factor since the cracks are already open for chlorides to reach the reinforcing bars. However, the relatively high difference that occurred in the 60 mm samples may be because some of the 20, 30, and 40 mm samples had reached a complete break in the sample before achieving a crack of 4 mm, which did not occur in any of the 60 mm cover samples.

The effect of the curing period on the damage times was found to be similar to that on the cracking times across all curing techniques. However, this effect showed to be slightly lower at the damage stage than at the cracking stage. For instance, when the water-curing period (at 23° C) was changed from 3 to 28 days, in 60 mm cover as an example, the measured times to damage increased by nearly 3%. On the other hand, increasing the cold-air curing (at 3-5° C) from 21 to 28 days and the heat curing (at 50° C) from 1 to 7 days resulted in a reduction in the damage periods by almost 3%. These results may also be attributed to the increasing width of cracks at this stage, which minimized the contribution of the concrete resistivity.

Tables 4.10 and 4.11 also show that higher chloride contents, higher passing currents, and higher percentage of mass loss existed at the damage stage. These higher values were expected owing to the effect of cracks, which are present at severe corrosion stage. It should again be noted that the first damaged samples were ones cured with technique 10 (7-days heat), while the last samples were cured using technique 2 (28-days water). Furthermore, neither the concrete cover nor the curing techniques showed any effect on the values of the chloride contents and percentages of mass loss at damage stage. However, the increase of the concrete cover from 20 to 60 mm resulted in a slight decrease of the passing currents and half-cell potentials at damage.

Table 4.11: Results for the 40 Samples in Severe Corrosion Stage

Prism Sample	Number of Cracks	Maximum Crack Size (mm)	Chloride Content at Damage %	Mass Loss at Damage %	Final Time at Damage (Days)	Damage Current (mA)	Damage Half-Cell (mV)
2-20-1	Broken	N/A	0.926	14.04	11	1830	-552
2-20-2	Broken	N/A	1.224	11.86	14	3020	-448
2-20-3	Broken	N/A	0.725	5.08	12.5	1990	-587
2-20-4	1	4	0.919	4.21	13.5	930	-523
2-20-5	1	4	0.884	8.47	12	360	-508
2-20-6	1	4	0.689	5.08	11	970	-444
2-20-7	1	4	0.825	9.75	10	3100	-628
2-20-8	1	4	0.625	3.81	10	440	-437
2-20-9	Broken	N/A	1.026	10.17	9	3720	-547
2-20-10	1	4	1.248	5.51	9	510	-509
2-30-1	Broken	N/A	1.606	8.62	17	860	-491
2-30-2	Broken	N/A	1.899	9.56	22.5	2800	-497
2-30-3	1	5	1.503	8.62	21.5	1360	-537
2-30-4	1	6	1.787	10.02	22	1690	-497
2-30-5	Broken	N/A	1.685	10.02	19	1200	-600
2-30-6	1	5	1.341	7.69	18	1670	-424
2-30-7	1	5	0.636	3.50	17	980	-462
2-30-8	Broken	N/A	2.065	10.96	15	1210	-450
2-30-9	1*	9	1.56	9.56	14	2340	-459
2-30-10	1	9	1.168	9.09	12	500	-332
2-40-1	3	4	1.035	12.21	26	930	-387
2-40-2	Broken	N/A	0.538	8.57	36	510	-496
2-40-3	2	4.5	0.727	6.22	33	525	-426
2-40-4	3	4	1.37	10.13	34	520	-136
2-40-5	2	8	0.974	11.17	32	785	-366
2-40-6	3	4	0.964	13.25	31	500	-241
2-40-7	2	4	0.866	16.36	29	470	-446
2-40-8	Broken	N/A	1.184	6.49	26	3350	-495
2-40-9	Broken	N/A	1.411	10.13	25	199	-413
2-40-10	1	7	1.046	9.09	24	286	-321
2-60-1	4	4.2	0.285	3.73	67	108.5	-350
2-60-2	4	4	0.502	15.25	76	86	-285
2-60-3	2	4.5	0.695	15.93	74	65.4	-350
2-60-4	4	4	0.351	14.58	75	174.4	-504
2-60-5	5	6	0.508	17.29	70	650	-505

2-60-6	4	4	0.471	22.37	69	139.5	-327
2-60-7	5	6	0.971	13.22	68	1220	-548
2-60-8	2	4	0.641	39.66	65	76.2	-385
2-60-9	1	5	0.712	38.31	65	66.3	-375
2-60-10	3	4	0.578	43.05	63	56.9	-326

* Almost Broken

4.3.4.3 Corrosion Initiation Times

The current and half-cell relationships were used to detect the corrosion initiation. Figure 4.26 demonstrates the general trend for the current versus time and half-cell potentials versus time relationships, for sample number 1-60-2, as an example. The time of "corrosion initiation" was detected at the point of the jump (sudden increase) in the current reading. It is clear that the corrosion started just after reaching a minimum value of the passing current (21.2), and a sudden increase can then be seen after this point from the top part of Figure 4.26. This point was also evaluated based on the reading of the half-cell potential test (-352). The half-cell readings indicate a greater than 90% probability that reinforcing steel corrosion is occurring, if the measured potentials for the sample are less than −350 mV.

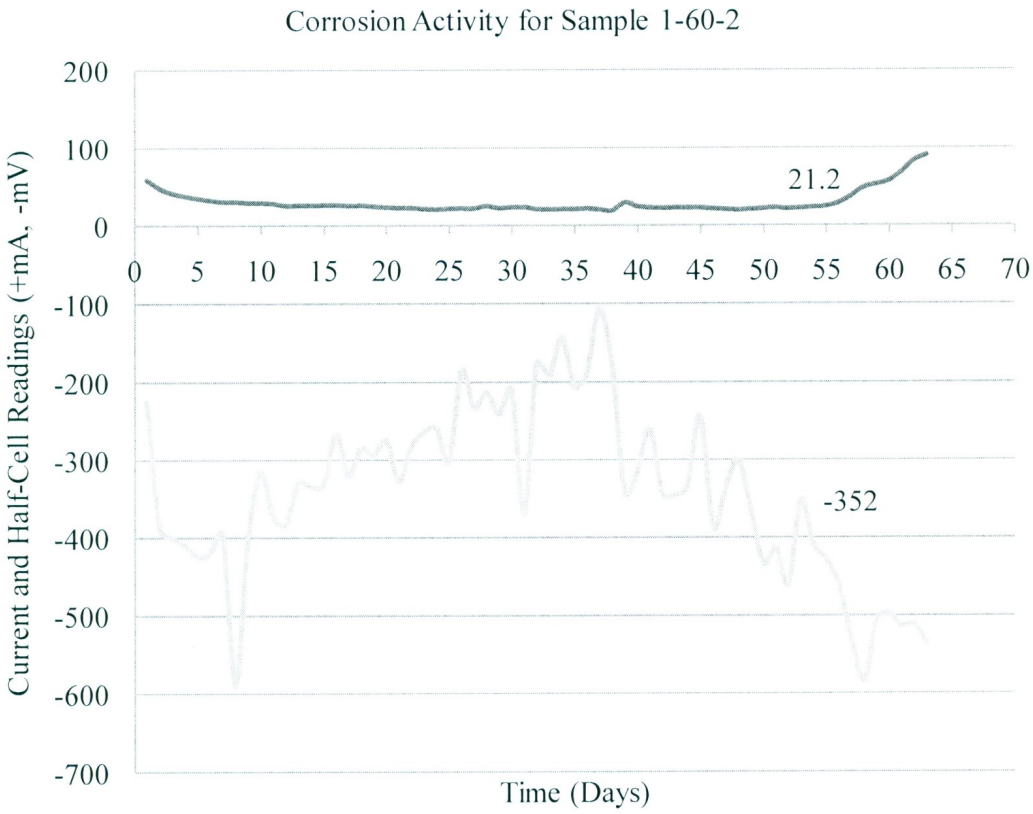

Figure 4.26: Time versus Current and Half-Cell Relationships for Sample 1-60-2

By reviewing the current and half-cell readings, the initiation of corrosion was identified for each sample from 1-20-1 to 1-60-10 and recorded, as demonstrated in Table 4.12. The table also demonstrates the currents and half-cell potentials associated with corrosion initiation of each sample. It should be noted that almost identical trends were obtained from both current and half-cell measurements versus time for the samples tested at stage 2 before reaching the severe corrosion.

Table 4.12: Corrosion Initiation Times for the 40 Samples in Non-Severe Corrosion Stage

Prism Sample	Chloride Diffusion Coefficient D_a (m^2/sec)	Initiation Time (Days)	Initiation Current (mA)	Initiation Half-Cell (mV)
1-20-1	1.50 E-11	1	67.8	-553
1-20-2	7.52 E-12	2	65.7	-557
1-20-3	8.86 E-12	2	64.8	-536
1-20-4	1.15 E-11	2	58.9	-550
1-20-5	7.89 E-12	1.5	77.35	510
1-20-6	7.85 E-12	1.5	74.3	-484
1-20-7	9.62 E-12	1	73.8	-537
1-20-8	1.22 E-11	1.5	80	-498
1-20-9	1.5 E-11	1	83.4	-562
1-20-10	1.8 E-11	1	77.8	-585
1-30-1	1.50 E-11	4	31.3	-504
1-30-2	7.52 E-12	6	42.1	-511
1-30-3	8.86 E-12	5	42.7	-502
1-30-4	1.15 E-11	5	39	-539
1-30-5	7.89 E-12	6	50.8	-492
1-30-6	7.85 E-12	5	47.8	-480
1-30-7	9.62 E-12	5	44.6	-511
1-30-8	1.22 E-11	5	51.8	-514
1-30-9	1.5 E-11	4	58.1	-507
1-30-10	1.8 E-11	3	61.2	-540
1-40-1	1.50 E-11	12	22	-362
1-40-2	7.52 E-12	20	32.2	-398
1-40-3	8.86 E-12	18	31.8	-400
1-40-4	1.15 E-11	19	31.8	-411
1-40-5	7.89 E-12	16	38.5	-432
1-40-6	7.85 E-12	14	33.6	-377
1-40-7	9.62 E-12	12	34	-400
1-40-8	1.22 E-11	10	41.1	-410
1-40-9	1.5 E-11	8	41.7	-510
1-40-10	1.8 E-11	7	40.8	-480
1-60-1	1.50 E-11	25	19.3	-440
1-60-2	7.52 E-12	53	21.9	-352
1-60-3	8.86 E-12	50	16.6	-377
1-60-4	1.15 E-11	52	21.1	-350
1-60-5	7.89 E-12	46	21.7	-401

1-60-6	7.85 E-12	43	24.5	-392
1-60-7	9.62 E-12	42	19.4	-357
1-60-8	1.22 E-11	21	28.1	-404
1-60-9	1.5 E-11	20	27.8	-357
1-60-10	1.8 E-11	18	29.3	-355

These results showed a minimum initiation period of 1 day associated with samples 1-20-1, 1-20-7, and 1-20-10, which had the minimum concrete cover along with high chloride permeability. On the other hand, the maximum period of 53 days was obtained from sample 1-60-2 with 60 mm cover, as expected. This sample had a superior performance owing to the minimum chloride permeability along with the biggest concrete cover, which increased the resistance to corrosion. The concrete cover significantly affected the corrosion initiation times, as expected, because it provided resistance to corrosion (Vu et al. 2000). For instance, the 20 mm cover had an average initiation period of 3 days versus 9, 18, and 43 days for 30, 40, and 60 mm covers, respectively (see Table 4.12).

On the other hand, different initiation times were warranted for each curing technique associated with a certain concrete cover. It is obvious from Table 4.12 that minimum initiation periods were obtained from curing regime 10 (heat curing at 50° C). The maximum initiation periods were seen in samples cured using technique 2 (water curing at 23° C). It is also clear that normal water-cured samples (techniques 2, 3, and 4) had the maximum times to corrosion, higher than both cold air- cured (techniques 5, 6, and 7) and heated water-cured (techniques 8, 9, and 10) samples. In addition, the normal temperature air-cured sample at 23° C (technique 1) had longer initiation periods than all heated water-cured samples. However, the differences among the normal water-cured, cold air-cured, and heated water-cured samples were not significant. These differences ranged

from 50 to 53 days, 42 to 46 days, and 18 to 21 days for normal water cured, cold air-cured, and heated water-cured samples, respectively, for 60 mm cover as an example. These results showed that increasing the water-curing period from 3 to 28 days (at 23° C) increased the initiation times by approximately 6%. On the contrary, increasing the cold air curing times (at 3-5° C) from 21 to 28 yielded a 9% reduction in the corrosion initiation times. Moreover, extending the heat-curing periods (at 50° C) from 1 to 7 was found to minimize the corrosion initiation times by almost 15%. These ranges were attributed to the fact that these samples in water, cold, and heat curing had almost the same chloride permeability, which represented the resistivity to rebar corrosion.

4.3.4.4 Comparison of Corrosion Initiation Times from Fick's Law

The corrosion initiation periods obtained from the accelerated corrosion test are compared to the expected periods using Fick's law of diffusion. The assumptions and procedures are similar to those previously mentioned in section 4.2.3 (second stage of the study). For simplifying the comparison, only 60 mm cover samples were included in this evaluation.

To be able to compare between the accelerated corrosion test and the predicted values from Fick's law, the results were normalized as a percentage of the maximum period obtained from sample 1-60-2. The results from the accelerated corrosion test are described as a percentage of days with respect to sample 1-60-2, while the results from Fick's law are shown as a percentage of years with respect to sample 1-60-2 (Figure 4.27). It is obvious from Figure 4.27 that the differences between both methods of prediction (accelerated corrosion versus Fick's law) were almost non-significant. Finally,

it should be noted that the accelerated corrosion test method showed to be more practical than other models for service life time prediction.

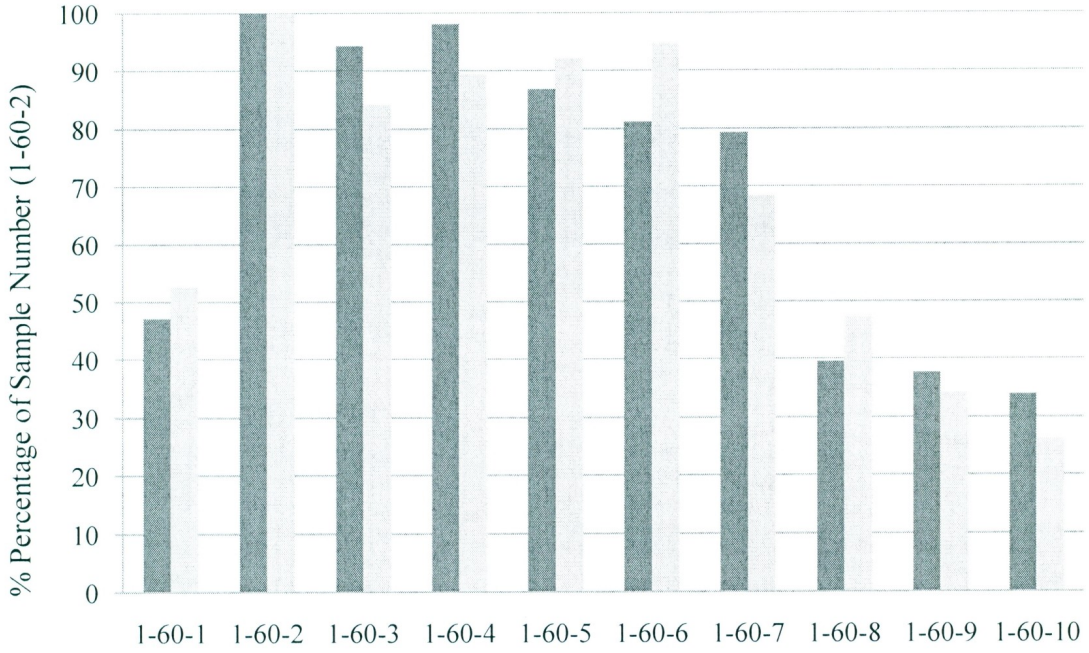

Figure 4.27: Initiation Periods from Fick's Law and Accelerated Corrosion Test for the 60 mm Cover Samples

5. Conclusions and Recommendations

The research program presented in this thesis was implemented throughout three successive experimental investigations divided into three stages. These stages included testing the strength and durability of mortars incorporating different SCM's, optimizing an HPSCC mixture containing MK, and testing corrosion of reinforcing steel resistance and service life time predictions of HPSCC mixtures. The analysis and discussion of the results from each stage were completed and the following conclusions were drawn:

5.1 Strength and Durability of Mortars Containing Different SCM's

- MK mortar mixture exhibited the maximum pozzolanic activity (compressive strength) after 7 days (14.5 MPa), followed by SF, SG, FA, and SB, respectively.
- 10% SB <20 μm mixture was the only SB mixture (among the four grain sizes tested SB samples) that fulfilled a strength greater than 5.5 MPa after 7 days (6.83 MPa) as per CSA A3004-E1 standard.
- Grinding SB to a finer particle size (from <75 to <20 μm) greatly improved the pozzolanic activity and slightly enhanced the durability performance of the sample.
- All SB samples (SB <75, <40, <30, and <20 μm) showed higher expansions in the alkali-silica reactivity and sulfate resistance tests compared to 30% FA, 20% MK, 30% SG, and 8% SF samples. However, 10% SB <30 μm showed lower expansion than the control mixture in both alkali-silica reactivity and sulfate resistance tests.

- All mortar mixtures (20% MK, 30% FA, 8% SF, 10% SB, and 30% SG) tested in the alkali-silica reactivity test had expansions higher than the maximum allowed expansion (0.1%) specified in CSA A23.2-25A after 14 days, except those with 20% MK and 30% FA.
- All mortar mixtures (20% MK, 30% FA, 8% SF, 10% SB, and 30% SG) tested in the sulfate resistance test had expansions lower than the maximum allowed expansion (0.1%) specified in CSA A3004-C8 after 8 months.
- The optimum strength and durability mixture among all tested mortar mixtures (20% MK, 30% FA, 8% SF, 10% SB, and 30% SG) was the 20% MK mixture. However, the 30% FA mixture had comparable durability to the 20% MK mixture, which exhibited approximately the same expansions as the 20% MK mixture in both alkali-silica reactivity and sulfate resistance tests.

5.2 Optimizing HPSCC Mixture Using Statistical Analysis (CCD Method)

- The effects of the three variables (binder content, water-to-binder ratio, and MK replacement) were all found to significantly affect the fresh, hardened, and durability properties and the expected service life times of HPSCC mixtures.
- The effects of the three tested variables were almost linear for the fresh properties tests; however, for the compressive strength and chloride permeability tests their effects were completely nonlinear.
- The increase in the binder content (420-480 kg/m^3) in the HPSCC mixtures resulted in decreasing the HRWRA demand, mixture viscosity, chloride

permeability; and in increasing the passing and flowing ability, segregation resistance, 28-days compressive strength, and the expected service life time.

- Increasing the water-to-binder ratio (0.37-0.43) in the tested mixtures showed an increase in the passing and flowing ability, segregation resistance, and chloride permeability; and a reduction in the HRWRA demand, mixture viscosity, 28-days compressive strength, and the expected service life time.
- Incorporating MK as a replacement of cement (5-20%) increased the HRWRA demand, mixture viscosity, passing and flowing ability, segregation resistance, 28-days compressive strength, and the expected service life time. In addition, this replacement decreased the chloride permeability of HPSCC, which resulted in obtaining higher predicted service life times.
- Different curing techniques had a significant effect on the compressive strength, chloride permeability, and the expected service life time of HPSCC mixtures. Water-cured samples had higher 28-days compressive strength, higher expected service life time, and lower chloride permeability than their air-cured counterparts.
- All tested mixtures exhibited a significant decrease in the RCPT values from 28 days to 180 days for both air and water curing systems.
- An optimum HPSCC mixture that can maintain the required balance between fresh properties, 28-days compressive strength, chloride permeability, and expected service life times showed to contain a total binder of 490 kg/m^3, a water-to-binder ratio of 0.39, and a replacement of MK by 19.9%.

- The developed statistical models can be used as a useful tool to evaluate different HPSCC mixtures containing MK. Testing the validated mixture showed results that almost matched the same results predicted from these models.
- The relationship between the RCPT values and chloride diffusion coefficients was almost linear in all air- and water-cured samples for all tested HPSCC containing MK and for HPSCC containing different SCM's.
- Comparing the optimum HPSCC mixture containing MK to those containing FA, SF, and SG showed that the MK mixture exhibited the lowest chloride permeability, highest HRWRA demand, highest viscosity, highest flowing and passing ability, highest segregation resistance, highest 28-days compressive strength, and longest service life time.
- The trapped air contents measured in all tested mixtures (NC and HPSCC) ranged from 0.9 to 3.3; however, no feasible relationships between the studied factors (binder content, water-to-binder ratio, and MK replacement) and the air contents were obtained.
- Increasing the coarse aggregate size in NC mixtures resulted in a reduction in the 28-days compressive strength; and an increase in the slump and chloride permeability/diffusion of NC mixtures.
- Based on comparing the 28-days compressive strength and chloride permeability of different SCM's in HPSCC and NC mixtures, the optimum mixtures can be defined as 20% MK and followed by 8% SF, 30% FA, 30% SG, NC1, and NC2, respectively.

5.3 Corrosion of Steel Reinforcement Resistance and Service Life Time Prediction

- For all curing techniques (air, water, cold, and heat curing), increasing the clear concrete cover resulted in longer periods for chlorides to penetrate through the cover reaching the embedded bars and eventually in longer times for corrosion initiation, cracking, and damage.
- The use of longer periods of water curing (at 23° C) decreased the chloride permeability and increased the time to corrosion obtained from both the accelerated corrosion test and Fick's second law of diffusion.
- Applying cold-air curing (at 3-5° C), and heated-water curing (at 50° C) for longer periods maximized the chloride permeability, reduced the 28-days compressive strength, and decreased the corrosion initiation, cracking, and damage periods.
- The water curing for a period of 28 days (at 23° C) proved to be the best curing system (compared to air, cold, and heat curing) in terms of compressive strength, chloride permeability, and corrosion resistance. The 28-days water-cured samples (curing technique 2) had the longest times to showing signs of corrosion initiation, cracking, and damage among all tested samples.
- The first samples that showed corrosion initiation, cracking, and damage were those cured in heated water for 7 days at 50° C (curing technique 10) in all values of concrete covers.
- Increasing the water curing period from 3 to 28 days (at 23° C) in techniques 2, 3, and 4, regardless of the concrete cover thickness, increased the corrosion

initiation, cracking, and damage times by approximately 6%, 10%, and 3%, respectively.

- The increase in the cold air curing times (at 3-5° C) from 21 to 28 days in techniques 5, 6, and 7 for all tested concrete covers yielded a reduction of the corrosion initiation, cracking, and damage times by about 9%, 6%, and 3%, respectively.
- Extending the heat curing periods (at 50° C) from 1 to 7 days in techniques 8, 9, and 10 for all 20, 30, 40, and 60 mm cover samples was found to reduce the corrosion initiation, cracking, and damage times by almost 14%, 15%, and 3%, respectively.
- The trend of the results of the corrosion initiation periods obtained from the accelerated corrosion test was similar to that obtained from Fick's second law of diffusion for counterpart samples.
- A linear relationship was warranted between the electrical current measurements and the half-cell potential values in the accelerated corrosion test in all samples.
- The corrosion initiation was found to occur at a half-cell potential reading of -350 mV, as shown during the accelerated corrosion experiments.
- The differences between the trends of the two methods of service life time prediction (accelerated corrosion versus Fick's law) were almost non-significant.
- The accelerated corrosion test method showed to be more practical than other models for service life time prediction.

5.4 Recommendations for Future Research

It is recommended to test the effect of the HRWRA dose/type on the fresh properties of HPSCC mixtures. It is also recommended to consider the comparison between the optimum MK mixture and the other SCM's at different levels of replacement. Finally, testing full-scale elements in the accelerated corrosion test is essential in evaluating the service life times.

References

ASTM C39-01, "Standard Test Method for Compressive Strength of Cylindrical Concrete Specimens." *ASTM International*, West Conshohocken (2001).

ASTM C109-11a, "Standard Test Method for Compressive Strength of Hydraulic Cement Mortars (Using 2-in. or [50-mm] Cube Specimens)." *ASTM International*, West Conshohocken (2011).

ASTM C157-08, "Standard Test Method for Length Change of Hardened Hydraulic-Cement Mortar and concrete." *ASTM International*, West Conshohocken (2008).

ASTM C230-08, "Standard Specification for Flow Table for Use in Tests of Hydraulic Cement." *ASTM International*, West Conshohocken (2008).

ASTM C231-10, "Standard Test Method for Air Content of Freshly Mixed Concrete by the Pressure Method." *ASTM International*, West Conshohocken (2010).

ASTM C876-91, "Standard Test Method for Half-Cell Potentials of Uncoated Reinforcing Steel in Concrete." *ASTM International*, West Conshohocken (1991).

ASTM C1202-97, "Standard Test Method for Electrical Indication of Concrete's Ability to Resist Chloride Ion Penetration." *ASTM International*, West Conshohocken (1997).

ASTM C1556-11a, "Standard Test Method for Determining the Apparent Chloride Diffusion Coefficient of Cementitious Mixtures by Bulk Diffusion." *ASTM International*, West Conshohocken (2011).

ASTM C1611-09be1, "Standard Test Method for Slump Flow of Self-Consolidating Concrete." *ASTM International*, West Conshohocken (2009).

ASTM C1621-09b, "Standard Test Method for Passing Ability of Self-Consolidating Concrete by J-Ring." *ASTM International*, West Conshohocken (2009).

Assaad, J., and Khayat, K. H., "Kinetics of Formwork Pressure Drop of Self-Consolidating Concrete Containing Various Types and Contents of Binder." *Cement and Concrete Research* 35 (2005): 1522-1530.

Bentz, E. C., and Thomas, M. D. A., "Life-365 ^{TM} Service Life Prediction Model ^{TM} and Computer Program for Predicting the Service Life and Life-Cycle Cost of Reinforced Concrete Exposed to Chlorides." Version 2.1, January 7, 2012, User Manual.

Boddy, A. M., Bentz, E. C., Thomas, M. D. A. and Hooton, R. D. "An Overview and Sensitivity Study of a Multi-Mechanistic Chloride Transport Model." *Cement and Concrete Research* 29 (1999): 827-837.

Boddy, A. M., Hooton, R. D., and Thomas, M. D. A., "The Effect of Product Form of Silica Fume on its Ability to Control Alkali Silica Reaction." *Cement and Concrete Research* 30 (2000): 1139-1150.

Boddy, A. M., Hooton, R. D., and Gruber, K. A., "Long-Term Testing of the Chloride Penetration Resistance of Concrete Containing High Reactivity Metakaolin." *Cement and Concrete Research* (2001): 759-76.

Copeland, L. E., and Bragg, R. H., "Self-Desiccation in Portland Cement Pastes." *Research Department Bulletin RX052*, Portland Cement Association, (1955): 13 pages.

CSA, Canadian Standards Association, "Test Method for Determination of Compressive Strengths." CSA A3004-C2, (2008) Rexdale, Ontario, Canada.

CSA, Canadian Standards Association, "Test Method for Determination of Expansion of Blended Hydraulic Cement Mortar Bars due to External Sulfate Attack." CSA A3004-C8, (2008) Rexdale, Ontario, Canada.

CSA, Canadian Standards Association, "Test Method for Detection of Alkali-Silica Reactive Aggregate by Accelerated Expansion of Mortar Bars." CSA A23.2-25A, (2008) Rexdale, Ontario, Canada.

Ehlen, M. A., Thomas, M. D. A., and Bentz, E. C., "Widely Used Software Helps Assess Uncertainties in Concrete Service Life and Life-Cycle Costs." *ACI Concrete international* (2009): 41-46.

Felekogl, B., Turkel, S., and Baradan, B., "Effect of Water/Cement Ratio on the Fresh and Hardened Properties of Self-Compacting Concrete." *Building and Environment* 42 (2007): 1795-1802.

Gencel, O, Ozel, C., Brostow, W., and Martinez-Barrera, G., "Mechanical Properties of Self-Compacting Concrete Reinforced with Polypropylene Fibers." *Materials Research Innovations* 15.3 (2011): 216-225.

Gonnerman, H. F., and Shuman, E. C., "Flexure and Tension Tests of Plain Concrete." Major Series 171, 209, and 210, *Report of the Director of Research,* Portland Cement Association (1928): 149-163.

Gjørv, O. E., "Durability and Service Life of Concrete Structures." *Proceedings 6, The First fib Congress*, Japan Prestressed Concrete Engineering Association, Tokyo (2002): 1-16.

Guneyisi, E., Gesoglu, M., and Ozbay, E., "Permeation Properties of Self-Consolidating Concretes with Mineral Admixtures." *ACI Materials Journal* 108, (2011): 150-158.

Hassan, A. A. A., Hossain, K. M. A., and Lachemi, M., "Corrosion Resistance of Self-Consolidating Concrete in Full-Scale Reinforced Beams." *Cement & Concrete Composites*, 31 (2009): 29-38.

Hassan, A. A. A., Hossain, K. M. A., and Lachemi, M., "Effect of Metakaolin and Silica Fume on Rheology of Self-Consolidating Concrete."*ACI Materials Journal* 109.6 (2012): 657-664.

Hassan, A. A. A., Hossain, K. M. A., Lachemi, M., "Effect of Metakaolin and Silica Fume on the Durability of Self-Consolidating Concrete." *Cement & Concrete Composites*, V. 34 (2012): 801-807.

Hooton, R. D., Geiker, M. R., and Bentz, E. C., "Effects of Curing on Chloride Ingress and Implications on Service Life." *ACI Materials Journal* 99, (2002): 201-206.

Khatib, J. M., "Metakaolin Concrete at a Low Water to Binder Ratio." *Construction and Building Materials* 22 (2008): 1691-1700.

Khayat, K. H., Manai, K., and Trudel, A., "In Situ Mechanical Properties of Wall Elements Using Self-Consolidating Concrete." *ACI Materials Journal 94* (1997): 491-500.

Khayat, K. H., "Workability, Testing, and Performance of Self-Consolidating Concrete." *ACI Materials Journal* 96 (1999): 346-353.

Khayat, K. H., "Optimization and Performance of Air-Entrained, Self-Consolidating Concrete." *ACI Materials Journal* 97.5 (2000): 526-535.

Khayat, K. H., and Assaad, J., "Air-Void Stability in Self-Consolidating Concrete." *ACI Materials Journal* 99.4 (2002): 408-416.

Khayat, K. H., Assaad, J., and Daczko, J., "Comparison of Field-Oriented Test Methods to Assess Dynamic Stability of Self-Consolidating Concrete." *ACI Materials Journal* 101 (2004): 168-176.

Koehler, E. P., "Aggregates in Self-Consolidating Concrete." PhD Thesis (2007).

Lachemi, M, Hossain, K. M. A., Lambros, V., and Bouzoubaâ, N., "Development of Cost-Effective Self-Consolidating Concrete Incorporating Fly Ash, Slag Cement, or Viscosity-Modifying Admixtures." *ACI Materials Journal* 100 (2003): 419-425.

Lachemi, M., Hossain, K. M. A., and Lambros, V. "Shear Resistance of Self-Consolidating Concrete Beams – Experimental Investigation." *Canadian Journal of Civil Engineering* 32 (2005): 1103-1113.

Larbi, J. A., "Microstructure of the Interfacial Zone around Aggregate Particles in Concrete." *Heron* 38 (1993): 69.

Madandoust, R., and Mousavi, S. Y., "Fresh and Hardened Properties of Self-Compacting Concrete Containing Metakaolin." *Construction and Building Materials* 35 (2012): 752-760.

Martin-Peréz, B., Pantazopoulou, S. J., and Thomas, M. D. A., "Finite Element Modelling of Corrosion in Highway Structures." *Second International Conference on Concrete under Severe Conditions CONSEC '98*, Tromso, Norway, (1998).

Mehta, P. K., "Studies on Blended Portland Cement Containing Santorin Earth." *Cement and Concrete Research* (1981): 507-518.

Mehta, P. K., and Monteiro, P. J. M., "Concrete: Structure, Properties and Materials." 2nd ed. *Prentice Hall* (1993).

Nanthagopalan, P., and Santhanam, M., "Experimental Investigations on the Influence of Paste Composition and Content on the Properties of Self-Compacting Concrete." *Construction and Building Materials* 23 (2009): 3443-3449.

Nokken, M., Boddy, A., Hooton, R. D., and Thomas, M. D. A, "Time Dependent Diffusion in Concrete: Three Laboratory Studies." *Cement and Concrete Research* (2006): 200-207.

Patel, R, Hossain, K. M. A., Shehata, M., Bouzoubaâ, N., and Lachemi, M., "Development of Statistical Models for Mixture Design of High-Volume Fly Ash Self-Consolidating Concrete." *ACI Materials Journal* 101 (2004): 294-302.

Pun, P. C. H., "Influence of Silica Fume on Chloride Resistance of Concrete." M.A.Sc. Thesis (1997), Department of Civil Engineering, University of Toronto.

Russell, H.G., "ACI defines high-performance concrete." *Concrete International* 21 (1999): 56-57.

Sadok, H., Kenai, A., Courard, L., and Darimont, A., "Microstructure and Durability of Mortars Modified with Medium Active Blast Furnace Slag." *Construction and Building Material,* 25 (2011): 1018-1025.

Safiuddin, Md., West, J. S., and Soudki, K. A., "Properties of Freshly Mixed Self-Consolidating Concrete Incorporating Rice Husk Ash as a Supplementary Cementing Material.", *Journal of Construction and Building Materials* (2012): 833-842.

Shamsad, A, "Techniques for Inducing Accelerated Corrosion of Steel in Concrete." *The Arabian Journal for Science and Engineering* (2009): 95-104.

Schmidt, S. R., and Launsby, R. G., "Understanding Industrial Designed Experiments." 4th Edition, M. J. Kiemele, ed., *Air Academic Press*, Colorado Springs, Colo. (1994): 1-48.

Sonebi, M., "Applications of Statistical Models in Proportioning Medium-Strength Self-Consolidating Concrete." *ACI Materials Journal 101* (2004): 339-346.

Su, N., Hsu, K. C., and Chai, H. W., "A Simple Mix Design Method for Self-Compacting Concrete." *Cement and Concrete Research* 31 (2001): 1799-1807.

Sujjavanich, S., Sida, V., and Suwanvitaya, P., "Chloride Permeability and Corrosion Risk of High-Volume Fly Ash Concrete with Mid-Range Water Reducer." *ACI Materials Journal* 102 (2005): 177-182.

The European Guidelines for Self-Compacting Concrete. *European Project Group* (2005).

Trejo, D, and Pillai, R. G., "Accelerated Chloride Threshold Testing: Part I - ASTM A 615 and A 706 Reinforcement." *ACI Materials Journal* (2003): 519-527.

Tuutti, K., "Corrosion of steel in concrete." *Swedish Cement and Concrete Research Institute*, Report No. 4-82. (1982).

Vejmelková, E., Keppert, M., Rovnaníková, P., Ondrácek, M., and Keršner, Z., "Properties of High Performance Concrete Containing Fine-Ground Ceramics as Supplementary Cementitious Material." *Cement and Concrete Composites* 34, (2012): 55-61.

Verbeck, G. J., and Helmuth, R. A., "Structures and Physical Properties of Cement Pastes." Proceedings, Fifth International Symposium on the Chemistry of Cement, V. III, *The Cement Association of Japan*, Tokyo, (1968).

Vu, K. A. T., and Stewart, M. G., "Structural Reliability of Concrete Bridges Including Improved Chloride-Induced Corrosion Models." *Structural Safety*, (2000): 313-333.

Zeljkovic, M, "Metakaolin Effects on Concrete Durability." M.A.Sc. Thesis, Department of Civil Engineering, University of Toronto (2009).

Zhu, W., and Bartos, P. J. M., "Permeation Properties of Self-Compacting Concrete." *Cement and Concrete Research* 33 (2003): 921-926.

Appendix A: Pictures of Alkali-Silica Reactivity Prisms at 14-Days

A1: Control

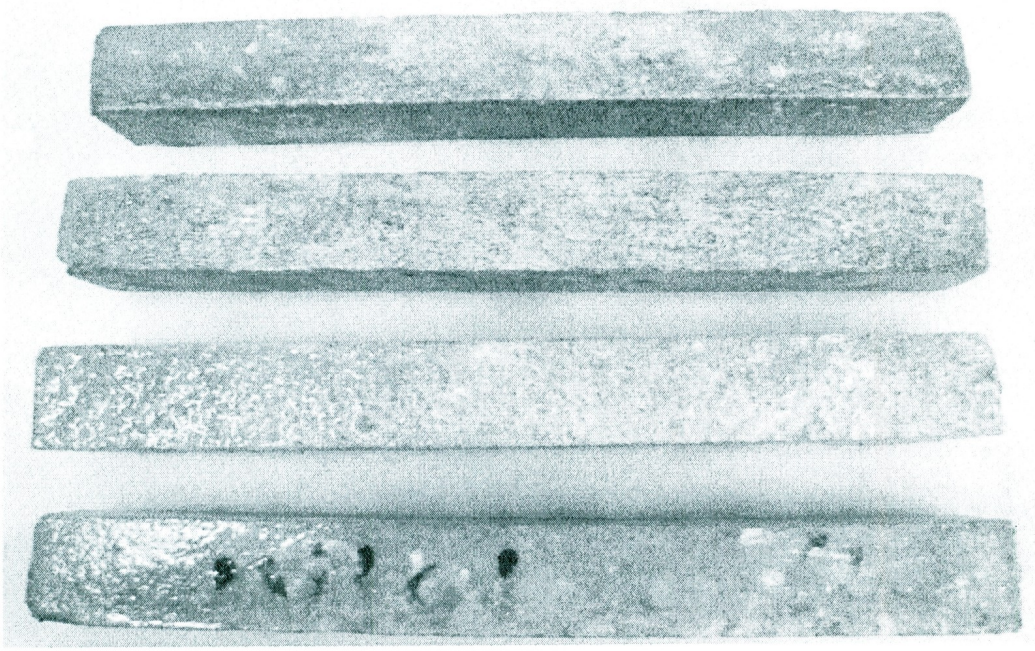

A2: FA

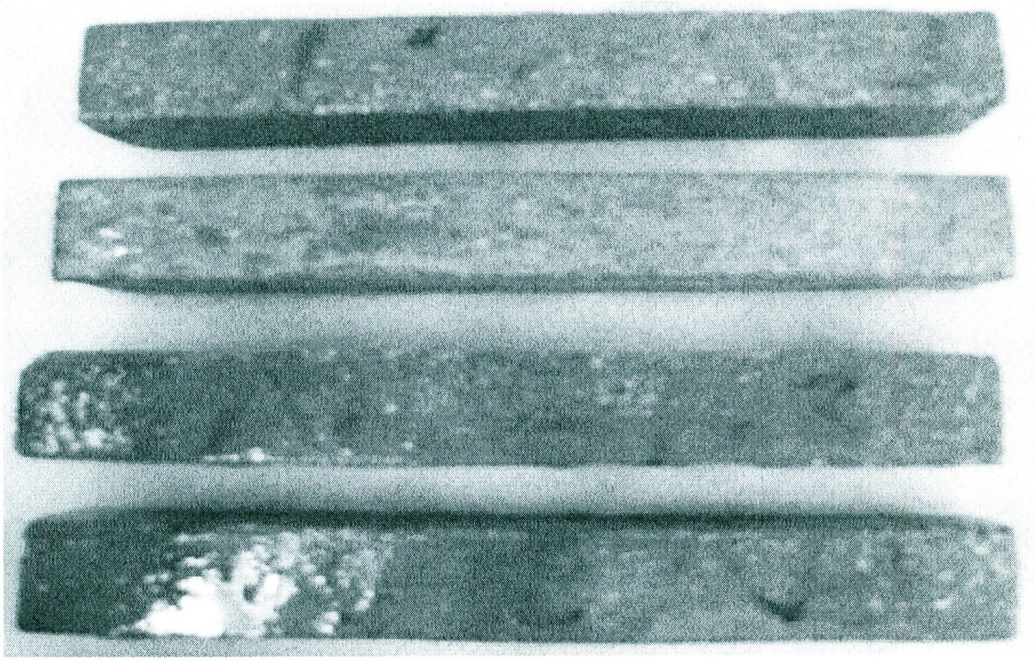

A3: MK

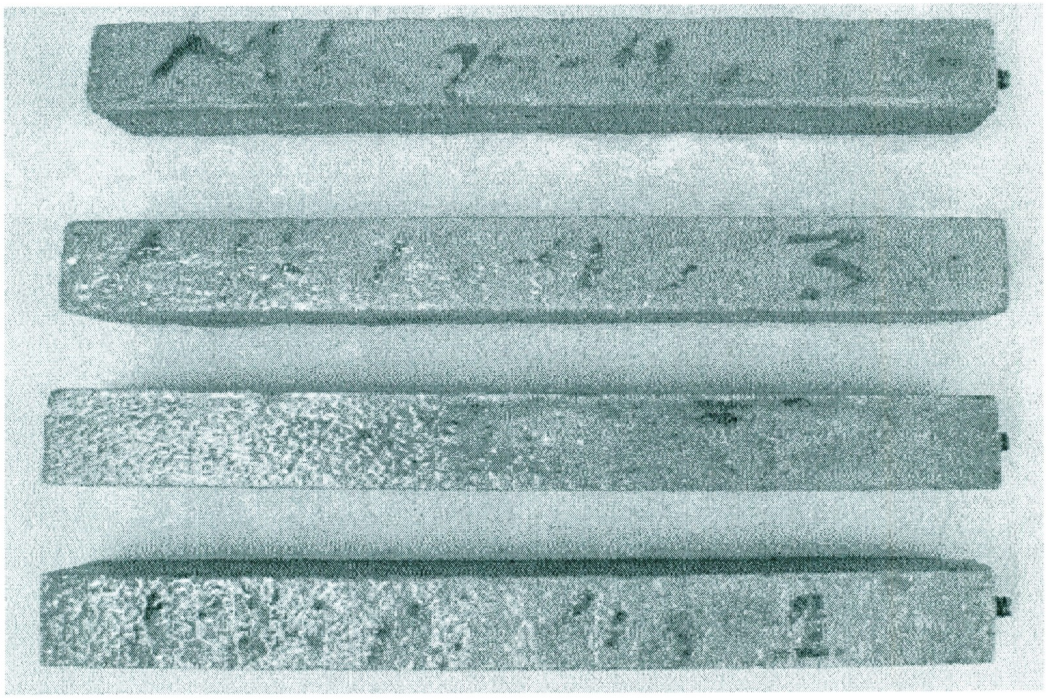

A4: SG

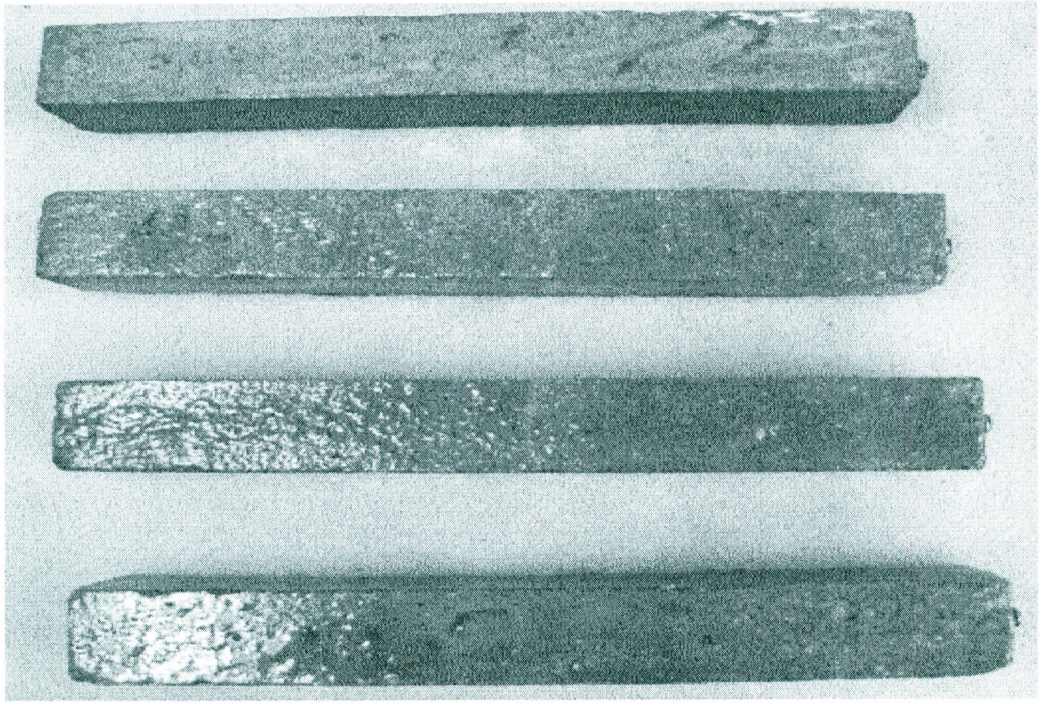

A5: SF

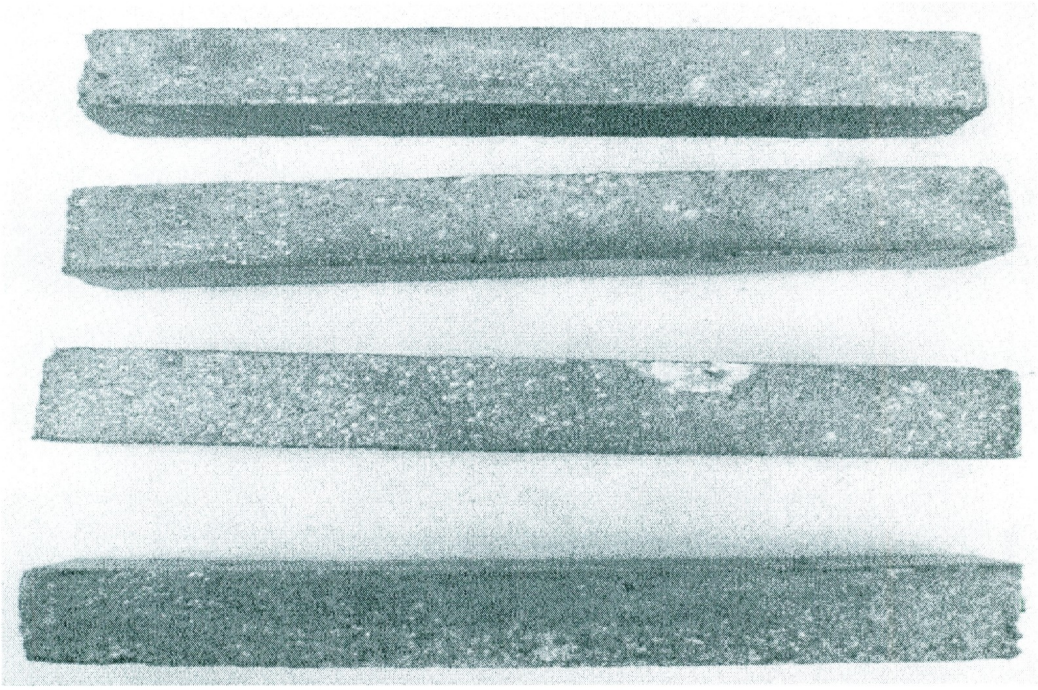

A6: SB <20 µm

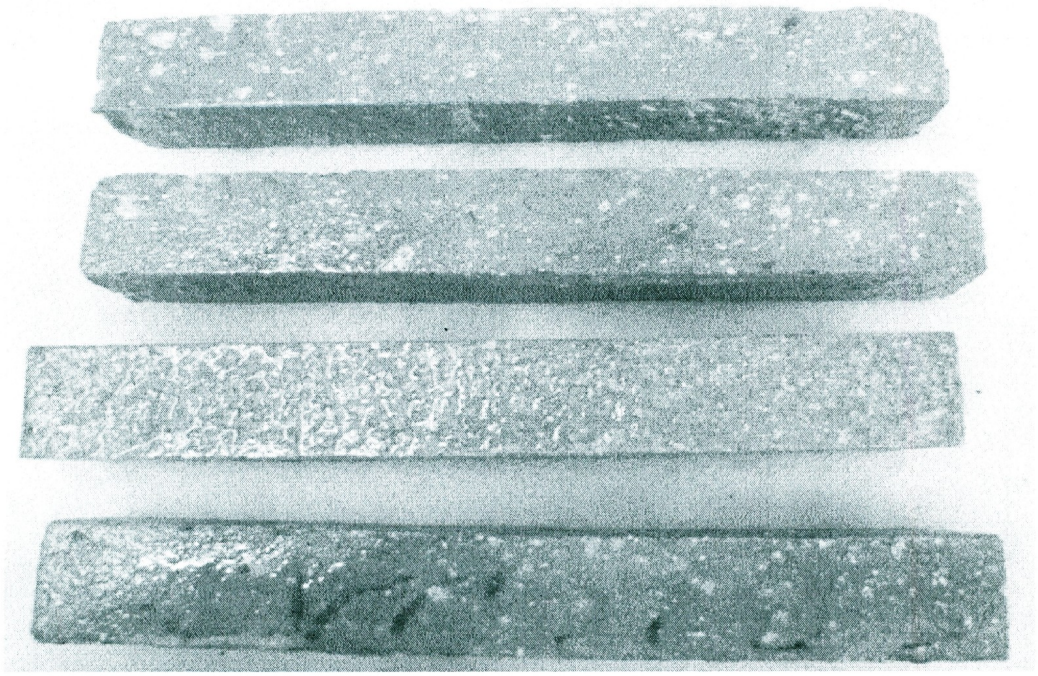

A7: SB <30 µm

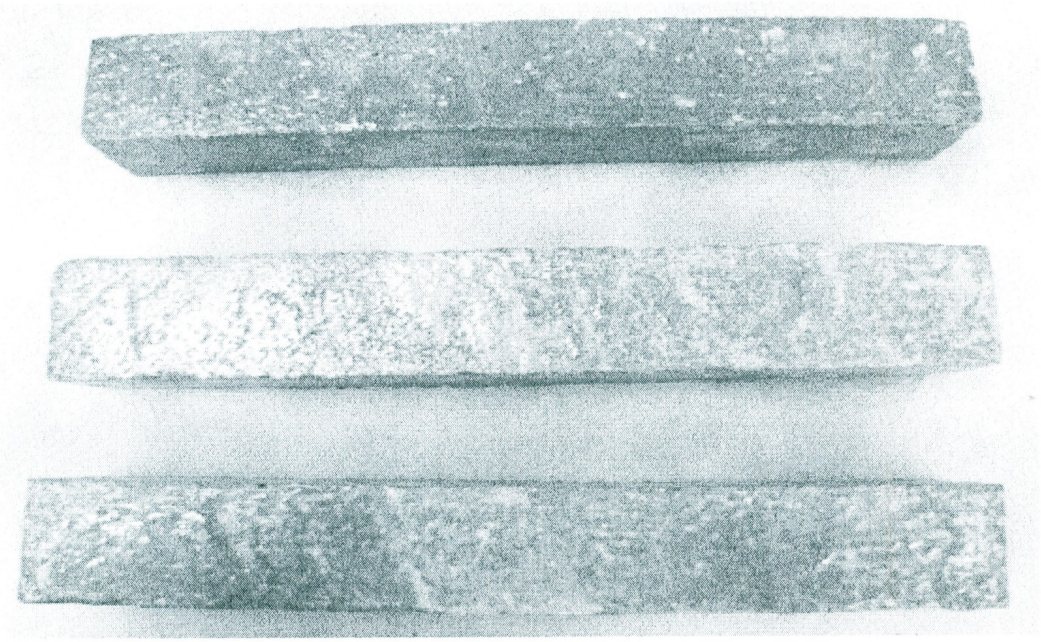

A8: SB <45 µm

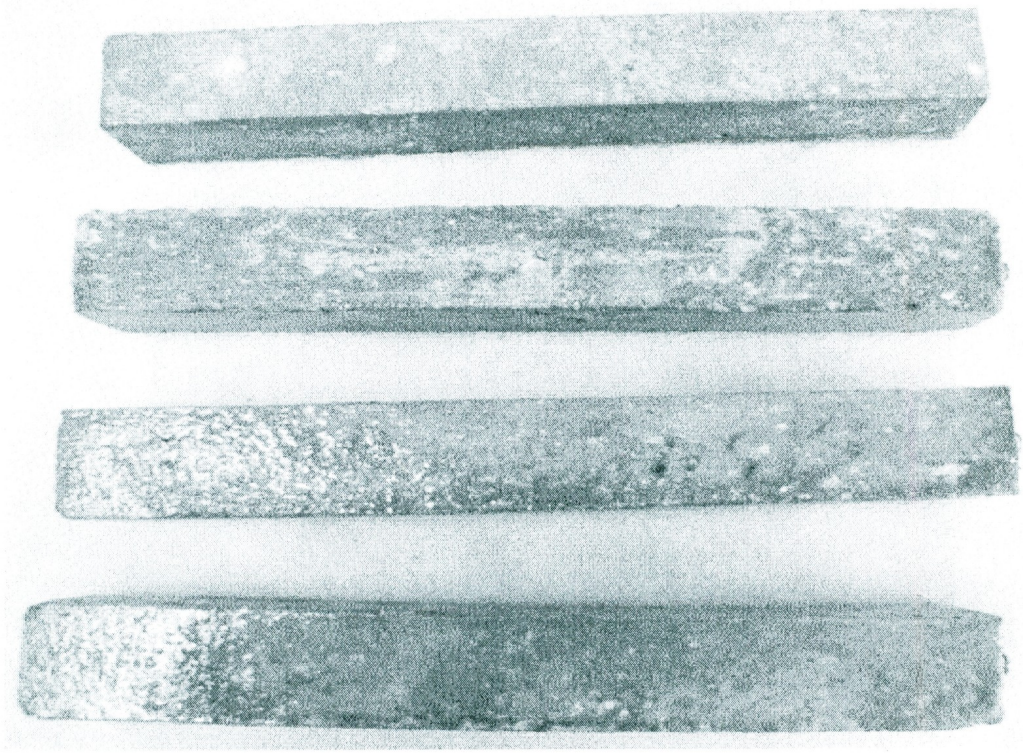

A9: SB <75 µm

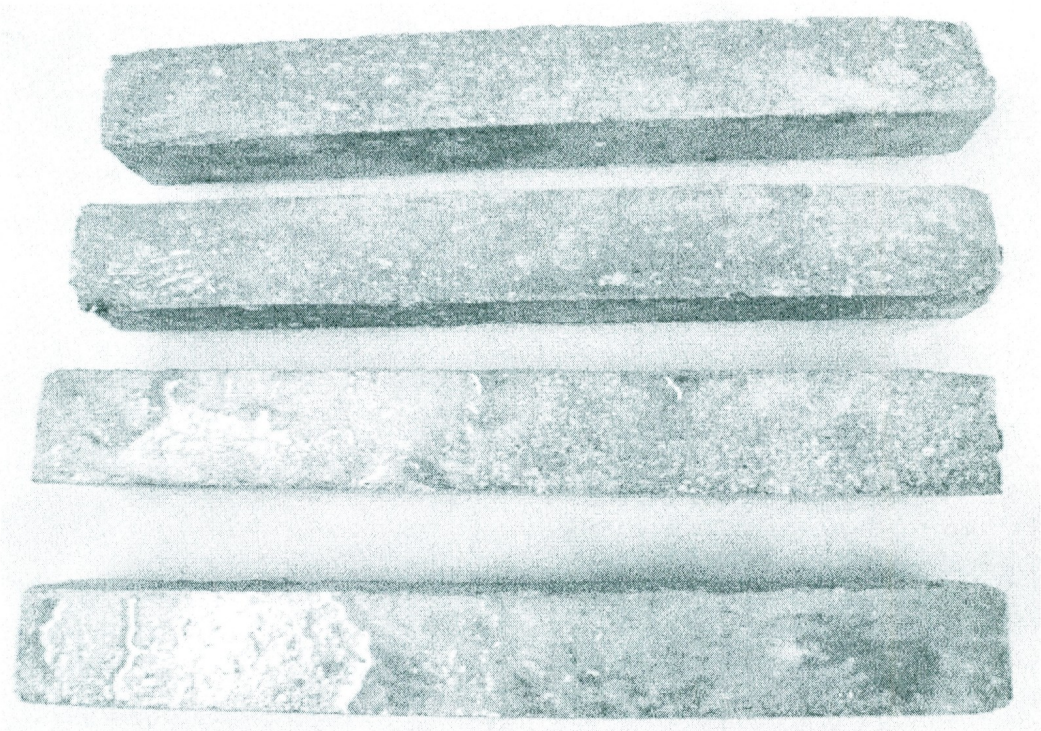

Appendix B: Pictures of Sulfate Resistance Prisms at 8-Months

B1: Control

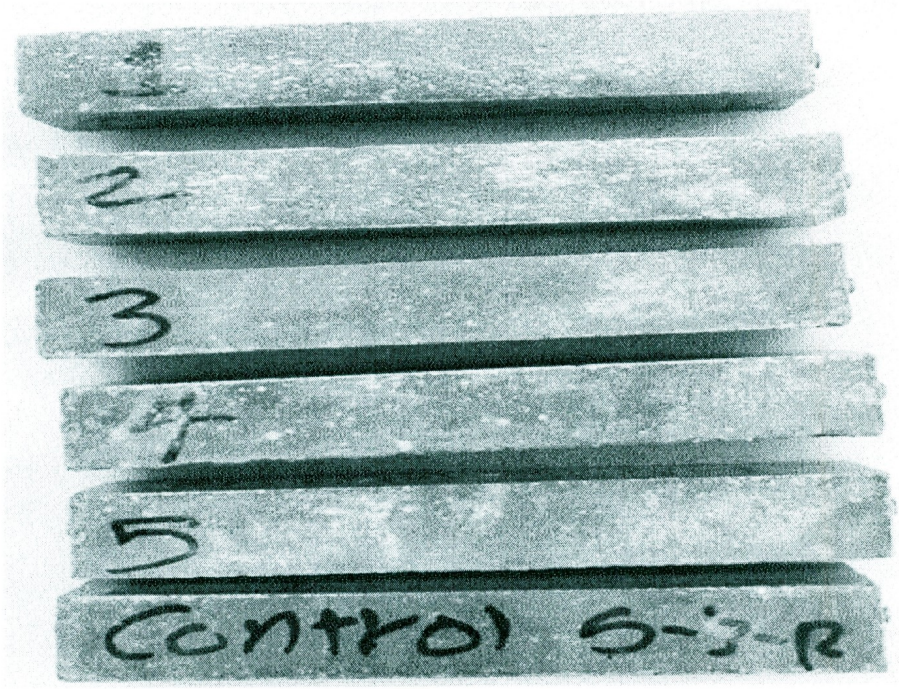

B2: FA

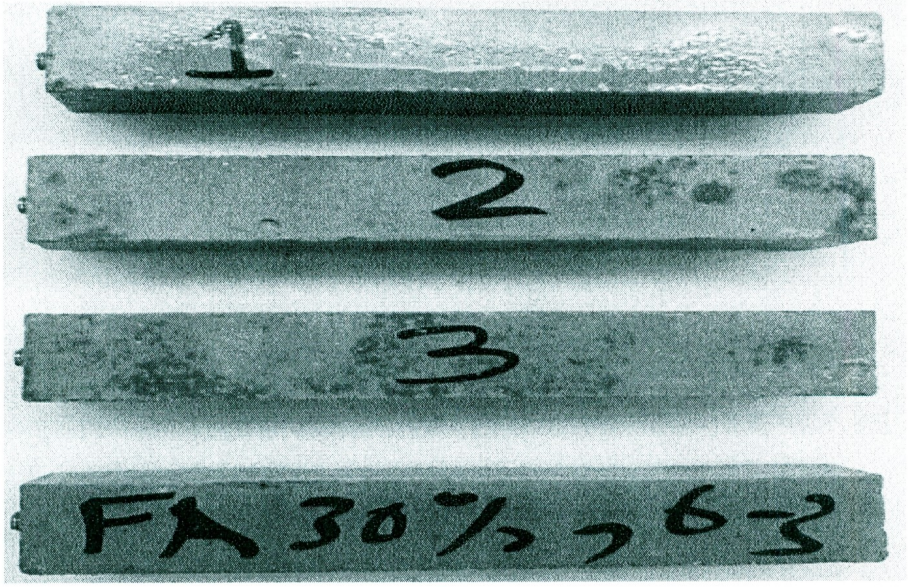

B3: MK

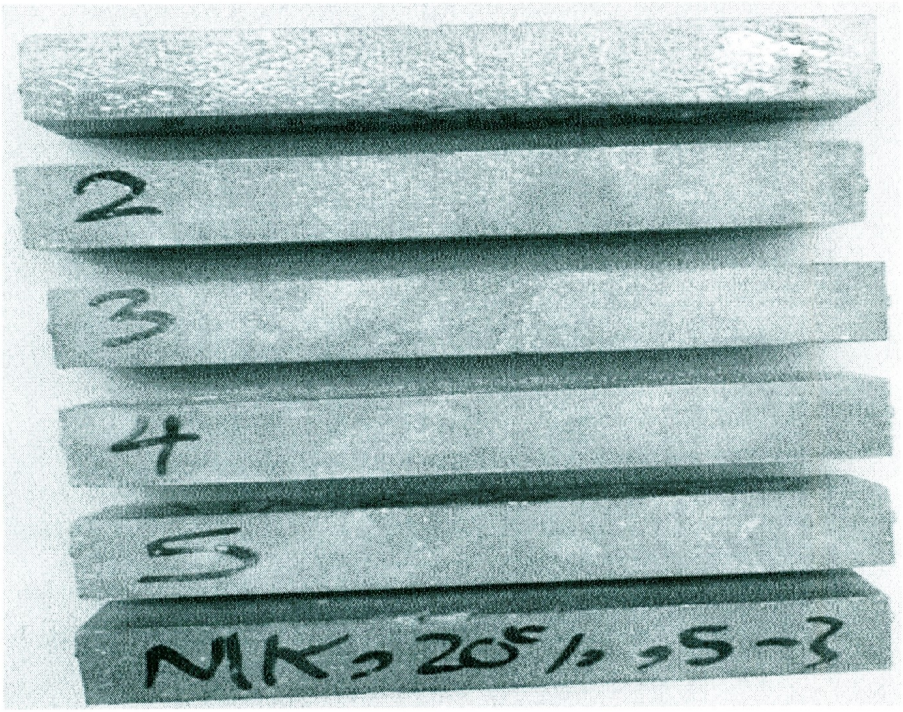

B4: SG

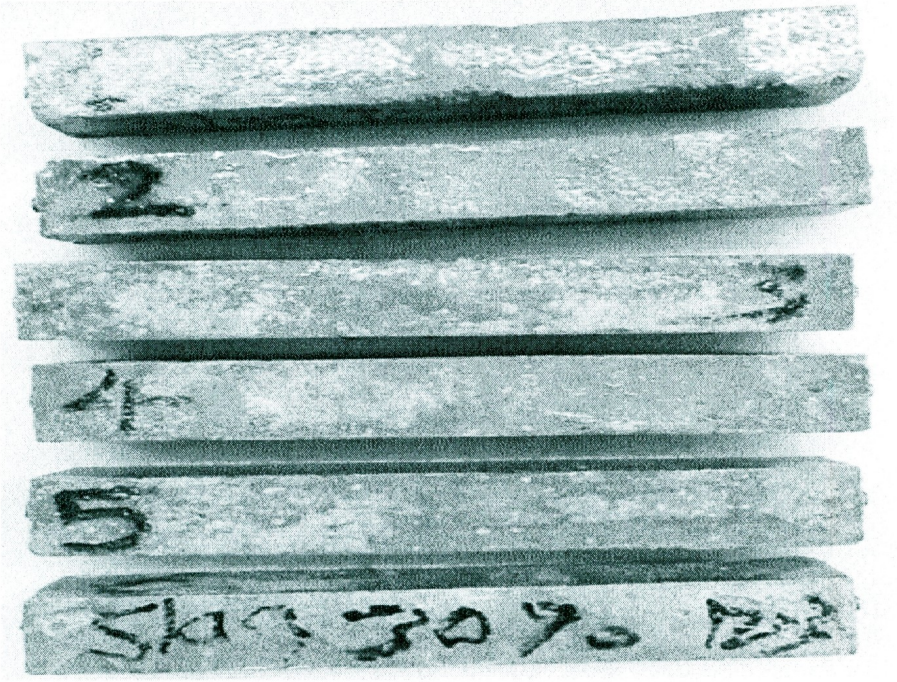

B5: SF

B6: SB <20 μm

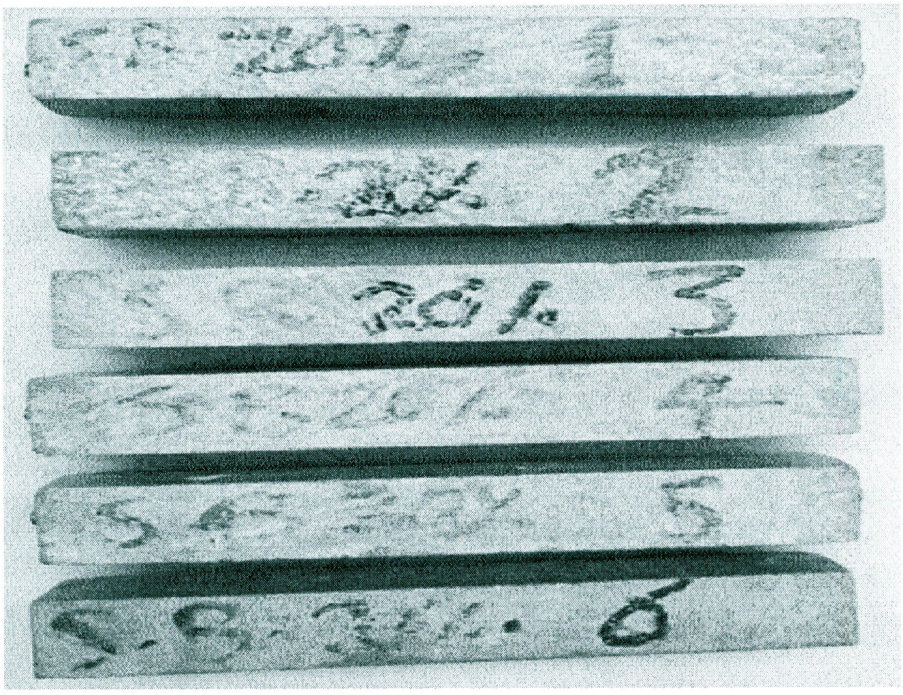

B7: SB <30 µm

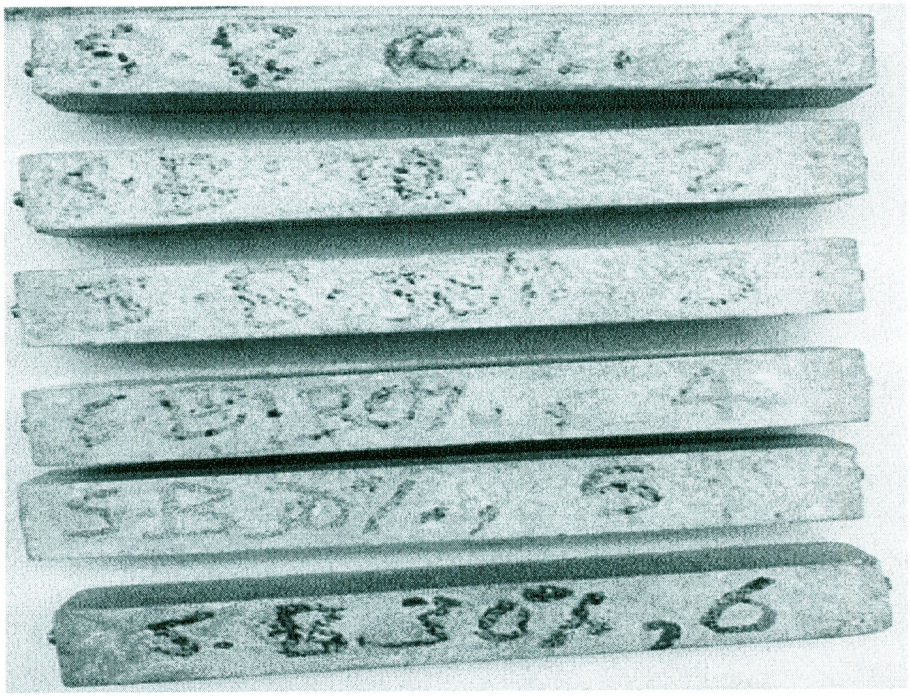

B8: SB <45 µm

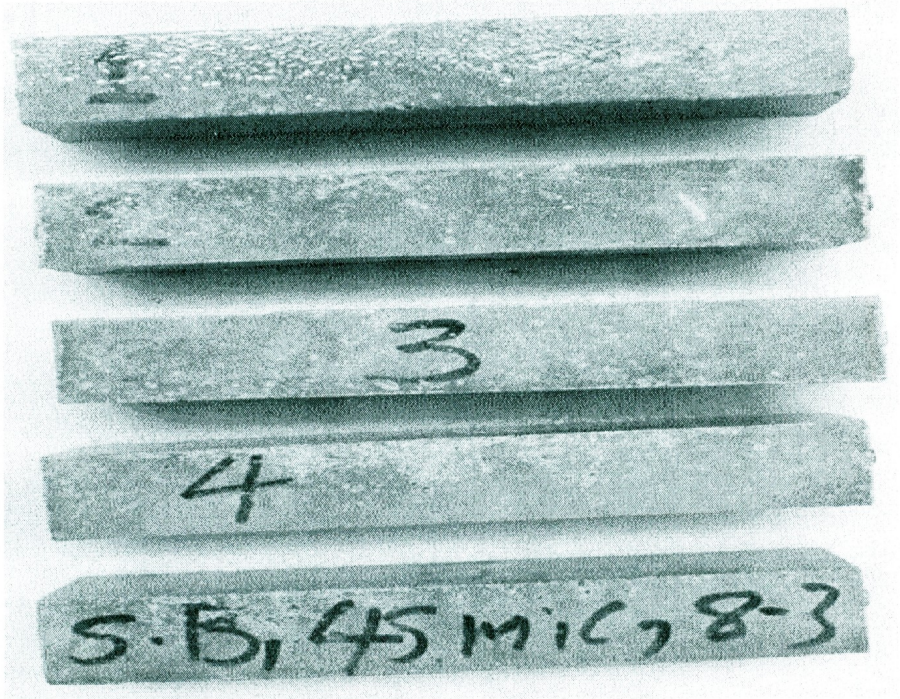

B9: SB <75 µm

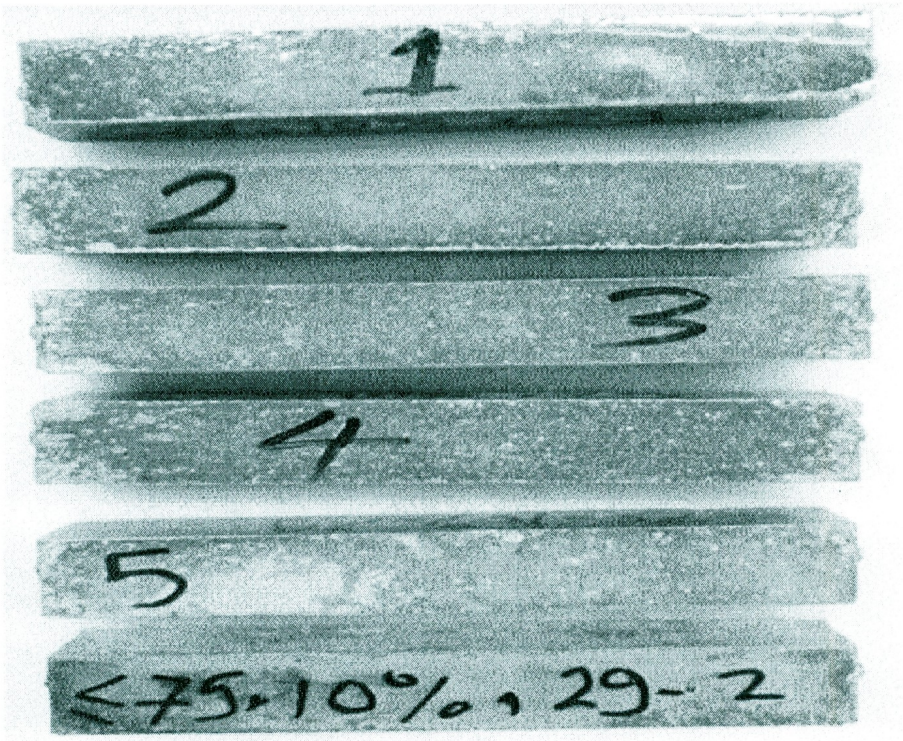

Appendix C: ANOVA Tables and Responses Charts for the 20 Mixtures

Response 2: T_{500}

ANOVA Table for Response 2: T_{500}

Response	2	T_{500}				
Transform:	Natural Log	Constant:	0			
ANOVA for Response Surface Linear Model						
Analysis of variance table [Partial sum of squares - Type III]						
Source	Sum of Squares	d_f	Mean Square	F-Value	P-Value (Prob. > F)	Significance
Model	3.49	3	1.16	28.67	< 0.0001	Significant
A-Binder Content	1.62	1	1.62	39.89	< 0.0001	Significant
B-W/B	1.50	1	1.50	36.97	< 0.0001	Significant
C-Replacement	0.37	1	0.37	9.14	0.0081	Significant
Residual	0.65	16	0.04			
Lack of Fit	0.57	11	0.05	3.33	0.0976	Not Significant
Pure Error	0.08	5	0.02			
Correlation Total	4.13	19				

d_f = Degrees of Freedom

C1: Effects of Factors A, B, and C on Response 2 (T_{500})

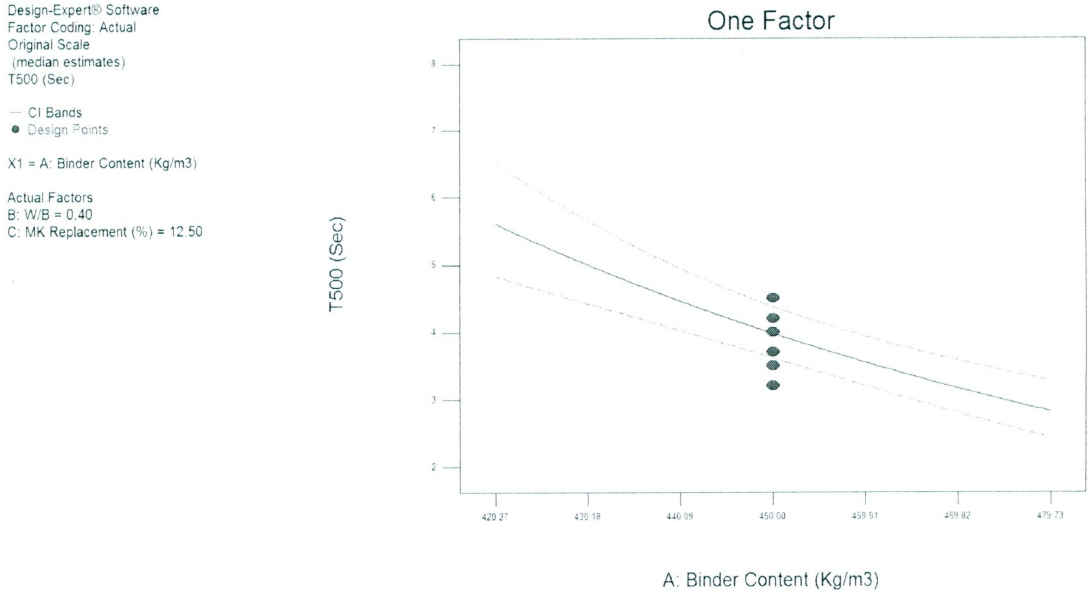

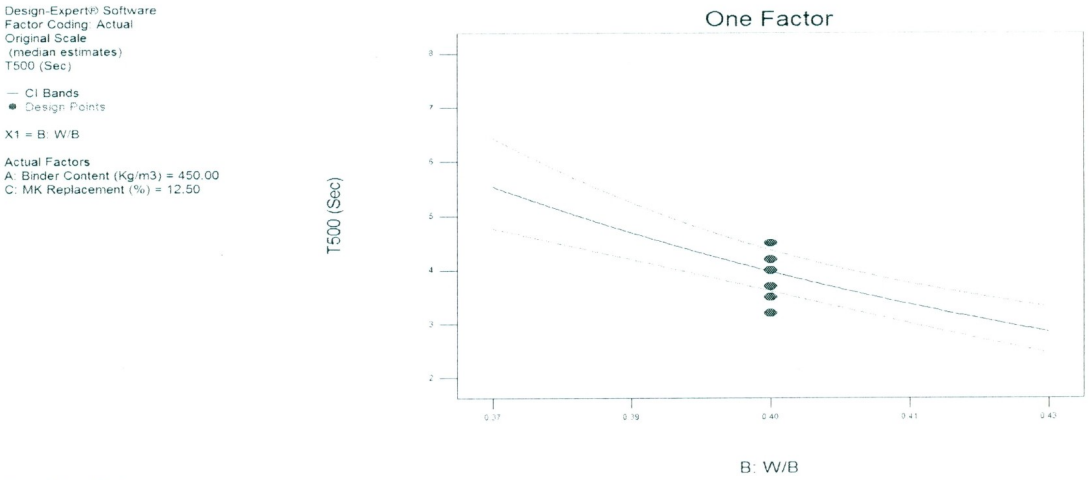

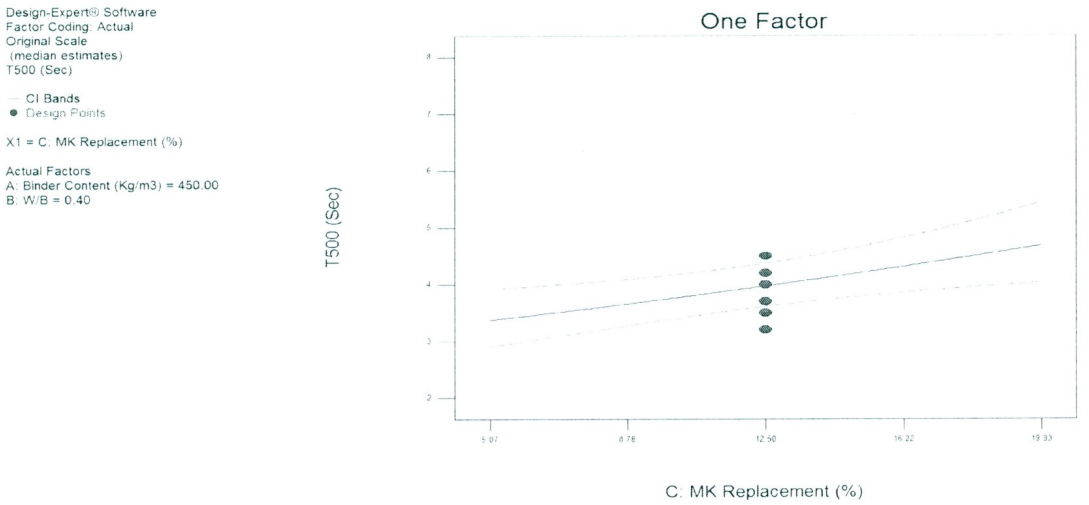

C2: Response Surfaces for factors A-B, A-C, and B-C for Response 2 (T_{500})

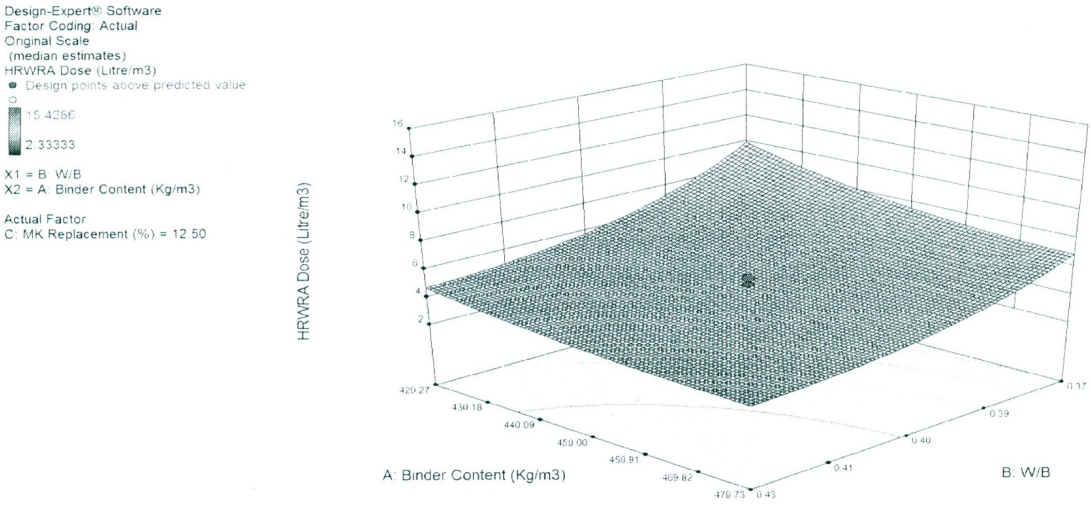

Design-Expert® Software
Factor Coding: Actual
Original Scale
(median estimates)
T500 (Sec)
● Design points above predicted value
○
9.5
1.5

X1 = C: MK Replacement (%)
X2 = A: Binder Content (Kg/m3)

Actual Factor
B: W/B = 0.40

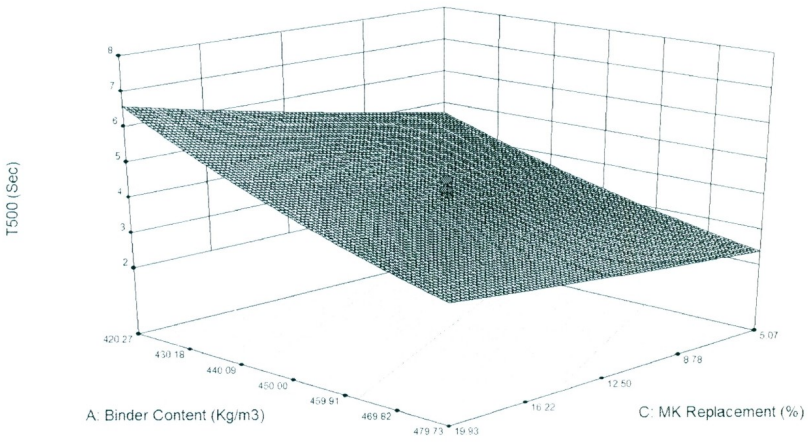

Design-Expert® Software
Factor Coding: Actual
Original Scale
(median estimates)
HRWRA Dose (Litre/m3)
● Design points above predicted value
○
15.4286
2.33333

X1 = B: W/B
X2 = C: MK Replacement (%)

Actual Factor
A: Binder Content (Kg/m3) = 450.00

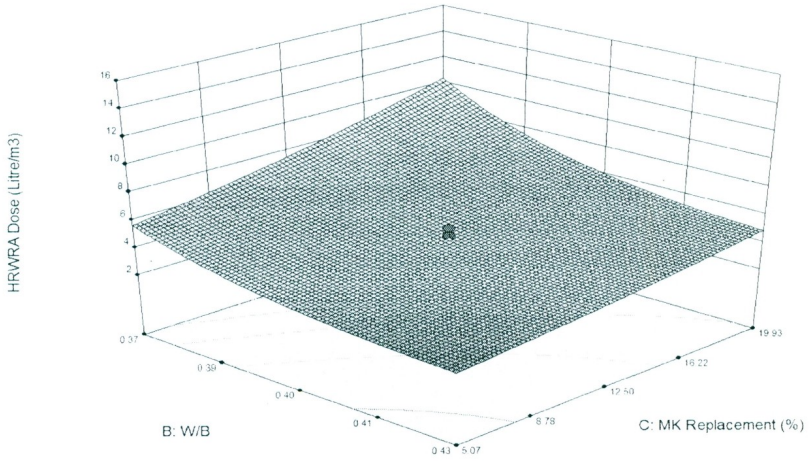

Response 3: Initial V-Funnel

ANOVA Table for Response 3: Initial V-Funnel

Response	3	Initial V-Funnel				
ANOVA for Response Surface Reduced 2FI Model						
Analysis of variance table [Partial sum of squares - Type III]						
Source	Sum of Squares	d_f	Mean Square	F-Value	P-Value (Prob. > F)	Significance
Model	2309.09	5	461.82	41.30	< 0.0001	Significant
A-Binder Content	626.51	1	626.51	56.03	< 0.0001	Significant
B-W/B	1236.59	1	1236.59	110.59	< 0.0001	Significant
C-Replacement	188.42	1	188.42	16.85	0.0011	Significant
AC	148.78	1	148.78	13.31	0.0026	Significant
BC	108.78	1	108.78	9.73	0.0075	Significant
Residual	156.55	14	11.18			
Lack of Fit	121.72	9	13.52	1.94	0.2407	Not Significant
Pure Error	34.83	5	6.97			
Correlation Total	2465.64	19				

d_f = Degrees of Freedom

C3: Effects of Factors A, B, and C on Response 3 (Initial V-Funnel)

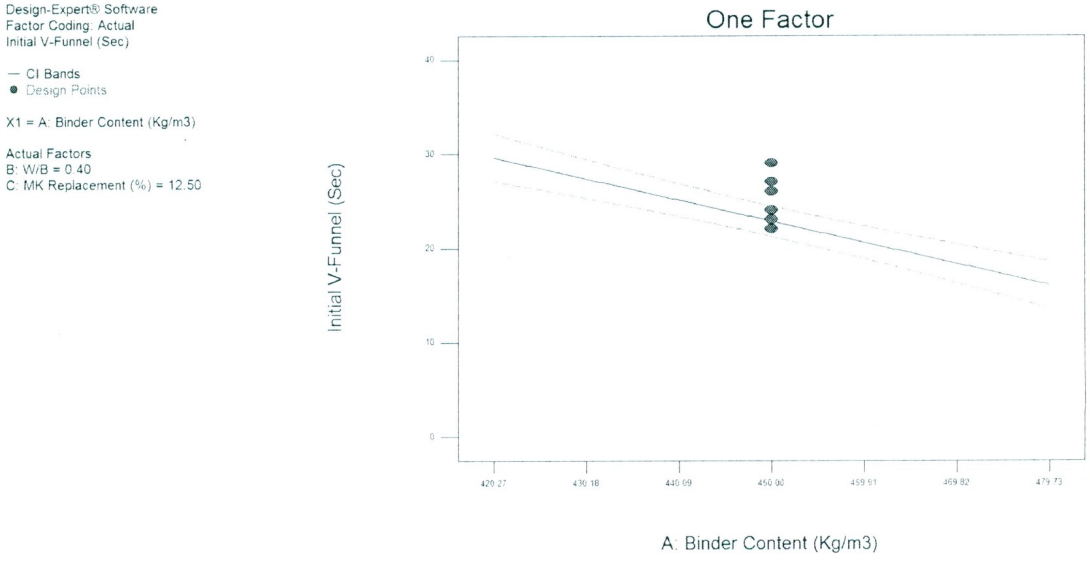

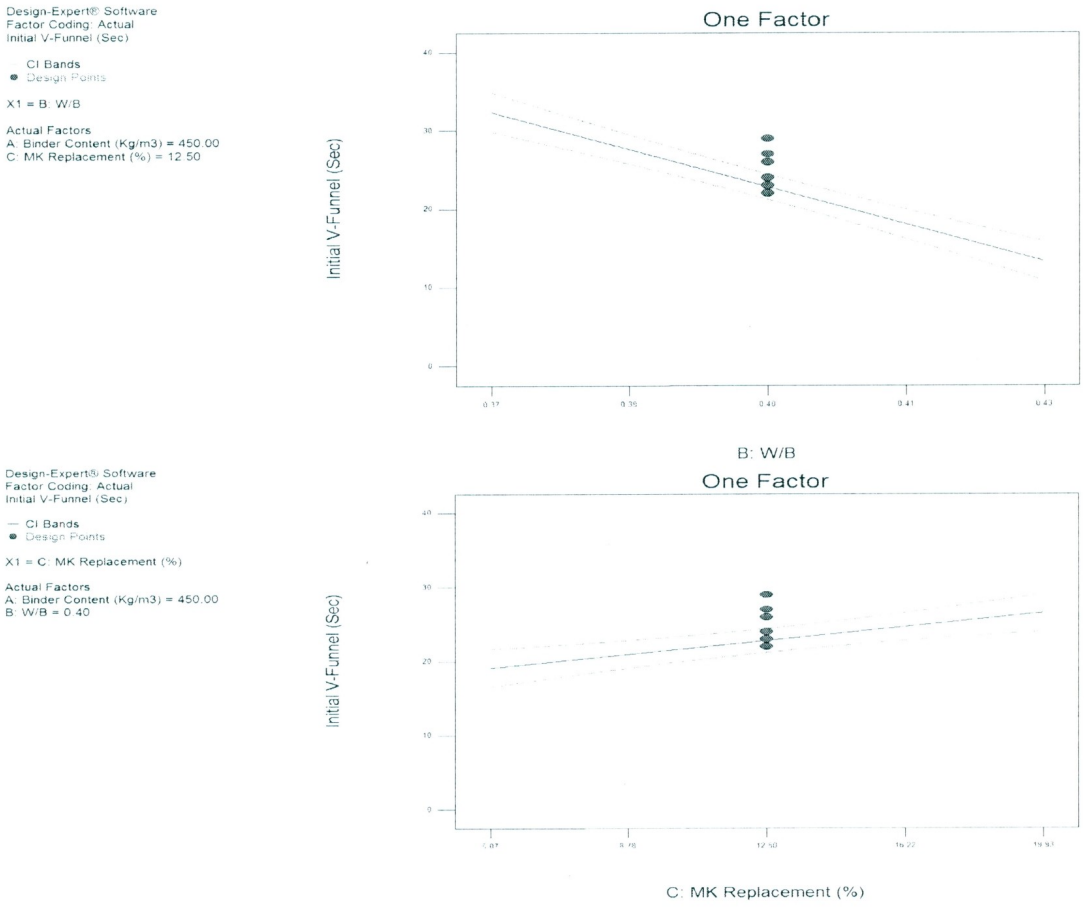

C4: Interaction Effects of Factors AC and BC on Response 3 (Initial V-Funnel)

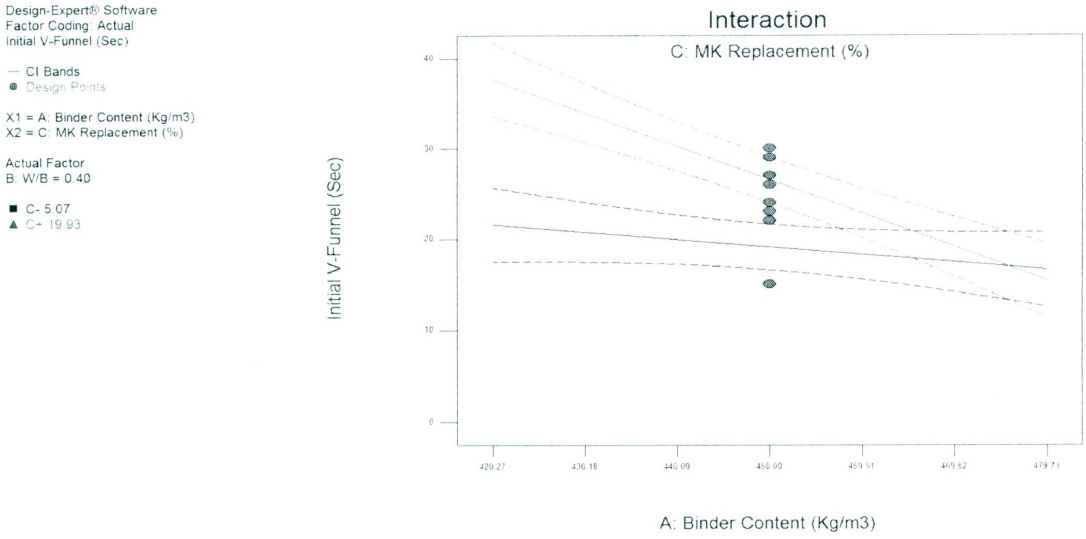

Design-Expert® Software
Factor Coding: Actual
Initial V-Funnel (Sec)

— CI Bands
● Design Points

X1 = C: MK Replacement (%)
X2 = A: Binder Content (Kg/m3)

Actual Factor
B: W/B = 0.40

■ A- 420.27
▲ A+ 479.73

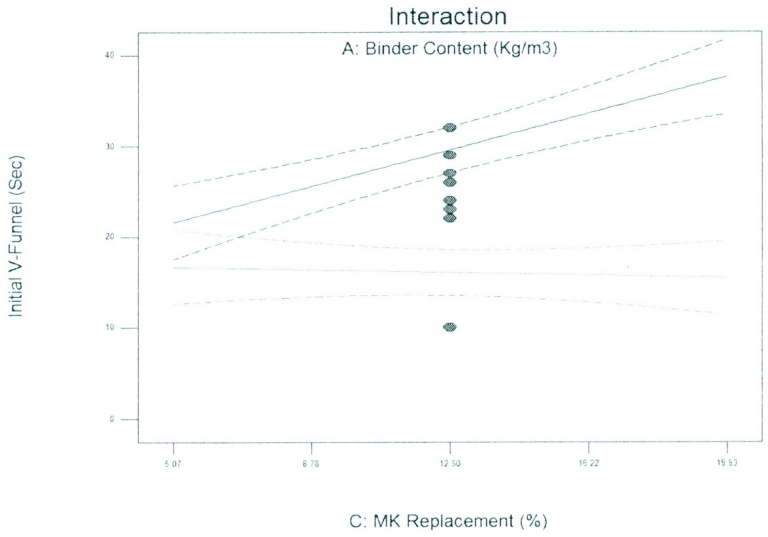

Design-Expert® Software
Factor Coding: Actual
Initial V-Funnel (Sec)

— CI Bands
● Design Points

X1 = B: W/B
X2 = C: MK Replacement (%)

Actual Factor
A: Binder Content (Kg/m3) = 450.00

■ C- 5.07
▲ C+ 19.93

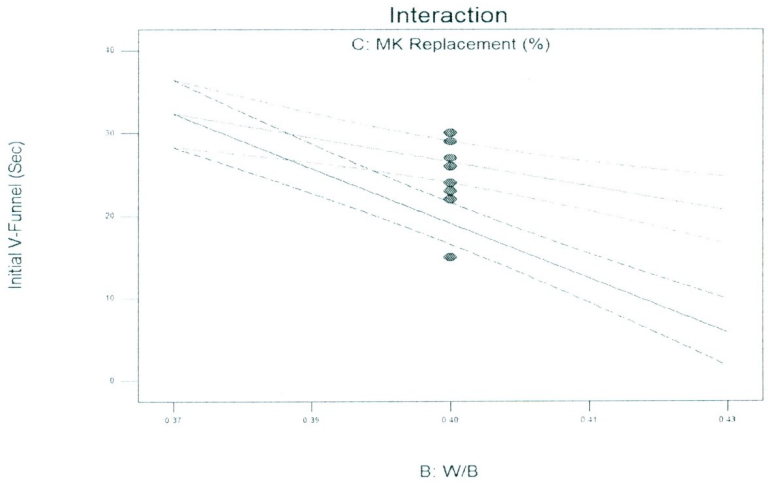

Design-Expert® Software
Factor Coding: Actual
Initial V-Funnel (Sec)

— CI Bands
● Design Points

X1 = C: MK Replacement (%)
X2 = B: W/B

Actual Factor
A: Binder Content (Kg/m3) = 450.00

■ B- 0.37
▲ B+ 0.43

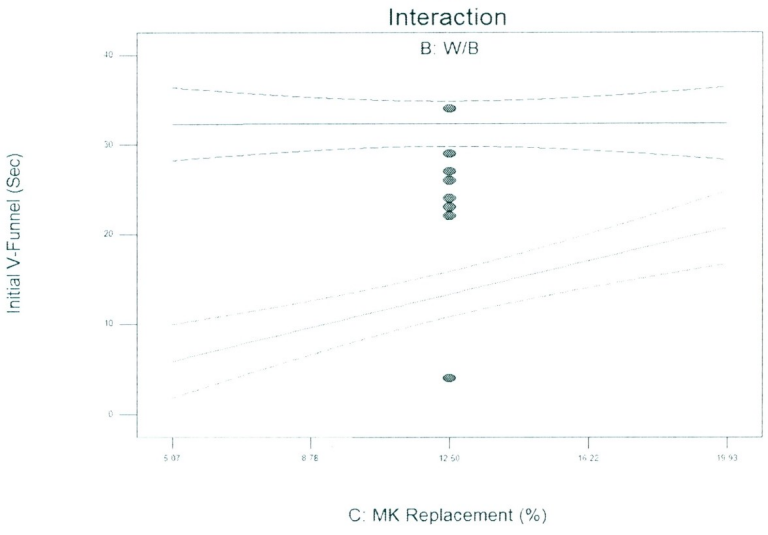

C5: Response Surfaces for factors A-B, A-C, and B-C for Response 3 (Initial V-Funnel)

Design-Expert® Software
Factor Coding: Actual
Initial V-Funnel (Sec)
Design points above predicted value
40
3.5
X1 = A: Binder Content (Kg/m3)
X2 = B: W/B
Actual Factor
C: MK Replacement (%) = 12.50

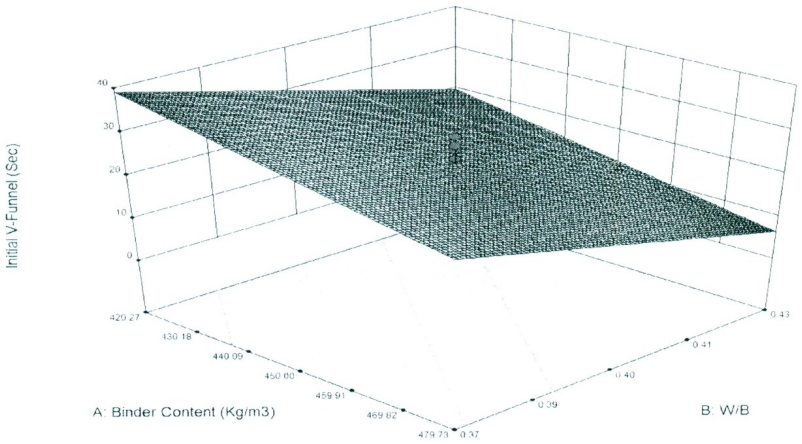

Design-Expert® Software
Factor Coding: Actual
Initial V-Funnel (Sec)
Design points above predicted value
40
3.5
X1 = A: Binder Content (Kg/m3)
X2 = C: MK Replacement (%)
Actual Factor
B: W/B = 0.40

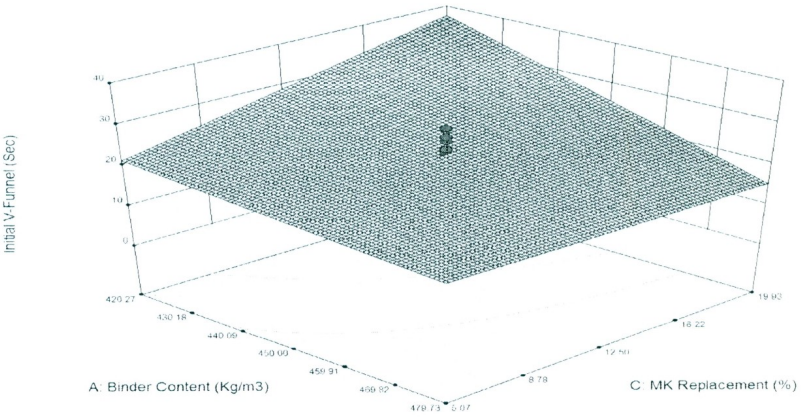

Design-Expert® Software
Factor Coding: Actual
Initial V-Funnel (Sec)
Design points above predicted value
40
3.5
X1 = C: MK Replacement (%)
X2 = B: W/B
Actual Factor
A: Binder Content (Kg/m3) = 450.00

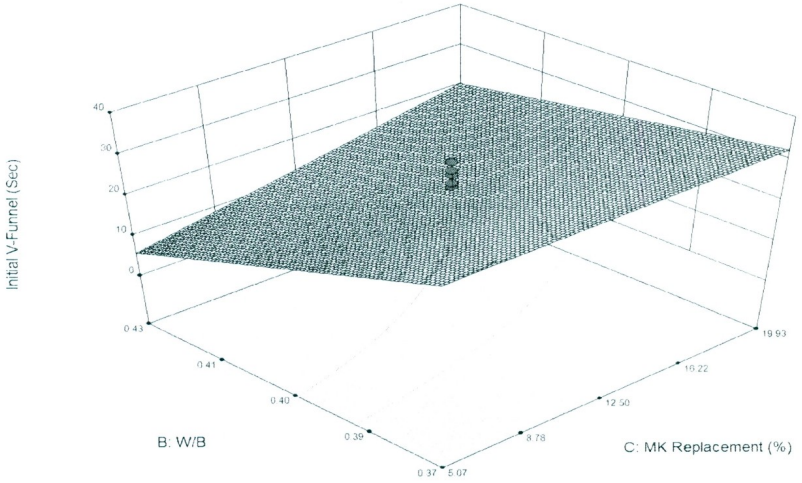

Response 4: Slump – J-Ring Diameter

ANOVA Table for Response 4: Slump – J-Ring Diameter

Response	4	Slump - J-Ring Diameter				
ANOVA for Response Surface Linear Model						
Analysis of variance table [Partial sum of squares - Type III]						
Source	Sum of Squares	d_f	Mean Square	F-Value	P-Value (Prob. > F)	Significance
Model	977.26	3	325.75	20.77	< 0.0001	Significant
A-Binder Content	107.00	1	107.00	6.82	0.0189	Significant
B-W/B	641.38	1	641.38	40.89	< 0.0001	Significant
C-Replacement	228.88	1	228.88	14.59	0.0015	Significant
Residual	250.94	16	15.68			
Lack of Fit	220.11	11	20.01	3.24	0.1021	Not Significant
Pure Error	30.83	5	6.17			
Correlation Total	1228.20	19				

d_f = Degrees of Freedom

C6: Effects of Factors A, B, and C on Response 4 (Slump – J-Ring Diameter)

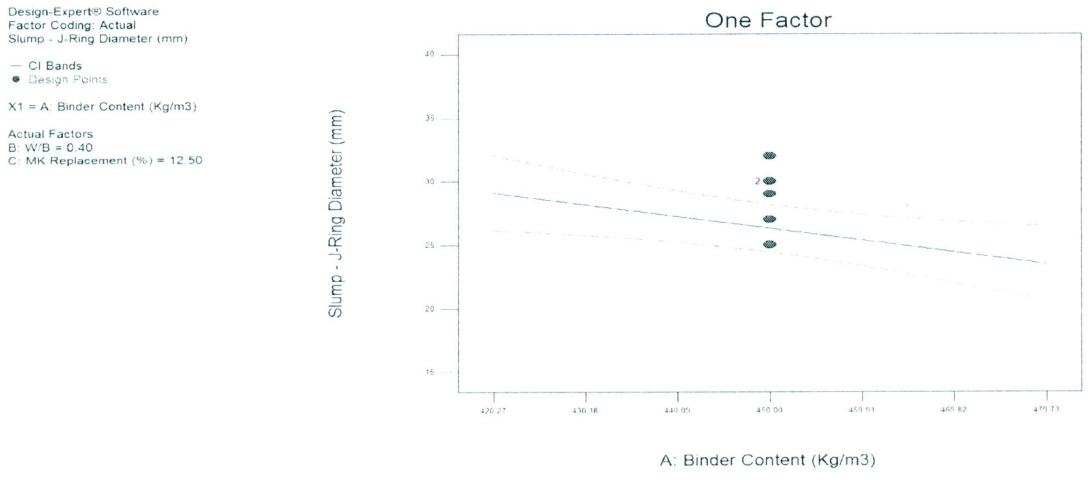

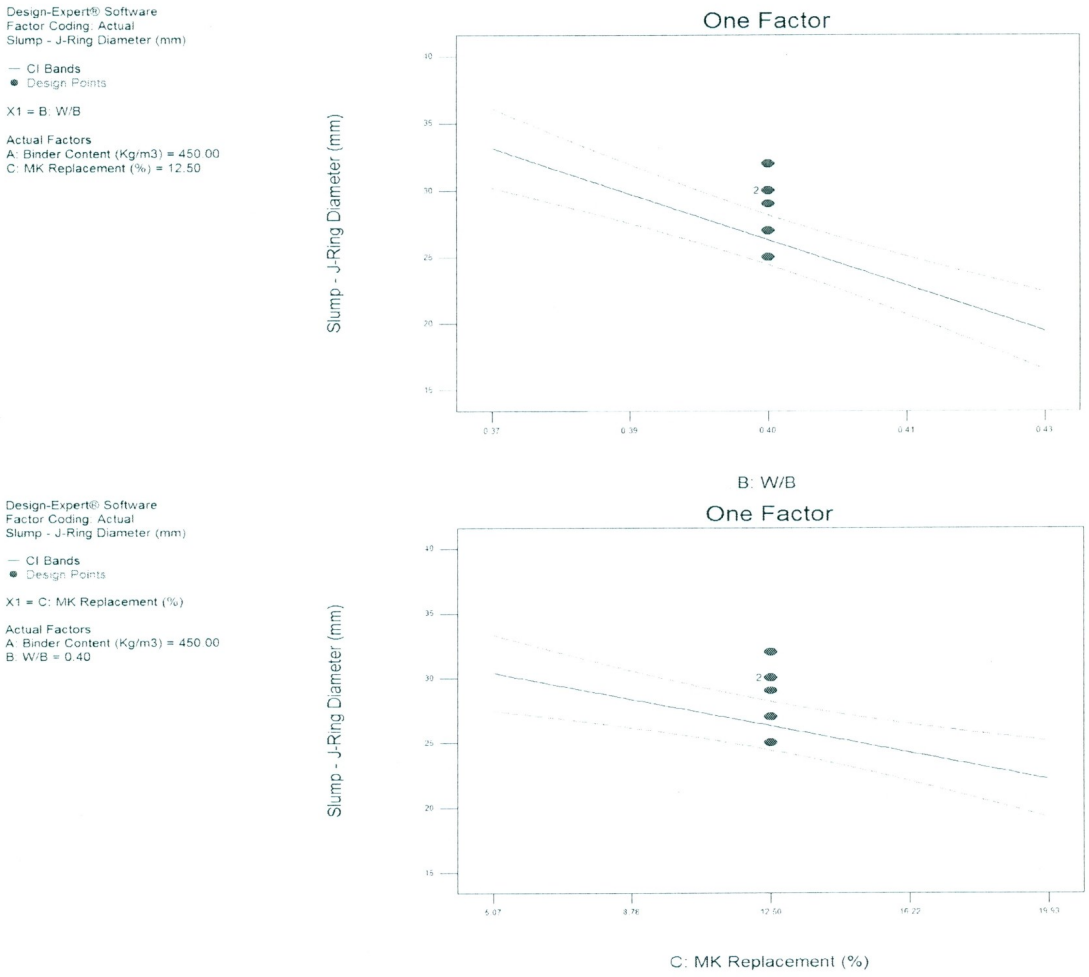

C7: Response Surfaces for factors A-B, A-C, and B-C for Response 4 (Slump – J-Ring Diameter)

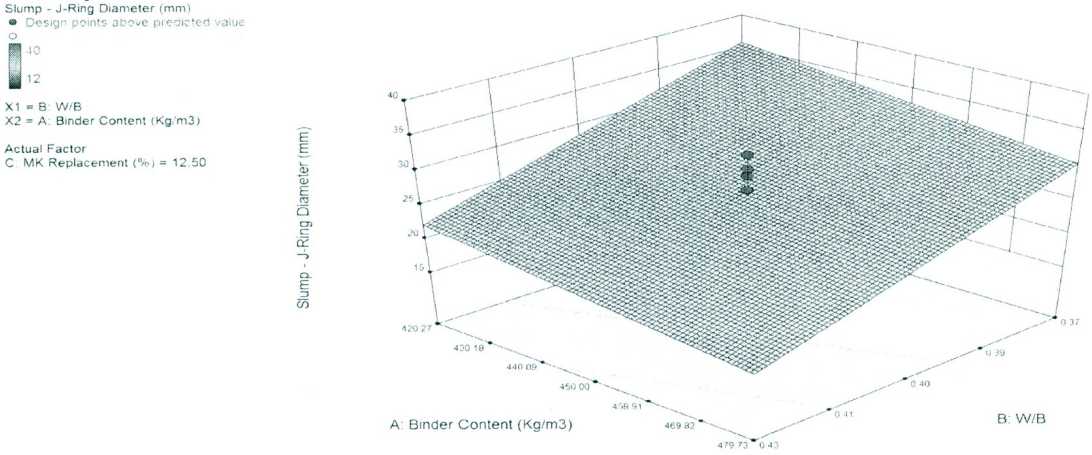

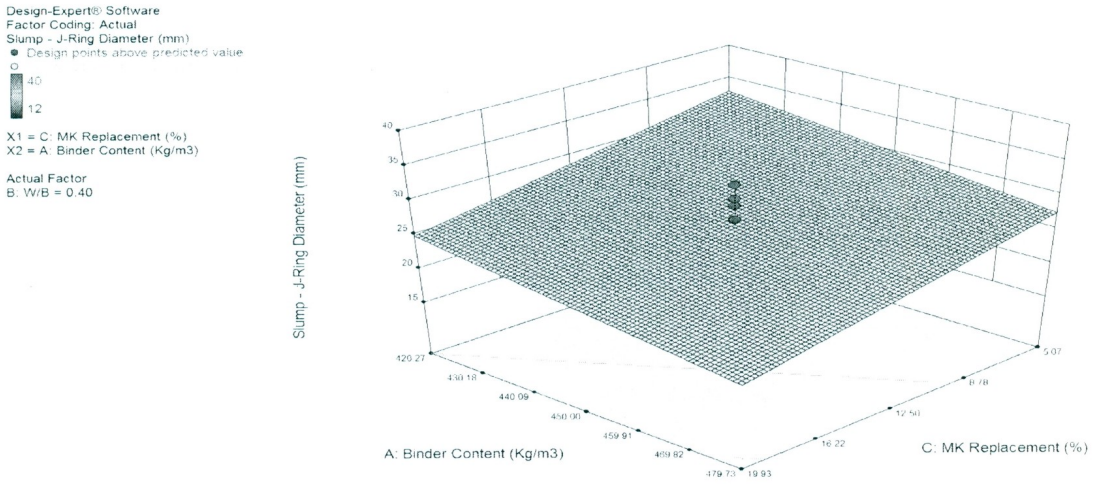
Design-Expert® Software
Factor Coding: Actual
Slump - J-Ring Diameter (mm)
Design points above predicted value
40
12
X1 = C: MK Replacement (%)
X2 = A: Binder Content (Kg/m3)
Actual Factor
B: W/B = 0.40
Slump - J-Ring Diameter (mm)
40
35
30
25
20
15
420.27
430.18
440.09
450.00
459.91
469.82
479.73
A: Binder Content (Kg/m3)
0.07
8.78
12.50
16.22
19.93
C: MK Replacement (%)

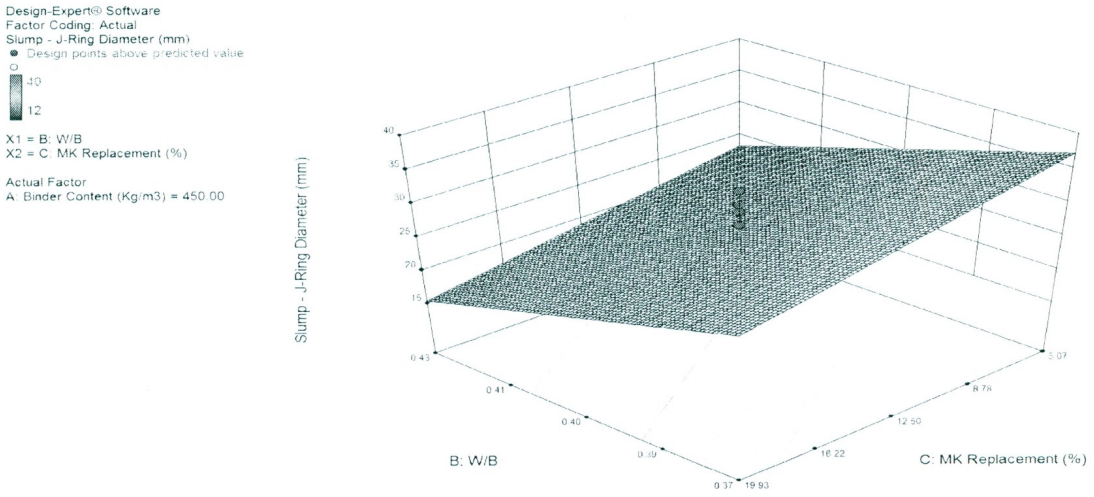
Design-Expert® Software
Factor Coding: Actual
Slump - J-Ring Diameter (mm)
Design points above predicted value
40
12
X1 = B: W/B
X2 = C: MK Replacement (%)
Actual Factor
A: Binder Content (Kg/m3) = 450.00
Slump - J-Ring Diameter (mm)
40
35
30
25
20
15
0.43
0.41
0.40
0.39
0.37
B: W/B
0.07
8.78
12.50
16.22
19.93
C: MK Replacement (%)

Response 5: H2/H1 L-Box

ANOVA Table for Response 5: H2/H1 L-Box

Response	5	H2/H1 L-Box				
ANOVA for Response Surface Linear Model						
Analysis of variance table [Partial sum of squares - Type III]						
Source	Sum of Squares	d_f	Mean Square	F-Value	P-Value (Prob. > F)	Significance
Model	0.24	3	0.079	33.51	< 0.0001	Significant
A-Binder Content	0.03	1	0.032	13.69	0.0019	Significant
B-W/B	0.10	1	0.096	40.52	< 0.0001	Significant
C-Replacement	0.11	1	0.110	46.31	< 0.0001	Significant
Residual	0.04	16	0.002			
Lack of Fit	0.03	11	0.003	1.73	0.2830	Not Significant
Pure Error	0.01	5	0.002			
Correlation Total	0.28	19				

d_f = Degrees of Freedom

C8: Effects of Factors A, B, and C on Response 5 (H2/H1 L-Box)

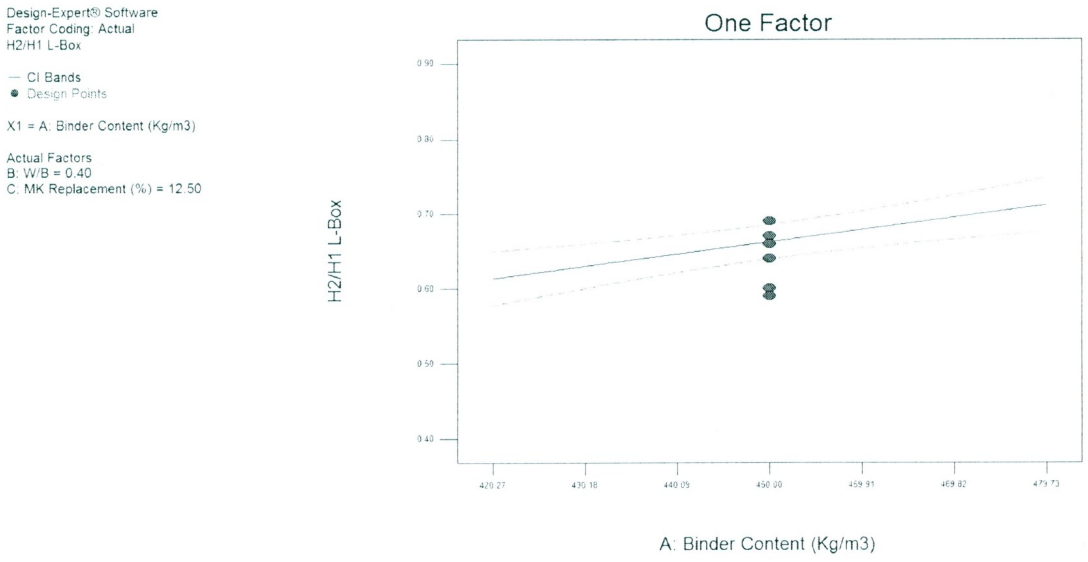

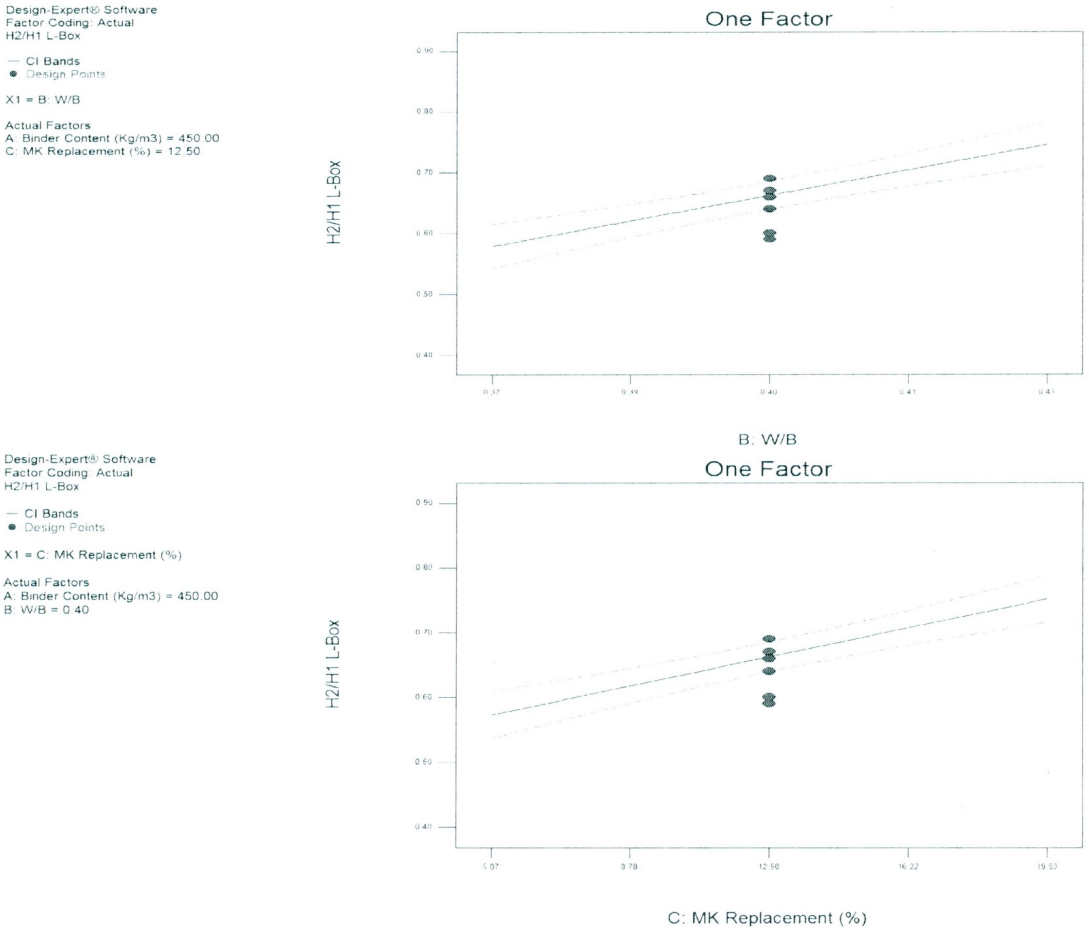

C9: Response Surfaces for factors A-B, A-C, and B-C for Response 5 (H2/H1 L-Box)

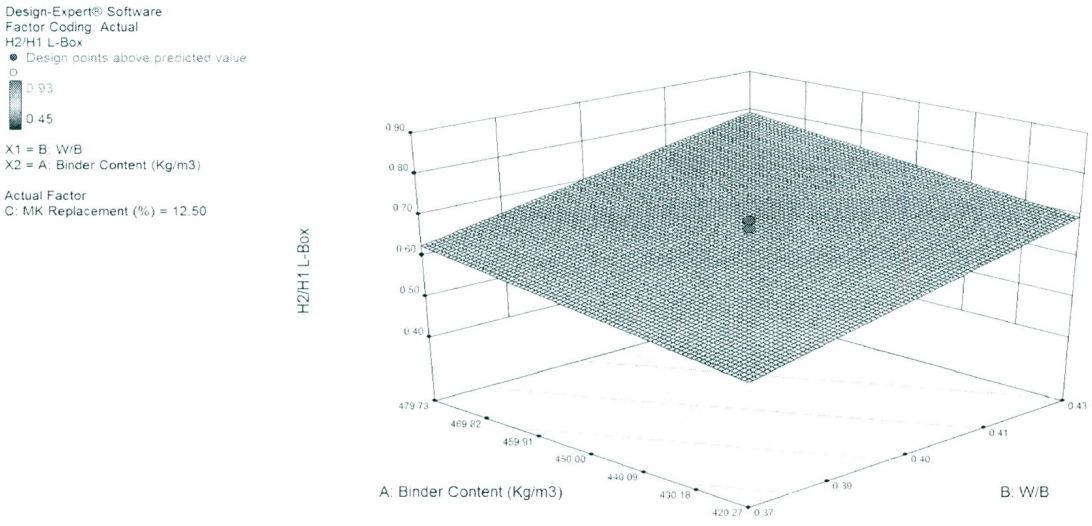

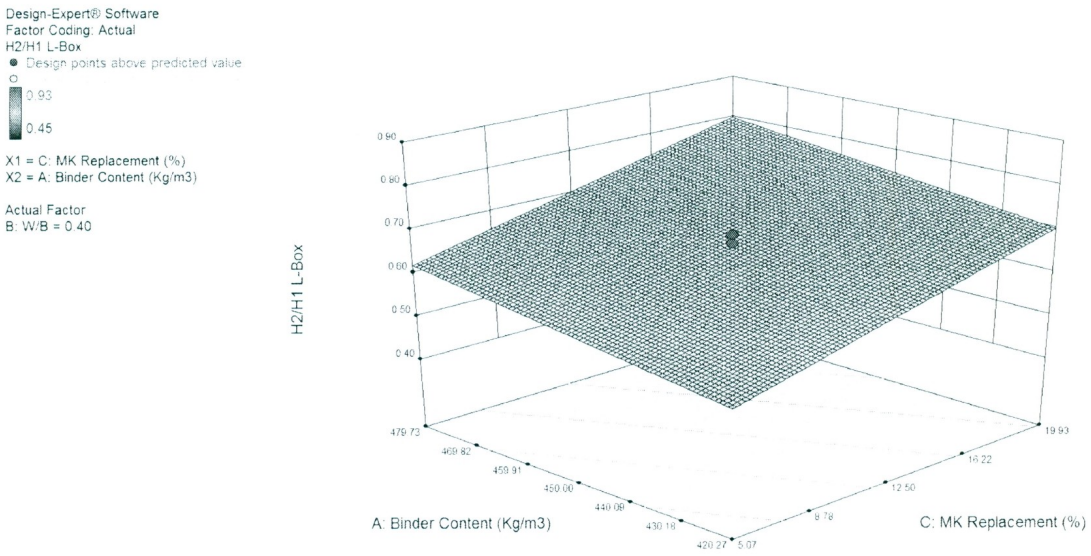
Design-Expert® Software
Factor Coding: Actual
H2/H1 L-Box
Design points above predicted value
0.93
0.45
X1 = C: MK Replacement (%)
X2 = A: Binder Content (Kg/m3)
Actual Factor
B: W/B = 0.40
H2/H1 L-Box
0.90
0.80
0.70
0.60
0.50
0.40
479.73
469.82
459.91
450.00
440.09
430.18
420.27
A: Binder Content (Kg/m3)
5.07
8.78
12.50
15.22
19.93
C: MK Replacement (%)

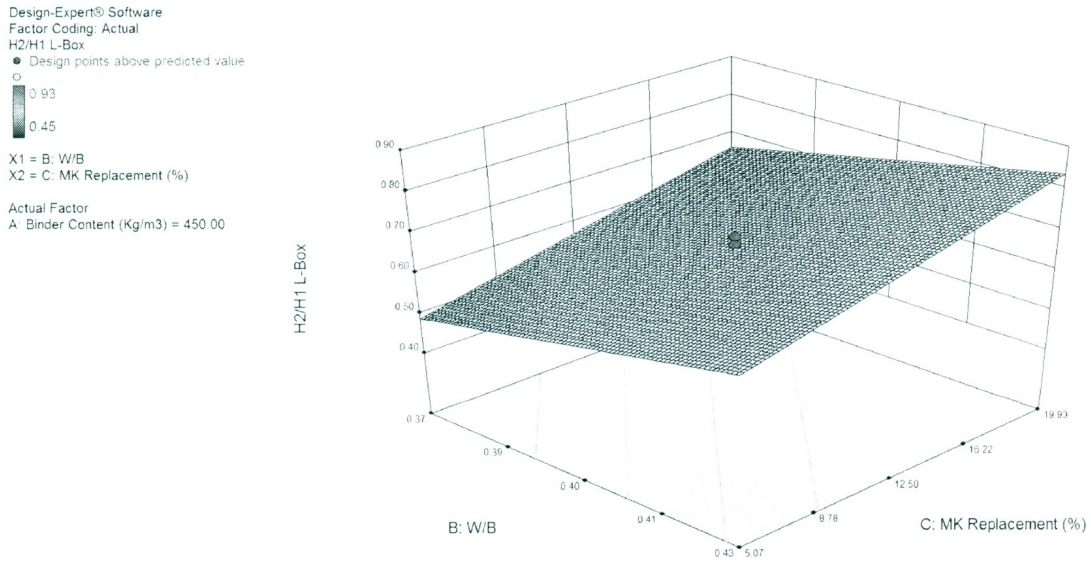
Design-Expert® Software
Factor Coding: Actual
H2/H1 L-Box
Design points above predicted value
0.93
0.45
X1 = B: W/B
X2 = C: MK Replacement (%)
Actual Factor
A: Binder Content (Kg/m3) = 450.00
H2/H1 L-Box
0.90
0.80
0.70
0.60
0.50
0.40
0.37
0.39
0.40
0.41
0.43
B: W/B
5.07
8.78
12.50
15.22
19.93
C: MK Replacement (%)

Response 6: $T_{500}J$

ANOVA Table for Response 6: $T_{500}J$

Response	6		T500J			
Transform:	Natural Log	Constant:	0			
ANOVA for Response Surface Linear Model						
Analysis of variance table [Partial sum of squares - Type III]						
Source	Sum of Squares	d_f	Mean Square	F-Value	P-Value (Prob. > F)	Significance
Model	3.24	3	1.08	41.04	< 0.0001	Significant
A-Binder Content	1.61	1	1.61	60.96	< 0.0001	Significant
B-W/B	1.47	1	1.47	55.68	< 0.0001	Significant
C-Replacement	0.17	1	0.17	6.47	0.0217	Significant
Residual	0.42	16	0.03			
Lack of Fit	0.36	11	0.03	2.71	0.1406	Not Significant
Pure Error	0.06	5	0.01			
Correlation Total	3.66	19				

d_f = Degrees of Freedom

C10: Effects of Factors A, B, and C on Response 6 ($T_{500}J$)

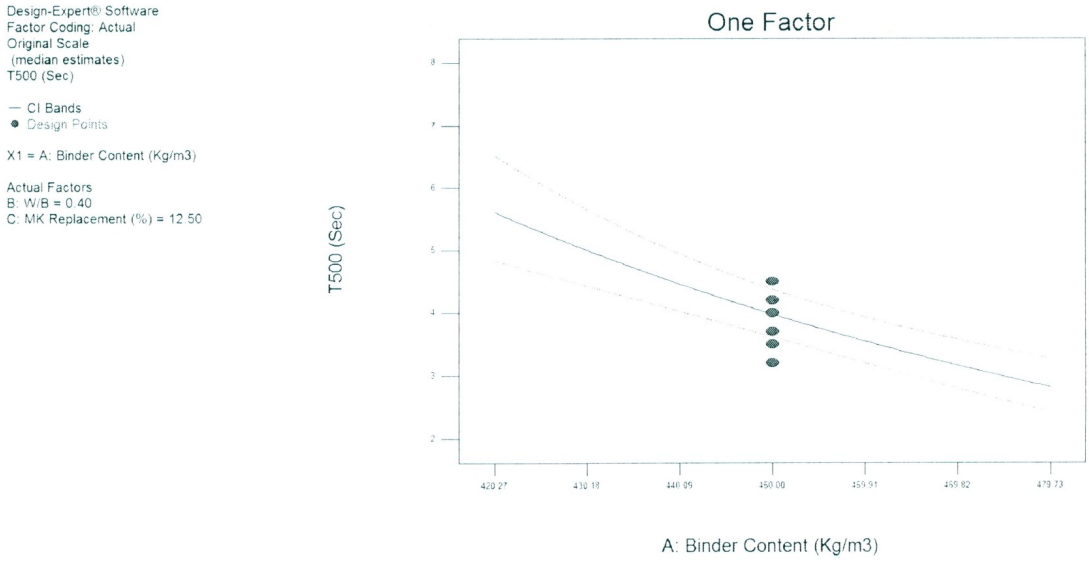

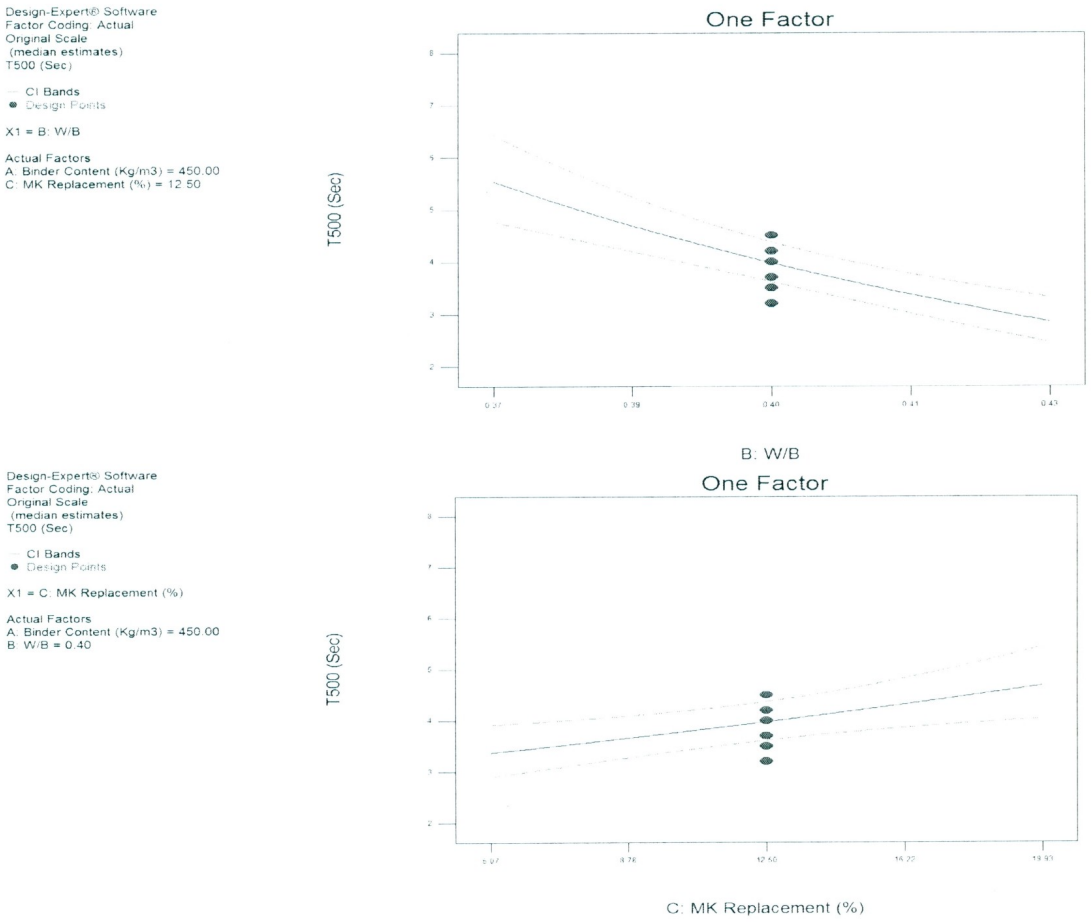

C11: Response Surfaces for factors A-B, A-C, and B-C for Response 6 ($T_{500}J$)

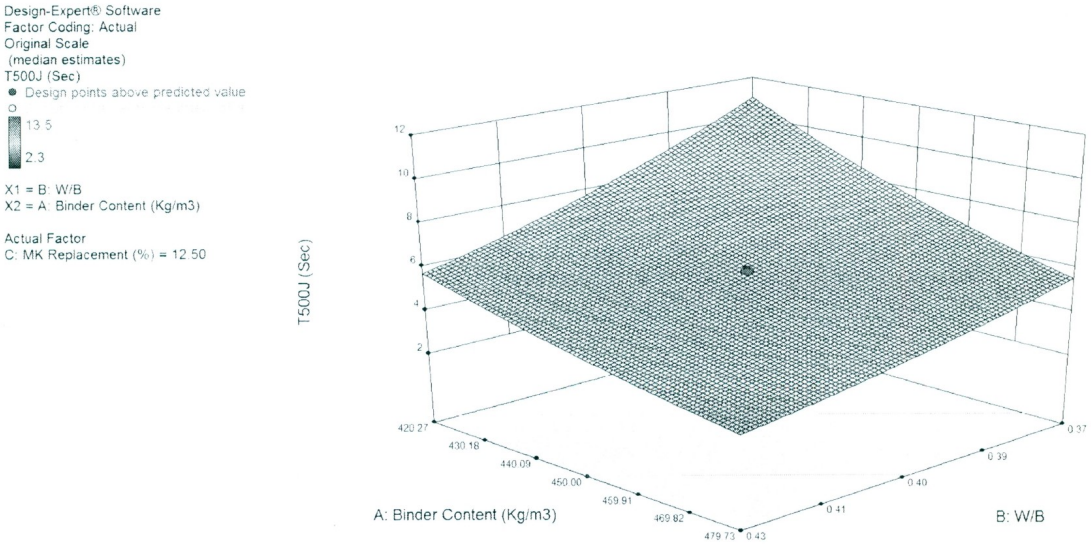

Design-Expert® Software
Factor Coding: Actual
Original Scale
(median estimates)
T500J (Sec)
● Design points above predicted value
○
13.5
2.3

X1 = A: Binder Content (Kg/m3)
X2 = C: MK Replacement (%)

Actual Factor
B: W/B = 0.40

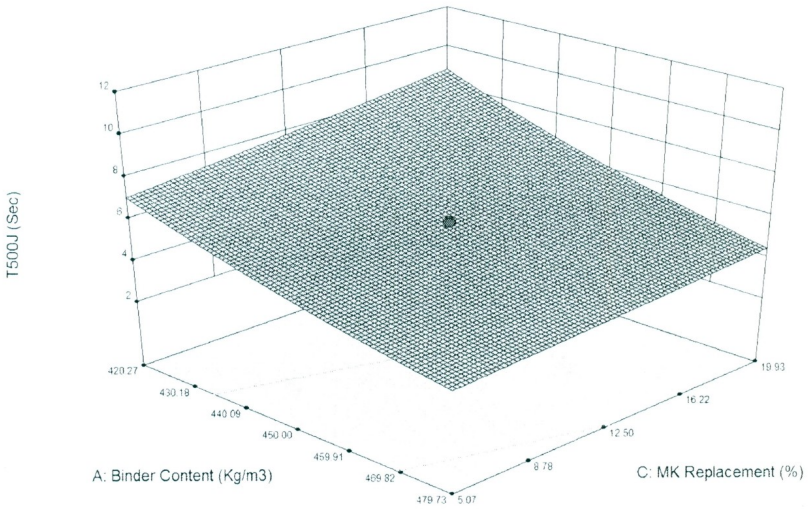

Design-Expert® Software
Factor Coding: Actual
Original Scale
(median estimates)
T500J (Sec)
● Design points above predicted value
○
13.5
2.3

X1 = B: W/B
X2 = C: MK Replacement (%)

Actual Factor
A: Binder Content (Kg/m3) = 450.00

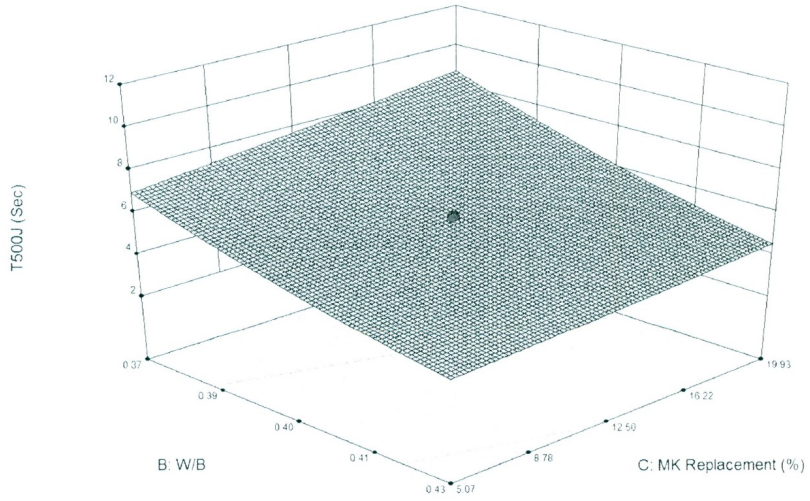

Response 7: Final V-Funnel

ANOVA Table for Response 7: Final V-Funnel

Response	7	Final V-Funnel				
ANOVA for Response Surface Reduced 2FI Model						
Analysis of variance table [Partial sum of squares - Type III]						
Source	Sum of Squares	d_f	Mean Square	F-Value	P-Value (Prob. > F)	Significance
Model	8098.86	4	2024.72	40.27	< 0.0001	Significant
A-Binder Content	2616.59	1	2616.59	52.05	< 0.0001	Significant
B-W/B	4769.45	1	4769.45	94.87	< 0.0001	Significant
C-Replacement	20.91	1	20.91	0.42	0.5287	Significant
BC	691.92	1	691.92	13.76	0.0021	Significant
Residual	754.13	15	50.28			
Lack of Fit	663.29	10	66.33	3.65	0.0828	Not Significant
Pure Error	90.83	5	18.17			
Correlation Total	8852.99	19				

d_f = Degrees of Freedom

C12: Effects of Factors A, B, and C on Response 7 (Final V-Funnel)

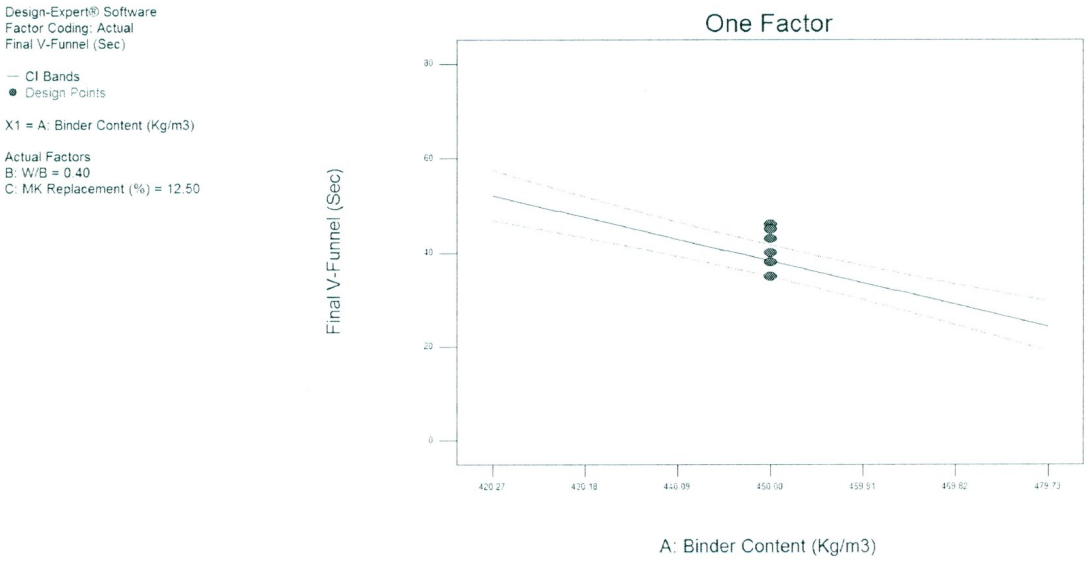

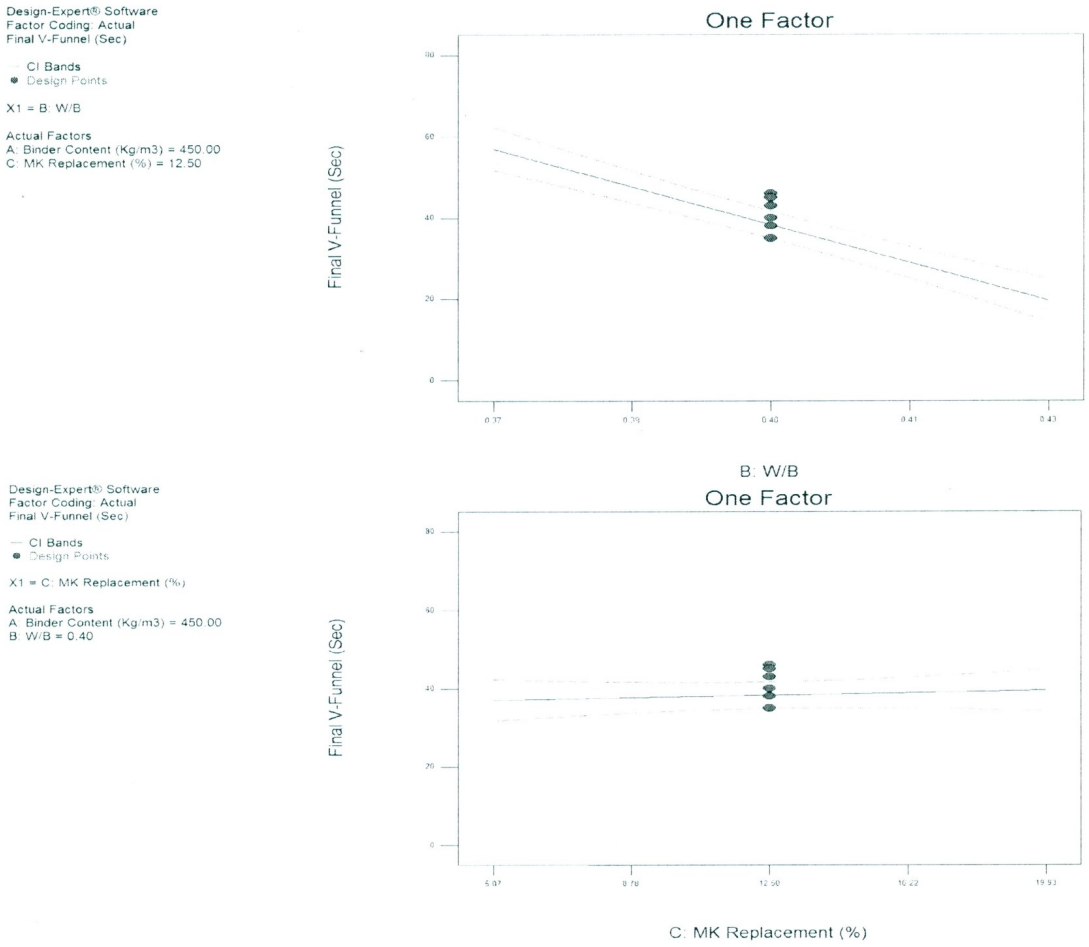

C13: Interaction Effect of BC on Response 7 (Final V-Funnel)

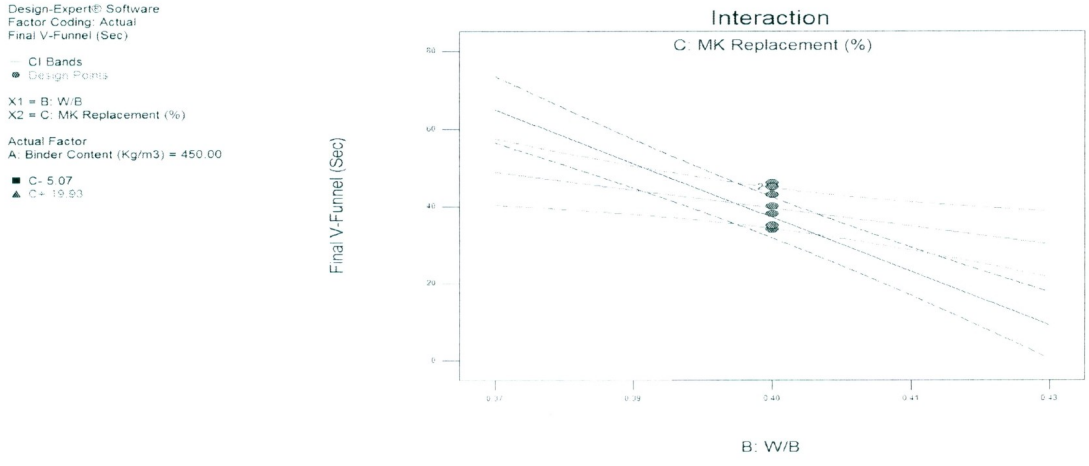

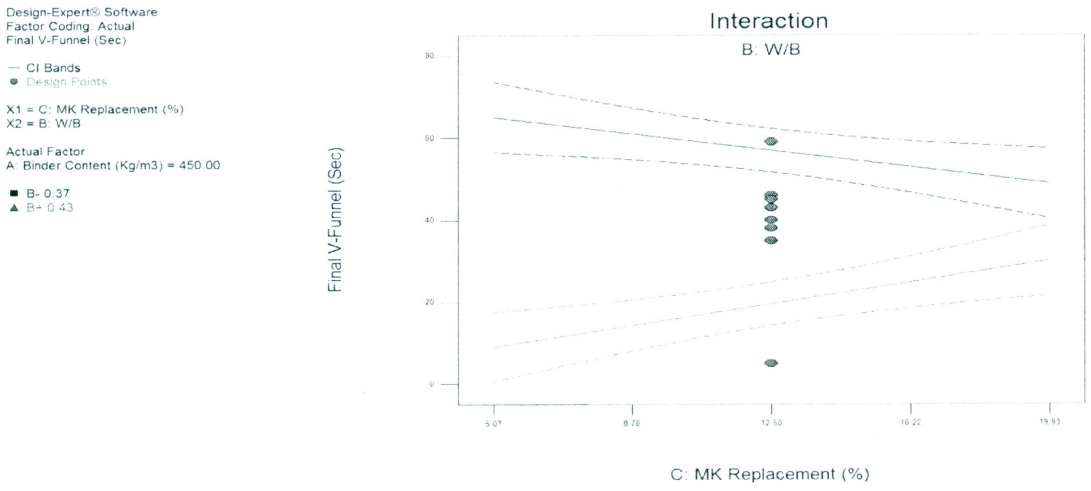

C14: Response Surfaces for factors A-B, A-C, and B-C for Response 7 (Final V-Funnel)

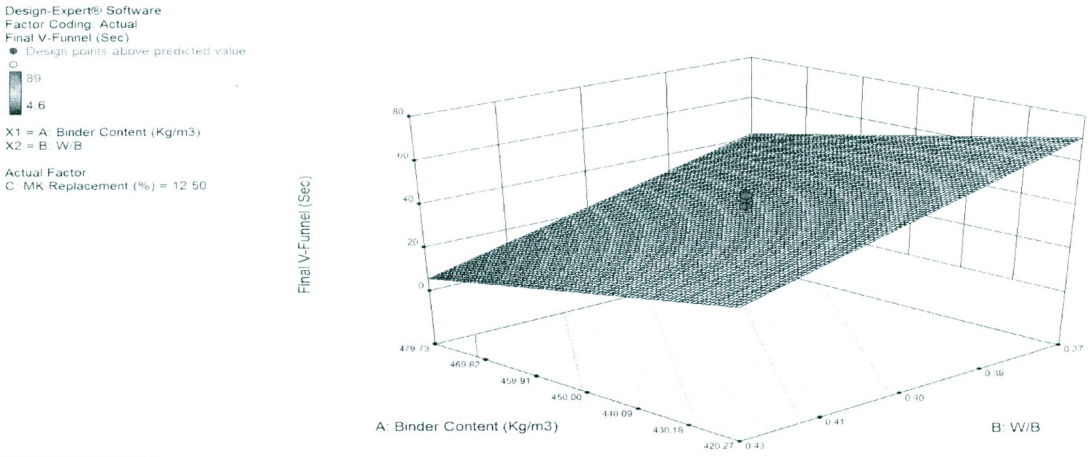

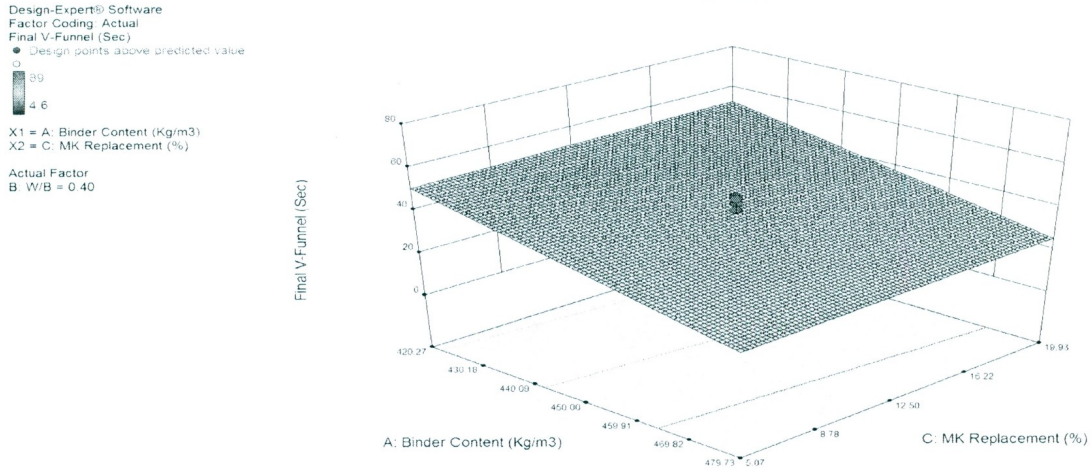

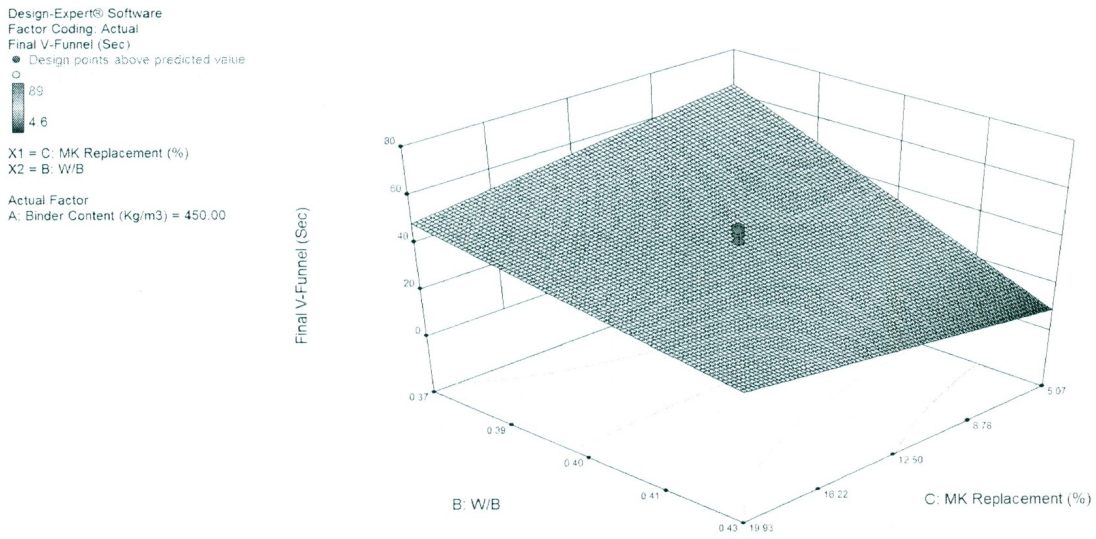

Response 8: Segregation Factor

ANOVA Table for Response 8: Segregation Factor

Response	8	Segregation Factor				
Transform:	Natural Log	Constant:	0			
ANOVA for Response Surface Reduced Quadratic Model						
Analysis of variance table [Partial sum of squares - Type III]						
Source	Sum of Squares	df	Mean Square	F-Value	P-Value (Prob. > F)	Significance
Model	4.27	7	0.61	50.26	< 0.0001	Significant
A-Binder Content	1.12	1	1.12	92.63	< 0.0001	Significant
B-W/B	1.53	1	1.53	125.82	< 0.0001	Significant
C-Replacement	0.93	1	0.93	76.21	< 0.0001	Significant
AC	0.07	1	0.07	5.38	0.0388	Significant
A^2	0.22	1	0.22	18.19	0.0011	Significant
B^2	0.33	1	0.33	27.53	0.0002	Significant
C^2	0.06	1	0.06	5.23	0.0412	Significant
Residual	0.15	12	0.01			
Lack of Fit	0.13	7	0.02	5.11	0.05	Not Significant
Pure Error	0.02	5	0.00			
Correlation Total	4.42	19				

d_f = Degrees of Freedom

C15: Effects of Factors A, B, and C on Response 8 (Segregation Factor)

Design-Expert® Software
Factor Coding: Actual
Original Scale
(median estimates)
Segregation Factor

— CI Bands
● Design Points

X1 = A: Binder Content (Kg/m3)

Actual Factors
B: W/B = 0.40
C: MK Replacement (%) = 12.50

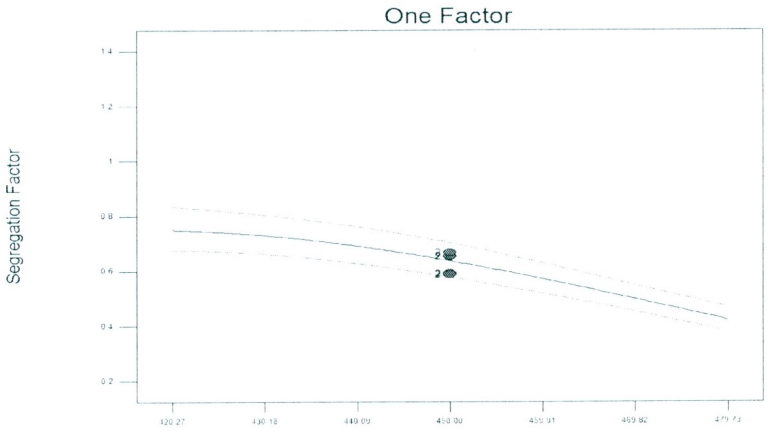

Design-Expert® Software
Factor Coding: Actual
Original Scale
(median estimates)
Segregation Factor

— CI Bands
● Design Points

X1 = B: W/B

Actual Factors
A: Binder Content (Kg/m3) = 450.00
C: MK Replacement (%) = 12.50

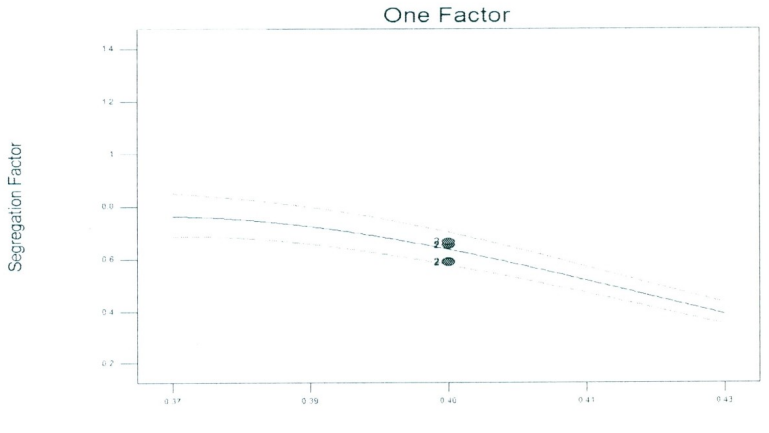

Design-Expert® Software
Factor Coding: Actual
Original Scale
(median estimates)
Segregation Factor

— CI Bands
● Design Points

X1 = C: MK Replacement (%)

Actual Factors
A: Binder Content (Kg/m3) = 450.00
B: W/B = 0.40

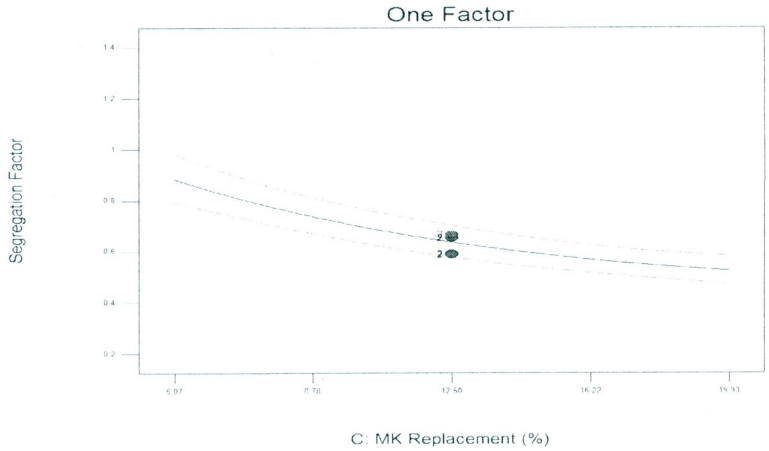

C16: Interaction Effect of AC on Response 8 (Segregation Factor)

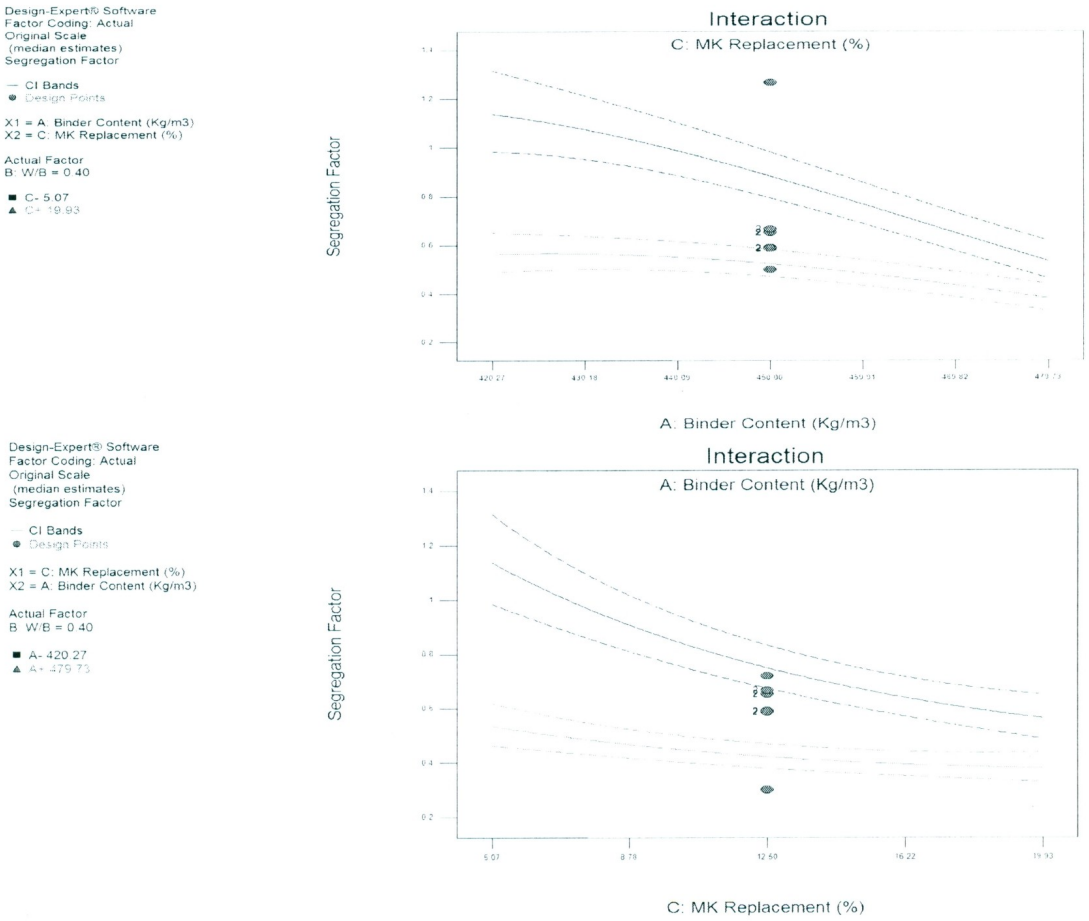

C17: Response Surfaces for factors A-B, A-C, and B-C for Response 8 (Segregation Factor)

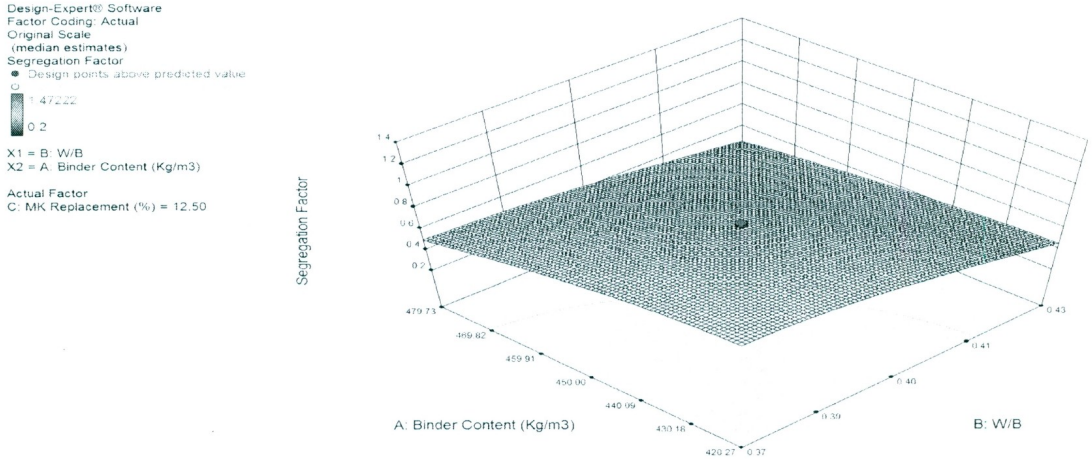

Design-Expert® Software
Factor Coding: Actual
Original Scale
(median estimates)
Segregation Factor
Design points above predicted value
1.47222
0.2

X1 = C: MK Replacement (%)
X2 = A: Binder Content (Kg/m3)

Actual Factor
B: W/B = 0.40

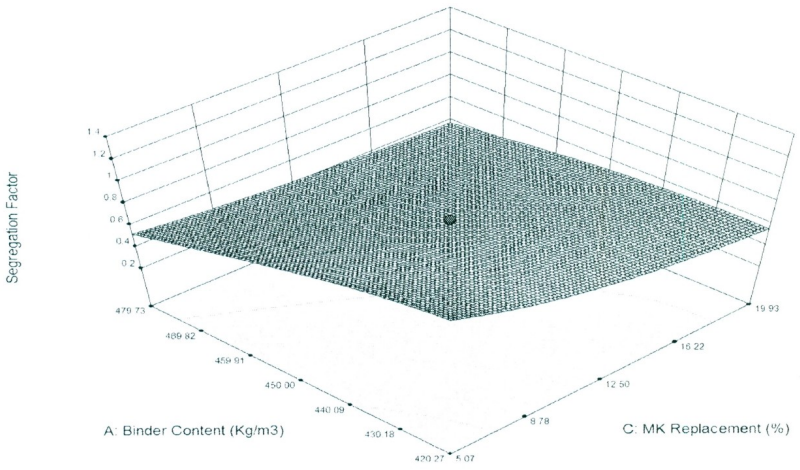

Design-Expert® Software
Factor Coding: Actual
Original Scale
(median estimates)
Segregation Factor
Design points above predicted value
1.47222
0.2

X1 = B: W/B
X2 = C: MK Replacement (%)

Actual Factor
A: Binder Content (Kg/m3) = 450.00

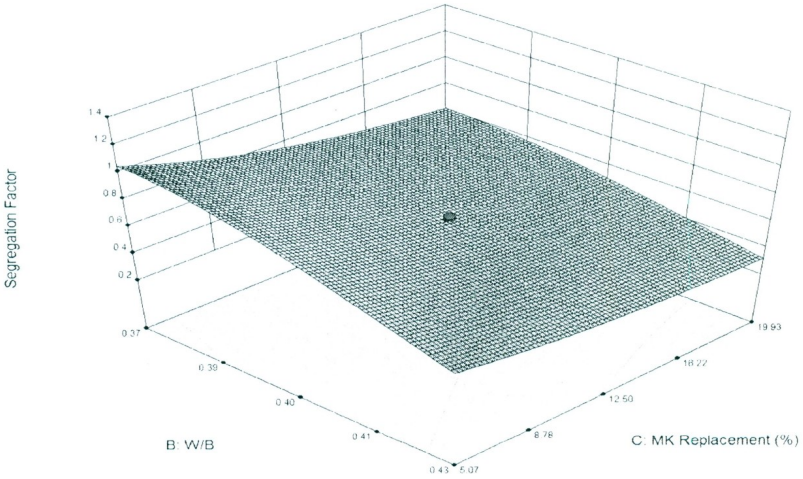

Response 9: Air Content

ANOVA Table for Response 9: Air Content

Response	9	Air Content				
ANOVA for Response Surface Reduced 2FI Model						
Analysis of variance table [Partial sum of squares - Type III]						
Source	Sum of Squares	d_f	Mean Square	F-Value	P-Value (Prob. > F)	Significance
Model	3.28	5	0.66	6.08	0.0034	Significant
A-Binder Content	0.11	1	0.11	1.06	0.3202	Significant
B-W/B	0.49	1	0.49	4.57	0.0506	Significant
C-Replacement	0.03	1	0.03	0.31	0.5848	Significant
AB	1.36	1	1.36	12.59	0.0032	Significant
BC	1.28	1	1.28	11.84	0.0040	Significant
Residual	1.51	14	0.11			
Lack of Fit	1.28	9	0.14	3.05	0.1163	Not Significant
Pure Error	0.23	5	0.05			
Correlation Total	4.80	19				

d_f = Degrees of Freedom

C18: Effects of Factors A, B, and C on Response 9 (Air Content)

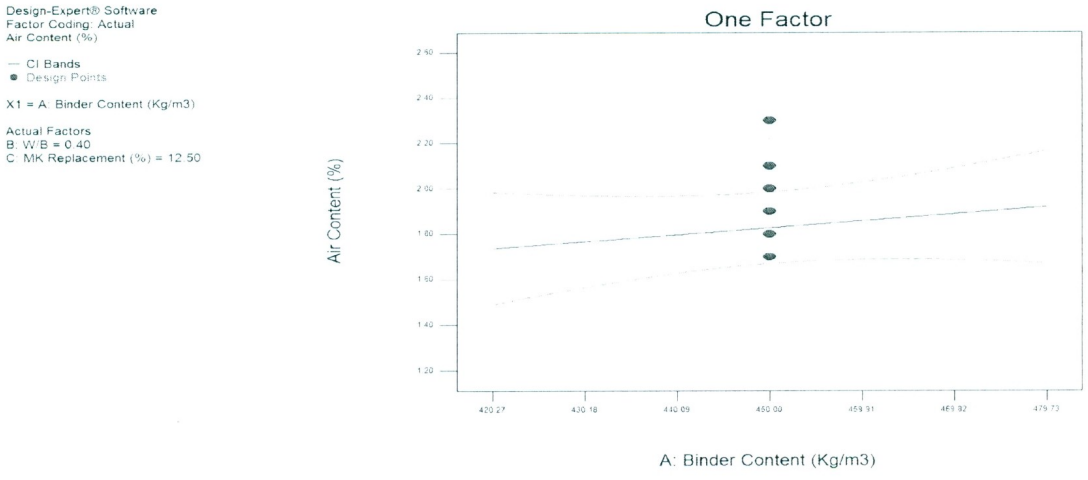

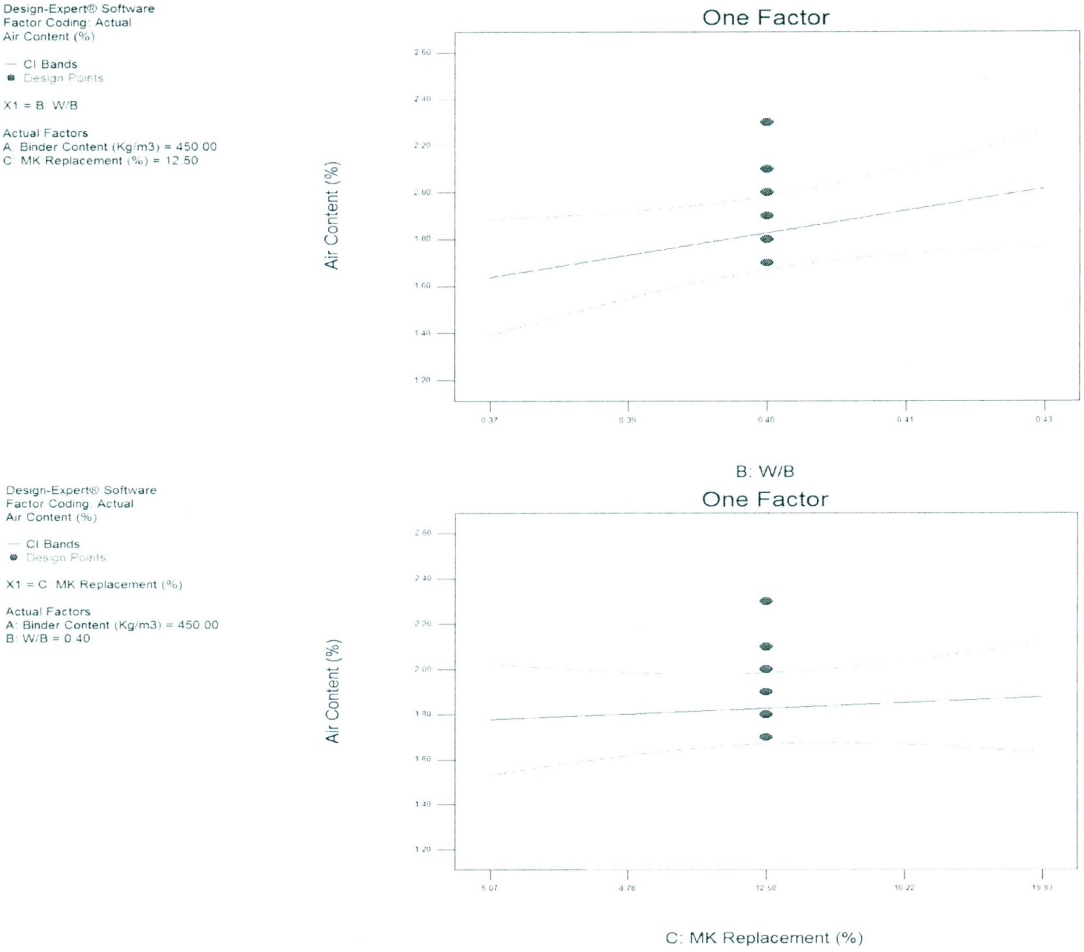

C19: Interaction Effects of Factors AB and BC on Response 9 (Air Content)

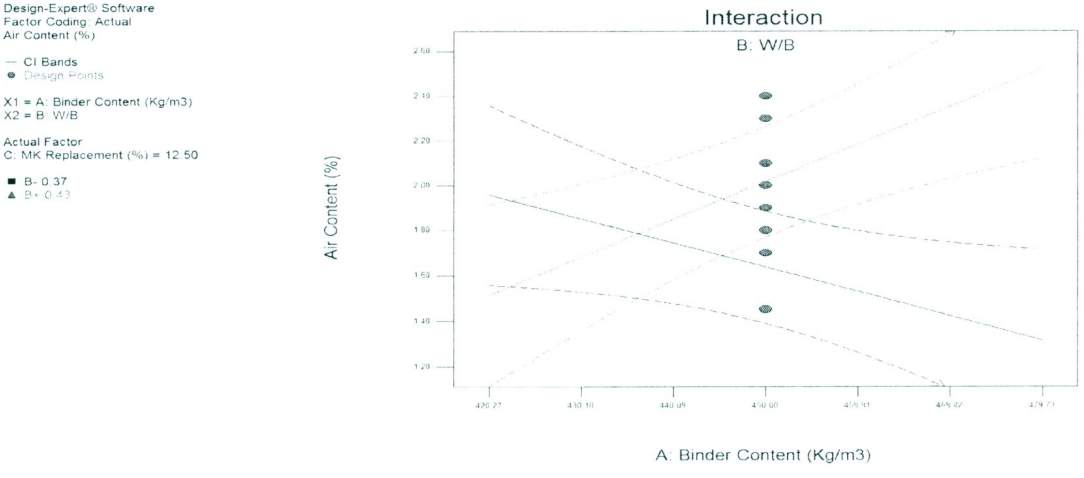

Design-Expert® Software
Factor Coding: Actual
Air Content (%)

— CI Bands
● Design Points

X1 = B: W/B
X2 = A: Binder Content (Kg/m3)

Actual Factor
C: MK Replacement (%) = 12.50

■ A- 420.27
▲ A+ 479.73

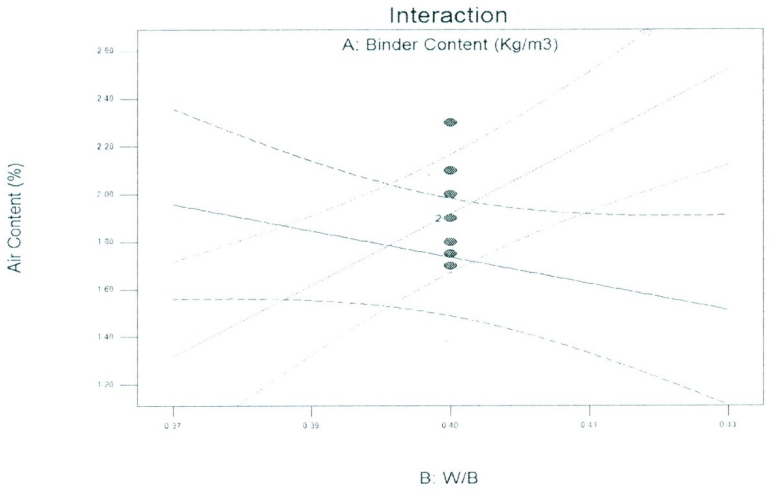

Design-Expert® Software
Factor Coding: Actual
Air Content (%)

— CI Bands
● Design Points

X1 = B: W/B
X2 = C: MK Replacement (%)

Actual Factor
A: Binder Content (Kg/m3) = 450.00

■ C- 5.07
▲ C+ 19.93

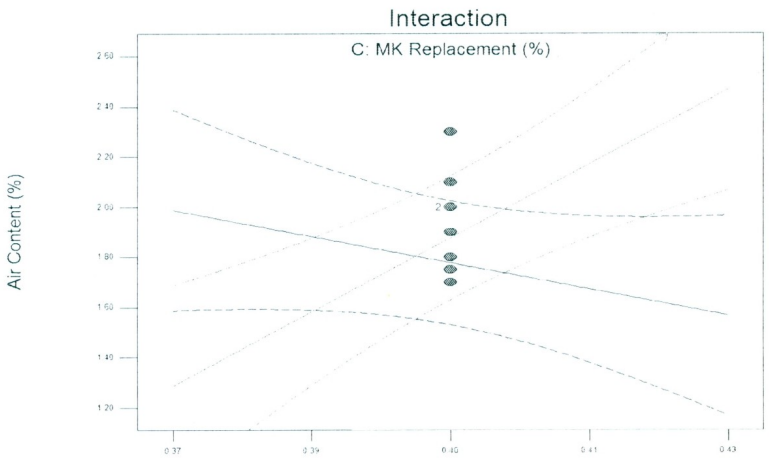

Design-Expert® Software
Factor Coding: Actual
Air Content (%)

— CI Bands
● Design Points

X1 = C: MK Replacement (%)
X2 = B: W/B

Actual Factor
A: Binder Content (Kg/m3) = 450.00

■ B- 0.37
▲ B+ 0.43

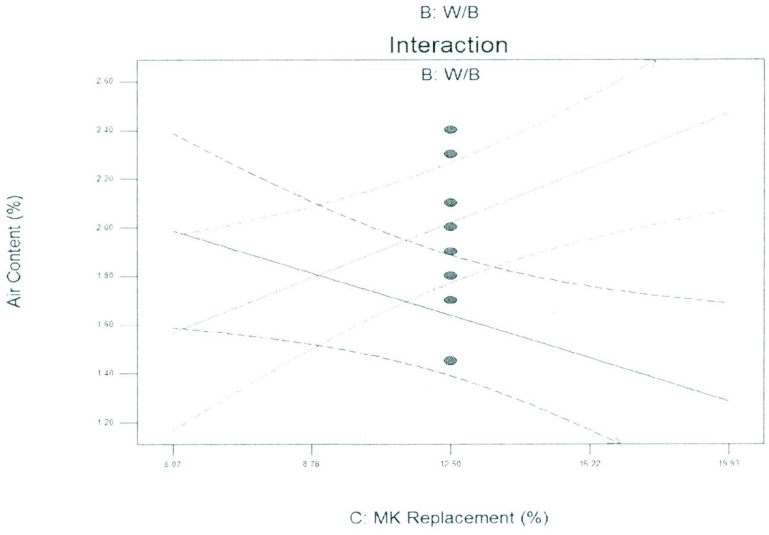

C20: Response Surfaces for factors A-B, A-C, and B-C for Response 9 (Air Content)

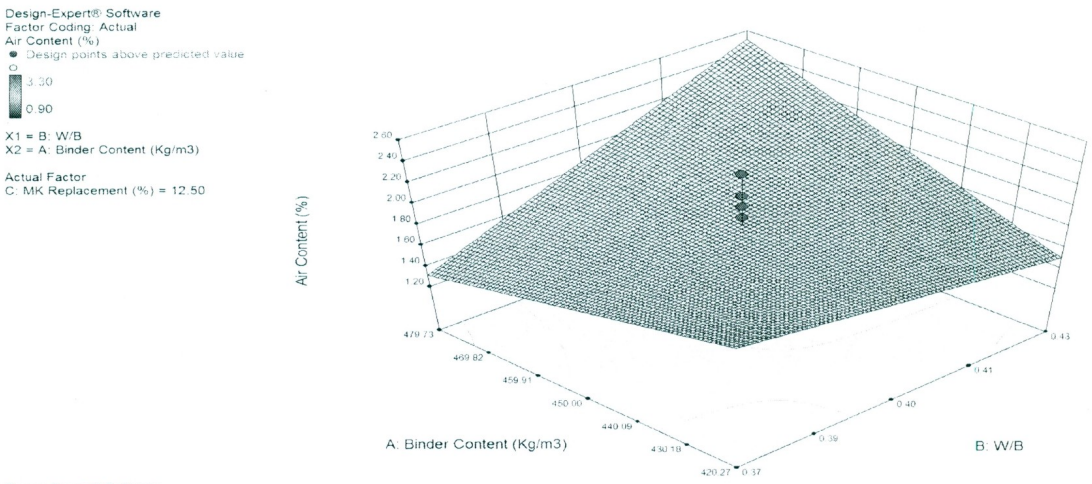

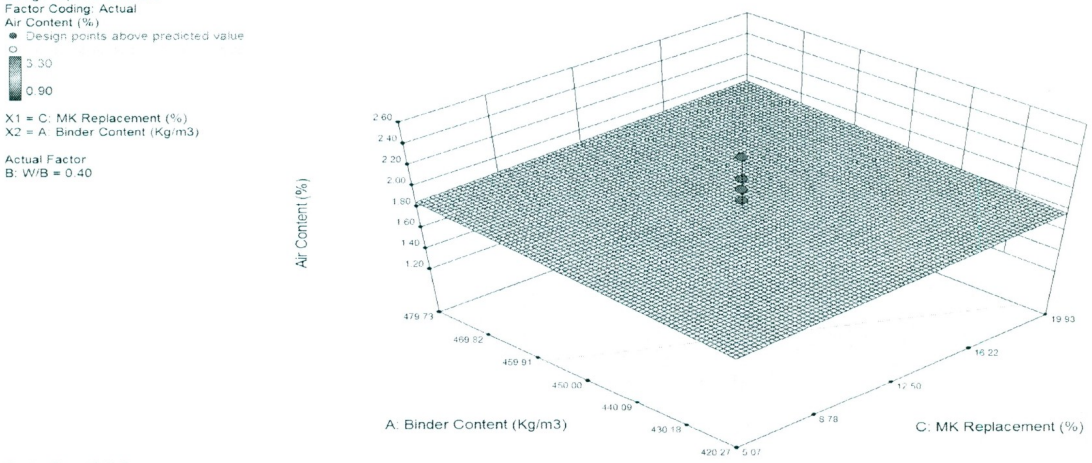

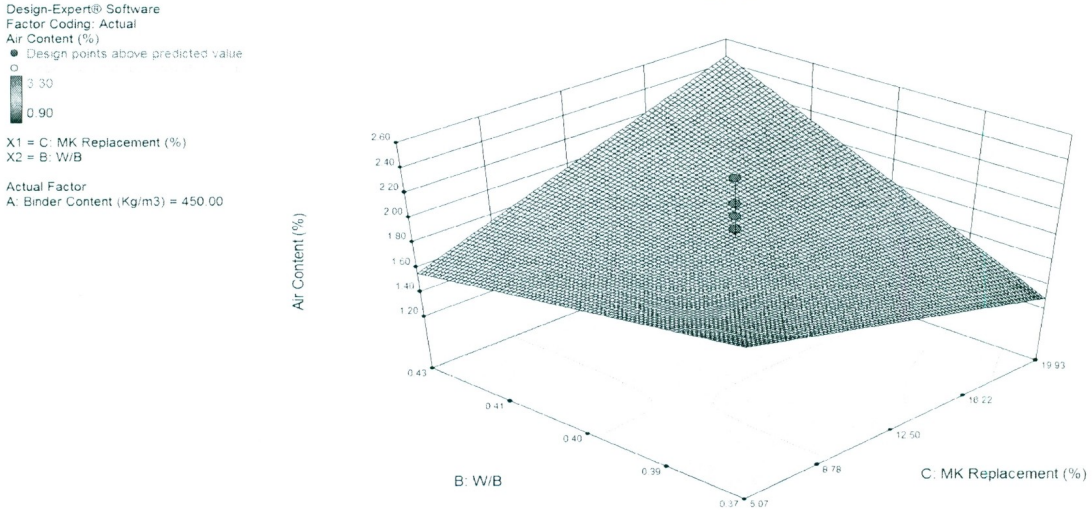

Response 10: Compressive Strength 28 Days (Air)

ANOVA Table for Response 10: Compressive Strength 28 Days (Air)

Response	10	Compressive Strength 28 Days (Air)				
ANOVA for Response Surface Reduced Quadratic Model						
Analysis of variance table [Partial sum of squares - Type III]						
Source	Sum of Squares	d_f	Mean Square	F-Value	P-Value (Prob. > F)	Significance
Model	1559.91	7	222.84	19.40	< 0.0001	Significant
A-Binder Content	325.15	1	325.15	28.30	0.0002	Significant
B-W/B	350.88	1	350.88	30.54	0.0001	Significant
C-Replacement	427.01	1	427.01	37.17	< 0.0001	Significant
AB	70.75	1	70.75	6.16	0.0289	Significant
A^2	88.38	1	88.38	7.69	0.0168	Significant
B^2	81.33	1	81.33	7.08	0.0208	Significant
C^2	280.54	1	280.54	24.42	0.0003	Significant
Residual	137.86	12	11.49			
Lack of Fit	120.22	7	17.17	4.87	0.0502	Not Significant
Pure Error	17.64	5	3.53			
Correlation Total	1697.77	19				

d_f = Degrees of Freedom

C21: Effects of Factors A, B, and C on Response 10 (Compressive Strength 28 Days-Air)

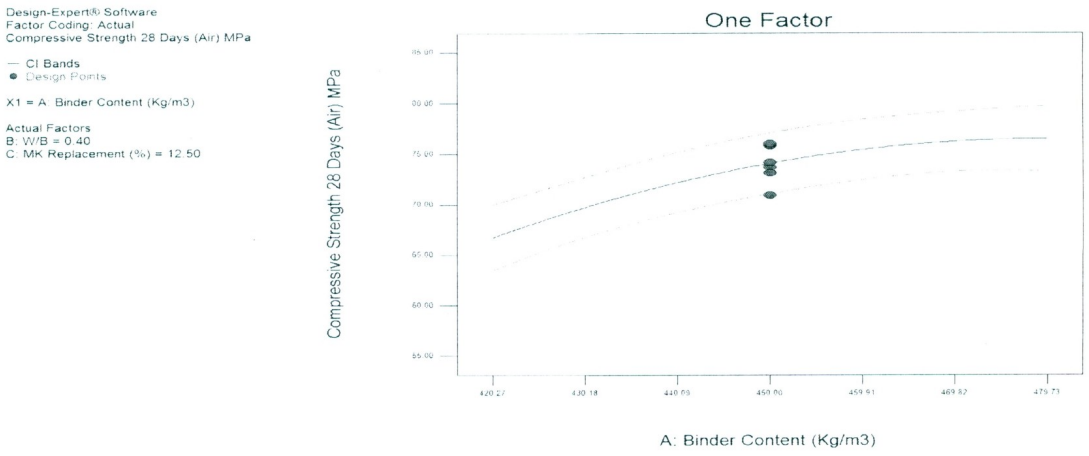

Design-Expert® Software
Factor Coding: Actual
Compressive Strength 28 Days (Air) MPa

— CI Bands
● Design Points

X1 = B: W/B

Actual Factors
A: Binder Content (Kg/m3) = 450.00
C: MK Replacement (%) = 12.50

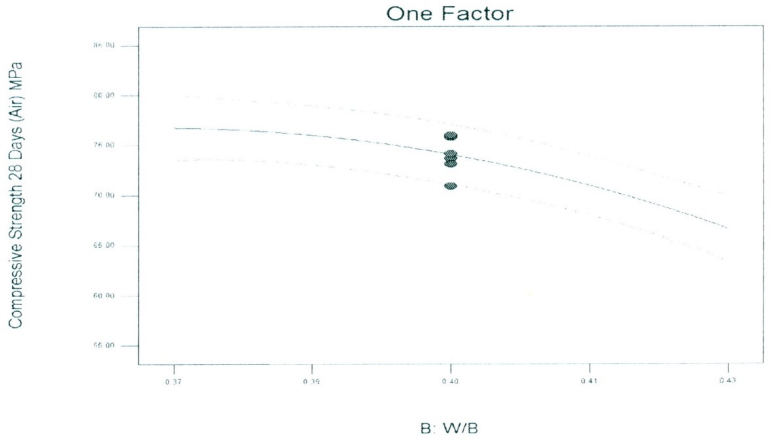

Design-Expert® Software
Factor Coding: Actual
Compressive Strength 28 Days (Air) MPa

— CI Bands
● Design Points

X1 = C: MK Replacement (%)

Actual Factors
A: Binder Content (Kg/m3) = 450.00
B: W/B = 0.40

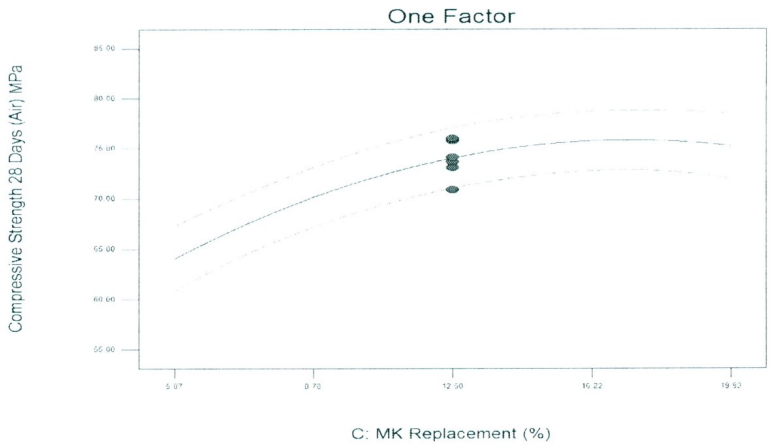

C22: Interaction Effect of Factor AB on Response 10 (Compressive Strength 28 Days-Air)

Design-Expert® Software
Factor Coding: Actual
Compressive Strength 28 Days (Air) MPa

— CI Bands
● Design Points

X1 = A: Binder Content (Kg/m3)
X2 = B: W/B

Actual Factor
C: MK Replacement (%) = 12.50

■ B- 0.37
▲ B+ 0.43

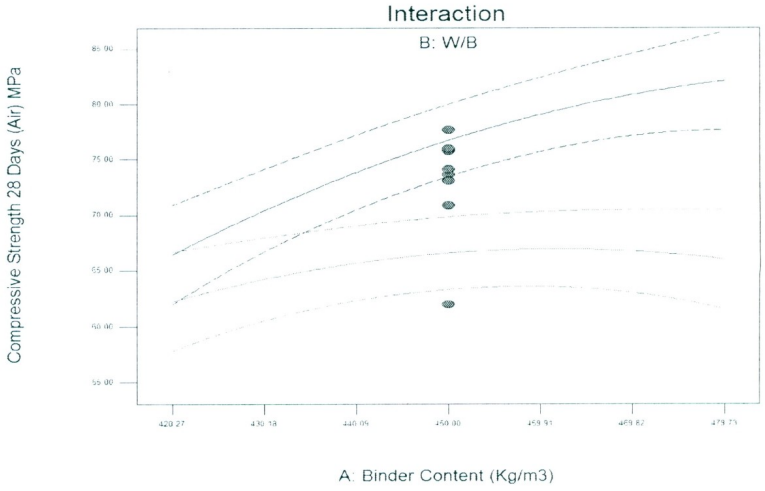

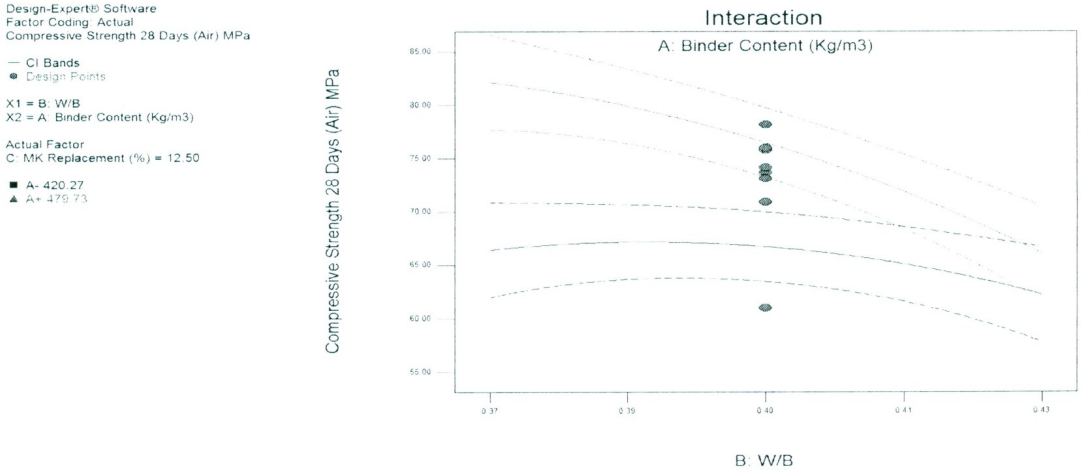

C23: Response Surfaces for factors A-B, A-C, and B-C for Response 10 (Compressive Strength 28 Days-Air)

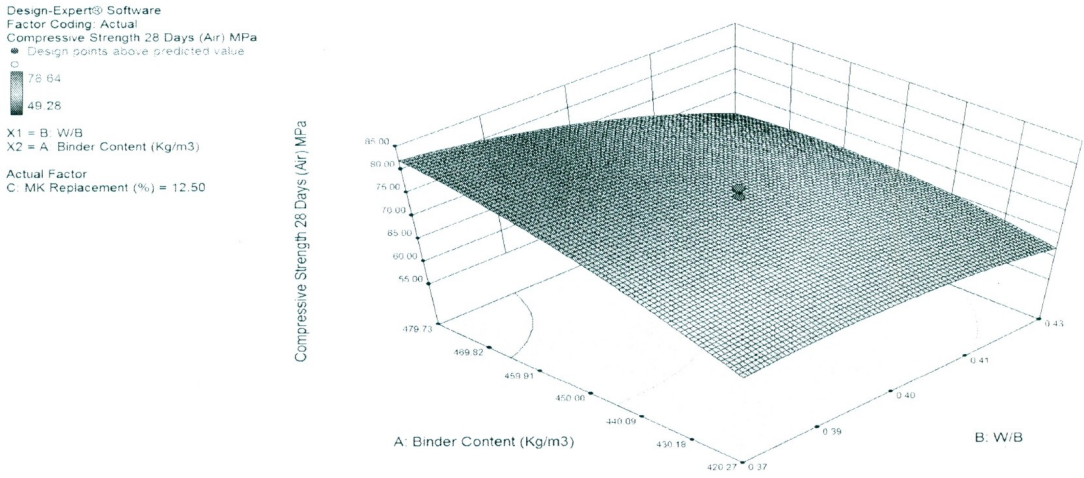

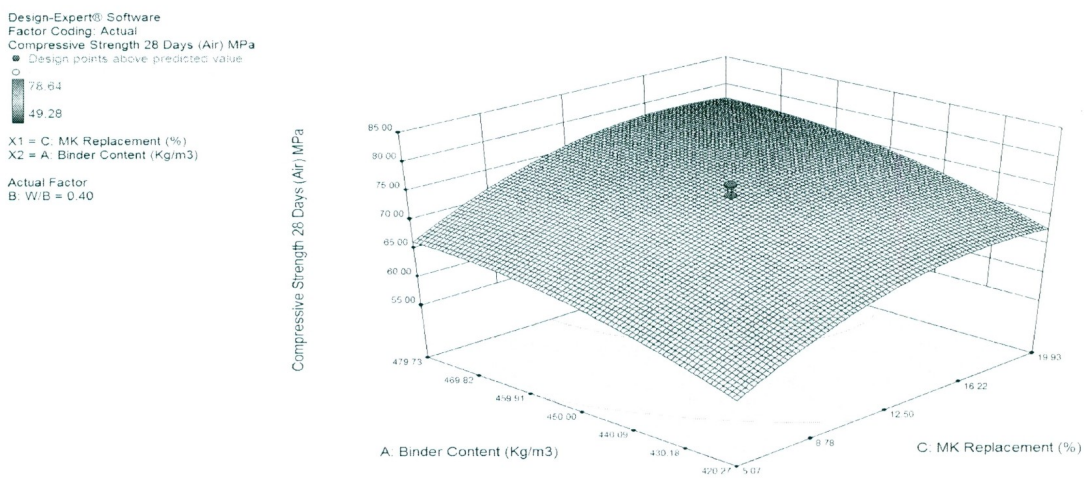

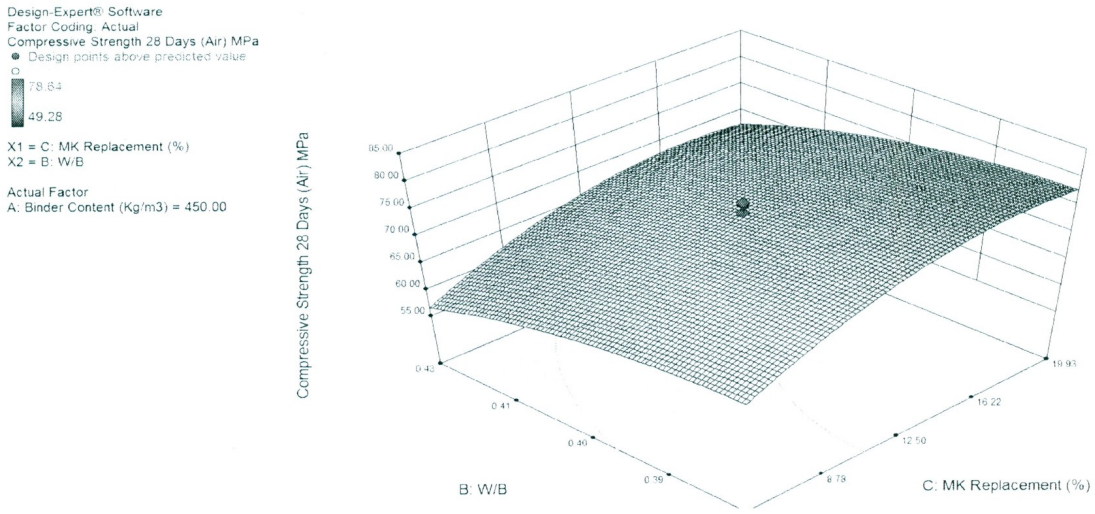

Response 11: Compressive Strength 28 Days (Water)

ANOVA Table for Response 11: Compressive Strength 28 Days (Water)

Response	11	Compressive Strength 28 Days (Water)				
ANOVA for Response Surface Reduced Quadratic Model						
Analysis of variance table [Partial sum of squares - Type III]						
Source	Sum of Squares	d_f	Mean Square	F-Value	P-Value (Prob. > F)	Significance
Model	1516.24	7	216.61	28.09	< 0.0001	Significant
A-Binder Content	336.64	1	336.64	43.65	< 0.0001	Significant
B-W/B	136.14	1	136.14	17.65	0.0012	Significant
C-Replacement	586.35	1	586.35	76.03	< 0.0001	Significant
AB	53.87	1	53.87	6.99	0.0215	Significant
A^2	121.28	1	121.28	15.73	0.0019	Significant
B^2	100.93	1	100.93	13.09	0.0035	Significant
C^2	254.46	1	254.46	33.00	< 0.0001	Significant
Residual	92.54	12	7.71			
Lack of Fit	73.45	7	10.49	2.75	0.1417	Not Significant
Pure Error	19.09	5	3.82			
Correlation Total	1608.78	19				

d_f = Degrees of Freedom

C24: Effects of Factors A, B, and C on Response 11 (Compressive Strength 28 Days-Water)

Design-Expert® Software
Factor Coding: Actual
Compressive Strength 28 Days (Water) MPa

— CI Bands
● Design Points

X1 = A: Binder Content (Kg/m3)

Actual Factors
B: W/B = 0.40
C: MK Replacement (%) = 12.50

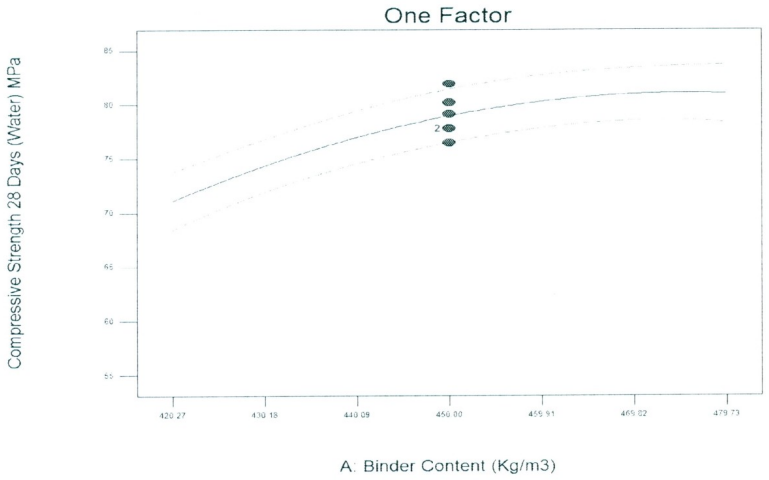

Design-Expert® Software
Factor Coding: Actual
Compressive Strength 28 Days (Water) MPa

— CI Bands
● Design Points

X1 = B: W/B

Actual Factors
A: Binder Content (Kg/m3) = 450.00
C: MK Replacement (%) = 12.50

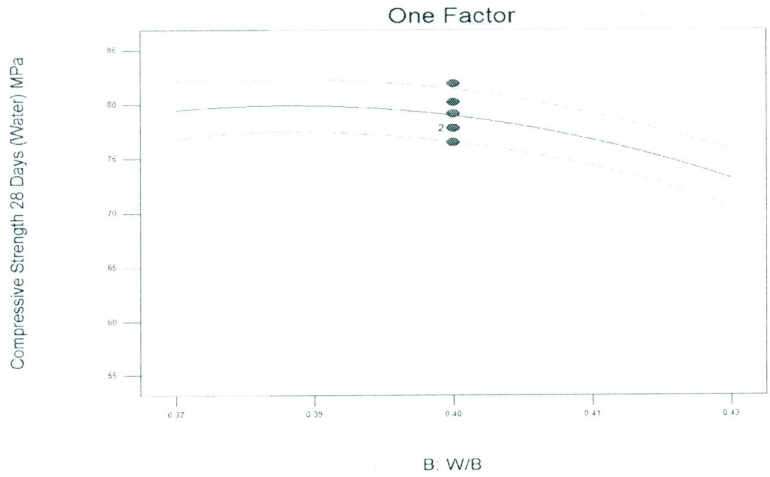

Design-Expert® Software
Factor Coding: Actual
Compressive Strength 28 Days (Water) MPa

— CI Bands
● Design Points

X1 = C: MK Replacement (%)

Actual Factors
A: Binder Content (Kg/m3) = 450.00
B: W/B = 0.40

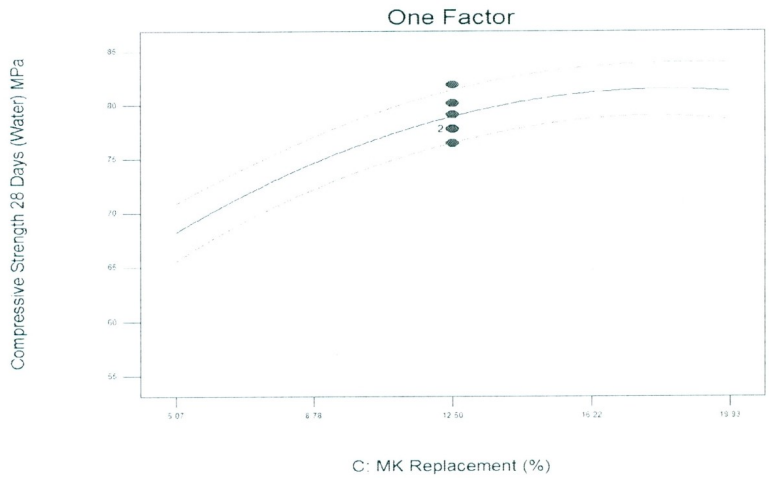

C25: Interaction Effect of Factor AB on Response 11: Compressive Strength 28 Days (Water)

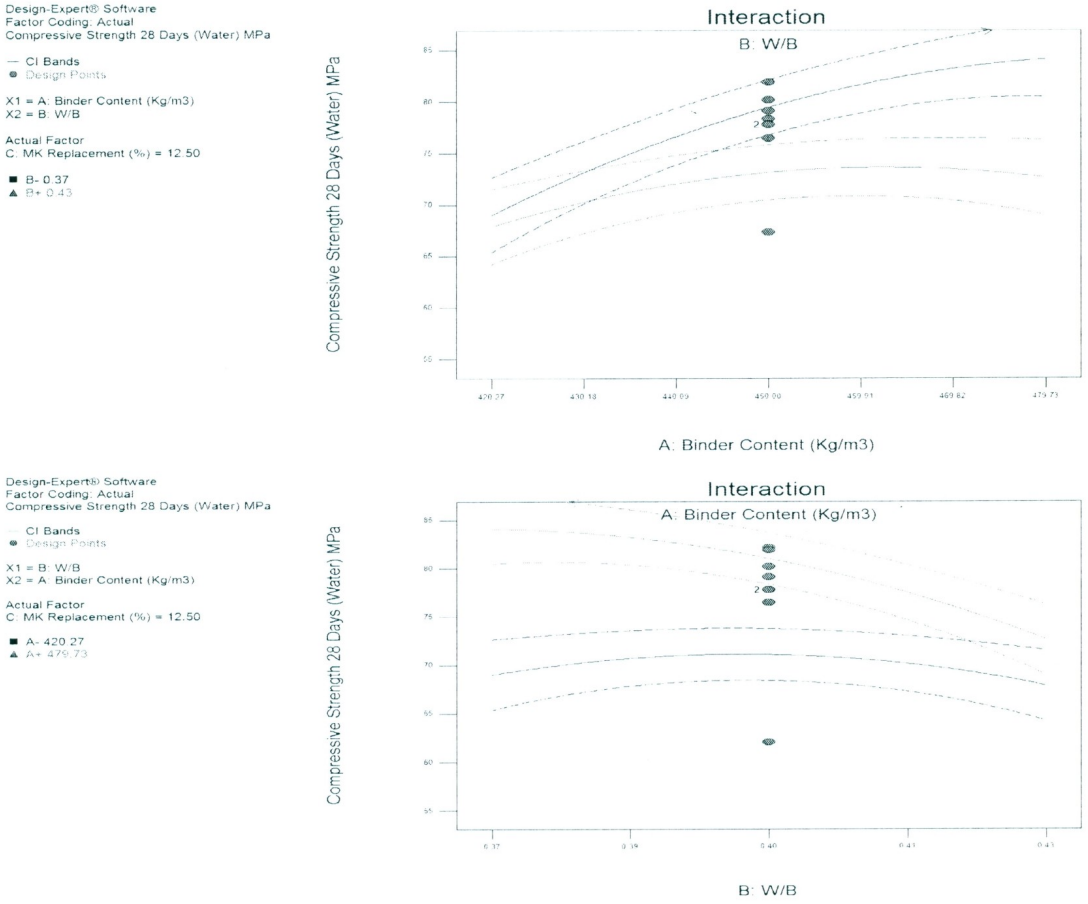

C26: Response Surfaces for factors A-B, A-C, and B-C for Response 11 (Compressive Strength 28 Days-Water)

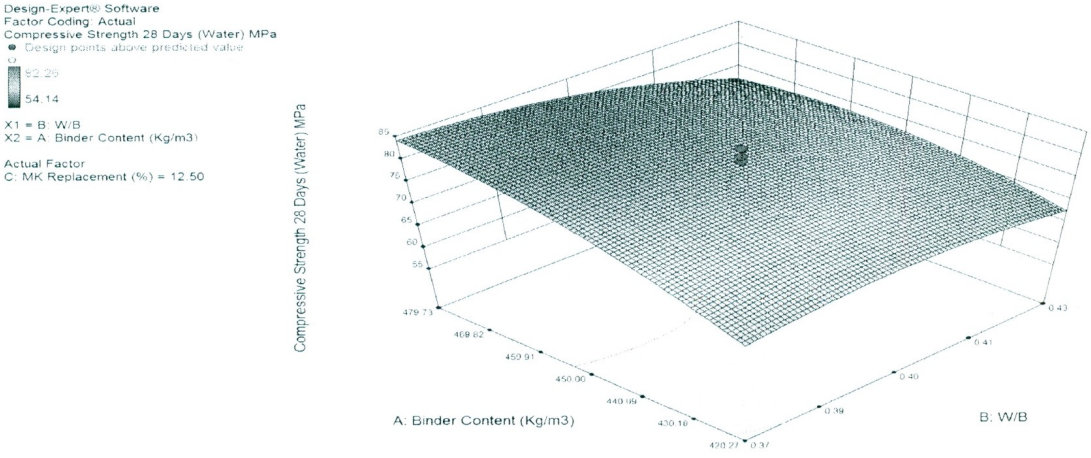

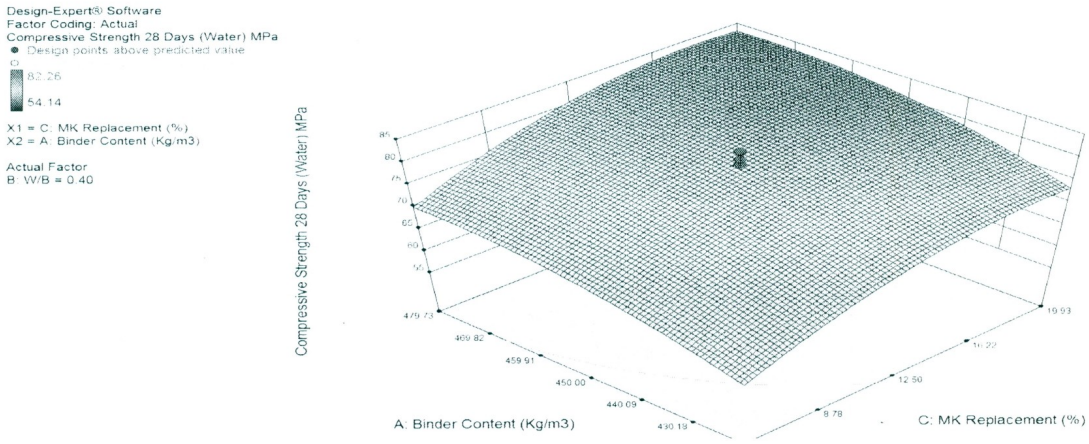
Design-Expert® Software
Factor Coding: Actual
Compressive Strength 28 Days (Water) MPa
Design points above predicted value
82.26
54.14
X1 = C: MK Replacement (%)
X2 = A: Binder Content (Kg/m3)
Actual Factor
B: W/B = 0.40
Compressive Strength 28 Days (Water) MPa
85
80
75
70
65
60
55
479.73
469.82
459.91
450.00
440.09
430.18
A: Binder Content (Kg/m3)
0.78
12.50
16.22
19.93
C: MK Replacement (%)

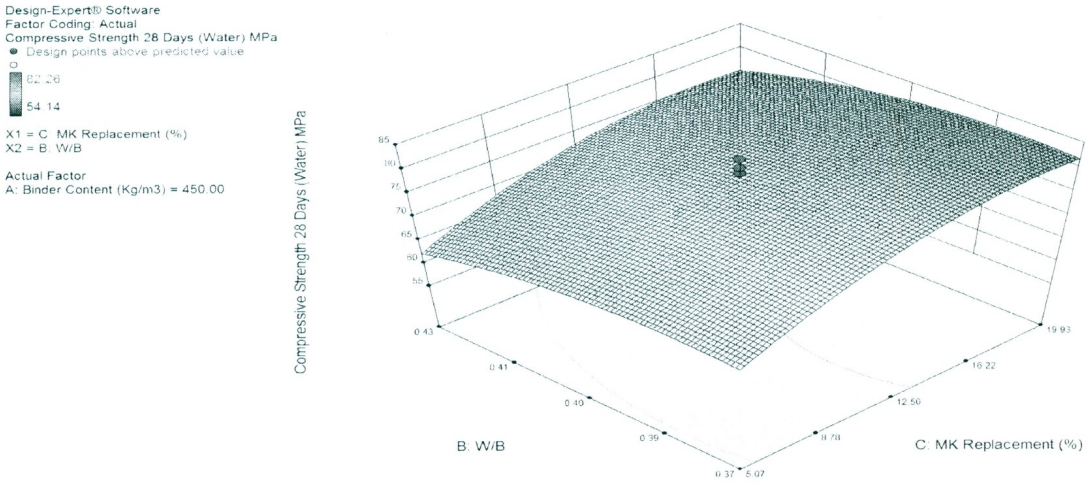
Design-Expert® Software
Factor Coding: Actual
Compressive Strength 28 Days (Water) MPa
Design points above predicted value
82.26
54.14
X1 = C: MK Replacement (%)
X2 = B: W/B
Actual Factor
A: Binder Content (Kg/m3) = 450.00
Compressive Strength 28 Days (Water) MPa
85
80
75
70
65
60
55
0.43
0.41
0.40
0.38
0.37
B: W/B
5.07
8.78
12.50
16.22
19.93
C: MK Replacement (%)

Response 12: 28-Days RCPT (Air)

ANOVA Table for Response 12: 28-Days RCPT (Air)

Response	12	28-Days RCPT (Air)				
Transform:	Natural Log	Constant:	0			
ANOVA for Response Surface Reduced Quadratic Model						
Analysis of variance table [Partial sum of squares - Type III]						
Source	Sum of Squares	d_f	Mean Square	F-Value	P-Value (Prob. > F)	Significance
Model	11.178	6	1.8630	70.39	< 0.0001	Significant
A-Binder Content	0.233	1	0.2328	8.80	0.0109	Significant
B-W/B	0.876	1	0.8756	33.08	< 0.0001	Significant
C-MK Replacement	6.623	1	6.6229	250.21	< 0.0001	Significant
A^2	0.138	1	0.1382	5.22	0.0398	Significant
B^2	0.303	1	0.3027	11.44	0.0049	Significant
C^2	3.283	1	3.2829	124.03	< 0.0001	Significant
Residual	0.344	13	0.0265			
Lack of Fit	0.342	8	0.0428	111.98	< 0.0001	Significant
Pure Error	0.002	5	0.0004			
Correlation Total	11.522	19				

d_f = Degrees of Freedom

C27: Effects of Factors A, B, and C on Response 12 (28-Days RCPT-Air)

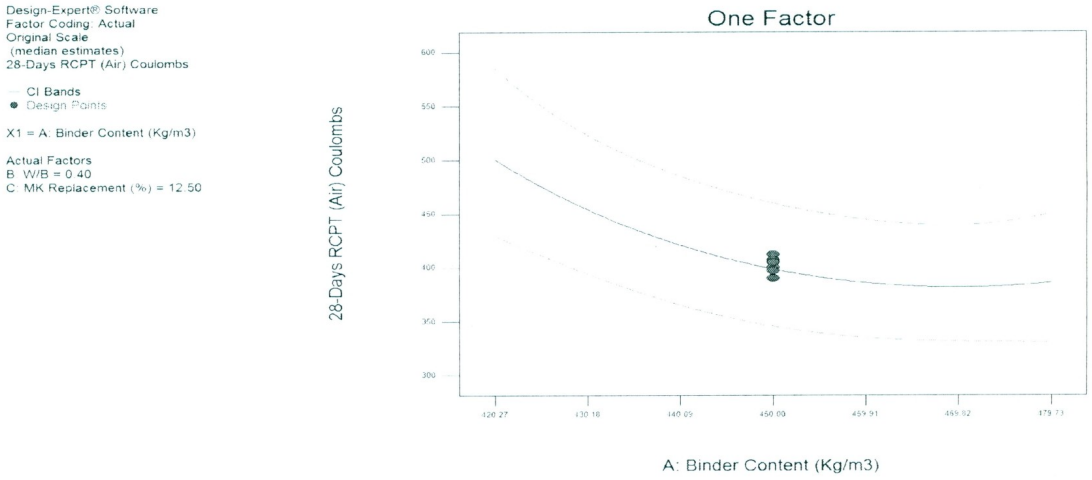

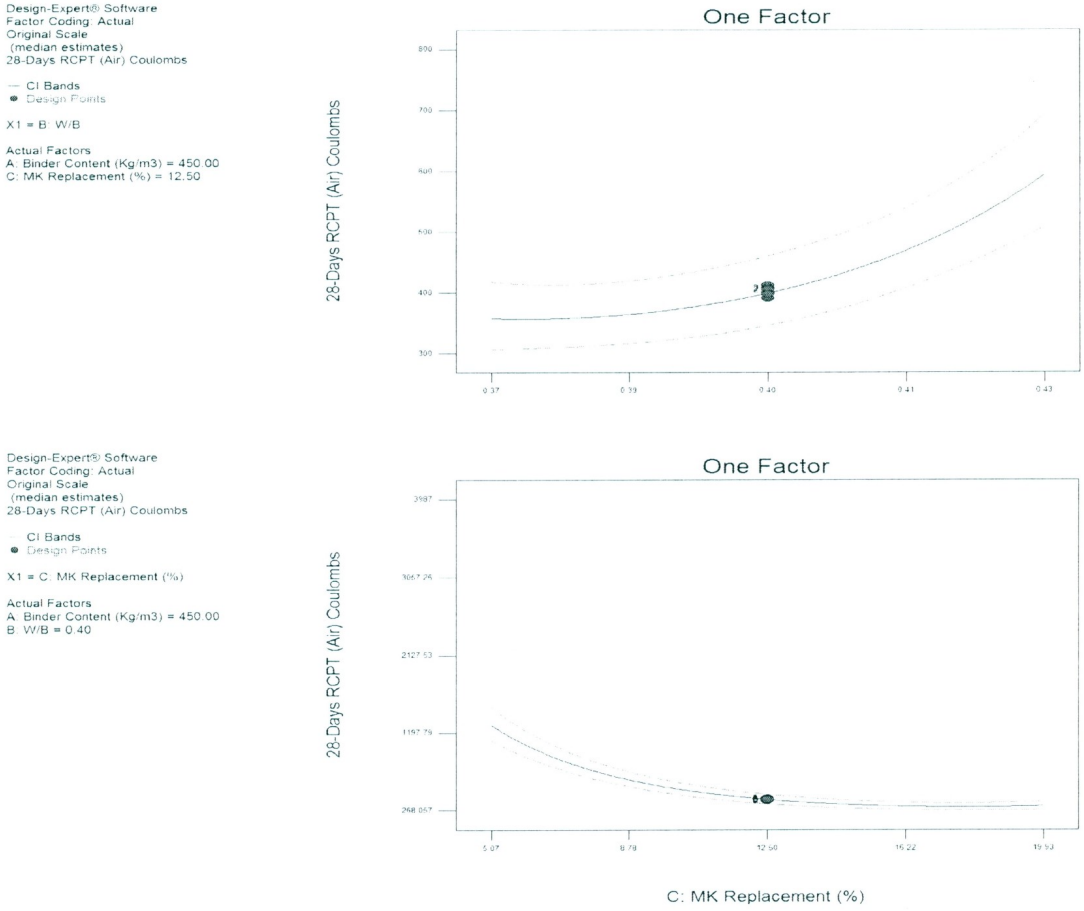

C28: Response Surfaces for factors A-B, A-C, and B-C for Response 12 (28-Days RCPT-Air)

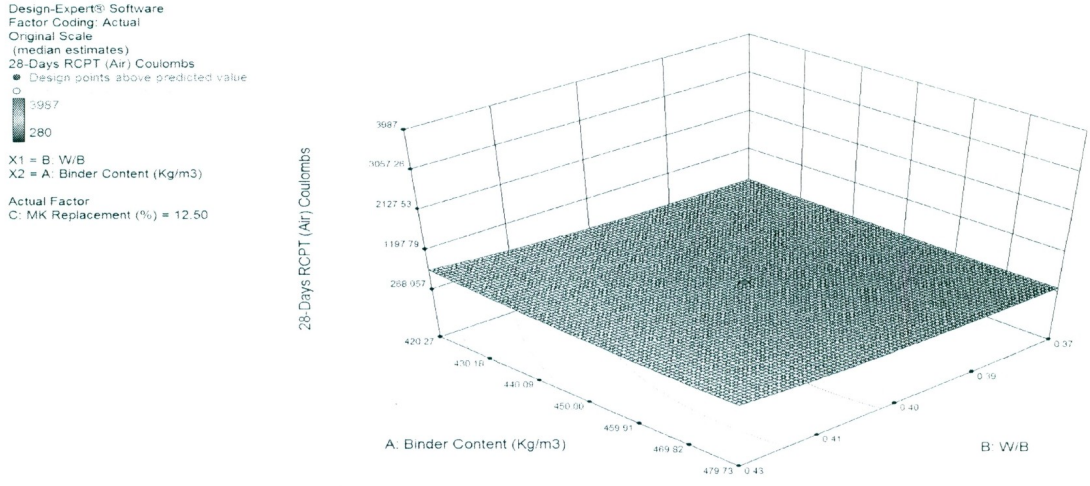

Design-Expert® Software
Factor Coding: Actual
Original Scale
(median estimates)
28-Days RCPT (Air) Coulombs
Design points above predicted value
3987
280

X1 = C: MK Replacement (%)
X2 = A: Binder Content (Kg/m3)

Actual Factor
B: W/B = 0.40

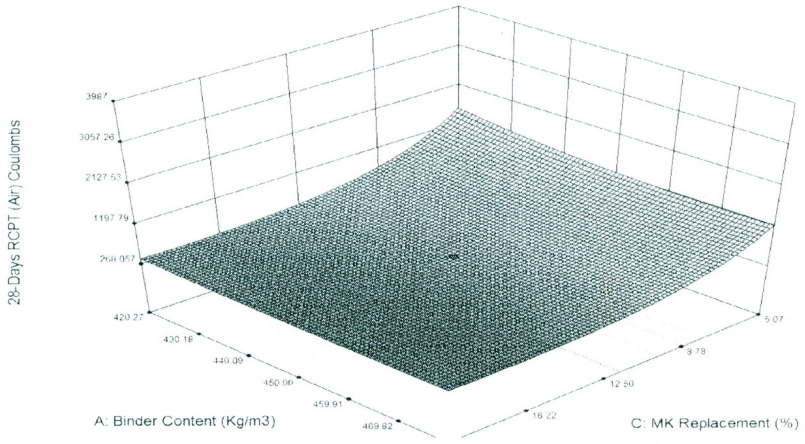

Design-Expert® Software
Factor Coding: Actual
Original Scale
(median estimates)
28-Days RCPT (Air) Coulombs
Design points above predicted value
3987
280

X1 = B: W/B
X2 = C: MK Replacement (%)

Actual Factor
A: Binder Content (Kg/m3) = 450.00

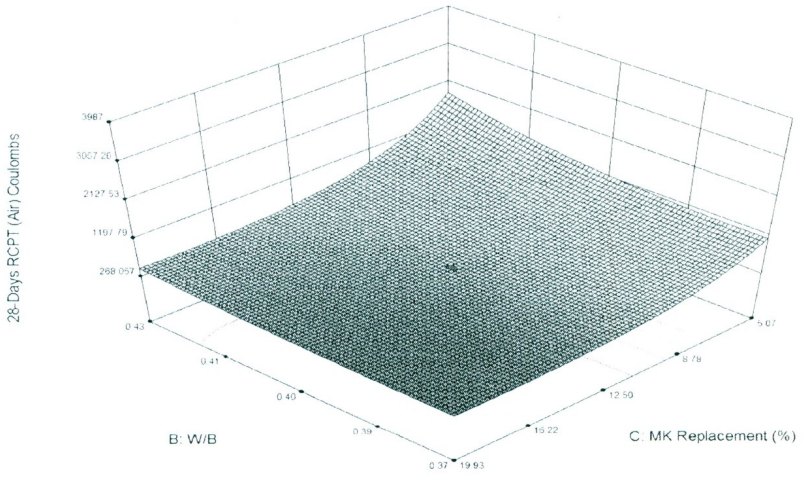

Response 13: 28-Days RCPT (Water)

ANOVA Table for Response 13: 28-Days RCPT (Water)

Response	13	28-Days RCPT (Water)				
Transform:	Natural Log	Constant:	0			
ANOVA for Response Surface Reduced Quadratic Model						
Analysis of variance table [Partial sum of squares - Type III]						
Source	Sum of Squares	d_f	Mean Square	F-Value	P-Value (Prob. > F)	Significance
Model	10.686	4	2.672	195.19	< 0.0001	Significant
A-Binder Content	0.058	1	0.058	4.22	0.0577	Significant
B-W/B	0.078	1	0.078	5.72	0.0303	Significant
C-MK Replacement	7.936	1	7.936	579.86	< 0.0001	Significant
C^2	2.614	1	2.614	190.96	< 0.0001	Significant
Residual	0.205	15	0.014			
Lack of Fit	0.192	10	0.019	7.39	0.0197	Significant
Pure Error	0.013	5	0.003			
Correlation Total	10.891	19				

d_f = Degrees of Freedom

C29: Effects of Factors A, B, and C on Response 13 (28-Days RCPT-Water)

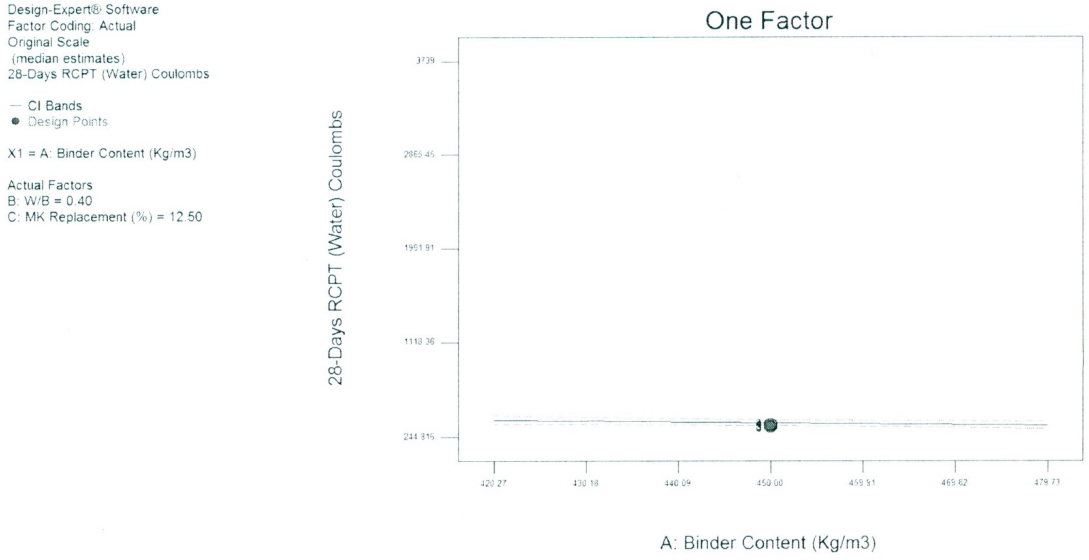

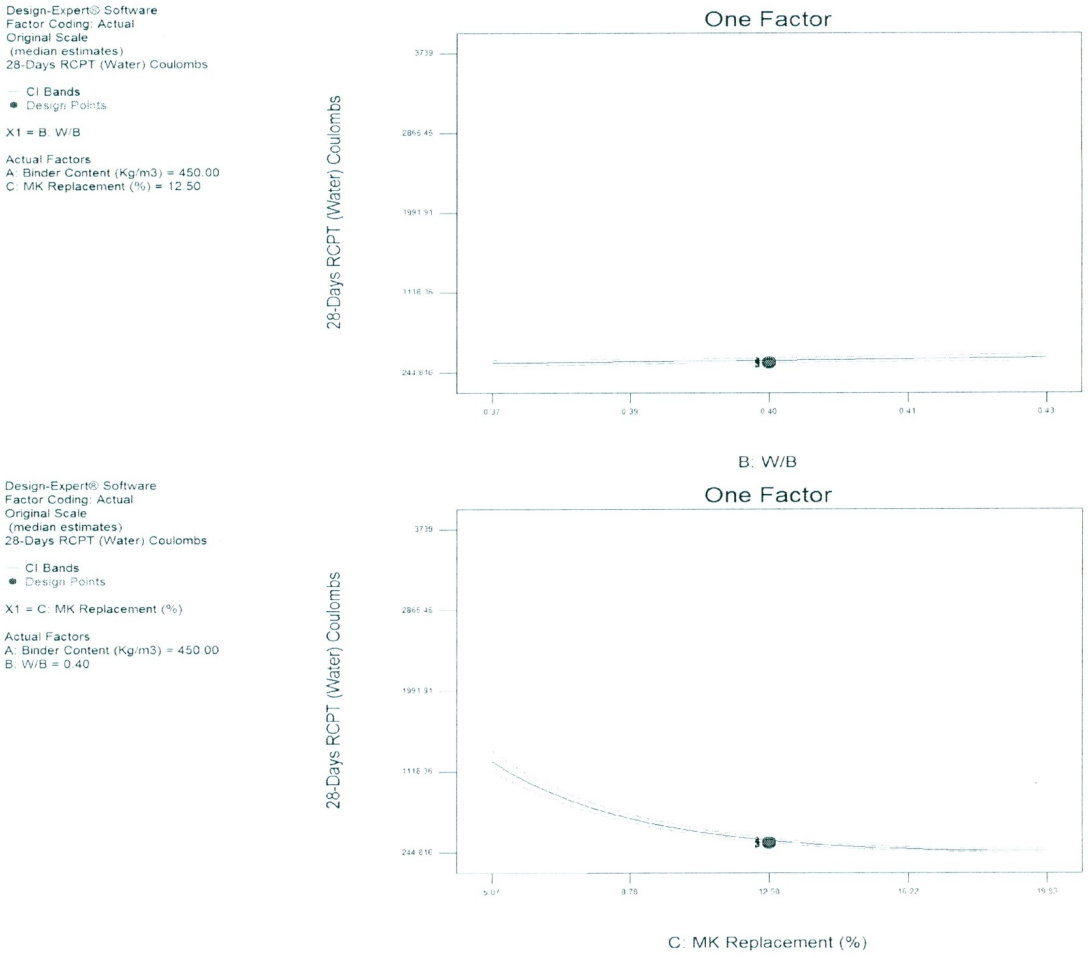

C30: Response Surfaces for factors A-B, A-C, and B-C for Response 13 (28-Days RCPT-Water)

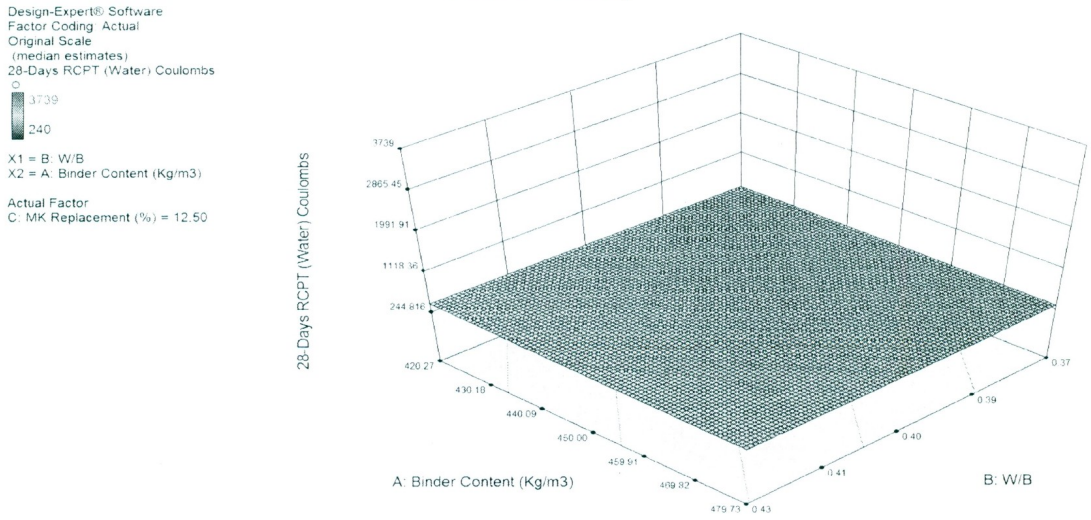

Design-Expert® Software
Factor Coding: Actual
Original Scale
(median estimates)
28-Days RCPT (Water) Coulombs

3739
240

X1 = C: MK Replacement (%)
X2 = A: Binder Content (Kg/m3)

Actual Factor
B: W/B = 0.40

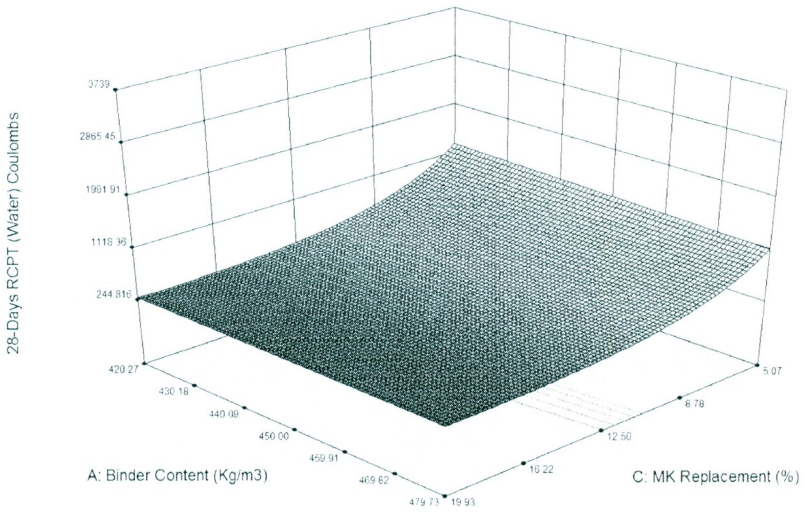

Design-Expert® Software
Factor Coding: Actual
Original Scale
(median estimates)
28-Days RCPT (Water) Coulombs

3739
240

X1 = B: W/B
X2 = C: MK Replacement (%)

Actual Factor
A: Binder Content (Kg/m3) = 450.00

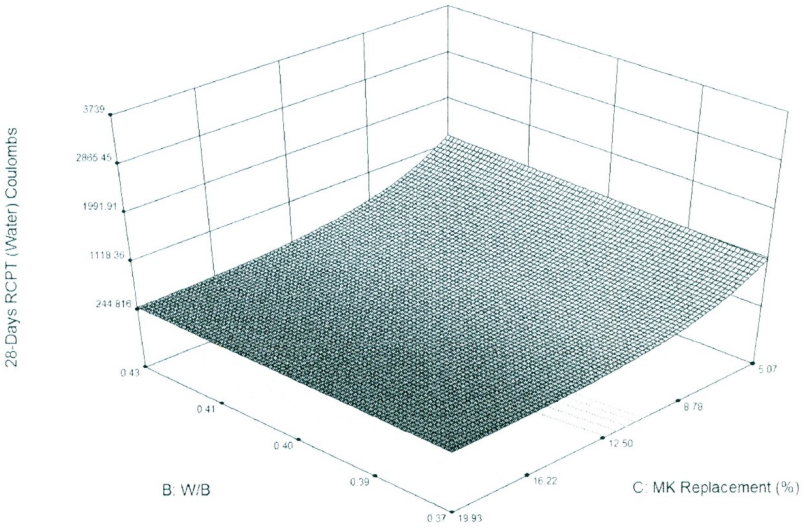

Response 14: 90-Days RCPT (Air)

ANOVA Table for Response 14: 90-Days RCPT (Air)

Response	14	90-Days RCPT (Air)				
Transform:	Natural Log	Constant:	0			
ANOVA for Response Surface Reduced Quadratic Model						
Analysis of variance table [Partial sum of squares - Type III]						
Source	Sum of Squares	d_f	Mean Square	F-Value	P-Value (Prob. > F)	Significance
Model	11.497	5	2.2994	79.87	< 0.0001	Significant
A-Binder Content	0.160	1	0.1596	5.55	0.0336	Significant
B-W/B	0.872	1	0.8718	30.28	< 0.0001	Significant
C-Replacement	8.164	1	8.1635	283.58	< 0.0001	Significant
B^2	0.339	1	0.3392	11.78	0.0040	Significant
C^2	2.096	1	2.0963	72.82	< 0.0001	Significant
Residual	0.403	14	0.0288			
Lack of Fit	0.401	9	0.0446	124	< 0.0001	Significant
Pure Error	0.002	5	0.0004			
Correlation Total	11.900	19				

d_f = Degrees of Freedom

C31: Effects of Factors A, B, and C on Response 14 (90-Days RCPT-Air)

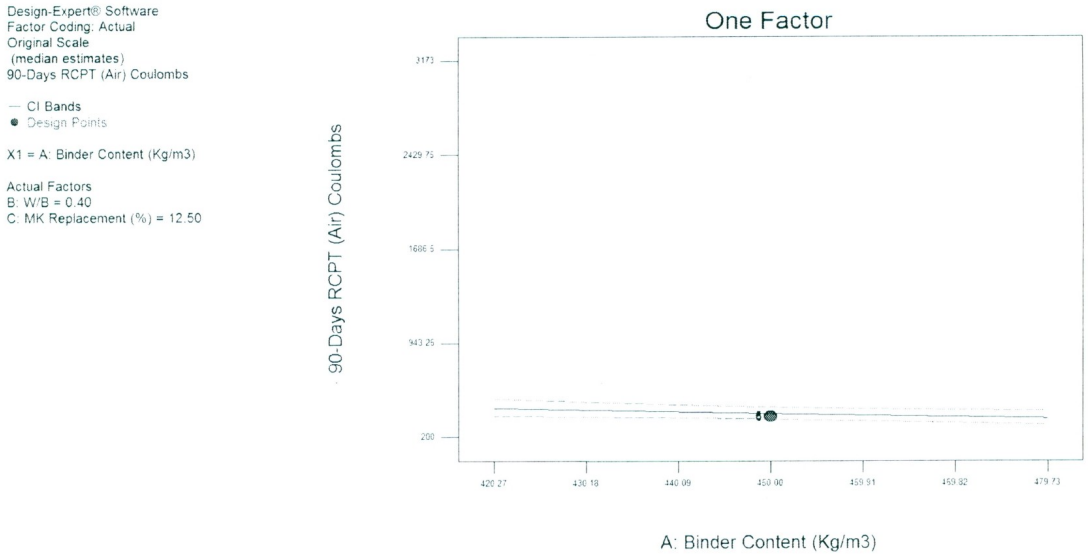

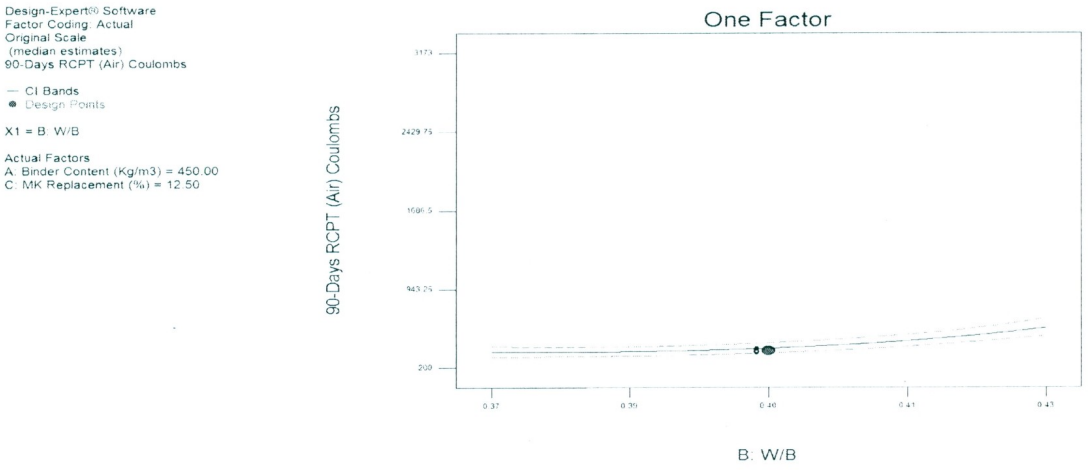

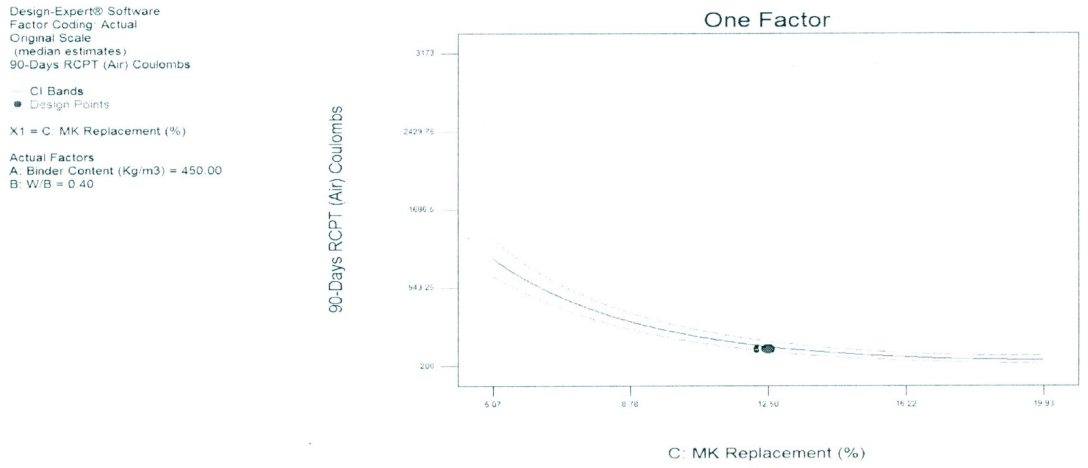

C32: Response Surfaces for factors A-B, A-C, and B-C for Response 14 (90-Days RCPT-Air)

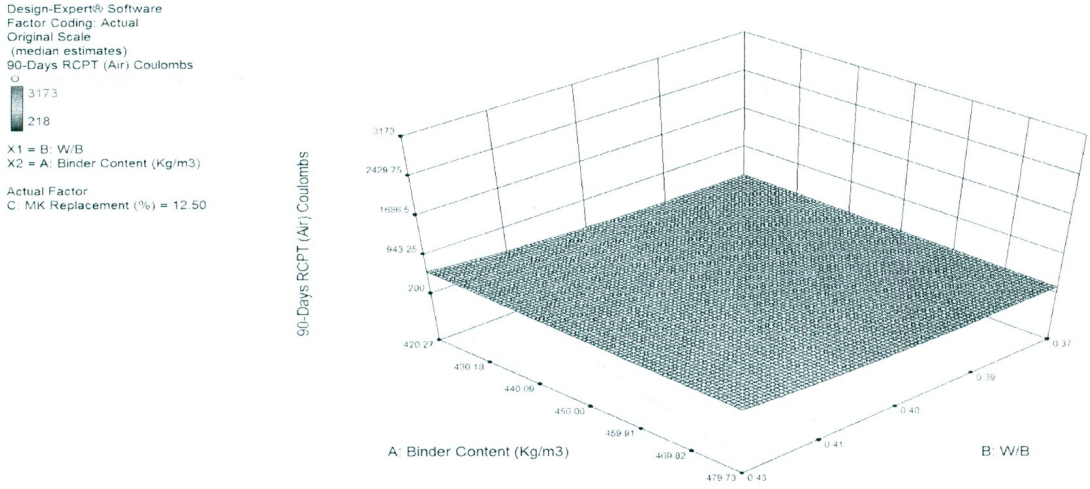

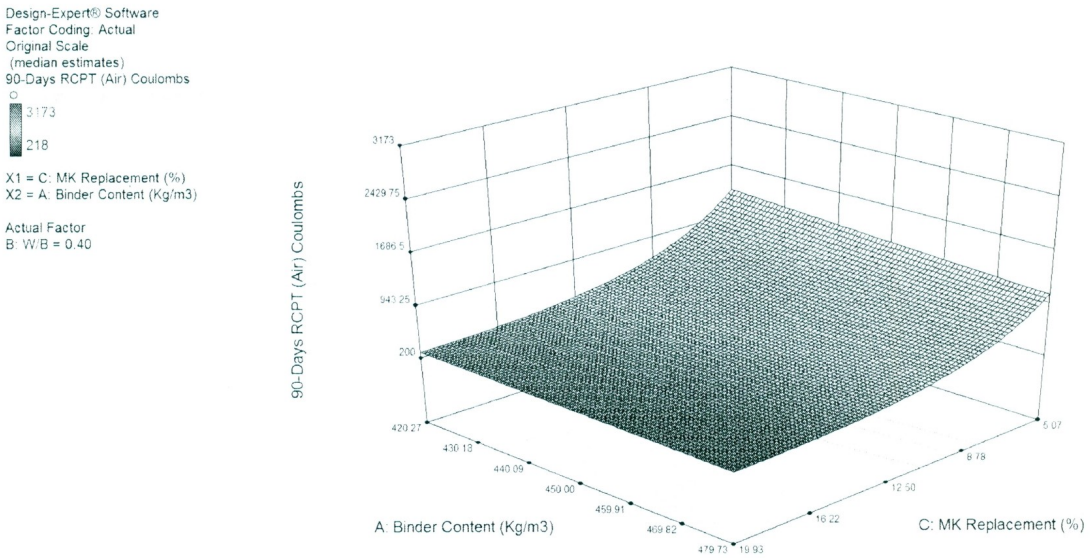
Design-Expert® Software
Factor Coding: Actual
Original Scale
(median estimates)
90-Days RCPT (Air) Coulombs
3173
218
X1 = C: MK Replacement (%)
X2 = A: Binder Content (Kg/m3)
Actual Factor
B: W/B = 0.40
90-Days RCPT (Air) Coulombs
3173
2429.75
1686.5
943.25
200
420.27
430.18
440.09
450.00
459.91
469.82
479.73
A: Binder Content (Kg/m3)
19.93
16.22
12.50
8.78
5.07
C: MK Replacement (%)

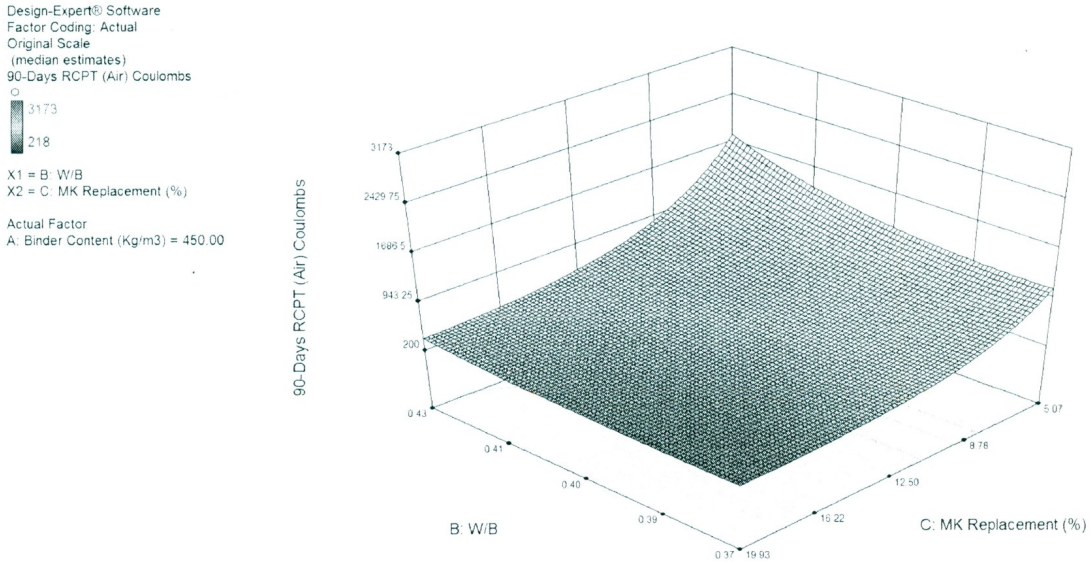
Design-Expert® Software
Factor Coding: Actual
Original Scale
(median estimates)
90-Days RCPT (Air) Coulombs
3173
218
X1 = B: W/B
X2 = C: MK Replacement (%)
Actual Factor
A: Binder Content (Kg/m3) = 450.00
90-Days RCPT (Air) Coulombs
3173
2429.75
1686.5
943.25
200
0.43
0.41
0.40
0.39
0.37
B: W/B
19.93
16.22
12.50
8.78
5.07
C: MK Replacement (%)

Response 15: 90-Days RCPT (Water)

ANOVA Table for Response 15: 90-Days RCPT (Water)

Response	15		90-Days RCPT (Water)			
Transform:	Natural Log	Constant:	0			
ANOVA for Response Surface Reduced Quadratic Model						
Analysis of variance table [Partial sum of squares - Type III]						
Source	Sum of Squares	d_f	Mean Square	F-Value	P-Value (Prob. > F)	Significance
Model	11.23	5	2.247	242.5	< 0.0001	Significant
A-Binder Content	0.02	1	0.020	2.1	0.1648	Significant
B-W/B	0.09	1	0.093	10.0	0.0069	Significant
C-Replacement	9.53	1	9.526	1028.1	< 0.0001	Significant
B^2	0.07	1	0.067	7.2	0.0178	Significant
C^2	1.57	1	1.572	169.7	< 0.0001	Significant
Residual	0.13	14	0.009			
Lack of Fit	0.11	9	0.013	3.7	0.0803	Not Significant
Pure Error	0.02	5	0.003			
Correlation Total	11.36	19				

d_f = Degrees of Freedom

C33: Effects of Factors A, B, and C on Response 15 (90-Days RCPT-Water)

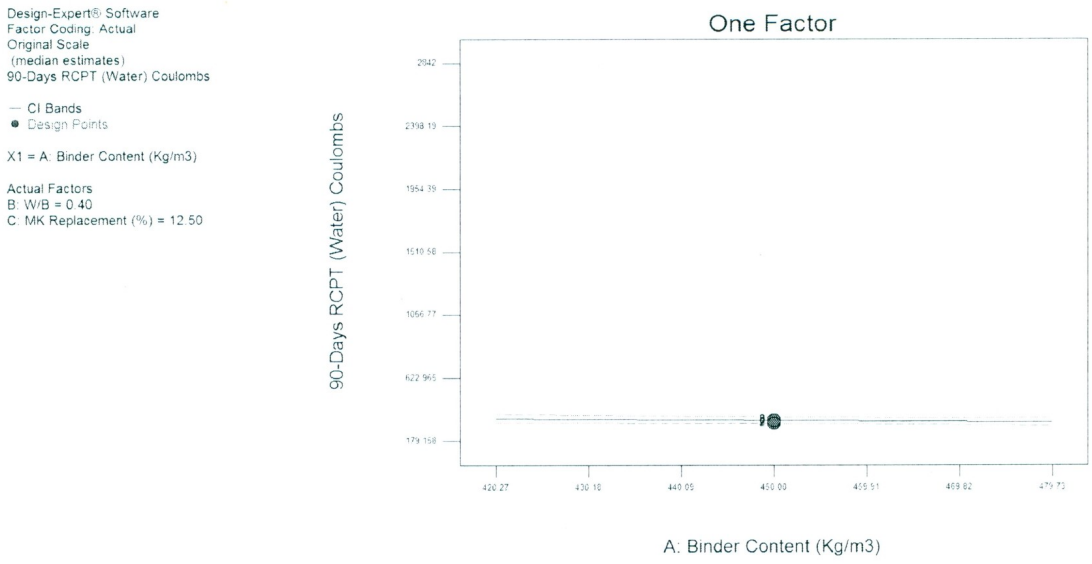

Design-Expert® Software
Factor Coding: Actual
Original Scale
(median estimates)
90-Days RCPT (Water) Coulombs

— CI Bands
● Design Points

X1 = B: W/B

Actual Factors
A: Binder Content (Kg/m3) = 450.00
C: MK Replacement (%) = 12.50

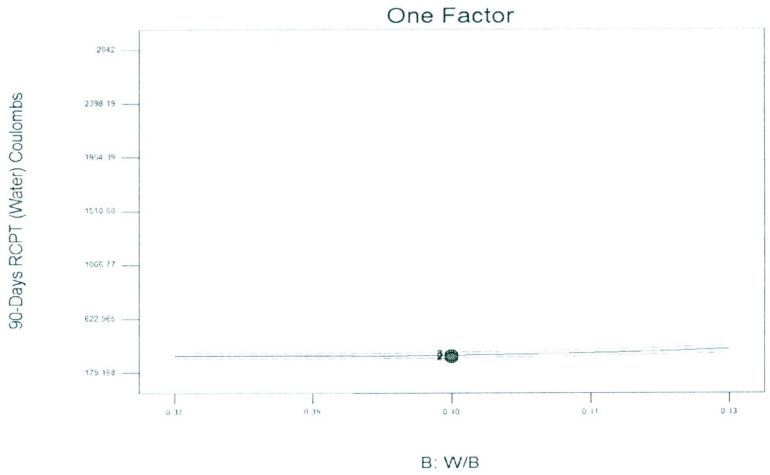

Design-Expert® Software
Factor Coding: Actual
Original Scale
(median estimates)
90-Days RCPT (Water) Coulombs

— CI Bands
● Design Points

X1 = C: MK Replacement (%)

Actual Factors
A: Binder Content (Kg/m3) = 450.00
B: W/B = 0.40

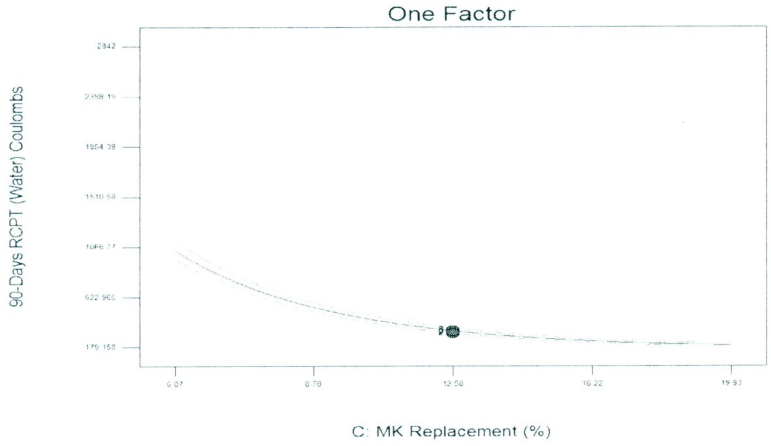

C34: Response Surfaces for factors A-B, A-C, and B-C for Response 15 (90-Days RCPT-Water)

Design-Expert® Software
Factor Coding: Actual
Original Scale
(median estimates)
90-Days RCPT (Water) Coulombs
● Design points above predicted value
○
2842
187

X1 = B: W/B
X2 = A: Binder Content (Kg/m3)

Actual Factor
C: MK Replacement (%) = 12.50

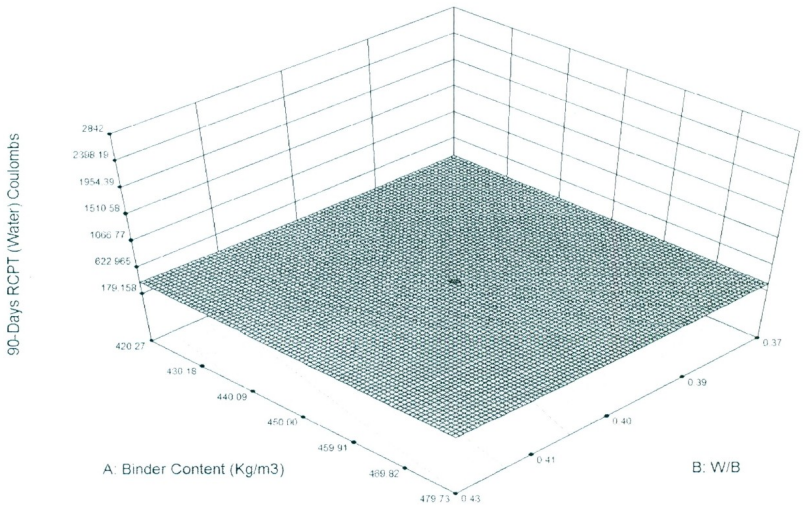

Design-Expert® Software
Factor Coding: Actual
Original Scale
(median estimates)
90-Days RCPT (Water) Coulombs
Design points above predicted value
2842
187

X1 = C: MK Replacement (%)
X2 = A: Binder Content (Kg/m3)

Actual Factor
B: W/B = 0.40

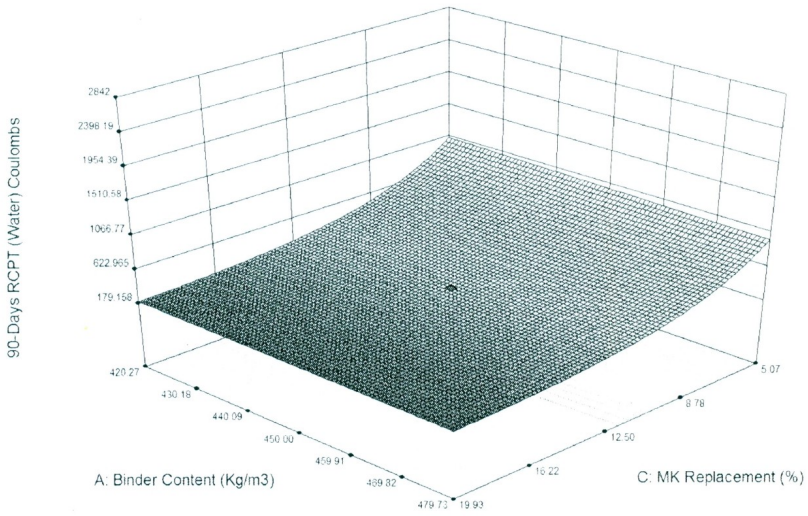

Design-Expert® Software
Factor Coding: Actual
Original Scale
(median estimates)
90-Days RCPT (Water) Coulombs
Design points above predicted value
2842
187

X1 = B: W/B
X2 = C: MK Replacement (%)

Actual Factor
A: Binder Content (Kg/m3) = 450.00

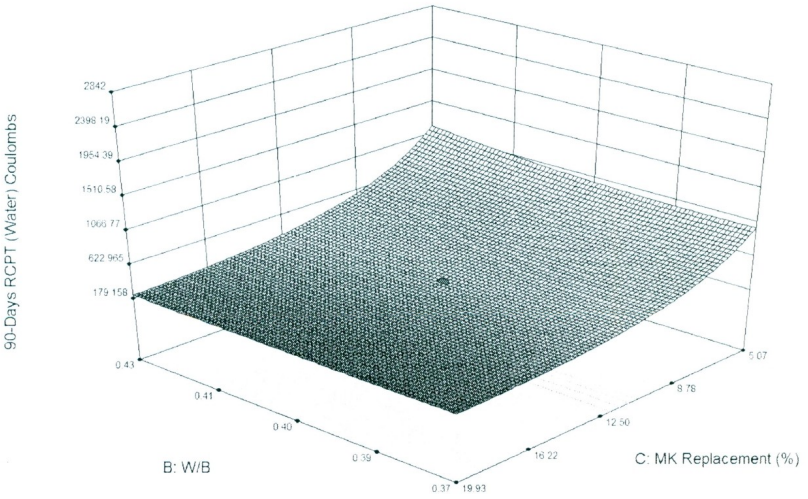

Response 16: 180-Days RCPT (Air)

ANOVA Table for Response 16: 180-Days RCPT (Air)

Response	16	180-Days RCPT (Air)				
Transform:	Natural Log	Constant:	0			
ANOVA for Response Surface Reduced Quadratic Model						
Analysis of variance table [Partial sum of squares - Type III]						
Source	Sum of Squares	d_f	Mean Square	F-Value	P-Value (Prob. > F)	Significance
Model	11.410	5	2.282	68.51	< 0.0001	Significant
A-Binder Content	0.119	1	0.119	3.57	0.0799	Significant
B-W/B	1.003	1	1.003	30.10	< 0.0001	Significant
C-Replacement	8.306	1	8.306	249.36	< 0.0001	Significant
B^2	0.398	1	0.398	11.95	0.0038	Significant
C^2	1.717	1	1.717	51.54	< 0.0001	Significant
Residual	0.466	14	0.033			
Lack of Fit	0.457	9	0.051	26.74	0.0010	Significant
Pure Error	0.009	5	0.002			
Correlation Total	11.876	19				

d_f = Degrees of Freedom

C35: Effects of Factors A, B, and C on Response 16 (180-Days RCPT-Air)

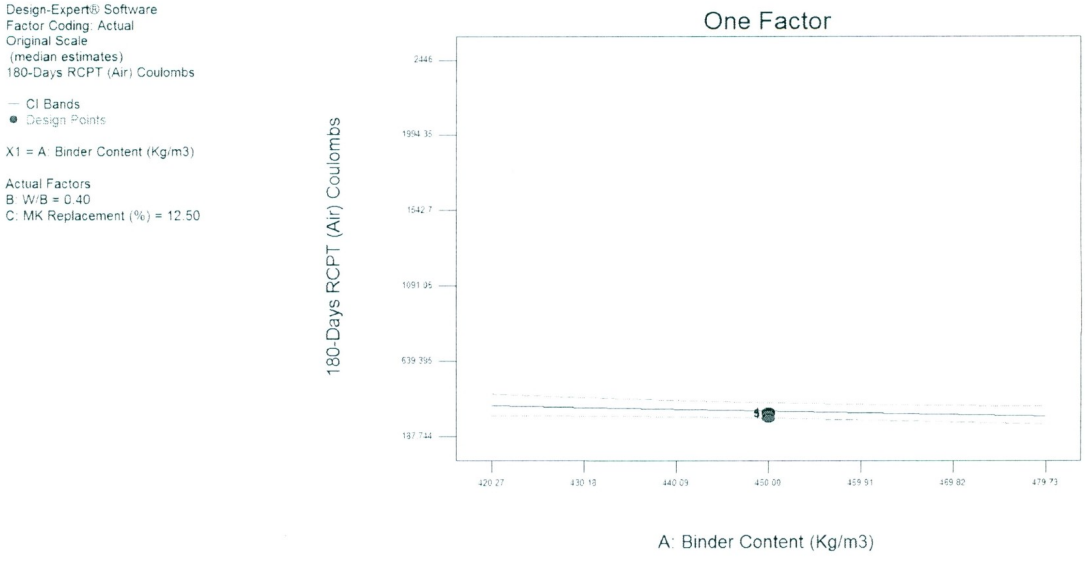

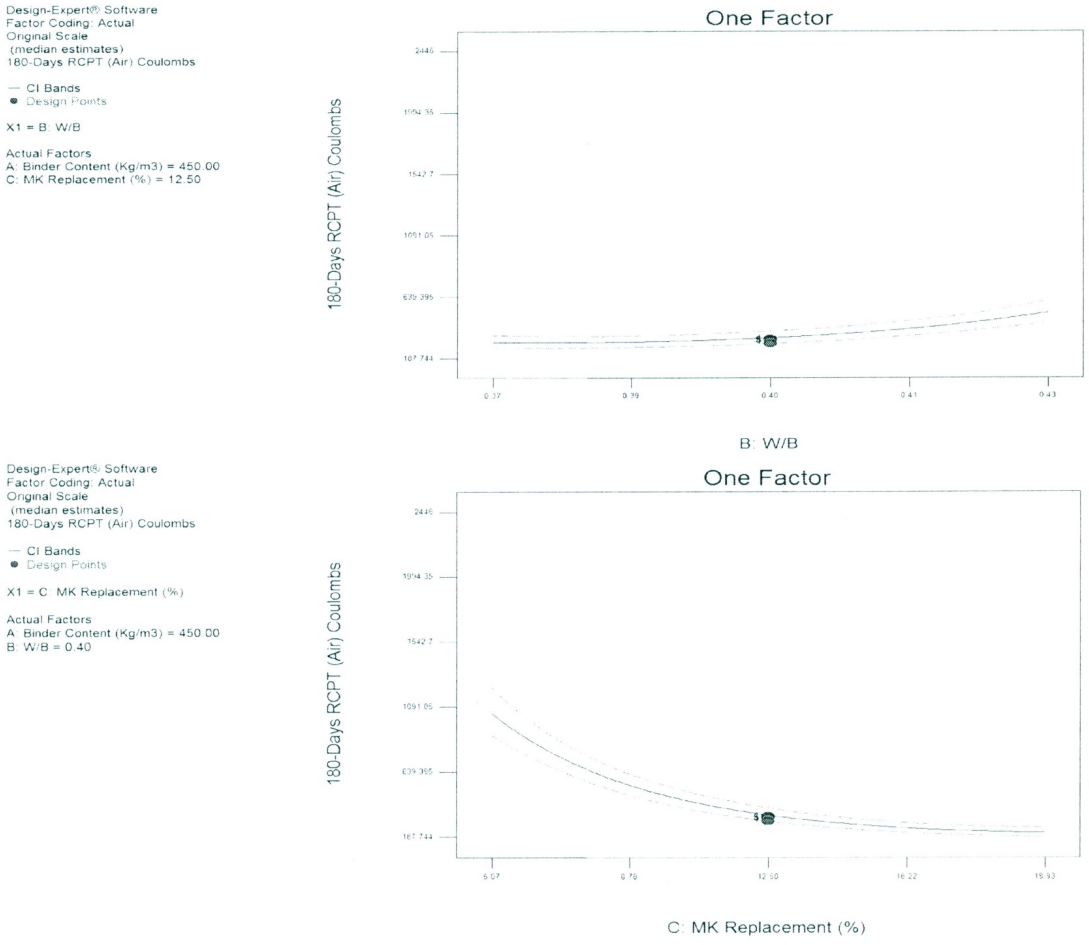

C36: Response Surfaces for factors A-B, A-C, and B-C for Response 16 (180-Days RCPT-Air)

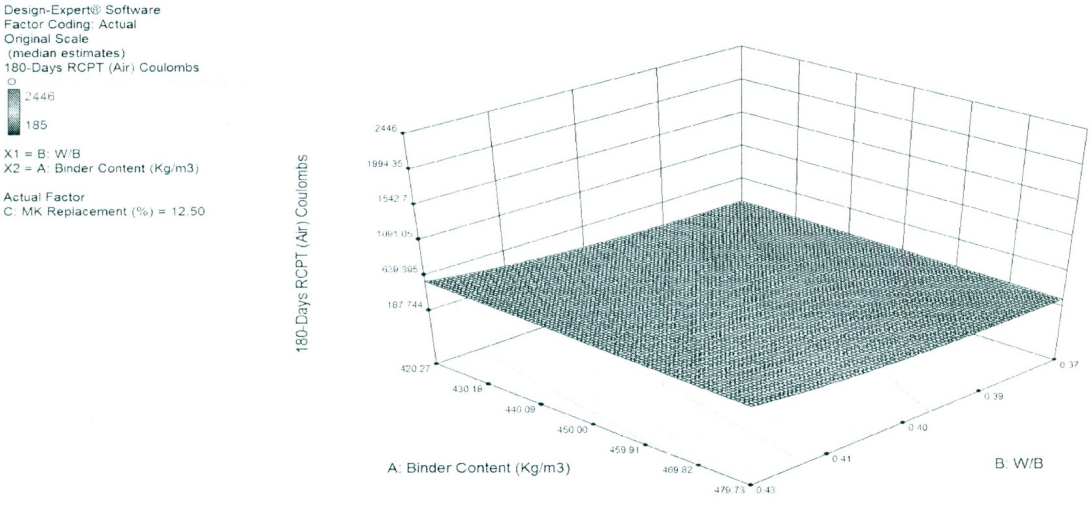

Design-Expert® Software
Factor Coding: Actual
Original Scale
(median estimates)
180-Days RCPT (Air) Coulombs

2446
185

X1 = C: MK Replacement (%)
X2 = A: Binder Content (Kg/m3)

Actual Factor
B: W/B = 0.40

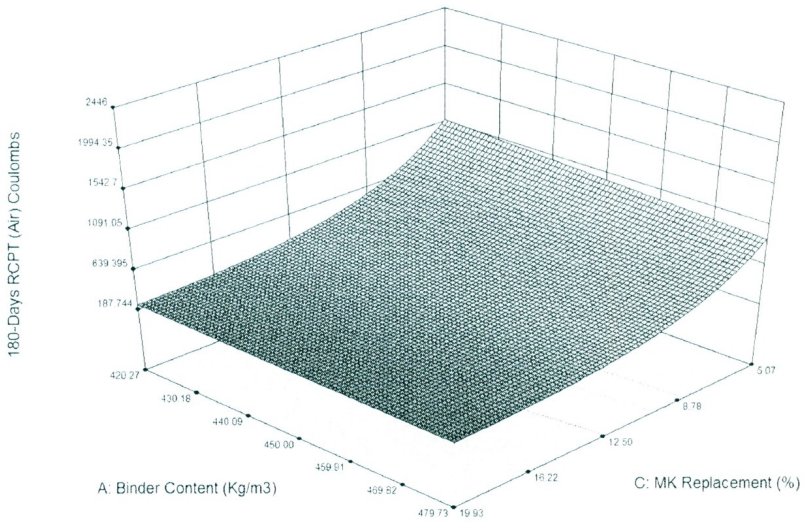

Design-Expert® Software
Factor Coding: Actual
Original Scale
(median estimates)
180-Days RCPT (Air) Coulombs

2446
185

X1 = B: W/B
X2 = C: MK Replacement (%)

Actual Factor
A: Binder Content (Kg/m3) = 450.00

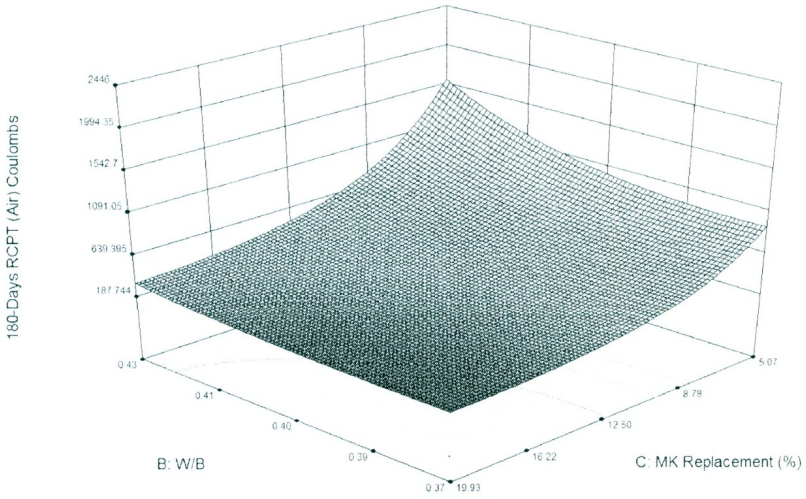

Response 17: 180-Days RCPT (Water)

ANOVA Table for Response 17: 180-Days RCPT (Water)

Response	17	180-Days RCPT (Water)				
Transform:	Natural Log	Constant:	0			
ANOVA for Response Surface Reduced Quadratic Model						
Analysis of variance table [Partial sum of squares - Type III]						
Source	Sum of Squares	df	Mean Square	F-Value	P-Value (Prob. > F)	Significance
Model	10.80	5	2.16	131.75	< 0.0001	Significant
A-Binder Content	0.01	1	0.01	0.37	0.5538	Significant
B-W/B	0.15	1	0.15	8.98	0.0096	Significant
C-Replacement	9.47	1	9.47	577.84	< 0.0001	Significant
B^2	0.09	1	0.09	5.46	0.0348	Significant
C^2	1.13	1	1.13	69.04	< 0.0001	Significant
Residual	0.23	14	0.02			
Lack of Fit	0.20	9	0.02	4.15	0.0657	Not Significant
Pure Error	0.03	5	0.01			
Correlation Total	11.03	19				

d_f = Degrees of Freedom

C37: Effects of Factors A, B, and C on Response 17 (180-Days RCPT-Water)

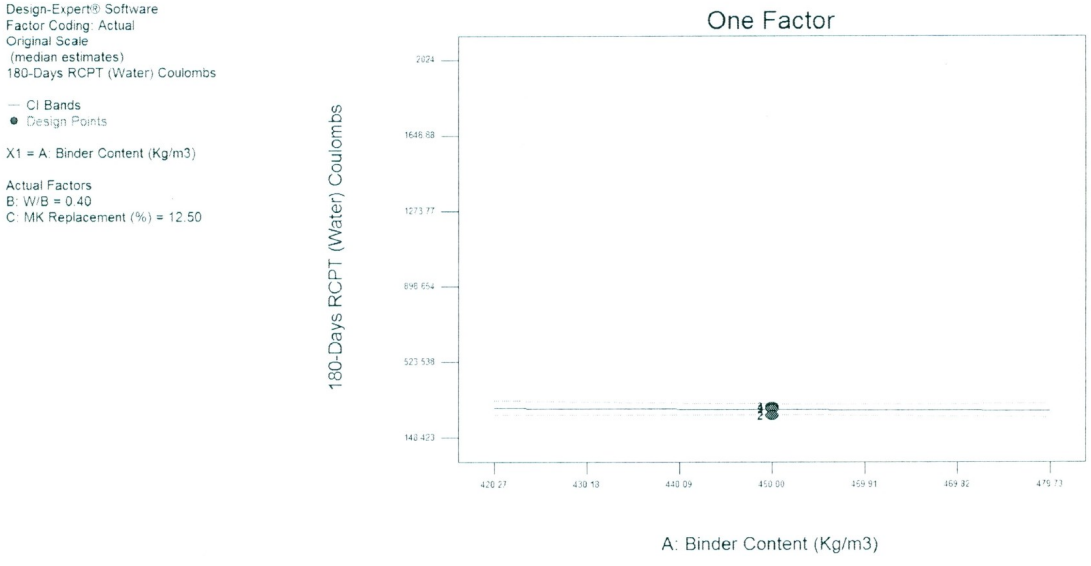

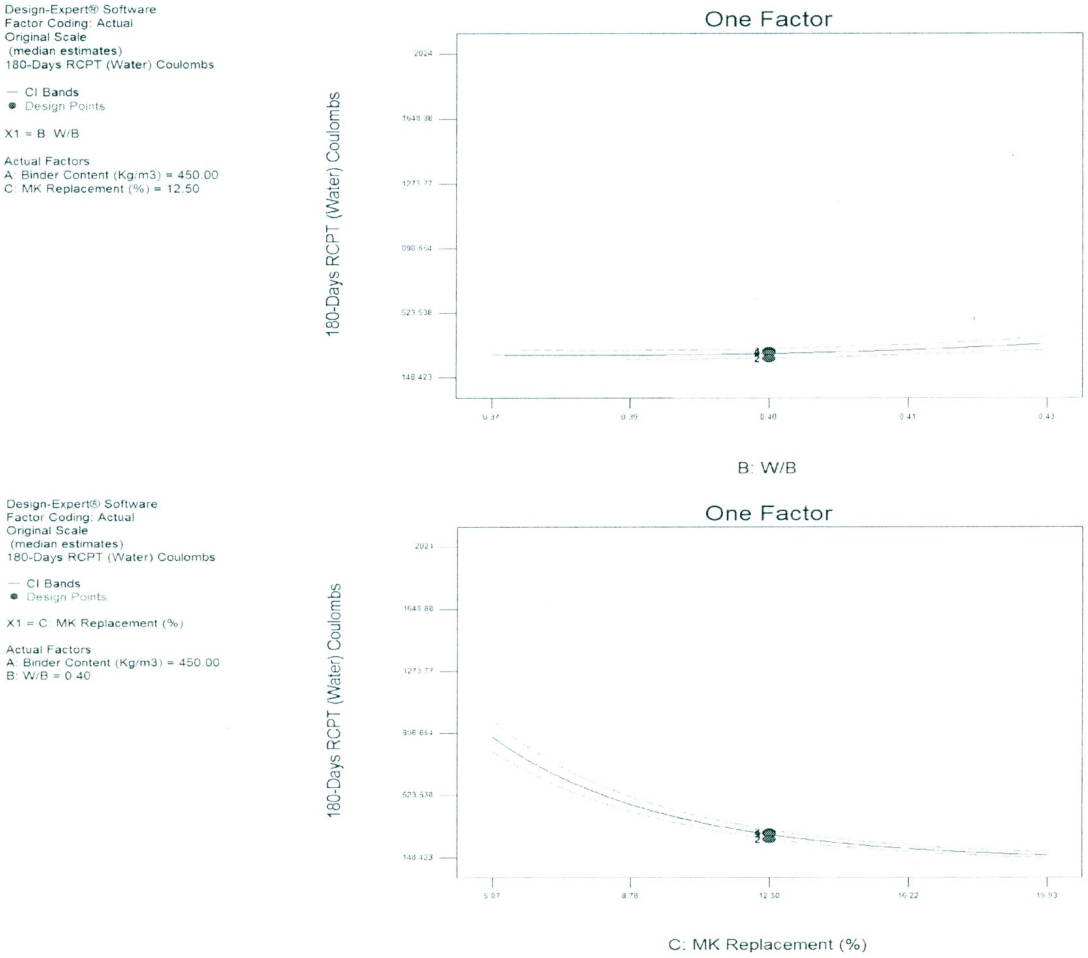

C38: Response Surfaces for factors A-B, A-C, and B-C for Response 17: 180-Days RCPT (Water)

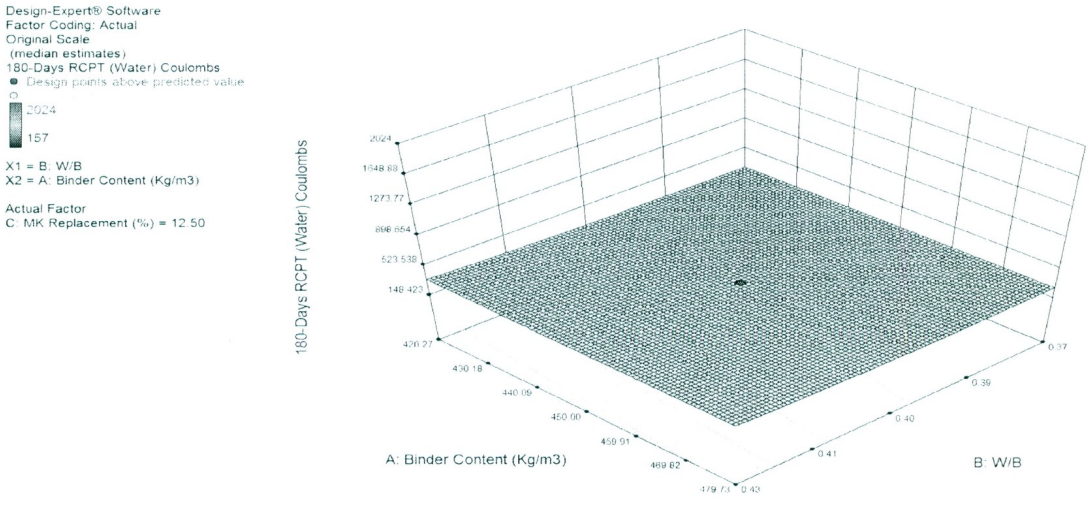

Design-Expert® Software
Factor Coding: Actual
Original Scale
(median estimates)
180-Days RCPT (Water) Coulombs
● Design points above predicted value
○
2024
157

X1 = C: MK Replacement (%)
X2 = A: Binder Content (Kg/m3)

Actual Factor
B: W/B = 0.40

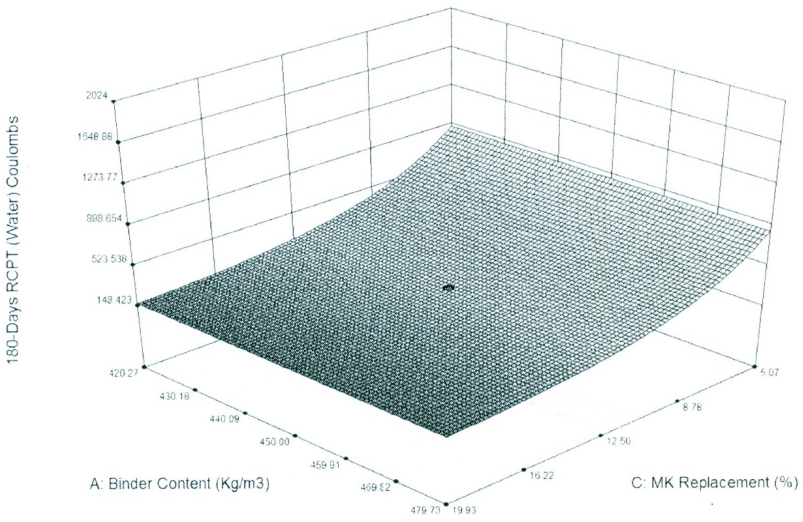

Design-Expert® Software
Factor Coding: Actual
Original Scale
(median estimates)
180-Days RCPT (Water) Coulombs
● Design points above predicted value
○
2024
157

X1 = B: W/B
X2 = C: MK Replacement (%)

Actual Factor
A: Binder Content (Kg/m3) = 450.00

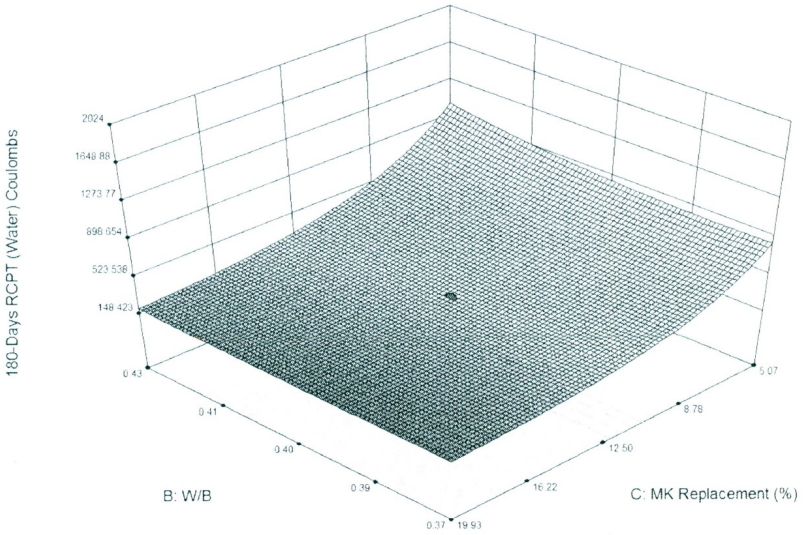

Response 18: *m* (Air)

ANOVA Table for Response 18: *m* (Air)

Response	18	*m* (air)			
ANOVA for Response Surface Reduced Quadratic Model					
Analysis of variance table [Partial sum of squares - Type III]					
Source	Sum of Squares	df	Mean Square	F-Value	P-Value (Prob. > F)	Significance
Model	0.106	5	0.0212	36.10	< 0.0001	Significant
A-Binder Content	0.005	1	0.0055	9.33	0.0086	Significant
B-W/B	0.001	1	0.0012	2.11	0.1681	Significant
C-Replacement	0.027	1	0.0275	46.72	< 0.0001	Significant
B^2	0.004	1	0.0038	6.51	0.0231	Significant
C^2	0.065	1	0.0647	110.00	< 0.0001	Significant
Residual	0.008	14	0.0006			
Lack of Fit	0.006	9	0.0007	1.42	0.3650	Not Significant
Pure Error	0.002	5	0.0005			
Correlation Total	0.114	19				

d_f = Degrees of Freedom

C39: Effects of Factors A, B, and C on Response 18 (*m*-Air)

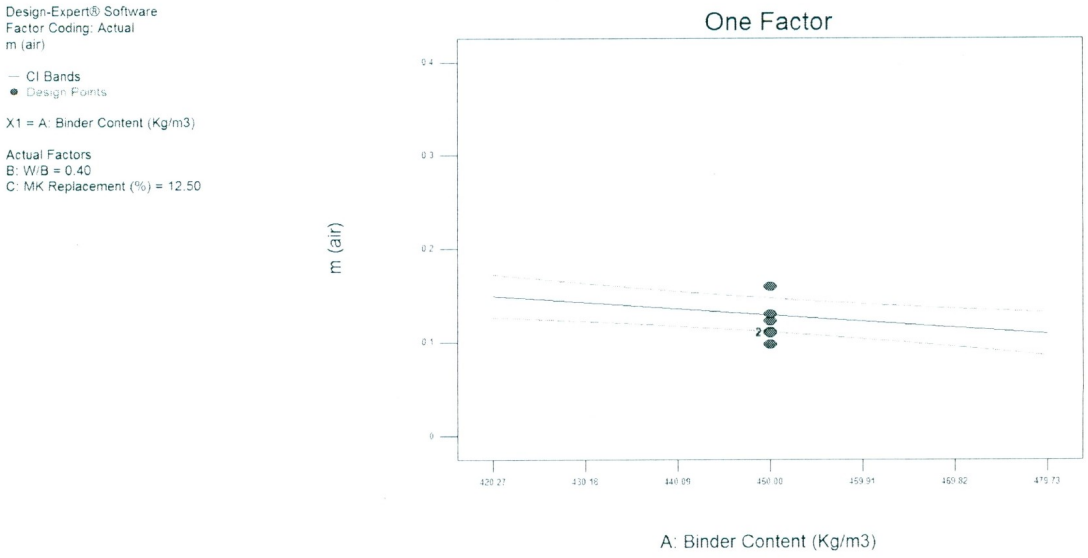

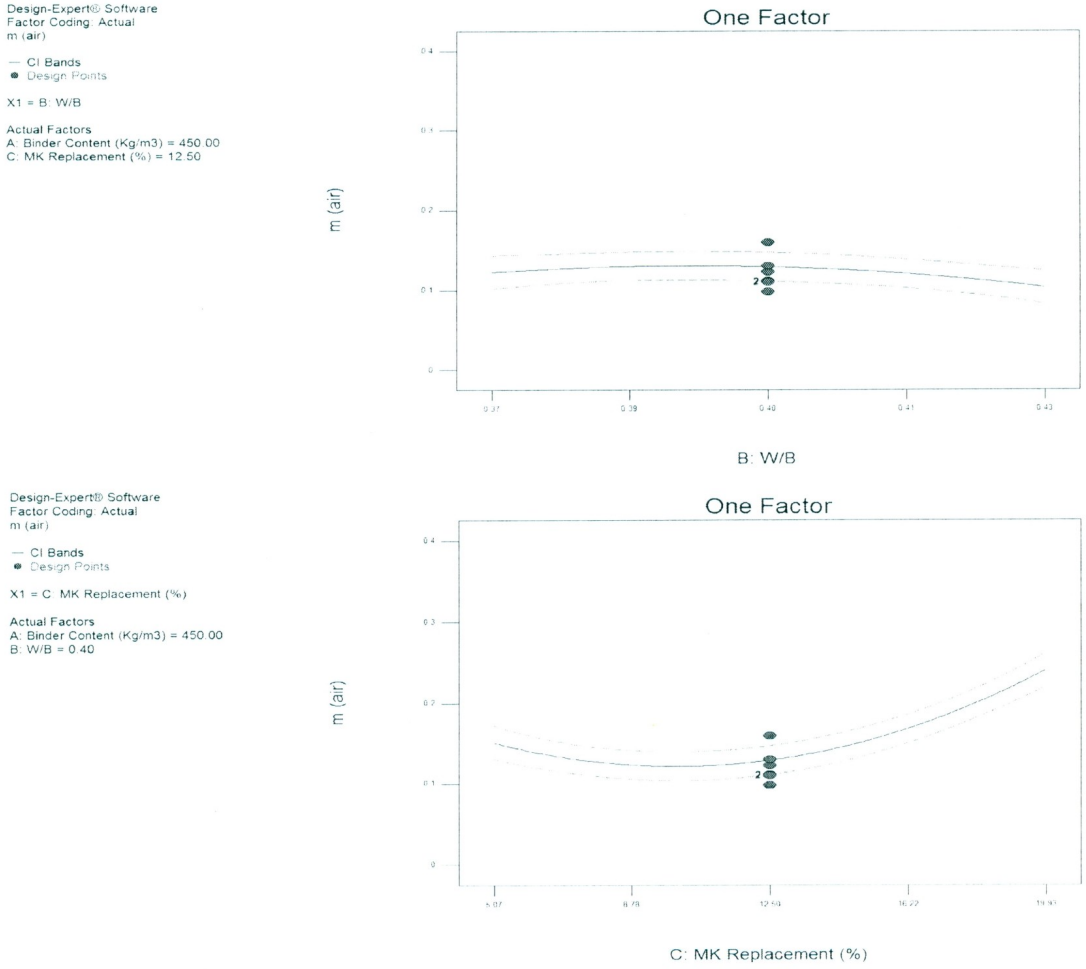

C40: Response Surfaces for factors A-B, A-C, and B-C for Response 18 (*m*-Air)

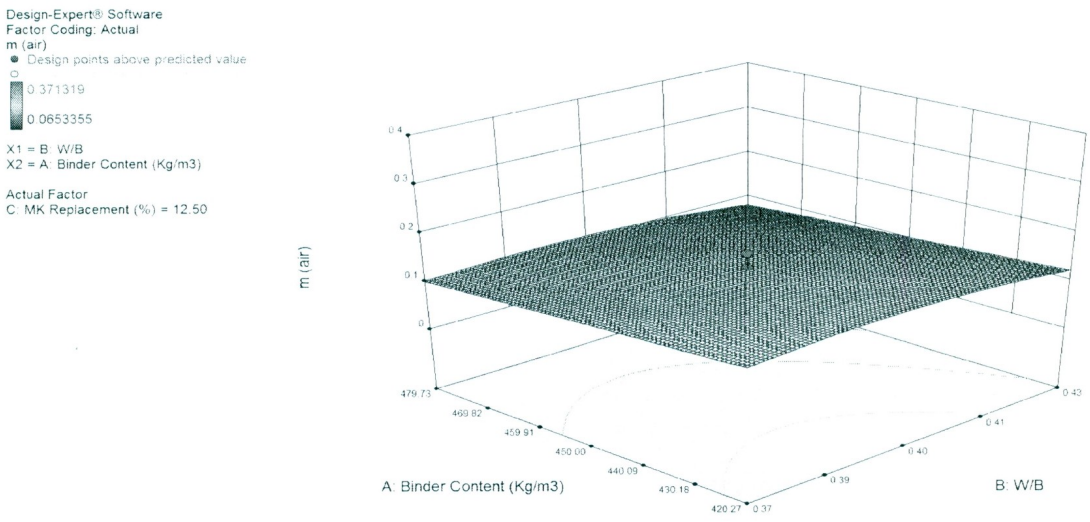

Design-Expert® Software
Factor Coding: Actual
m (air)
● Design points above predicted value
○
0.371319
0.0653355

X1 = C: MK Replacement (%)
X2 = A: Binder Content (Kg/m3)

Actual Factor
B: W/B = 0.40

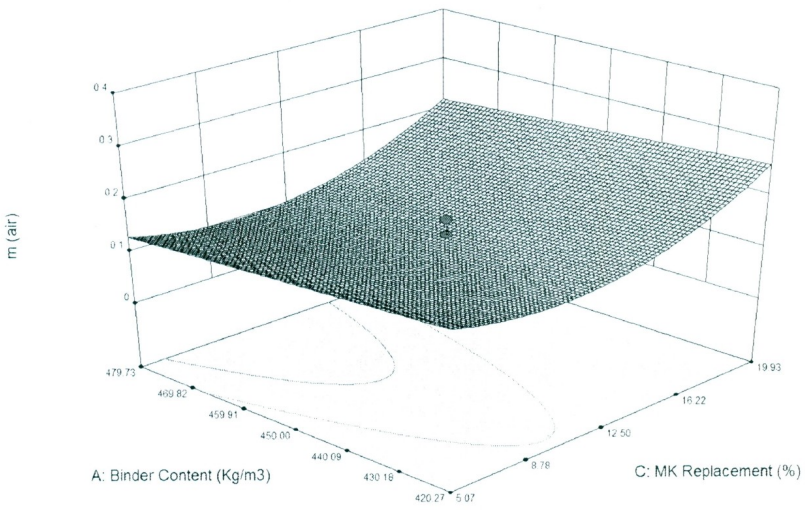

Design-Expert® Software
Factor Coding: Actual
m (air)
● Design points above predicted value
○
0.371319
0.0653355

X1 = B: W/B
X2 = C: MK Replacement (%)

Actual Factor
A: Binder Content (Kg/m3) = 450.00

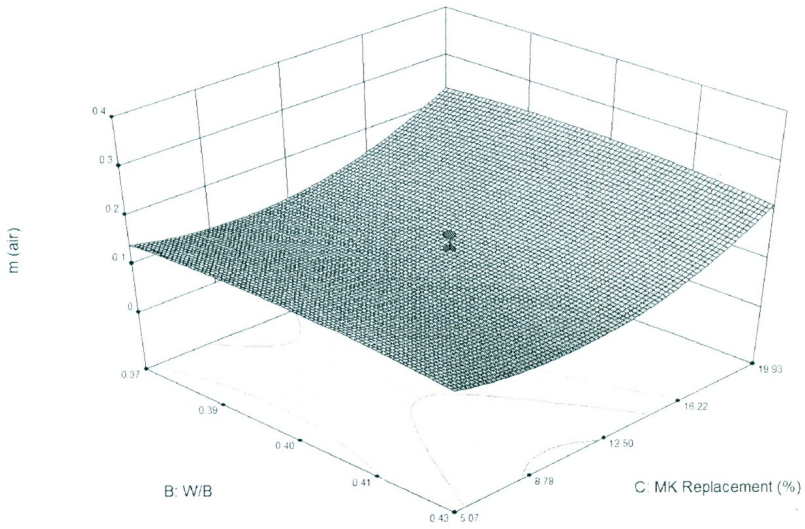

Response 19: *m* (Water)

ANOVA Table for Response 19: *m* (Water)

Response	19	m (water)				
ANOVA for Response Surface Reduced Quadratic Model						
Analysis of variance table [Partial sum of squares - Type III]						
Source	Sum of Squares	df	Mean Square	F-Value	P-Value (Prob. > F)	Significance
Model	0.123	3	0.041	26.02	< 0.0001	Significant
A-Binder Content	0.008	1	0.0077	4.86	0.0425	Significant
C-Replacement	0.020	1	0.0196	12.43	0.0028	Significant
C^2	0.096	1	0.0957	60.75	< 0.0001	Significant
Residual	0.025	16	0.0016			
Lack of Fit	0.022	11	0.002	3.31	0.0985	Not Significant
Pure Error	0.003	5	0.0006			
Correlation Total	0.148	19				

d_f = Degrees of Freedom

C41: Effects of Factors A and C on Response 19 (*m*-Water)

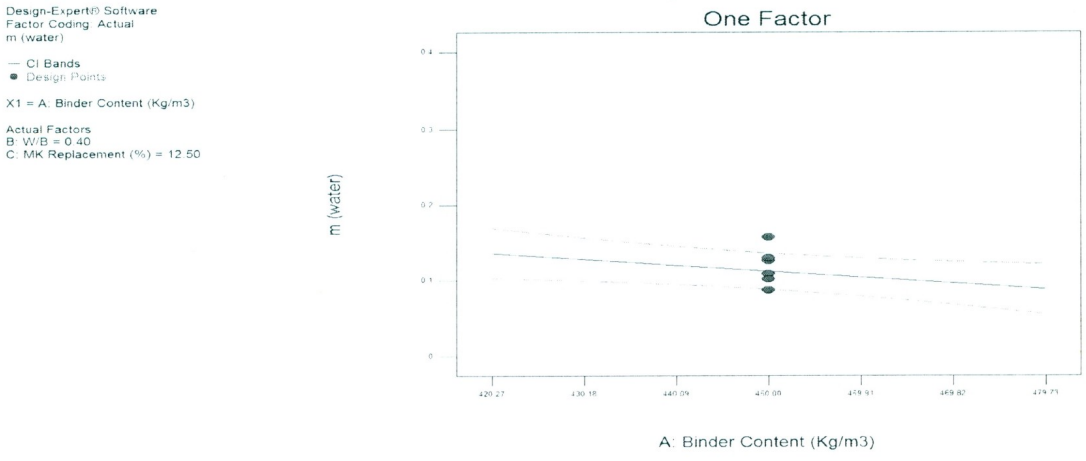

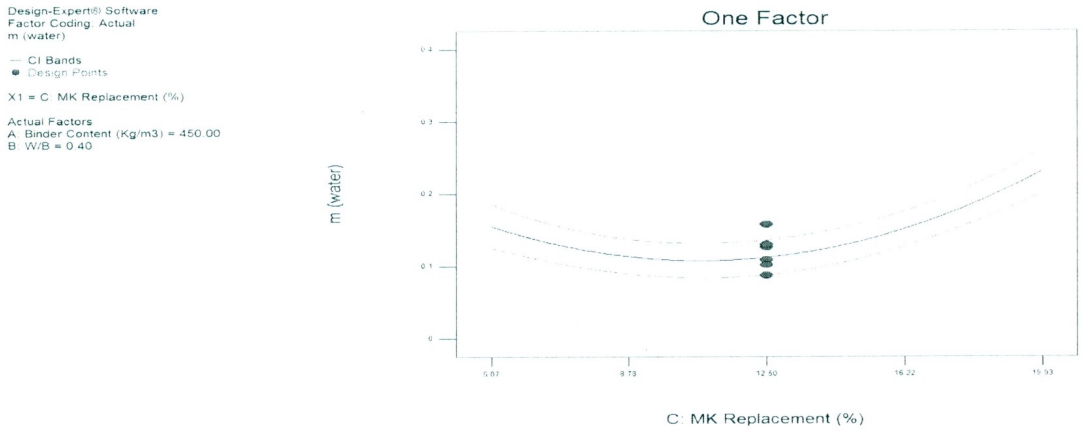

C42: Response Surfaces for factors A-B, A-C, and B-C for Response 19 (*m*-Water)

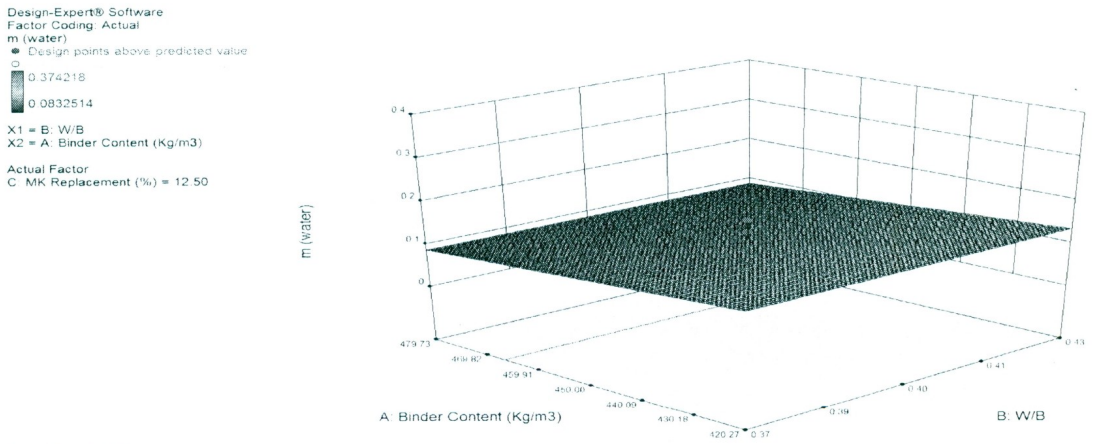

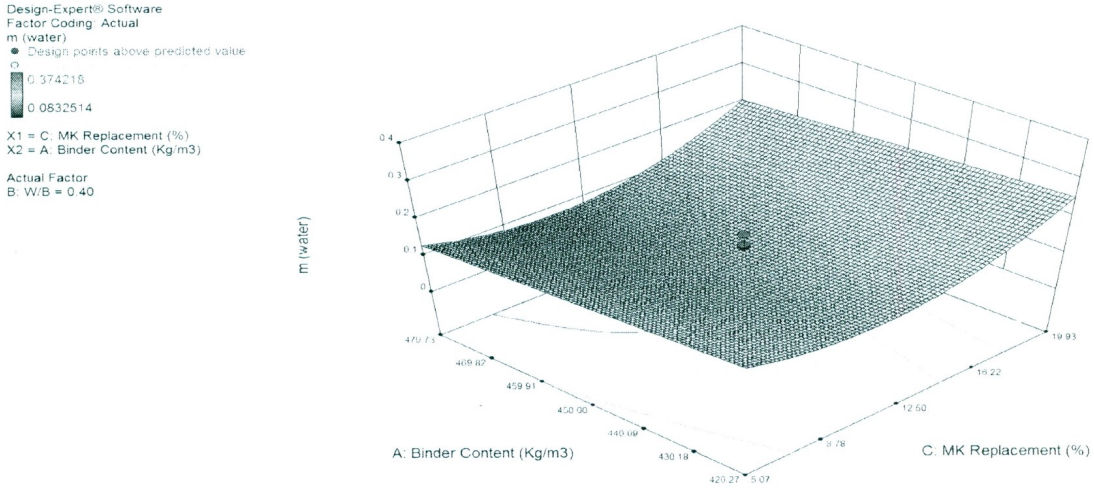

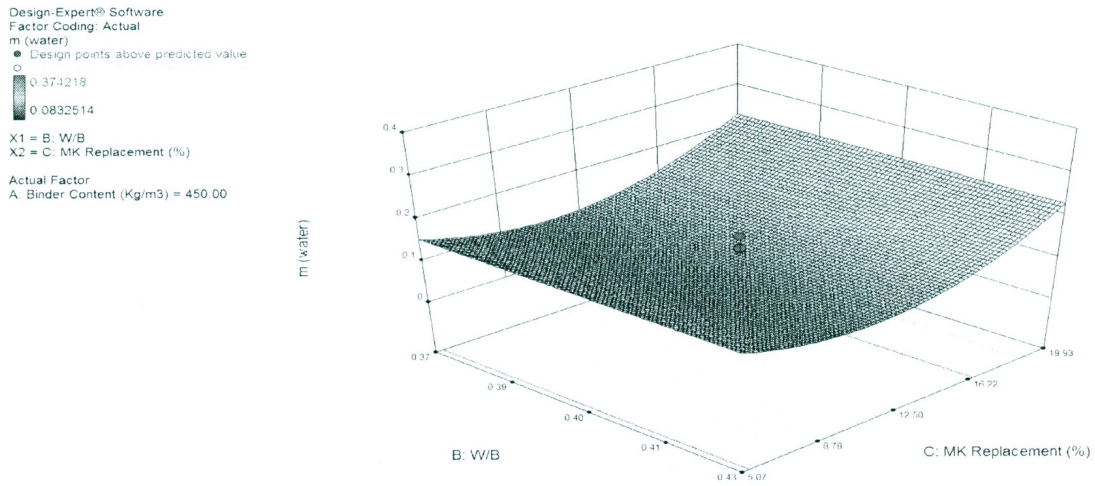

Response 20: 28-Days D_a (Air)

ANOVA Table for Response 20: 28-Days D_a (Air)

Response	20	28-Days D_a (Air)				
Transform:	Natural Log	Constant:	0			
ANOVA for Response Surface Reduced Quadratic Model						
Analysis of variance table [Partial sum of squares - Type III]						
Source	Sum of Squares	d_f	Mean Square	F-Value	P-Value (Prob. > F)	Significance
Model	8.30	5	1.66	46.99	< 0.0001	Significant
A-Binder Content	0.27	1	0.27	7.76	0.0146	Significant
B-W/B	1.60	1	1.60	45.33	< 0.0001	Significant
C-Replacement	4.54	1	4.54	128.53	< 0.0001	Significant
BC	0.51	1	0.51	14.47	0.0019	Significant
C^2	1.37	1	1.37	38.88	< 0.0001	Significant
Residual	0.49	14	0.04			
Lack of Fit	0.46	9	0.05	8.73	0.0140	Significant
Pure Error	0.03	5	0.01			
Correlation Total	8.79	19				

d_f = Degrees of Freedom

C43: Effects of Factors A, B, and C on Response 20 (28-Days D_a-Air)

Design-Expert® Software
Factor Coding: Actual
Original Scale
(median estimates)
28-Days Da (Air) *E-14 m2/sec

— CI Bands
● Design Points

X1 = A: Binder Content (Kg/m3)

Actual Factors
B: W/B = 0.40
C: MK Replacement (%) = 12.50

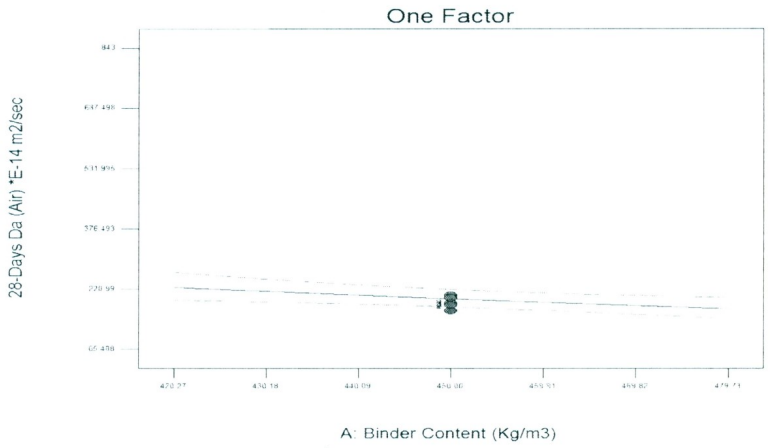

Design-Expert® Software
Factor Coding: Actual
Original Scale
(median estimates)
28-Days Da (Air) *E-14 m2/sec

CI Bands
● Design Points

X1 = B: W/B

Actual Factors
A: Binder Content (Kg/m3) = 450.00
C: MK Replacement (%) = 12.50

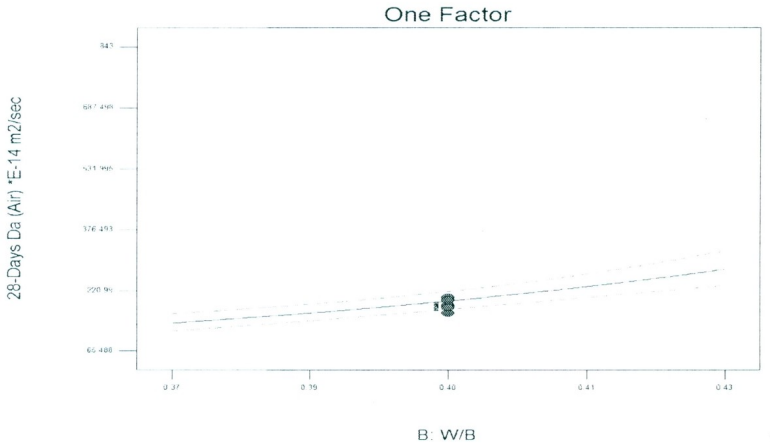

Design-Expert® Software
Factor Coding: Actual
Original Scale
(median estimates)
28-Days Da (Air) *E-14 m2/sec

— CI Bands
● Design Points

X1 = C: MK Replacement (%)

Actual Factors
A: Binder Content (Kg/m3) = 450.00
B: W/B = 0.40

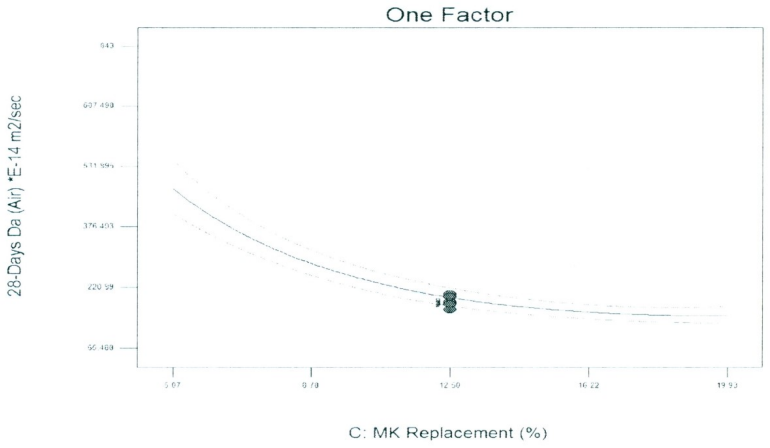

C44: Interaction Effect of Factor BC on Response 20 (28-Days D_a-Air)

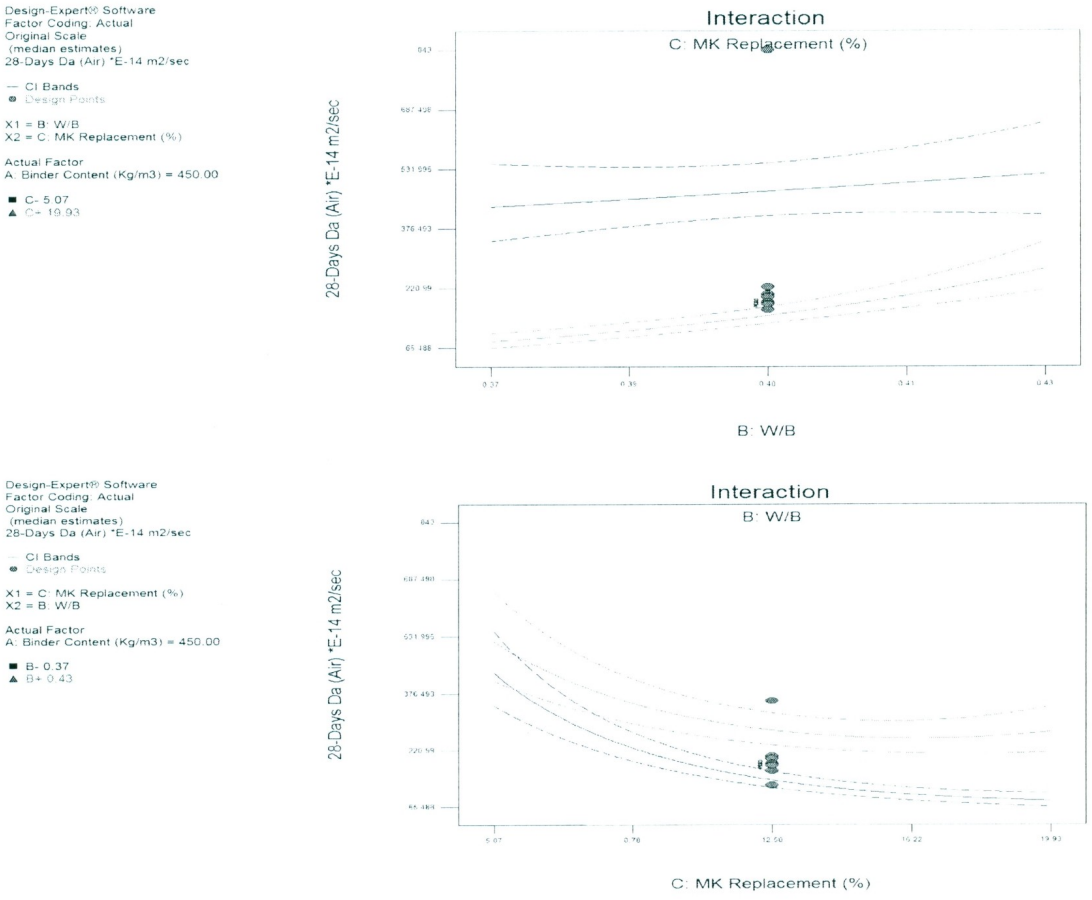

C45: Response Surfaces for factors A-B, A-C, and B-C for Response 20 (28-Days D_a-Air)

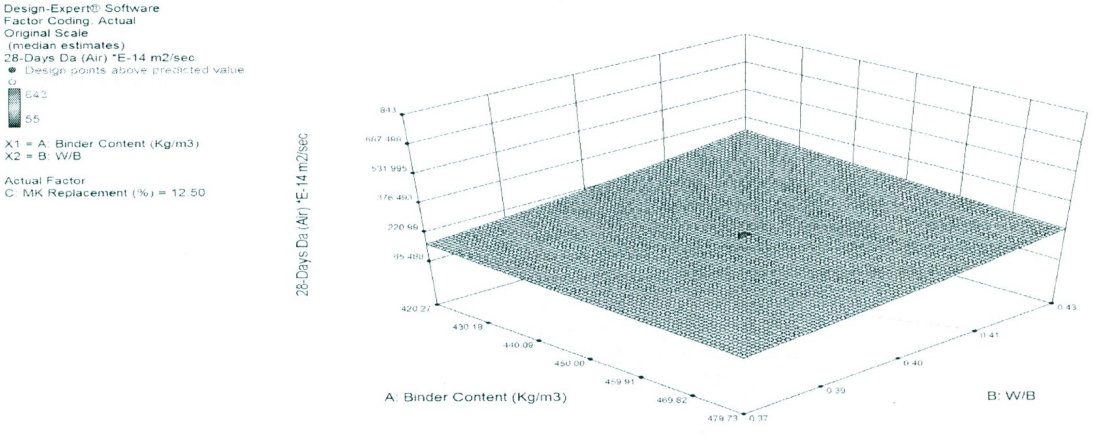

Design-Expert® Software
Factor Coding: Actual
Original Scale
(median estimates)
28-Days Da (Air) *E-14 m2/sec
● Design points above predicted value
○
843
55

X1 = A: Binder Content (Kg/m3)
X2 = C: MK Replacement (%)

Actual Factor
B: W/B = 0.40

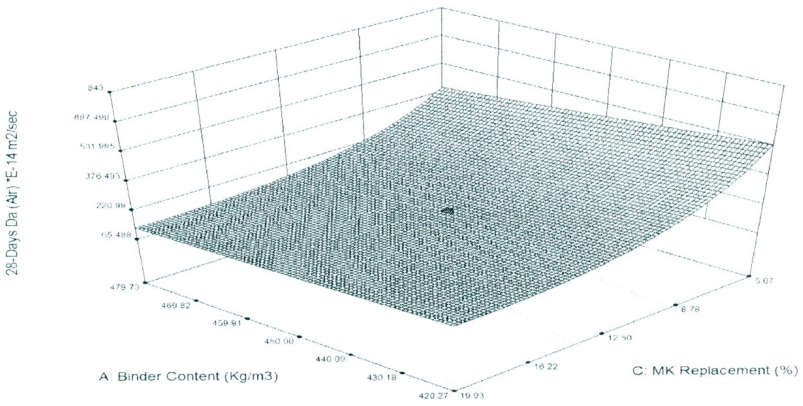

Design-Expert® Software
Factor Coding: Actual
Original Scale
(median estimates)
28-Days Da (Air) *E-14 m2/sec
● Design points above predicted value
○
843
55

X1 = C: MK Replacement (%)
X2 = B: W/B

Actual Factor
A: Binder Content (Kg/m3) = 450.00

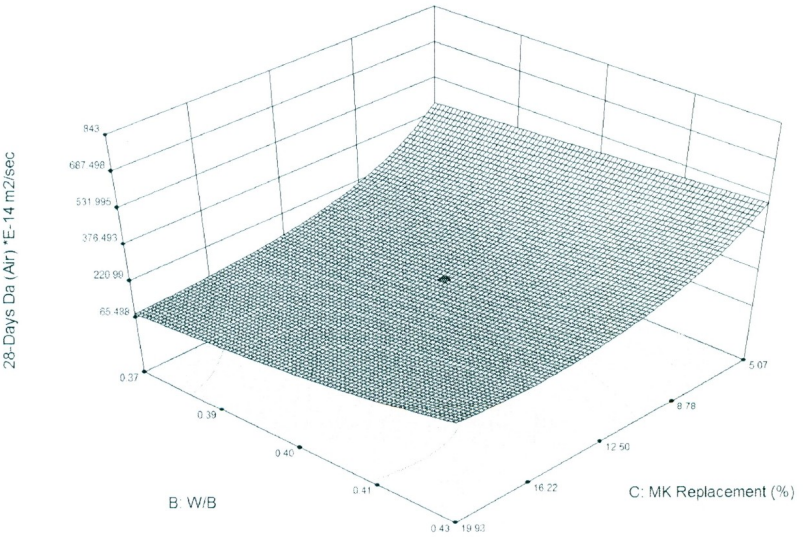

Response 21: 28-Days D_a (Water)

ANOVA Table for Response 21: 28-Days D_a (Water)

Response	21	28-Days D_a (Water)				
Transform:	Natural Log	Constant:	0			
ANOVA for Response Surface Reduced Quadratic Model						
Analysis of variance table [Partial sum of squares - Type III]						
Source	Sum of Squares	d_f	Mean Square	F-Value	P-Value (Prob. > F)	Significance
Model	11.27	5	2.253	47.25	< 0.0001	Significant
A-Binder Content	0.28	1	0.282	5.91	0.0290	Significant
B-W/B	0.38	1	0.382	8.02	0.0133	Significant
C-Replacement	8.61	1	8.611	180.59	< 0.0001	Significant
B^2	0.32	1	0.321	6.72	0.0213	Significant
C^2	1.79	1	1.791	37.56	< 0.0001	Significant
Residual	0.67	14	0.048			
Lack of Fit	0.66	9	0.073	35.76	0.0005	Significant
Pure Error	0.01	5	0.002			
Correlation Total	11.93	19				

d_f = Degrees of Freedom

C46: Effects of Factors A, B, and C on Response 21 (28-Days D_a-Water)

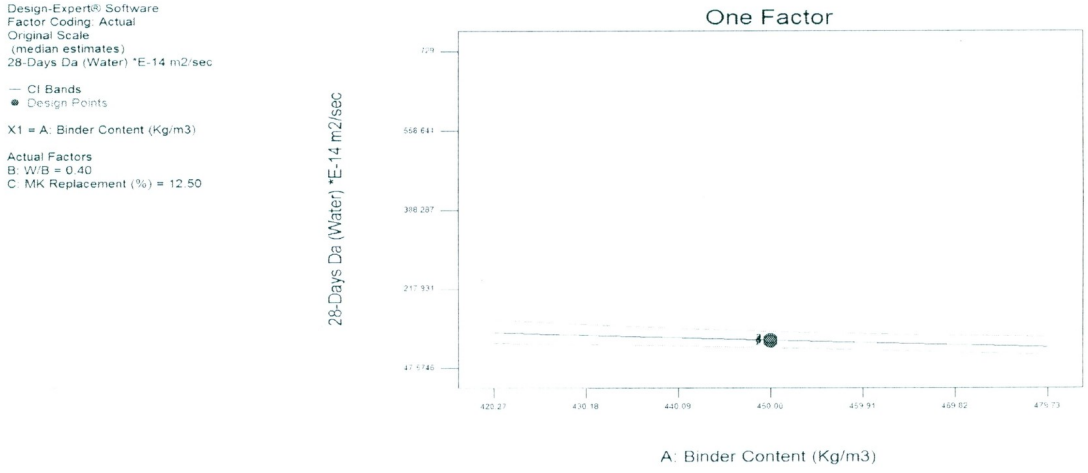

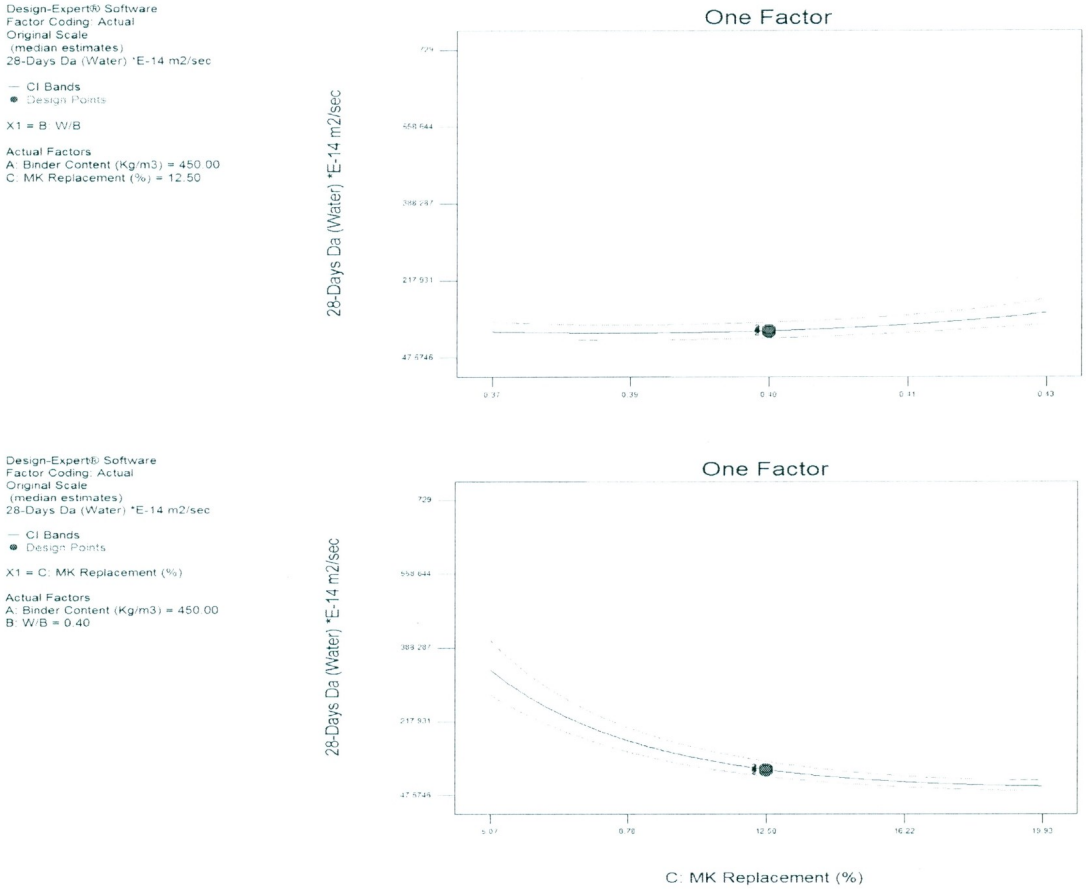

C47: Response Surfaces for factors A-B, A-C, and B-C for Response 21 (28-Days D_a-Water)

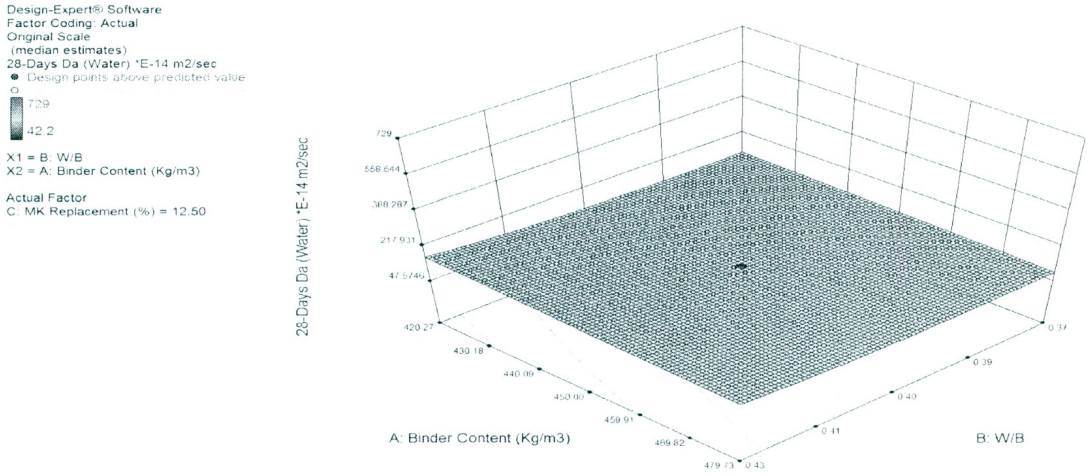

Design-Expert® Software
Factor Coding: Actual
Original Scale
(median estimates)
28-Days Da (Water) *E-14 m2/sec
● Design points above predicted value
○
729
42.2

X1 = C: MK Replacement (%)
X2 = A: Binder Content (Kg/m3)

Actual Factor
B: W/B = 0.40

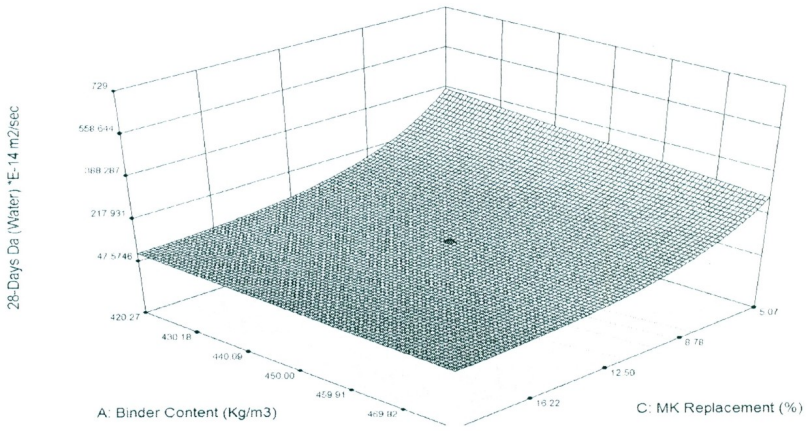

Design-Expert® Software
Factor Coding: Actual
Original Scale
(median estimates)
28-Days Da (Water) *E-14 m2/sec
● Design points above predicted value
○
729
42.2

X1 = B: W/B
X2 = C: MK Replacement (%)

Actual Factor
A: Binder Content (Kg/m3) = 450.00

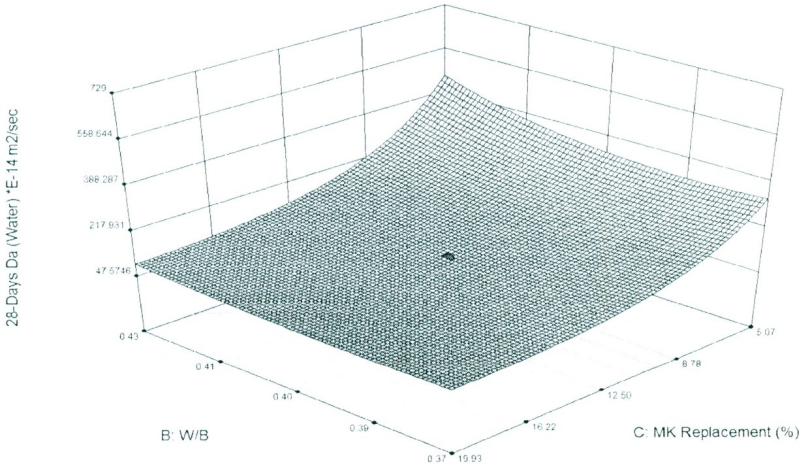

Response 22: Corrosion Initiation Time (Air)

ANOVA Table for Response 22: Corrosion Initiation Time (Air)

Response	22	Corrosion Initiation Time (Air)				
Transform:	Natural Log	Constant:	0			
ANOVA for Response Surface Reduced 2FI Model						
Analysis of variance table [Partial sum of squares - Type III]						
Source	Sum of Squares	d_f	Mean Square	F-Value	P-Value (Prob. > F)	Significance
Model	13.903005	3	4.6343	73.083	< 0.0001	Significant
B-W/B	2.4029998	1	2.403	37.895	< 0.0001	Significant
C-Replacement	10.719706	1	10.72	169.05	< 0.0001	Significant
BC	0.7802996	1	0.7803	12.305	0.0029	Significant
Residual	1.014589	16	0.0634			
Lack of Fit	0.9489469	11	0.0863	6.5711	0.0250	Significant
Pure Error	0.0656422	5	0.0131			
Correlation Total	14.917594	19				

d_f = Degrees of Freedom

C48: Effects of Factors B and C on Response 22 (Corrosion Initiation Time-Air)

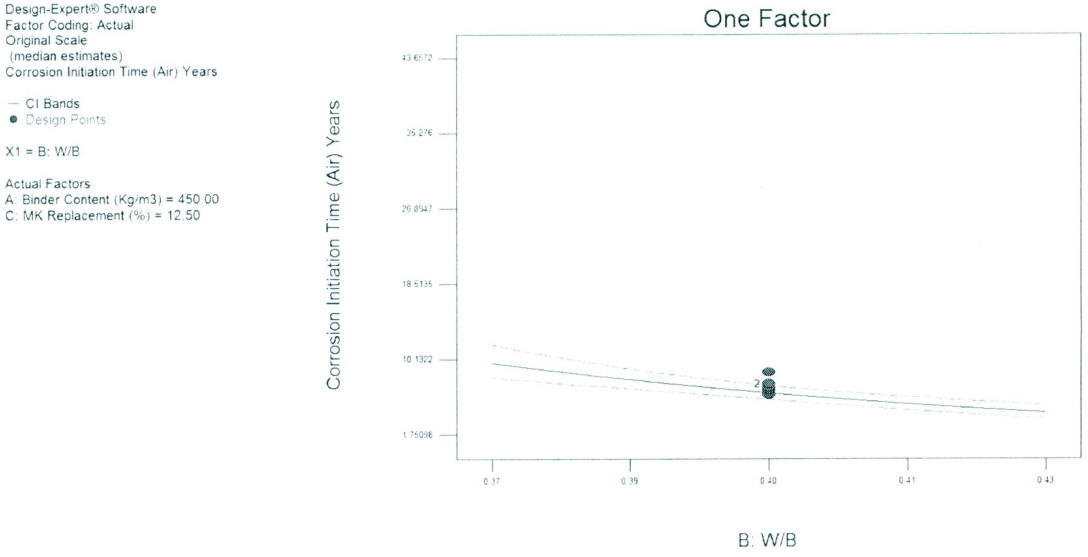

Design-Expert® Software
Factor Coding: Actual
Original Scale
(median estimates)
Corrosion Initiation Time (Air) Years

— CI Bands
● Design Points

X1 = C: MK Replacement (%)

Actual Factors
A: Binder Content (Kg/m3) = 450.00
B: W/B = 0.40

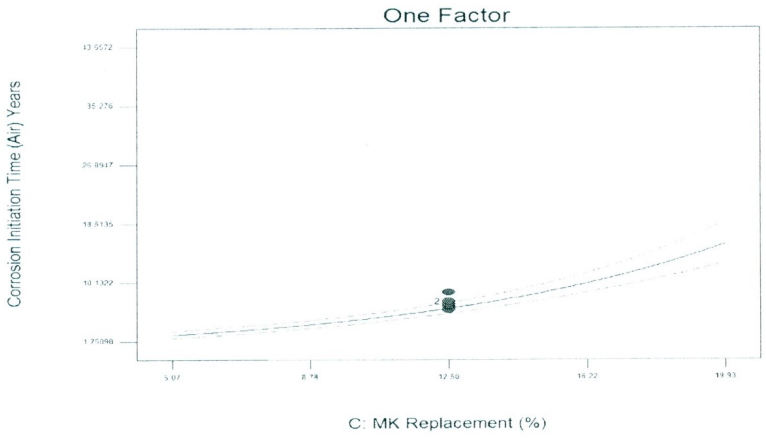

C49: Interaction Effect of Factor BC on Response 22 (Corrosion Initiation Time-Air)

Design-Expert® Software
Factor Coding: Actual
Original Scale
(median estimates)
Corrosion Initiation Time (Air) Years

— CI Bands
● Design Points

X1 = B: W/B
X2 = C: MK Replacement (%)

Actual Factor
A: Binder Content (Kg/m3) = 450.00

■ C- 5.07
▲ C+ 19.93

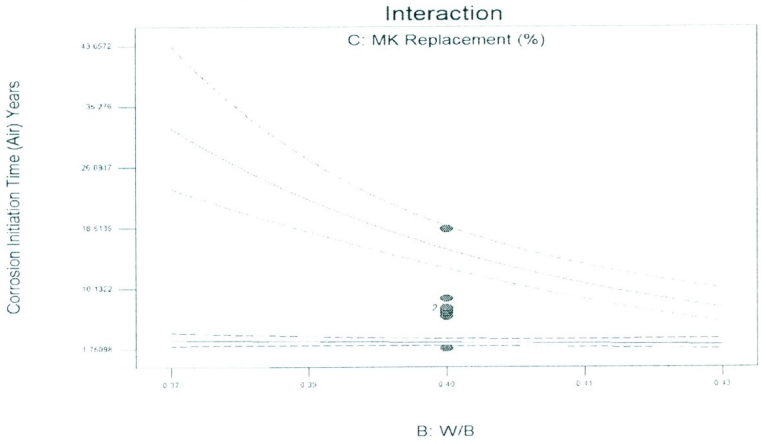

Design-Expert® Software
Factor Coding: Actual
Original Scale
(median estimates)
Corrosion Initiation Time (Air) Years

— CI Bands
● Design Points

X1 = C: MK Replacement (%)
X2 = B: W/B

Actual Factor
A: Binder Content (Kg/m3) = 450.00

■ B- 0.37
▲ B+ 0.43

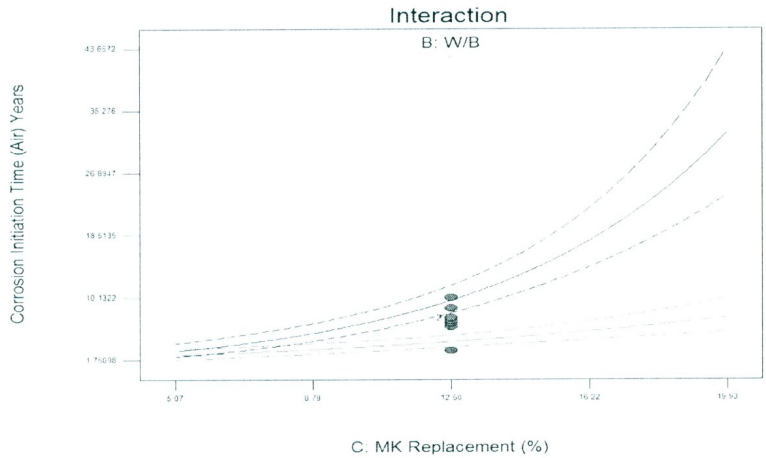

C50: Response Surfaces for factors A-B, A-C, and B-C for Response 22 (Corrosion Initiation Time-Air)

Design-Expert® Software
Factor Coding: Actual
Original Scale
(median estimates)
Corrosion Initiation Time (Air) Years
● Design points above predicted value
○
48.9
1.7

X1 = B: W/B
X2 = A: Binder Content (Kg/m3)

Actual Factor
C: MK Replacement (%) = 12.50

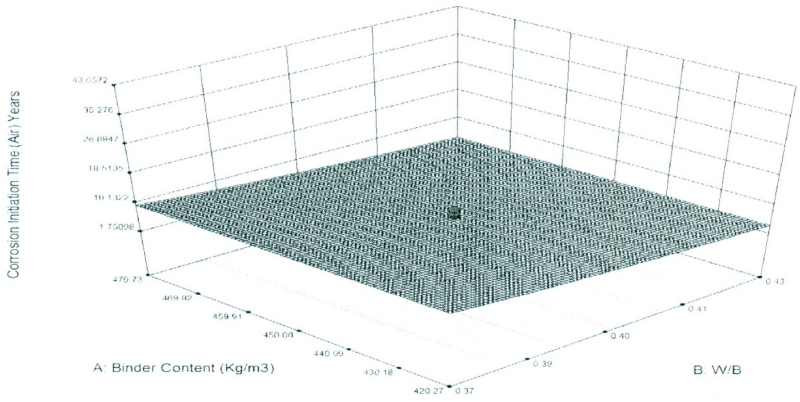

Design-Expert® Software
Factor Coding: Actual
Original Scale
(median estimates)
Corrosion Initiation Time (Air) Years
● Design points above predicted value
○
48.9
1.7

X1 = C: MK Replacement (%)
X2 = A: Binder Content (Kg/m3)

Actual Factor
B: W/B = 0.40

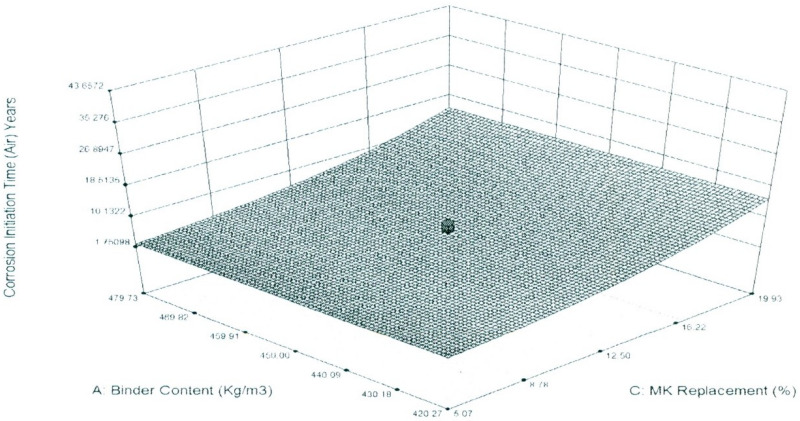

Design-Expert® Software
Factor Coding: Actual
Original Scale
(median estimates)
Corrosion Initiation Time (Air) Years
● Design points above predicted value
○
48.9
1.7

X1 = B: W/B
X2 = C: MK Replacement (%)

Actual Factor
A: Binder Content (Kg/m3) = 450.00

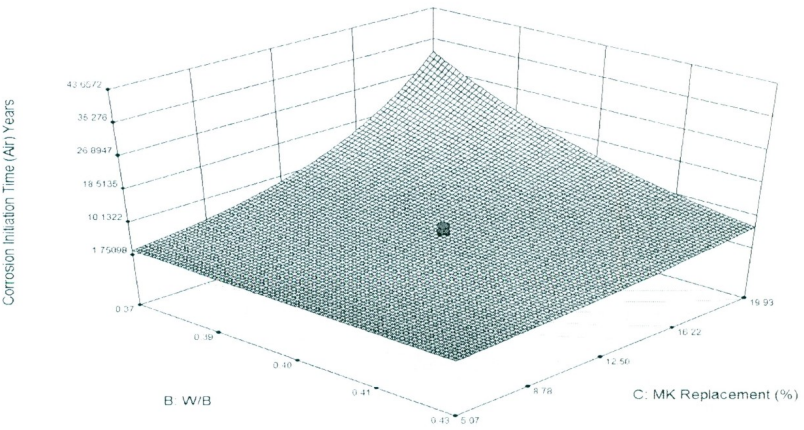

Response 23: Corrosion Initiation Time (Water)

ANOVA Table for Response 23: Corrosion Initiation Time (Water)

Response	23	Corrosion Initiation Period (Water)				
Transform:	Natural Log	Constant:	0			
ANOVA for Response Surface Reduced Linear Model						
Analysis of variance table [Partial sum of squares - Type III]						
Source	Sum of Squares	df	Mean Square	F-Value	P-Value (Prob. > F)	Significance
Model	19.30	2	9.65	96.06	< 0.0001	Significant
B-W/B	0.80	1	0.80	7.92	0.0120	Significant
C-Replacement	18.50	1	18.50	184.20	< 0.0001	Significant
Residual	1.71	17	0.10			
Lack of Fit	1.64	12	0.14	10.06	0.0096	Significant
Pure Error	0.07	5	0.01			
Correlation Total	21.00	19				

d_f = Degrees of Freedom

C51: Effects of Factors B and C on Response 23 (Corrosion Initiation Time-Water)

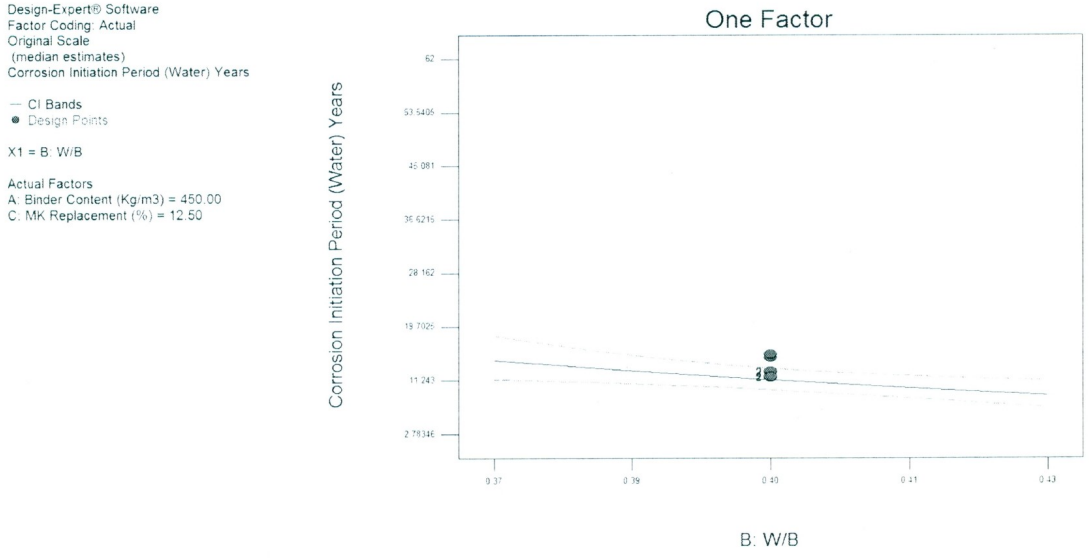

Design-Expert® Software
Factor Coding: Actual
Original Scale
(median estimates)
Corrosion Initiation Period (Water) Years

— CI Bands
● Design Points

X1 = C: MK Replacement (%)

Actual Factors
A: Binder Content (Kg/m3) = 450.00
B: W/B = 0.40

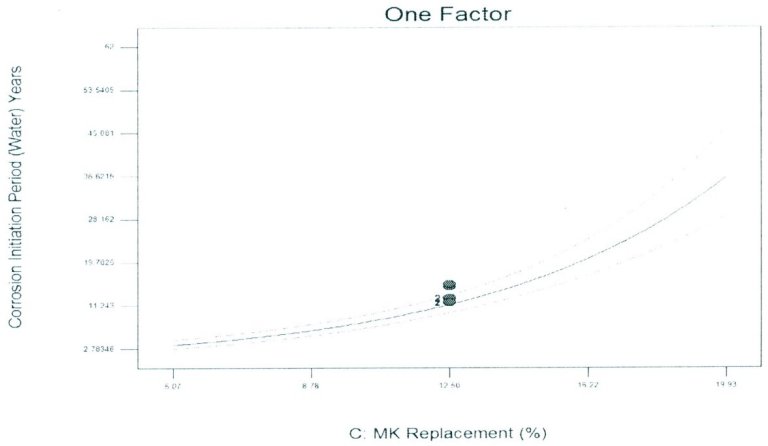

C52: Response Surfaces for factors A-B, A-C, and B-C for Response 23: Corrosion Initiation Time (Water)

Design-Expert® Software
Factor Coding: Actual
Original Scale
(median estimates)
Corrosion Initiation Period (Water) Years
● Design points above predicted value
65.1
2.2

X1 = B: W/B
X2 = A: Binder Content (Kg/m3)

Actual Factor
C: MK Replacement (%) = 12.50

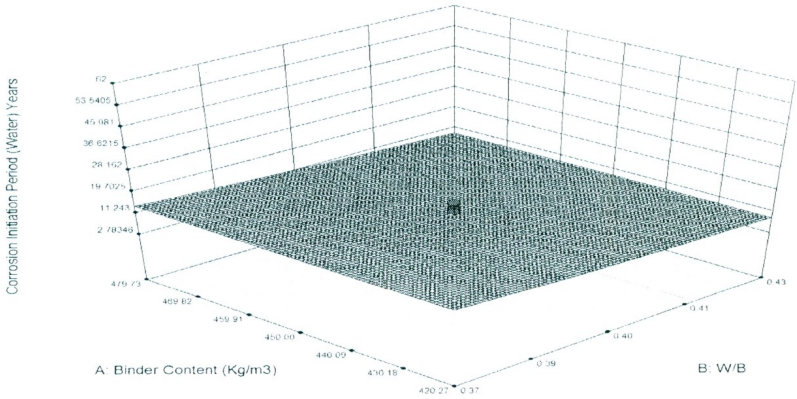

Design-Expert® Software
Factor Coding: Actual
Original Scale
(median estimates)
Corrosion Initiation Period (Water) Years
● Design points above predicted value
65.1
2.2

X1 = C: MK Replacement (%)
X2 = A: Binder Content (Kg/m3)

Actual Factor
B: W/B = 0.40

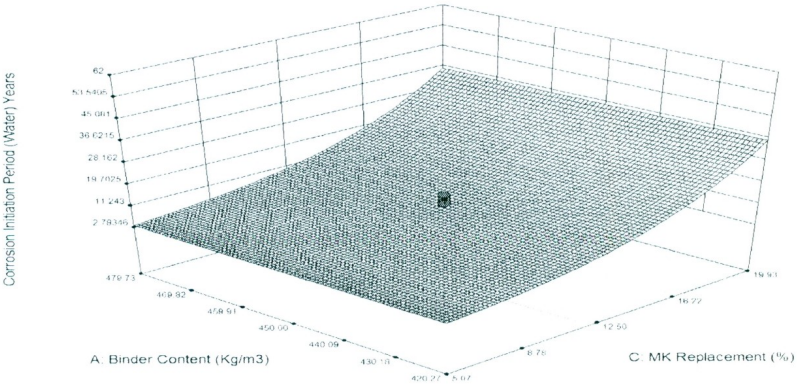

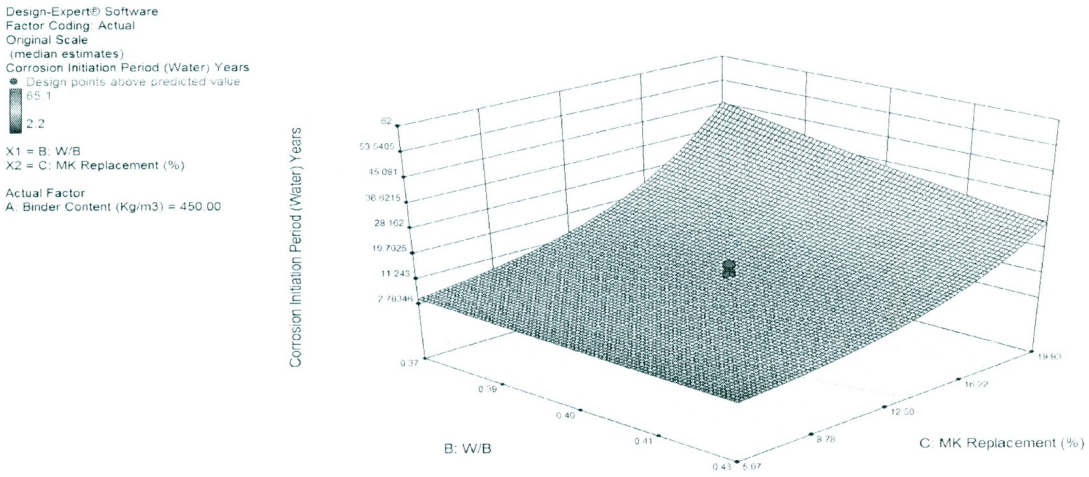
Design-Expert® Software
Factor Coding: Actual
Original Scale
(median estimates)
Corrosion Initiation Period (Water) Years
Design points above predicted value
65.1
2.2
X1 = B: W/B
X2 = C: MK Replacement (%)
Actual Factor
A: Binder Content (Kg/m3) = 450.00
Corrosion Initiation Period (Water) Years
62
53.5405
45.081
36.6215
28.162
19.7025
11.243
2.78346
0.37
0.39
0.40
0.41
0.43
B: W/B
5.67
8.78
12.50
16.22
19.93
C: MK Replacement (%)